THE GEOLOGY OF

Antelope Island

DAVIS COUNTY, UTAH

Jon K. King and Grant C. Willis, editors

THE GEOLOGY OF ANTELOPE ISLAND, DAVIS COUNTY, UTAH

Jon K. King and Grant C. Willis, editors

ISBN 1-55791-647-0

2000

Miscellaneous Publication 00-1
UTAH GEOLOGICAL SURVEY
a division of
Utah Department of Natural Resources

STATE OF UTAH

Michael O. Leavitt, Governor

DEPARTMENT OF NATURAL RESOURCES

Kathleen Clarke, Executive Director

UTAH GEOLOGICAL SURVEY

Kimm M. Harty, Acting Director

UGS Board

Member	Representing
Craig Nelson (Chairman)	Civil Engineering
D. Cary Smith	Mineral Industry
C. William Berge	Mineral Industry
E.H. Deedee O'Brien	Public-at-Large
Robert Robison	Mineral Industry
Charles Semborski	Mineral Industry
Richard R. Kennedy	Economics-Business/Scientific
David Terry, Director, Trust Lands Administration	*Ex officio member*

UTAH GEOLOGICAL SURVEY

The **UTAH GEOLOGICAL SURVEY** is organized into five geologic programs with Administration, Editorial, and Computer Resources providing necessary support to the programs. The **ECONOMIC GEOLOGY PROGRAM** undertakes studies to identify coal, geothermal, uranium, hydrocarbon, and industrial and metallic resources; initiates detailed studies of these resources including mining district and field studies; develops computerized resource data bases, to answer state, federal, and industry requests for information; and encourages the prudent development of Utah's geologic resources. The **APPLIED GEOLOGY PROGRAM** responds to requests from local and state governmental entities for engineering-geologic investigations; and identifies, documents, and interprets Utah's geologic hazards. The **GEOLOGIC MAPPING PROGRAM** maps the bedrock and surficial geology of the state at a regional scale by county and at a more detailed scale by quadrangle. The **GEOLOGIC EXTENSION SERVICE** answers inquiries from the public and provides information about Utah's geology in a non-technical format. The **ENVIRONMENTAL SCIENCES PROGRAM** maintains and publishes records of Utah's fossil resources, provides paleontological and archeological recovery services to state and local governments, conducts studies of environmental change to aid resource management, and evaluates the quantity and quality of Utah's ground-water resources.

The UGS Library is open to the public and contains many reference works on Utah geology and many unpublished documents on aspects of Utah geology by UGS staff and others. The UGS has several computer data bases with information on mineral and energy resources, geologic hazards, stratigraphic sections, and bibliographic references. Most files may be viewed by using the UGS Library. The UGS also manages a sample library which contains core, cuttings, and soil samples from mineral and petroleum drill holes and engineering geology investigations. Samples may be viewed at the Sample Library or requested as a loan for outside study.

The UGS publishes the results of its investigations in the form of maps, reports, and compilations of data that are accessible to the public. For information on UGS publications, contact the Natural Resources Map/Bookstore, 1594 W. North Temple, Salt Lake City, Utah 84116, (801) 537-3320 or 1-888-UTAH MAP. E-mail: nrugs.geostore@state.ut.us and visit our web site at http://www.ugs.state.ut.us.

UGS Editorial Staff

J. Stringfellow	Editor
Vicky Clarke, Sharon Hamre	Graphic Artists
Patricia H. Speranza, James W. Parker, Lori Douglas	Cartographers

3/00

The Miscellaneous Publication series of the Utah Geological Survey provides non-UGS authors with a high-quality format for papers concerning Utah geology. Although some reviews have been incorporated, this publication does not necessarily conform to UGS technical, policy, or editorial standards.

Many of the papers in this Miscellaneous Publication were written in the early 1990s and have not been fully updated with information or research completed since that time. The extent of peer review varies between papers.

TABLE OF CONTENTS

INTRODUCTION TO THE GEOLOGY OF ANTELOPE ISLAND, UTAH

by
Grant C. Willis, Jon K. King, and Hellmut H. Doelling
Utah Geological Survey

Antelope Island, the largest of Great Salt Lake's eight major islands, is about 15 miles (24 km) long and up to 5 miles (8 km) wide, and covers approximately 40 square miles (104 km^2). Frary Peak, the island's highest point, is 6,597 feet (2,010 m) above sea level and about 2,400 feet (730 m) above the lake's historical average level. Although the island is perhaps best known for its wildlife and relatively pristine condition, the island is also fascinating from a geological standpoint.

GEOLOGIC MAPPING

Captain Howard Stansbury, who explored the valley of Great Salt Lake in 1850, first described the geology of the island (Stansbury, 1852). Stansbury turned his notes and rock samples over to the prominent New York professor, James Hall, who noted in an appendix to Stansbury's report that the rocks of the island "...consist of granite, or perhaps an altered sedimentary quartz or siliceous sandstone" (Hall, 1852). In the 1870s, Clarence King, S.F. Emmons and Arnold Hague of the 40th Parallel Survey and other government surveyors explored and mapped much of the west (King, 1876, 1878; Hague and Emmons, 1877). Their geologic map of northern Utah showed the island as Archean rocks surrounded by Quaternary deposits (King, 1876). After climbing to the top of Frary Peak, Hague and Emmons (1877) described the Archean rocks as "...mostly gneisses, with some quartzites and mica-slates."

George G. Bywater and Joseph A. Barlow (1909) produced the first large-scale geologic map of Antelope Island (1 inch = 1 mile). Their map included two Precambrian units - "granite" and "gneiss," and four Cambrian units - "basal conglomerate," "limestone," "slate," and "quartzite and conglomerate." They also made note of the "shoreline of an ancient ocean" (Pleistocene Lake Bonneville), marked by accumulations of sand and gravel deposits, and Paleozoic boulders. A.J. Eardley and R.A. Hatch (1940a, 1940b) divided the Precambrian crystalline rocks into three lithologic units and discussed overlying sedimentary rocks and quartzite at the north end of the island.

Willard Larsen (1957) produced a detailed study of the petrology and structure of Antelope Island, and a 1:24,000-scale (1 inch = 0.379 miles) geologic map. He divided the Precambrian crystalline rocks into three lithologic parts, which he treated as stratigraphic units: the lower, mainly on the west side of the island; the middle, including a major shear zone, in the center of the island; and the upper, covering all of the southern and most of the eastern part of the island. He also noted the presence of Tertiary rocks on the island.

In 1987, the Utah Geological and Mineral Survey (now the Utah Geological Survey), in cooperation with the Utah Division of Parks and Recreation, began a multifaceted project to map the island, study mineral and water resources, and assess geologic hazards. This comprehensive study resulted in the following publications: *Geology and Antelope Island State Park, Utah* (Doelling and others, 1988); *Antelope Island State Park - the History, the Geology, and Wise Planning for Future Development* (Doelling, 1989); and the *Geologic Map of Antelope Island*, a 1:24,000-scale geologic map and accompanying text booklet (Doelling and others, 1990), that were used in developing the Antelope Island State Park Master Plan. Doelling and others (1990) mapped the island's rocks and sediments in greater detail than previous studies, showed scarps and faults, identified potential geologic hazards, and discussed engineering aspects. This new volume contains the results of various technical studies completed as part of, or in cooperation with, the UGS Antelope Island study begun in 1987.

GEOLOGIC HISTORY

Some of Utah's oldest and youngest rocks are preserved on the island. They consist of six formations separated by unconformities: Farmington Canyon Complex, Mineral Fork Formation, Kelley Canyon Formation, Tintic Quartzite, an unnamed Tertiary conglomeratic unit, and Salt Lake Formation (figure 1) (Doelling and others, 1990).

The oldest rocks, the Farmington Canyon Complex, are exposed on the southern two-thirds of the island. Some of these rocks may be more than 2.5 billion years old, and were overprinted by high-grade metamorphism and intrusions about 1.7 billion years ago. Yonkee and others (this volume) describe these rocks.

The Mineral Fork Formation consists of diamictite deposited about 750 million years ago (late Proterozoic) during continental glaciation. The slightly younger, but closely associated, Kelley Canyon Formation overlies the Mineral Fork rocks. The Kelley Canyon consists of slightly metamor-

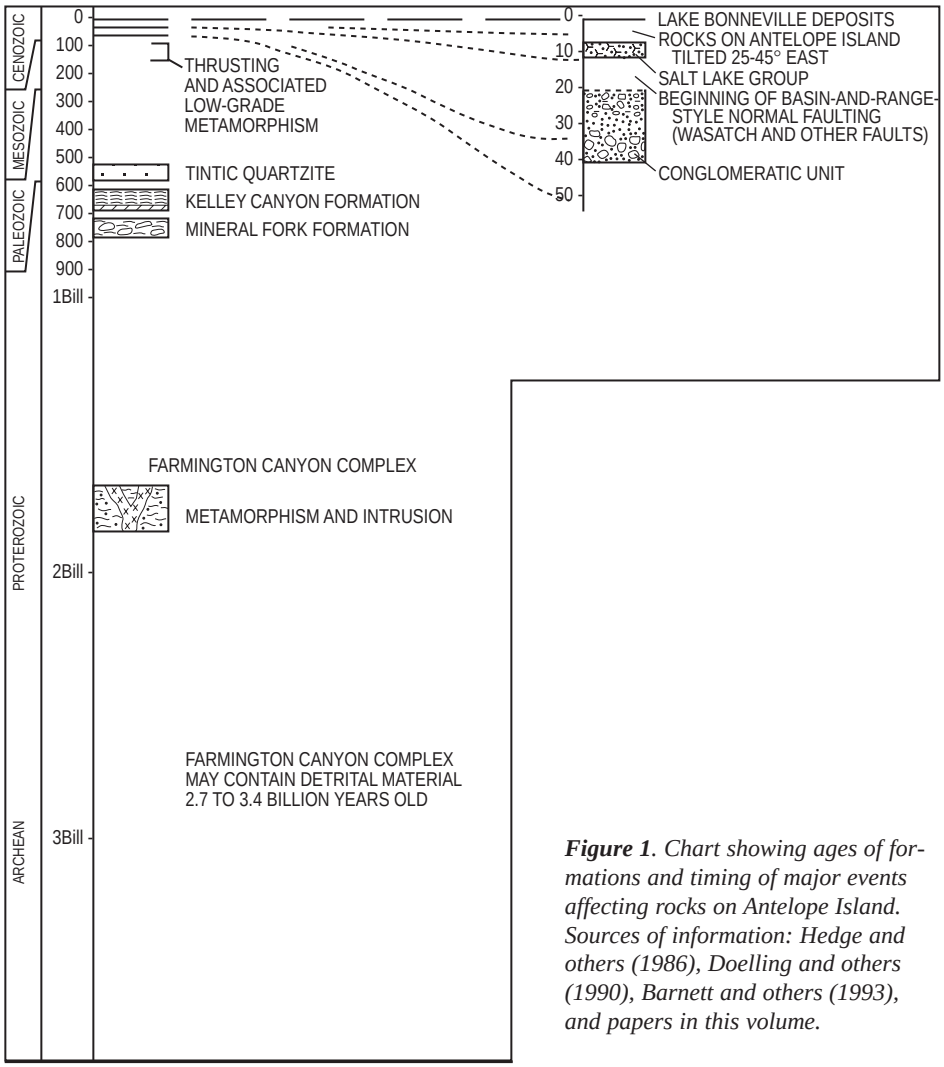

***Figure 1**. Chart showing ages of formations and timing of major events affecting rocks on Antelope Island. Sources of information: Hedge and others (1986), Doelling and others (1990), Barnett and others (1993), and papers in this volume.*

phosed dolomite and slate deposited in an ancient ocean between 600 and 700 million years ago. About 550 million years ago, during the early part of the Cambrian period, rocks of the Tintic Quartzite were deposited in lower coastal plain and shoreline environments near the margins of an ancient ocean. Tintic rocks cover the northern part of the island. Yonkee and others (this volume) describe the Mineral Fork, Kelley Canyon, and Tintic Formations. During the Late Jurassic to early Tertiary Sevier orogeny, island rocks were involved in intense semi-brittle to brittle deformation in which they were folded, faulted, sheared, retrogressively metamorphosed, uplifted, and eroded (Doelling and others, 1990; Yonkee, 1992). Hansen and McCarley (this volume) discuss some local Sevier orogeny and later basin-and-range deformation on Antelope Island.

The next group of rocks is middle Tertiary in age, and overlies an unconformity representing about 500 million years. During the early Tertiary, about 40 to 50 million years ago, very coarse conglomerate, sandstone, and mudstone were deposited in the area. This unnamed conglomerate unit is exposed on the east side of the island. These rocks may be equivalent in part to the Wasatch Formation, Fowkes Formation, or Norwood Tuff that are common in northeastern Utah. Large boulders in the conglomerate were eroded from Precambrian and Paleozoic formations, most of which are no longer preserved on the island, and some clasts contain fossils of corals, brachipods, crinoids, and other marine fauna.

After another interval of erosion, upper Tertiary rocks making up the Salt Lake Formation were deposited, probably 11 to 8 million years ago. They consist of sandstone, conglomerate, mudstone, and volcanic ash deposited in basins between mountain ranges. These rocks are now steeply tilted to the east and are faulted, reflecting late Cenozoic basin-and-range deformation that commenced about 17 million years ago and created the island block. Willis and Jensen (this volume) discuss the Tertiary rocks and their relationship to rocks of similar age and lithology in other parts of northern Utah. This latest phase of mountain building continues today. Deep basins, typically with no external drainage, developed between the ranges and are filled with sediments transported by rivers and streams from the surrounding mountains. Along with the rest of the Great Basin, Antelope Island continues to be active geologically. Movement occurs periodically along bounding faults, tilting the island more and changing the lake and island elevations.

One of the latest influences to shape Antelope Island was Lake Bonneville, which was 1,000 feet (300 m) deep and covered over 20,000 square miles (50,000 km^2) of western Utah, eastern Nevada, and southern Idaho during the last ice age (Currey and others, 1984; Oviatt and others, 1992). Lake Bonneville's various shorelines are etched on Antelope Island, and sand and gravel were deposited over most of the island by the lake's strong wave action. Lake Bonneville expanded gradually from a small saline lake about 30,000 years ago to its highest level, the "Bonneville" level (at approximately 5,200 feet [1,585 m] in elevation) about 15,000 years ago. At this level it was nearly the size of present Lake Michigan. This level was maintained until about 14,500 years ago when a breach at Red Rock Pass in southern Idaho released a catastrophic flood into the Snake River Plain, quickly lowering the water surface about 350 feet (107 m) to the "Provo" level. This level, at about 4,820 feet (1,469 m), was maintained until increased evaporation associated with climatic changes caused the lake to nearly dry up about 12,000 years ago. Several other levels, including the "Stansbury" at approximately 4,450 feet (1,356 m), and the "Gilbert" at about 4,250 feet (1,295 m), form less-prominent shorelines on the island (Oviatt and others, 1992). Over the last 10,000 years, lake levels have fluctuated near the present level of Great Salt Lake.

GREAT SALT LAKE

The present Great Salt Lake, approximately 40 miles (64 km) wide and 80 miles (128 km) long, is the largest lake in the U.S. after the Great Lakes. It is a shallow body of water - it is slightly over 30 feet (9 m) deep in the deepest part, and averages just 13 feet (4 m) deep when at a "typical" lake surface elevation of 4,202 feet (1,280.8 m) above sea level. Because it has no outlet, variations in precipitation in the drainage basin result in constant fluctuations in the lake level, size, and salinity. From 1850 until the present, the lake level has fluctuated more than 20 feet (6 m), from 4,191 to 4,212 feet (1,277.4-1,283.8 m) above sea level, changing its area from 970 to 2,280 square miles (2,512-5,905 km^2). When the lake is below a level of 4,200 feet (1,280 m), Antelope Island is connected to the mainland by a broad mudflat. During these fluctuations, lake salinity varies from 5 to over 25 percent. In contrast, ocean water contains a little over 3 percent salt. Five major ions are present in the waters of the lake: sodium, magnesium, potassium, chlorine, and sulfate. Calcium, lithium, bromine, and boron are present in lesser but significant quantities (Gwynn, 1997). Gwynn (this volume) discusses the hydrology of Great Salt Lake. Just as Lake Bonneville did before, the rising and falling Great Salt Lake leaves shoreline traces on Antelope Island. Atwood and Mabey (this volume), and Murchison and Mulvey (this volume) present more information on historical and late prehistoric Great Salt Lake shoreline features. Burke and Gerhard (this volume) discuss cementation and sedimentary structures associated with Great Salt Lake.

ROCK AND MINERAL RESOURCES

Slate was mined from outcrops in the Kelley Canyon Formation by the early pioneers. Over the years, prospectors searched for copper and gold because the island is aligned with the Oquirrh Mountains, the location of the productive Bingham mining district. Copper mineralization is prominent on some outcrops, but significant mineralization has not been discovered. Today, the chief resources of the island are sand, gravel, and quartzite boulders suitable for riprap, roadfill, and concrete aggregate. In 1979 and 1980, approximately 16 million cubic yards (12 million m^3) of sand and gravel were excavated from 2.5 square miles (6.5 km^2) of alluvial fans and beach deposits in the southeast part of the island and transported on a 13-mile-long (21-km) conveyor belt (the longest in the world at the time) for use in the construction of Interstate 80 between Saltair and Salt Lake City. The northern and western beaches have abundant deposits of fine oolitic calcium carbonate sand. Davis (this volume) discusses construction materials on the island.

SPRINGS AND GROUND WATER

Antelope Island has several springs, primarily found above an elevation of 4,400 feet (1,340 m) on the east side of the island. These springs are thought to be recharged by rain and snowmelt that percolates into fractured rocks at higher elevations. The water quality is good, but with higher sodium and chloride concentrations than water flowing from springs in the Wasatch Range. Mayo and Klauk (1991; this volume) evaluate water chemistry on the island. Locations of septic drainfields and public facilities must be carefully evaluated to assure that the limited ground water is not polluted.

GEOLOGIC HAZARDS

Landslides, rock falls, and debris flows have created scars and deposits that can be seen on the island, sand dunes have migrated onto recently constructed roads, and unpaved roads on steep hillsides consisting of loose material have contributed to erosion. Several major active faults are near the island, and earthquake shaking could seriously damage or destroy man-made structures, trigger landslides and rock falls, and cause damaging waves on Great Salt Lake. Unusually high precipitation in the early 1980s produced a harsh reminder of the fluctuating levels of Great Salt Lake. A drastic rise in the lake level destroyed road access to Antelope Island, flooded beaches, destroyed public facilities, and caused over $300 million in damage to facilities around the lake (mostly on the mainland). Any future development on the island or on the causeway to the island should take into account the natural fluctuations of Great Salt Lake. Hecker and Case (this volume) discuss geologic hazards and engineering geology of the island.

REFERENCES

Barnett, Daniel, Bowman, J.R., and Smith, H.A., 1993, Petrologic and geochronologic studies in the Farmington Canyon Complex, Wasatch Mountains and Antelope Island, Utah: Utah Geological Survey Contract Report 93-5, 34 p.

Bywater, G.G., and Barlow, J.A., 1909, Antelope Island, Great Salt Lake: Salt Lake City, University of Utah, B.S. thesis, 21 p., scale 1:63,360.

Currey, D.R., Atwood, Genevieve, and Mabey, D.R., 1984, Major levels of Great Salt Lake and Lake Bonneville: Utah Geological and Mineral Survey Map 73, scale 1:750,000.

Doelling, H.H., 1989, Antelope Island State Park; the history, the geology and wise planning for future development: Utah Geological and Mineral Survey, Survey Notes, v. 23, no. 1, p. 2-14.

Doelling, H.H., Willis, G.C., Jensen, M.E., Davis, F.D., Gwynn, J.W., Case, W.F., Hecker, Suzanne, Atwood, Genevieve, and Klauk, R.H., 1988, Geology and Antelope Island State Park, Utah: Utah Geological and Mineral Survey, in cooperation with Division of Parks and Recreation, Miscellaneous Publication 88-2, 20 p.

Doelling, H.H., Willis, G.C., Jensen, M.E., Hecker, Suzanne, Case, W.F., and Hand, J.S., 1990, Geologic map of Antelope Island, Davis County, Utah: Utah Geological and Mineral Survey Map 127, 27 p. pamphlet, scale 1:24,000.

Eardley, A.J., and Hatch, R.A., 1940a, Pre-Cambrian crystalline rocks of north-central Utah: Journal of Geology, v. 48, p. 58-72.

Eardley, A.J. and Hatch, R.A., 1940b, Proterozic(?) rocks in Utah: Geological Society of America Bulletin, v. 51, p. 795-844.

Gwynn, J.W., 1997, Brine properties, mineral extraction industries, and salt load of Great Salt Lake, Utah: Utah Geological Survey Public Information Series PI-51, 2 p.

Hague, Arnold, and Emmons, S.F., 1877, Descriptive geology, *in* Report of the Geological exploration of the fortieth parallel: Professional Papers of the Engineer Department, U.S. Army, no. 18, v. II, 890 p.

Hall, J.E., 1852, Appendix E, a letter from professor James Hall ...containing observations on the geology and paleontology of the country traversed by the expedition, *in* Stansbury, Howard, Exploration and survey of the valley of the Great Salt Lake, including a reconnaissance of a new route through the Rocky Mountains: Philadelphia, Lippincott, Grambo & Co., p. 401-414 (U.S. 32nd Congress, Special Session, Senate Executive Document 3) (reprinted in 1988 with the title "Exploration of the valley of the Great Salt Lake" by Smithsonian Institution Press, Washington, D.C., 421 p.)

Hedge, C.E., Houston, R.S., Tweto, O.L., Peterman, Z.E., Harrison, J.E., and Reid, R.R., 1986, The Precambrian of the Rocky Mountain region: U.S. Geological Survey Professional Paper 1241-D, 17 p.

King, Clarence, 1876, Geological and topographical atlas accompanying the Report of the geological exploration of the fortieth parallel: Professional Papers of the Engineer Department, U.S. Army, no. 18, 10 maps, scale about 1:250,000 for Utah area.

King, Clarence, 1878, Systematic geology, *in* Report of the geological exploration of the fortieth parallel: Professional Papers of the Engineer Department, U.S. Army, no. 18, v. I, 803 p.

Larsen, W.N., 1957, Petrology and structure of Antelope Island, Davis County, Utah: Salt Lake City, University of Utah, Ph.D. dissertation, 142 p., scale 1:24,000.

Mayo, A.L., and Klauk, R.H., 1991, Contributions to the solute and isotopic groundwater geochemistry, Antelope Island, Great Salt Lake, Utah: Journal of Hydrology, v. 127, p. 307-335.

Oviatt, C.G., Currey, D.R., and Sack, Dorothy, 1992, Radiocarbon chronology of Lake Bonneville, eastern Great Basin, USA: Palaeogeography, Palaeoclimatology, Palaeoecology, v. 99, p. 225-241.

Stansbury, Howard, 1852, Exploration and survey of the valley of the Great Salt Lake, including a reconnaissance of a new route through the Rocky Mountains: Philadelphia, Lippincott, Grambo & Co., 487 p. [U.S. 32nd Congress, Special Session, Senate Executive Document 3](reprinted in 1988 with the title "Exploration of the valley of the Great Salt Lake" by Smithsonian Institution Press, Washington, D.C., 421 p.)

Yonkee, W.A., 1992, Basement-cover relations, Sevier orogenic belt, northern Utah: Geological Society of America Bulletin, v. 104, no. 3, p. 280-302.

PETROLOGY AND GEOLOGIC HISTORY OF THE PRECAMBRIAN FARMINGTON CANYON COMPLEX, ANTELOPE ISLAND, UTAH

by
W. A. Yonkee[1], G. C. Willis, and H. H. Doelling
Utah Geological Survey

[1]now at Department of Geosciences
Weber State University, Ogden, Utah

ABSTRACT

Precambrian high-grade metamorphic and igneous rocks of the Farmington Canyon Complex exposed on Antelope Island provide a partial record of the early geologic history of northern Utah. Rock types include: (1) layered gneiss; (2) biotite schist; (3) quartz-rich gneiss; (4) metamorphosed ultramafic rock; (5) hornblende-plagioclase gneiss; (6) banded gneiss; (7) granitic gneiss; (8) granite and pegmatite; (9) chloritic gneiss; and (10) phyllonite and mylonite.

Layered gneiss and intercalated lenses of biotite schist and quartz-rich gneiss probably represent a deformed sedimentary sequence. Hornblende-plagioclase gneiss and isolated lenses of metamorphosed ultramafic rock probably represent deformed mafic and ultramafic igneous rocks emplaced over a protracted history. Granitic gneiss and banded gneiss probably represent a deformed, complexly zoned pluton intruded during a main phase of metamorphism and deformation. Non-foliated smaller granite plutons crosscut earlier structures and were intruded after peak deformation. Pegmatite forms foliated concordant to non-foliated discordant dikes that were emplaced over a protracted history. Chloritic gneiss displays fractures and variable retrograde greenschist alteration that crosscut earlier high-grade structures. Phyllonite and mylonite within shear zones display pervasive retrograde alteration and concentrated plastic deformation. Chloritic gneiss, phyllonite, and mylonite formed during deformation associated with Mesozoic thrusting.

Layered gneiss contains biotite, garnet, sillimanite, K-feldspar, and cordierite, recording high temperatures (about 700°C) and relatively low lithostatic pressures (about 3 to 5 kilobar) during main-phase metamorphism. Compositions of banded and granitic gneiss are consistent with crystallization at temperatures of 650 to 700°C from magma derived by partial melting of tonalitic to granodioritic gneiss. A dominant foliation formed in the gneisses during main-phase deformation and metamorphism, but complex fold interference patterns and multiple foliations in layered gneiss may record earlier deformation.

An interpretive geologic history has the following idealized stages: (1) Archean (?) deposition of a supracrustal sequence; (2) Late Archean (?) metamorphism and deformation; (3) Early Proterozoic granitic intrusion; (4) Early Proterozoic main-phase metamorphism and deformation; (5) Proterozoic intrusion of late-stage granites; (6) Middle to Late Proterozoic uplift and erosion; (7) Late Proterozoic to Mesozoic deposition of sedimentary rocks; (8) Mesozoic deformation and retrograde alteration; and (9) Cenozoic extension.

INTRODUCTION

High-grade metamorphic and igneous rocks are well exposed on Antelope Island (figure 1), and provide a partial record of the Precambrian geologic history of northern Utah (Bryant, 1988a; Doelling and others, 1990). In this paper we

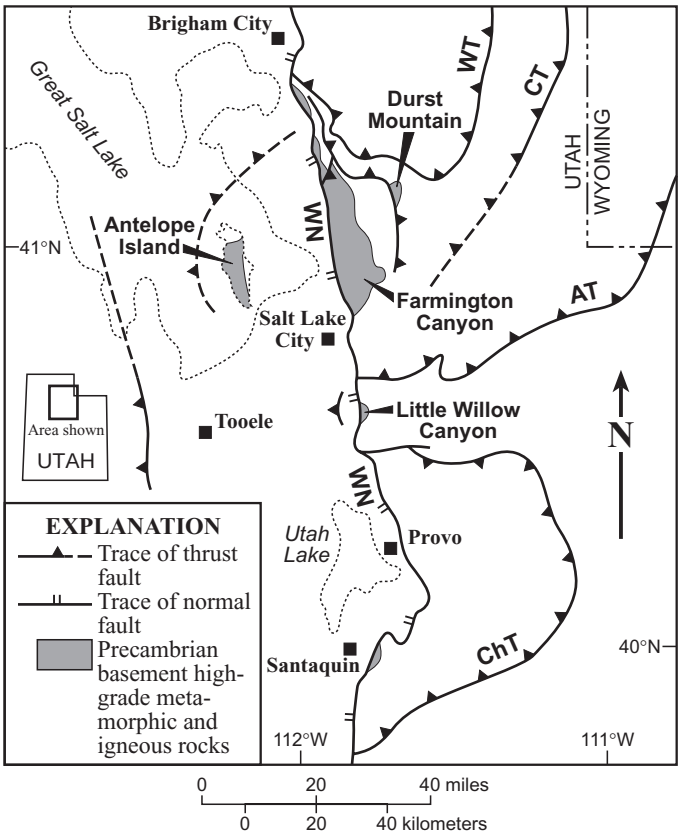

Figure 1. *Index map showing tectonic setting and locations of Precambrian basement outcrops in northern Utah. Major fault traces are labeled: AT- Absaroka thrust system; CT- Crawford thrust; ChT- Charleston thrust system; OT- Ogden thrust system; WT- Willard thrust; WN- Wasatch normal fault zone. Modified from Hintze and Stokes (1964) and Bryant (1988b).*

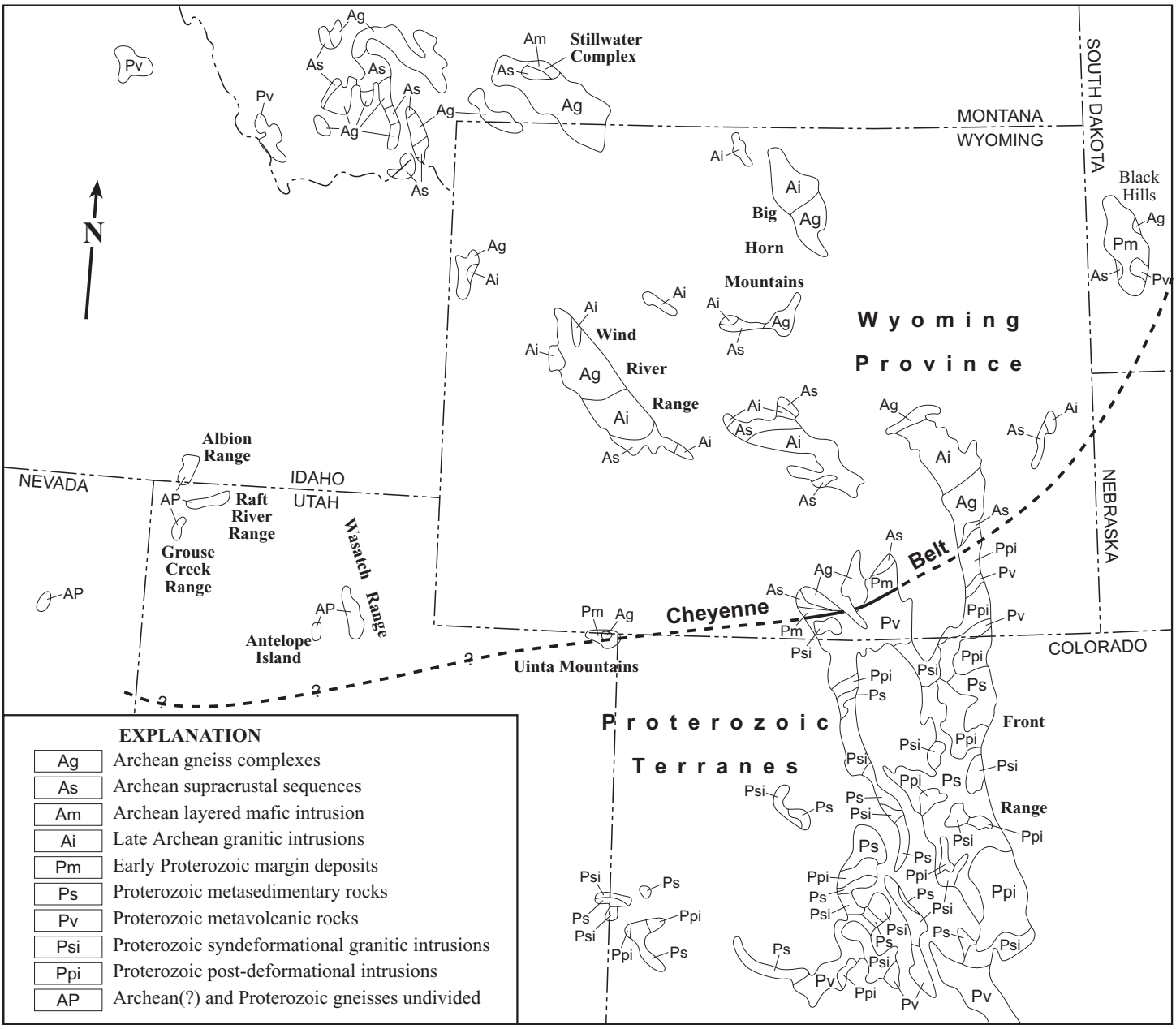

Figure 2. *Locations of Precambrian basement terranes and rock types in the Rocky Mountain region. Approximate boundary of Wyoming Province indicated by dashed line. Modified from Karlstrom and Houston (1984), Hedge and others (1986), Tweto (1987), and Bryant (1988a).*

discuss the outcrop and petrographic characteristics of basement rocks on Antelope Island. We also briefly discuss the geochemistry, metamorphic conditions, and geochronology of these rocks. These data are used to interpret the origin of the rocks, to develop a generalized geologic history for the area, and to regionally correlate basement rocks on Antelope Island with other Precambrian rocks exposed in the Rocky Mountain area.

Crystalline basement with similar characteristics is exposed to the east in the Wasatch Range near Farmington Canyon (figure 1), and was named the Farmington Canyon Complex by Eardley and Hatch (1940). Limited exposures of crystalline basement are also found at Durst Mountain, at Little Willow Canyon near Salt Lake City, and near Santaquin, Utah (figure 1).

Previous workers outlined the general characteristics of the Farmington Canyon Complex. Bell (1951) did a detailed study of basement rocks in part of the Wasatch Range, and Larsen (1957) conducted a geological study of Antelope Island. Bryant (1988b) discussed results of a reconnaissance study of the structure and geochemistry of the Farmington Canyon Complex, and Hedge and others (1983) conducted a geochronologic study of part of the complex. Basement and sedimentary rocks on Antelope Island were described and mapped in detail by Doelling and others (1990).

During the Precambrian, the Farmington Canyon Complex underwent a complicated history of deformation, intrusion, and metamorphism (Hedge and others, 1983; Bryant, 1988b). Late Proterozoic to Mesozoic sedimentary rocks were deposited unconformably over the crystalline basement. The basement and the sedimentary rocks were thrust eastward and internally deformed in the Late Mesozoic during the Sevier orogeny (Yonkee, 1990). An anastomosing network of shear zones developed during thrusting and these zones over-

printed Precambrian high-grade structures (Yonkee, 1992). Cenozoic normal faulting further modified structures and is partly responsible for the current topography and exposure.

REGIONAL SETTING

The Rocky Mountain region contains several distinct Precambrian terranes that are characterized by different ages, lithologies, and interpreted tectonic settings (Hedge and others, 1986; Tweto, 1987). Correlation of the Farmington Canyon Complex with these other terranes and interpretation of tectonic setting remain problematic, partly because of limited petrologic and geochronologic data. We briefly summarize characteristics of Precambrian terranes in the Rocky Mountain region, and then discuss alternative correlations of the Farmington Canyon Complex.

An Archean terrane termed the Wyoming Province covers a broad circular area within the north-central Rocky Mountains (figure 2) (Hedge and others, 1986). The terrane consists principally of high-grade gneiss complexes, granitic to granodioritic plutons, and interspersed belts of supracrustal rocks. Gneisses in the central part of the province are as old as 3,300 million years (Ma), but ages decrease overall toward the margins of the province. Many areas underwent metamorphism and intrusion of large granitic plutons between 2,700 and 2,500 Ma (Hedge and others, 1986).

A belt of variably metamorphosed Early Proterozoic margin deposits, now exposed in southern Wyoming and South Dakota, accumulated along the southern and eastern edges of the Wyoming Province (figure 2) (Hedge and others, 1986). The belt contains thick sequences of quartzose to argillaceous metasedimentary rocks and mafic meta-igneous rocks that probably accumulated along a rifted passive margin between 2,300 and 1,800 Ma (Karlstrom and Houston, 1984).

A wide zone of deformation, called the Cheyenne belt (Karlstrom and Houston, 1984), juxtaposes Archean basement of the Wyoming Province and the overlying sequence of Early Proterozoic margin deposits on the north side against terranes of strongly deformed Proterozoic metavolcanic and metasedimentary rocks on the south side (figure 2). The belt is interpreted to record a collisional orogeny and accretion of island arc terranes onto the southern margin of the Archean Wyoming Province between about 1,800 and 1,600 Ma (Karlstrom and Houston, 1984; Duebendorfer and Houston, 1987).

The Proterozoic terranes south of the Cheyenne belt are well exposed in parts of Colorado and consist mostly of: (1) felsic and hornblendic gneisses that represent metamorphosed rhyolitic and basaltic volcanic rocks; (2) quartz-plagioclase-biotite gneiss and schist that represent metamorphosed sedimentary rocks including graywacke, sandstone, and shale; and (3) large granodioritic to granitic calc-alkaline intrusive complexes (figure 2) (Hedge and others, 1986; Tweto, 1987). Protoliths for meta-volcanic and meta-sedimentary rocks probably accumulated in or near island arcs about 1,800 million years ago. Widespread metamorphism and intense deformation that affected these rocks peaked at about 1,700 Ma, synchronous with intrusion of the calc-alkaline granitic complexes, but the duration of the deformation is uncertain (Hedge and others, 1986; Duebendorfer and Houston, 1987).

The Cheyenne belt is well exposed in southeastern Wyoming, but its westward extension is uncertain (figure 2). Early Proterozoic margin deposits of the Red Creek Quartzite are juxtaposed over gneisses of the Late Archean Owiyukuts Complex within the Uinta Mountains (Sears and others, 1982), indicating that the southern margin of the Wyoming Province may continue westward in the subsurface beneath the northern margin of the Uinta Mountains (Graff and others, 1980; Bryant, 1988a). Crystalline gneisses in the Albion, Raft River, and Grouse Creek Ranges of northwestern Utah and southeastern Idaho may also contain Archean components (Armstrong, 1968; Compton and others, 1977). Mesozoic and Tertiary deformation and metamorphism have largely obliterated evidence of the early history of these gneisses such that the western margin of the Wyoming Province is poorly constrained. Rocks of the Farmington Canyon Complex display similarities with both the Archean Wyoming Province and the Proterozoic terranes of Colorado and southern Utah.

GENERAL DESCRIPTION OF BASEMENT ROCK TYPES

We divide the crystalline basement rocks on Antelope Island into ten types based on petrographic and outcrop characteristics. These rock types roughly correspond to map units discussed by Doelling and others (1990). Basement rock types are: (1) layered gneiss, which corresponds to parts of their layered and mixed gneiss map units; (2) biotite schist, which forms lenses within layered gneiss; (3) quartz-rich gneiss, which corresponds to their quartz-plagioclase gneiss map unit; (4) metamorphosed ultramafic rock, which forms isolated lenses within layered gneiss; (5) hornblende-plagioclase gneiss, which corresponds to their amphibolite map unit and which also forms thin lenses in other units; (6) banded gneiss, which corresponds to part of their mixed gneiss map unit; (7) granitic gneiss, which corresponds to their red granitic gneiss and migmatitic granitic gneiss map units; (8) granite and pegmatite, which correspond to their coarse-grained granite and pegmatitic granite map units and which form small pods within other units; (9) chloritic gneiss; and (10) phyllonite and mylonite within shear zones. The last two rock types correspond to the chloritized gneiss, mylonite, and phyllonite map unit of Doelling and others (1990), and are characterized by Cretaceous retrograde alteration and deformation that overprint earlier structures (Yonkee, 1992).

Layered gneiss, with lenses of biotite schist and quartz-rich gneiss, and rare pods of metamorphosed ultramafic and mafic rock, forms elongate regions within the southern and central parts of the island (figure 3a). Hornblende-plagioclase gneiss forms elongate pods in other units and is abundant within a large banded gneiss body in the central part of the island. Granitic gneiss is exposed in a large elliptical area on the west-central part of the island and in a smaller area to the northeast. Banded gneiss, the dominant rock type within the central and eastern parts of the island, surrounds the granitic gneiss. Granite and pegmatite form small plutons and stringers within other units and form several larger plutons on the eastern part of the island. Chloritic gneiss, phyllonite, and mylonite are found along shear zones, including a major shear zone in the central part of the island, and near the

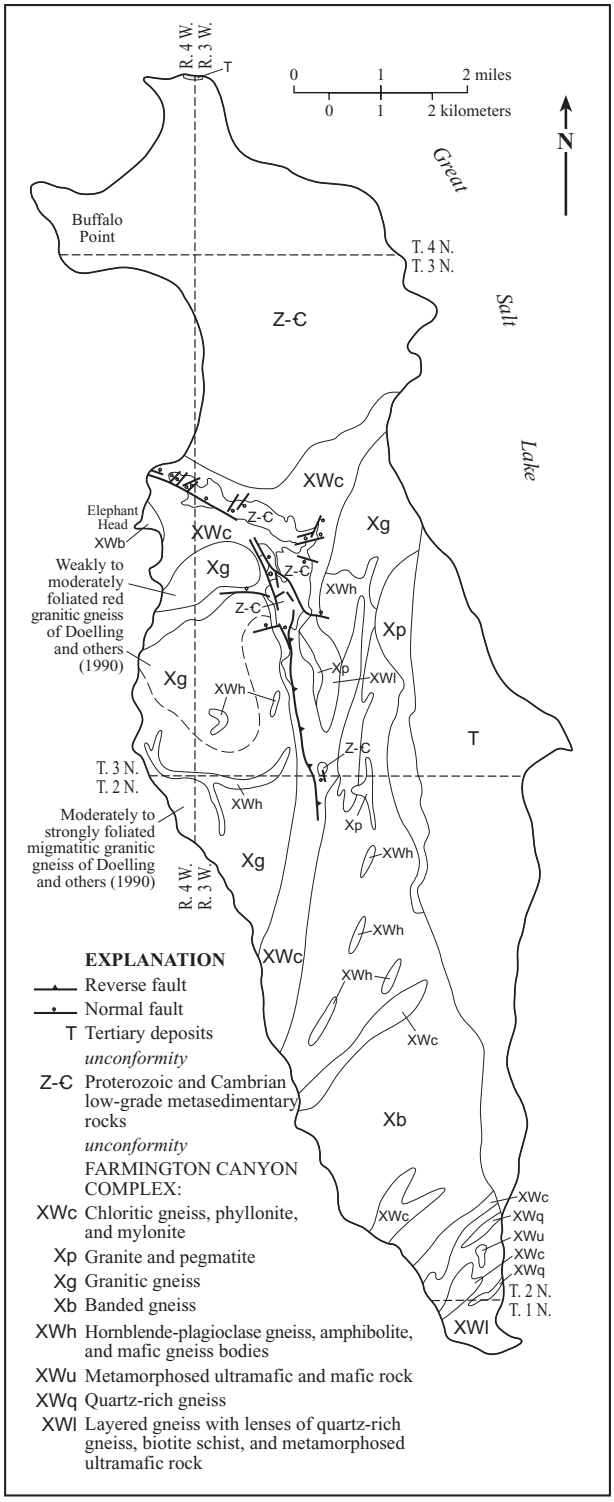

Figure 3a. *Generalized geologic map of Antelope Island, illustrating subcrop distributions of different rock types discussed in text. Modified from Doelling and others (1990).*

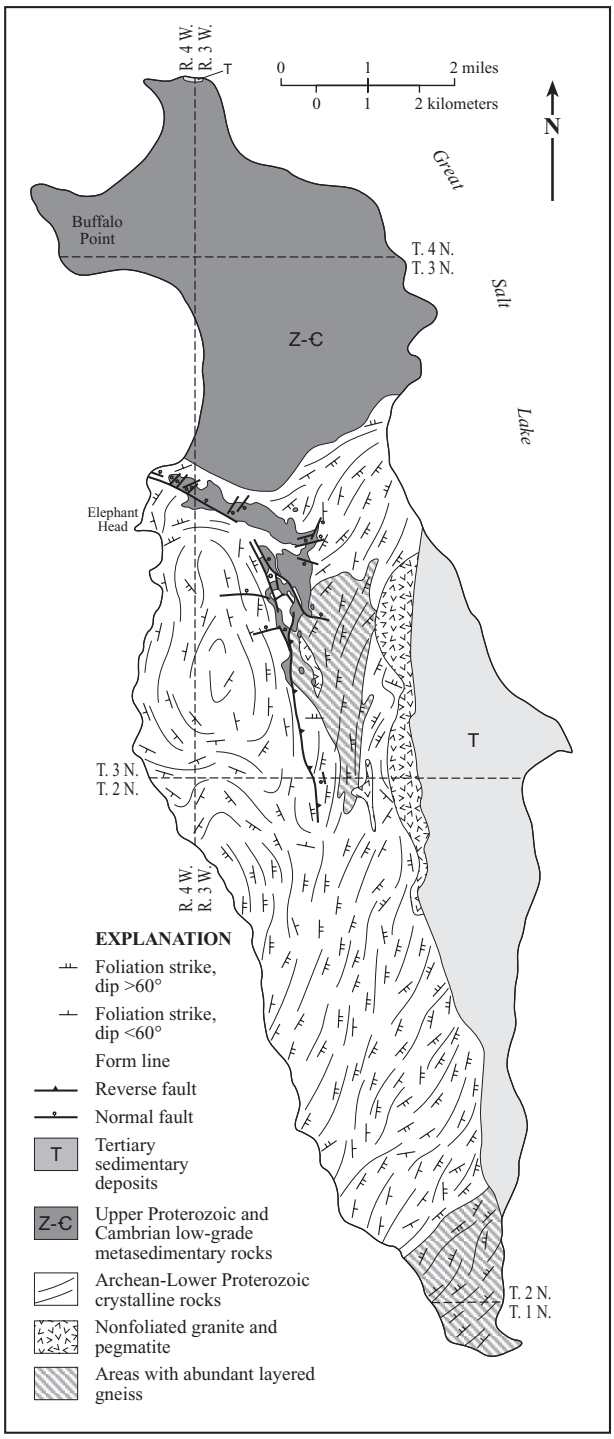

Figure 3b. *Strikes and dips of main-phase foliation and form lines parallel to general foliation strikes. Foliation is north- to northeast-striking except for elliptical pattern within granitic gneiss on the western part of the island. Areas of more complexly deformed layered gneiss with lenses of biotite schist and quartz-rich gneiss are indicated by fine dotted pattern and areas of non-foliated granite and pegmatite are indicated by coarse dotted pattern.*

contact with the overlying sedimentary cover.

Layered gneiss and lenses of biotite-schist and quartz-rich gneiss are isoclinally folded and have a dominant north- to northeast-striking foliation related to a main phase of deformation (figure 3b). This foliation is parallel to axial surfaces of most folds. However, these rocks locally display complex fold interference patterns and multiple foliations in some fold hinges, probably recording an earlier period of deformation. Banded gneiss displays a single strong north- to northeast-striking foliation related to main-phase deformation (figure 3b). Granitic gneiss displays a single weak to strong foliation that defines an elliptical pattern parallel to the contact with the banded gneiss (figure 3b). These relations are interpreted to record intrusion of a large pluton, now represented by banded and granitic gneiss, approximately synchronous with main-phase deformation. Larger granite and peg-

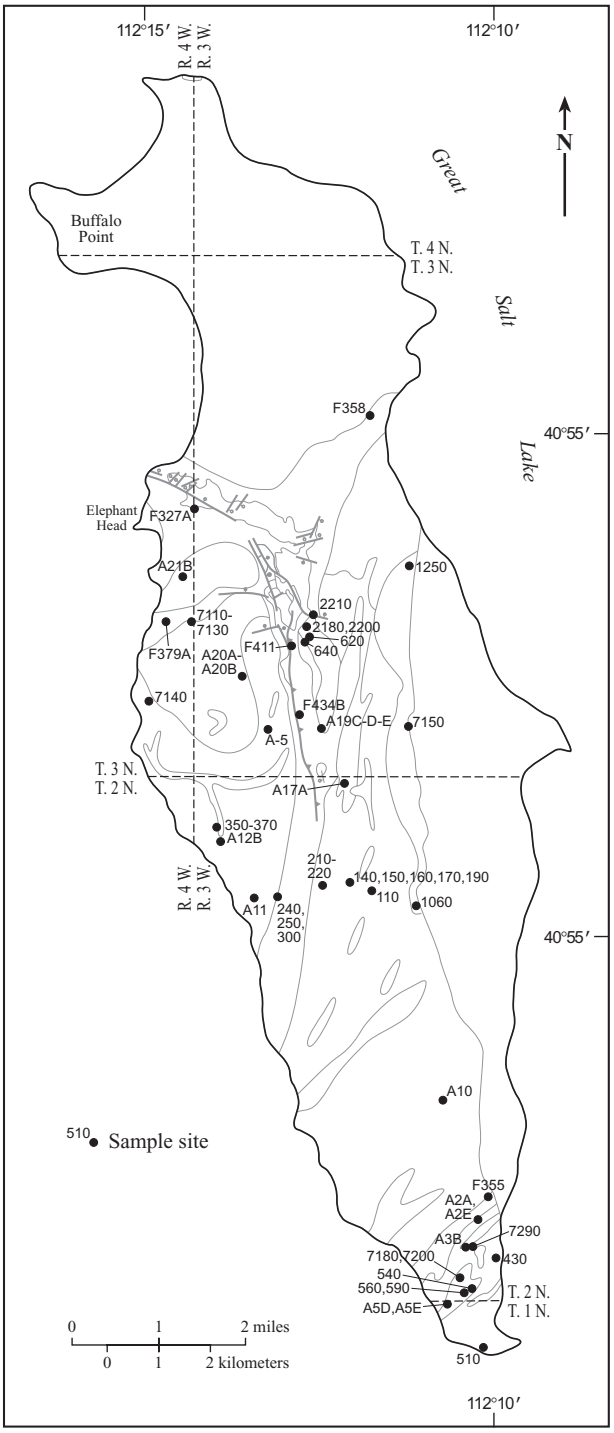

Figure 3c. *Locations of samples listed in tables; rock types are discussed in text. Table 4 gives sample locations.*

matitic intrusions are non-foliated, crosscut earlier structures, and were emplaced after main-phase deformation.

Basement rocks exposed to the east in the Wasatch Range are similar to rocks on Antelope Island and form a heterogeneous package that was intensely deformed and metamorphosed to upper amphibolite facies during a complicated Precambrian history (Hedge and others, 1983; Bryant, 1988b). Complexly deformed layered gneiss in the Wasatch Range also contains lenses of biotite schist and quartz-rich gneiss, and probably represents sedimentary rocks that underwent multiple periods of metamorphism and deformation. Large outcrops of granitic gneiss in the Wasatch Range display simple foliation patterns and probably represent granitic plutons that intruded layered gneiss, roughly synchronous with a main phase of deformation and regional metamorphism (Bryant, 1988a).

Retrograde greenschist-facies alteration and shear zones locally overprint high-grade features in basement rocks on Antelope Island and in the Wasatch Range (Yonkee, 1990). $^{40}Ar/^{39}Ar$ ages for syndeformational muscovite from phyllonite within these shear zones are mostly between 110 and 140 million years (Yonkee, 1990), recording localized deformation associated with thrusting during the Sevier orogeny.

OUTCROP AND PETROGRAPHIC CHARACTERISTICS OF BASEMENT ROCK TYPES

Photographs of outcrops and hand samples of different rock types are illustrated in figure 4, and microscopic textures for different rock types are illustrated in figure 5. Estimates of mineral abundances, based on 400 to 500 point counts per sample, are summarized in table 1. Most samples of basement rock have undergone minor retrograde alteration during Sevier deformation, and mineral abundances were slightly different prior to alteration. Table 1 lists both observed mineral abundances, and estimated abundances prior to alteration, for samples in which original mineralogy could be interpreted from preserved textures. Only observed mineral abundances are reported for samples of biotite schist, chloritic gneiss, phyllonite, and mylonite, because alteration has obliterated most evidence of original mineralogy.

Layered Gneiss

This rock type displays well-developed, continuous compositional layering, and consists of abundant, though variable, amounts of quartz, feldspar, and biotite (figures 4a, 4b). Some layers contain garnet, sillimanite, and rare cordierite. The gneiss weathers to form heterogenous gray to brown to pink outcrops of variable erosional resistance. Alternating quartzo-feldspathic, biotite-rich, quartz-rich, and amphibolite layers generally have thicknesses between 0.05 and 2 meters (0.2-6 ft), and are continuous over lengths of 10 to 100 meters (30-300 ft). Strongly developed foliation, defined by preferred orientation of mica and quartz aggregates, parallels compositional layering in most outcrops. In many areas, the gneiss is migmatitic, with development of alternating stringers of biotite-rich and leucocratic material probably recording local partial melting. Tight minor folds with wavelengths of 0.1 to 10 meters (0.3-30 ft) are widely developed, and mineral lineations generally parallel fold hinges. Preservation of two foliations in some fold hinges, and complex fold interference patterns record protracted or multiple deformation.

Layered gneiss locally grades into biotite schist and quartz-rich gneiss, consistent with a sedimentary protolith. Some outcrops, however, contain layers of more massive granitic gneiss that may have an igneous protolith. Gneissic layering probably developed by a combination of metamorphic differentiation, injection of dikes, and transposition of primary layering.

Mineral abundances of layered gneiss are variable; sam-

Figure 4. *Outcrop and sample photographs of different rock types.*

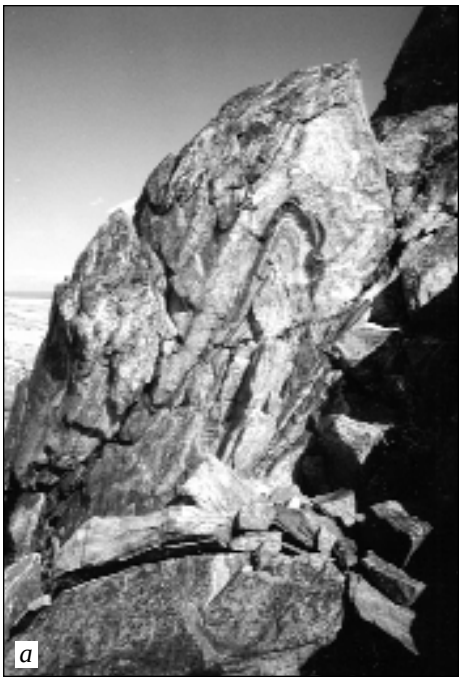

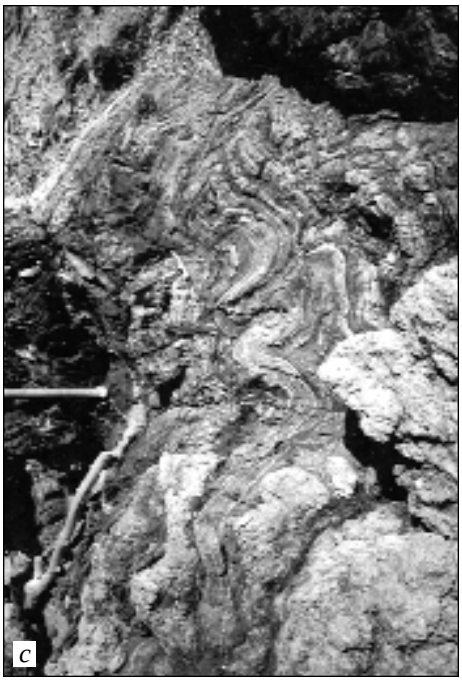

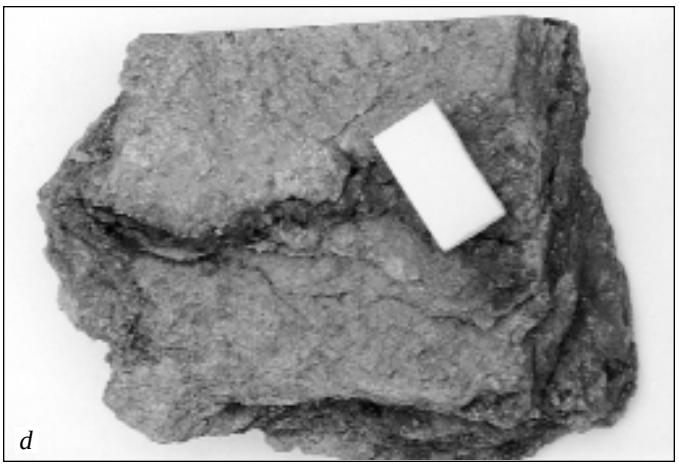

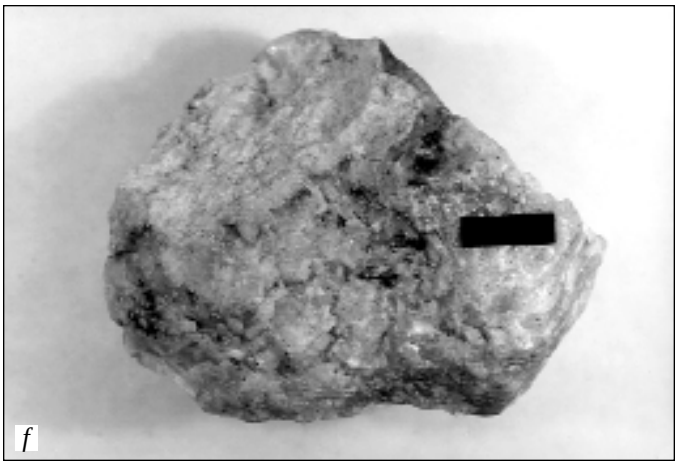

a. *Outcrop of layered gneiss on southern part of the island consists of alternating gray quartzo-feldspathic, white quartz-rich, and dark biotite-rich layers. Hammer located near core of tight fold in center of photograph is 30 centimeters (12 in) long.*

b. *Alternating lighter quartz-rich and darker biotite-rich layers are locally isoclinally folded on the southern part of the island. Hammer is 30 centimeters (12 in) long.*

c. *Outcrop of finely layered and folded biotite schist. Light-colored concordant pegmatitic layers in schist may represent partial melts. Coarse-grained, less deformed pegmatite body crosscuts layering. Hammer in central part of photograph is 30 centimeters (12 in) long.*

d. *Sample of dark biotite schist with micaceous foliation. Small garnet grains appear darker gray. Scale bar is 2.5 centimeters (1 in) long.*

e. *Quartz-rich gneiss has milky white appearance and forms resistant, blocky outcrops. Pen in central part of photograph is 15 centimeters (6 in) long.*

f. *Sample of vitreous quartz-rich gneiss contains minor amounts of dark oxides and creamy white plagioclase. Scale bar is 2.5 centimeters (1 in) long.*

g. *Outcrop of black hornblende-plagioclase gneiss. Light-colored pegmatite veinlets cut the gneiss and are overall concordant with foliation. Hammer in left part of photograph is 30 centimeters (12 in) long.*

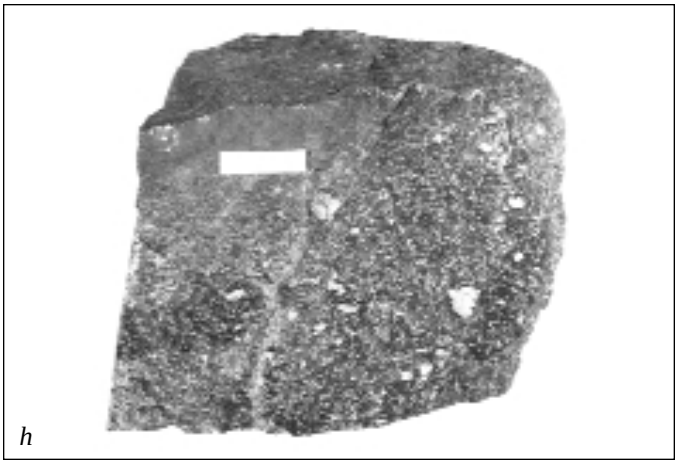

h. *Sample of hornblende-plagioclase gneiss from center of a dike. Sample has weak foliation and locally ophitic texture with interlocking light plagioclase and dark hornblende grains. Scale bar is 2.5 centimeters (1 in) long.*

i. *Outcrop of banded gneiss displays well-developed foliation and alternating thin layers of gray granodioritic gneiss and white leucocratic material. Later, undeformed pegmatite dikes crosscut layering. Stereoscope for scale is 12.5 centimeters (5 in) long.*

j. *Sample of medium-grained banded gneiss displays foliation defined by preferred orientations of dark hornblende and biotite grains. Stringers of white leucocratic material are approximately parallel foliation. Scale bar is 2.5 centimeters (1 in) long.*

k. *Alternating dark mafic layers and light leucocratic pods define migmatitic texture in complexly folded banded gneiss. Pencil in right part of photograph is about 15 centimeters (6 in) long.*

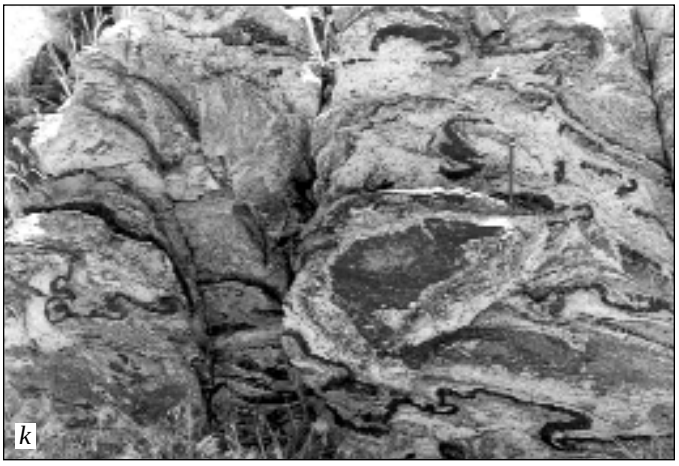

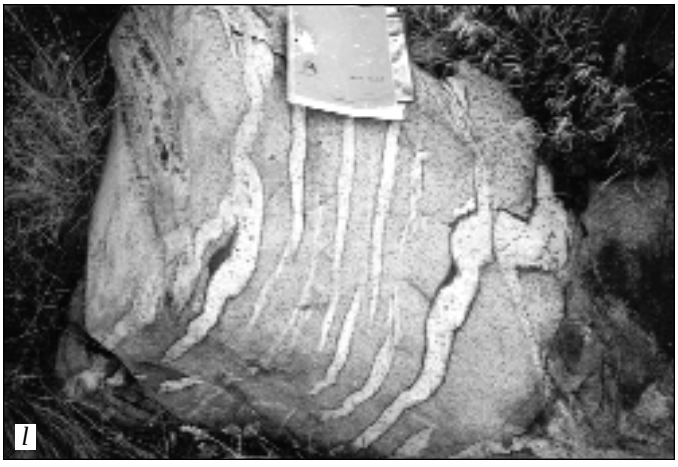

l. *A set of subparallel leucocratic pods and stringers cut weakly foliated block of granitic gneiss. Dark mafic minerals are locally concentrated along pod margins. Notebook is 22 centimeters (8.5 in) wide.*

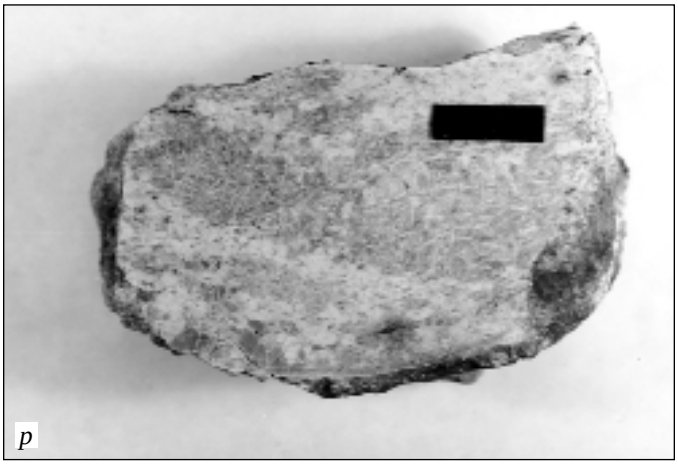

m. *Granitic gneiss forms light-colored, variably foliated, blocky outcrops on west side of island. Widely spaced, white pegmatitic veinlets define crude banding.*

n. *Sample of medium- to coarse-grained granitic gneiss contains abundant light-colored quartz and feldspar, and minor dark hornblende. Sample displays weak foliation and is cut by diffuse regions of leucocratic material. Scale bar is 2.5 centimeters (1 in) long.*

o. *Nonfoliated, light-colored pegmatite surrounds angular blocks of hornblende-plagioclase gneiss. Pegmatite forms resistant, knobby outcrops. Pack at bottom of photograph is about 0.5 meter (1.5 ft) tall.*

p. *Sample of red granite is composed dominantly of coarse-grained, fractured K-feldspar (gray), plagioclase (light gray), and quartz (white). Mafic minerals are rare and foliation is absent. Scale bar is 2.5 centimeters (1 in) long.*

q. *A set of thin, diffuse pegmatitic veinlets is concordant to foliation in an outcrop of banded gneiss. The early veinlets are cut by an early set of thicker, locally folded and foliated, pegmatite dikes. Later pegmatite dikes are planar, very coarse-grained, and crosscut foliation.*

r. *Some pegmatite dikes cut and offset dark hornblende-plagioclase dike, but dark dike offsets other deformed pegmatite dikes, recording multiple periods of pegmatite and mafic intrusion within outcrop of banded gneiss. Brunton compass for scale in center of photograph.*

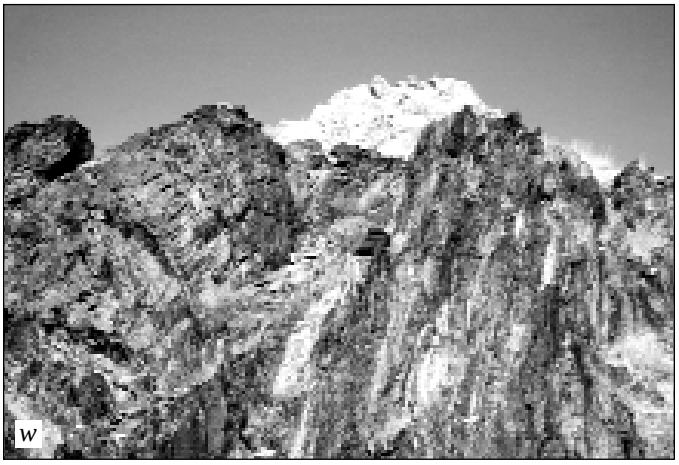

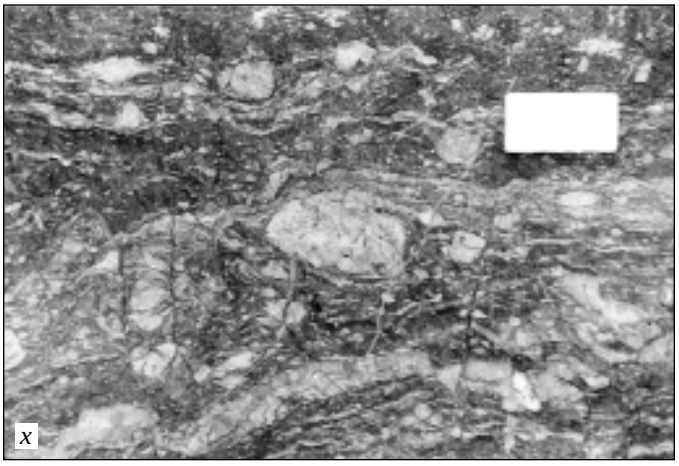

s. *Outcrop of darker chloritic gneiss is cut by en echelon arrays of white, quartz-filled veins. Locally developed cleavage dips to the left (west) parallel to parting. Outcrop is about 1.5 meters (5 ft) high.*

t. *Sample of chloritic gneiss is cut by anastomosing sets of dark fractures along which chlorite-epidote-sericite alteration is concentrated. A darker chloritic shear zone cuts the base of the sample. Scale bar is 2.5 centimeters (1 in) long.*

u. *Quartz veins cut and surround fragments of fractured chloritic gneiss. Veins vary from undeformed and crosscutting, to being recrystallized and sheared. Pencil for scale.*

v. *Steeply dipping phyllonitic cleavage crenulates gently dipping Precambrian foliation and compositional layering in outcrop of chloritic gneiss. Abundant chlorite and minor hematite produced during retrograde alteration give the outcrop a dark appearance. Brunton compass for scale.*

w. *Steeply dipping zone of phyllonite with pervasive alteration and well-developed cleavage in right half of photograph crosscuts basement foliation and layering. Cleavage and alteration continue across contact with overlying Late Proterozoic Mineral Fork diamictite near top of dark exposures. Light outcrops at top of photograph are dolomite of the Late Proterozoic Kelley Canyon Formation. Pack in center part of photograph is about 0.5 meter (1.5 ft) high.*

x. *Mylonite sample displays cleavage defined by stretched pods of light-gray quartz and preferred orientation of darker chlorite and sericite. More equant gray feldspar augen are fractured and have recrystallized tails. Shear fractures locally offset cleavage. Scale bar is 2.5 cm (1 in) long.*

Figure 5. *Photomicrographs of different rock types. (Bars indicate scale.) Symbols are: Q- quartz, K- K-feldspar, P- plagioclase, B-biotite, H-hornblende, G-garnet, S-sillimanite, C-chlorite, M-fine-grained muscovite (sericite), Cp-clinopyroxene, Cd-cordierite.*

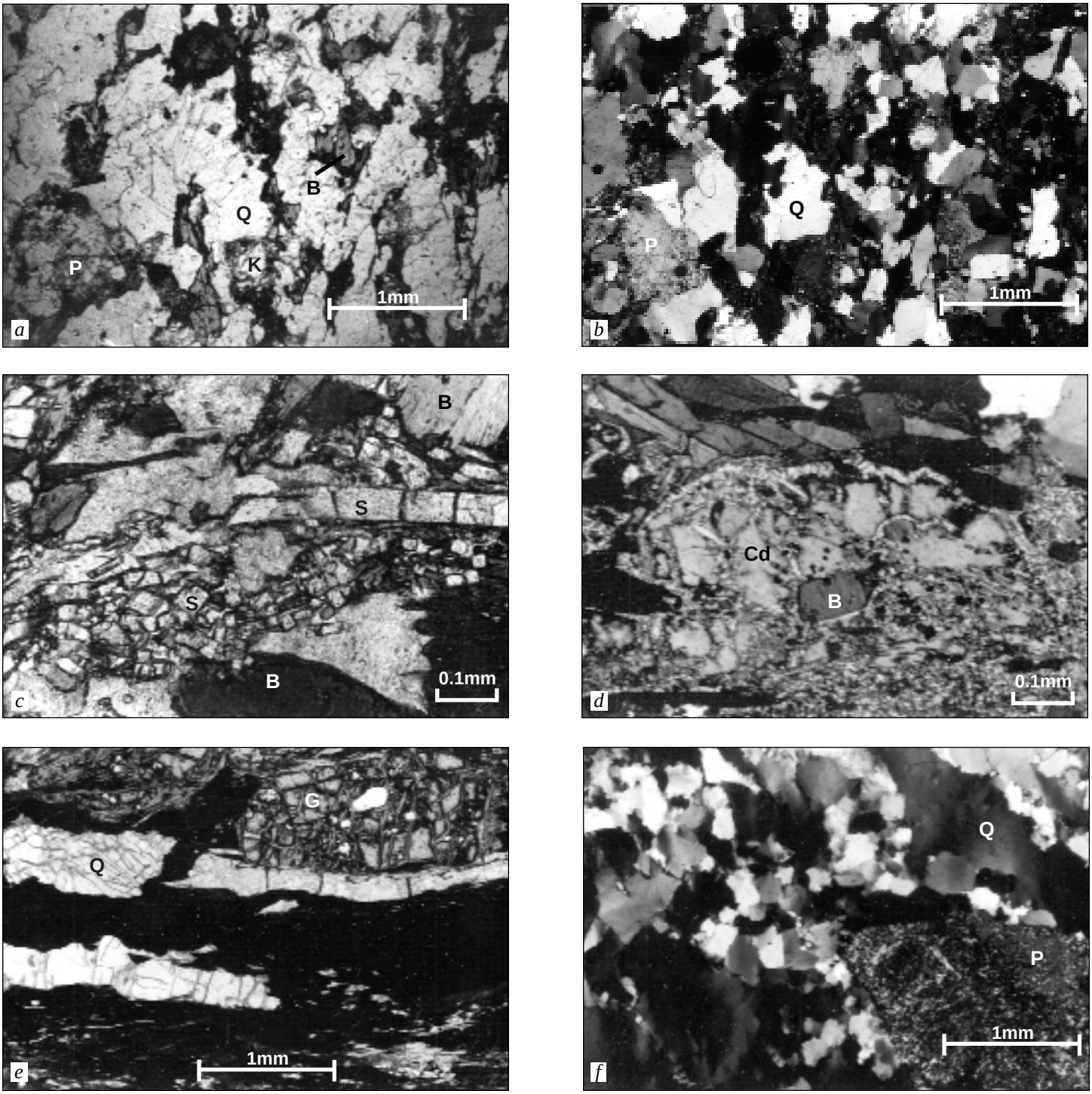

a. *Layered gneiss, viewed with uncrossed Nicols (non-polarized light), consists of medium-grained plagioclase, quartz, K-feldspar, biotite, and minor garnet. Subvertical preferred orientation of biotite is subparallel to macroscopic foliation.*

b. *Same view as (a) with crossed Nicols (polarized light). Plagioclase is partly altered to sericite.*

c. *Sillimanite forms prismatic cross sections in biotite-rich layer in layered gneiss.*

d. *Cordierite grain in layered gneiss is largely altered to pinite and contains biotite inclusions.*

e. *Biotite schist, viewed with uncrossed Nicols, contains abundant, dark biotite aligned parallel to foliation, poikiloblastic garnet, and polycrystalline ribbons of quartz. Some biotite grains contain small sericite pseudomorphs after sillimanite.*

f. *Quartz-rich gneiss, viewed with crossed Nicols, displays polygonal aggregate of recrystallized quartz grains. Large grain of plagioclase is partly altered to sericite.*

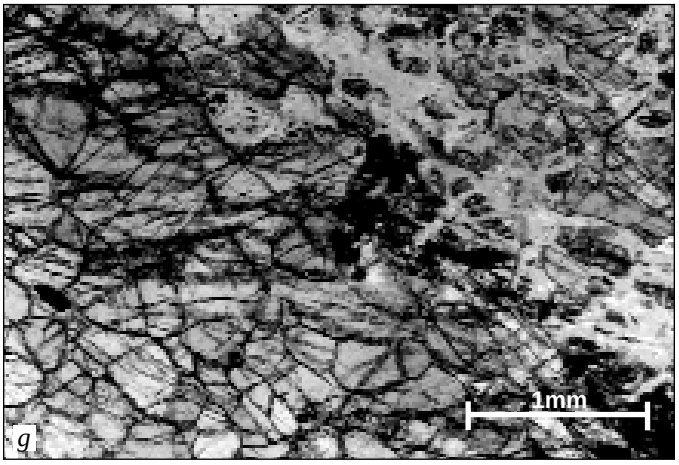

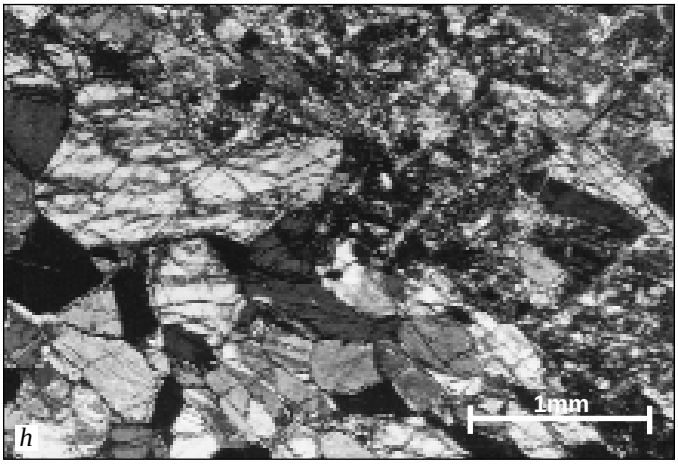

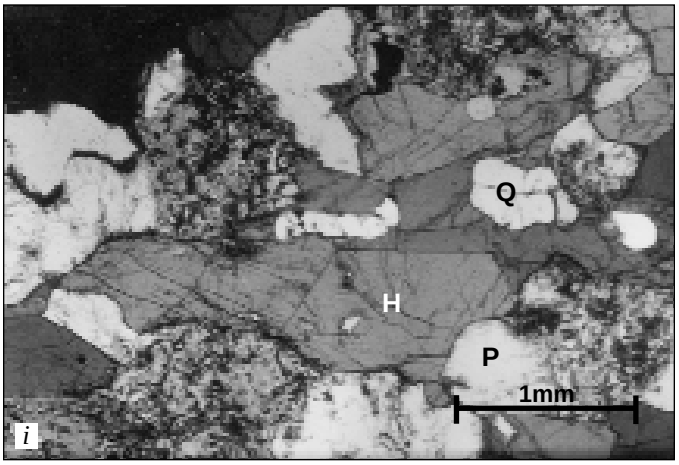

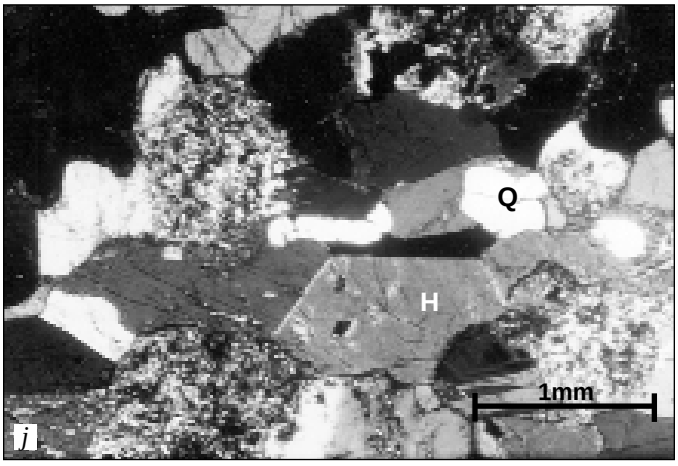

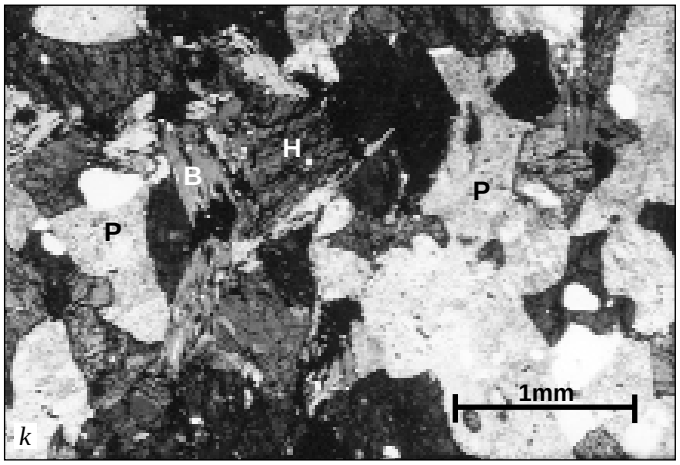

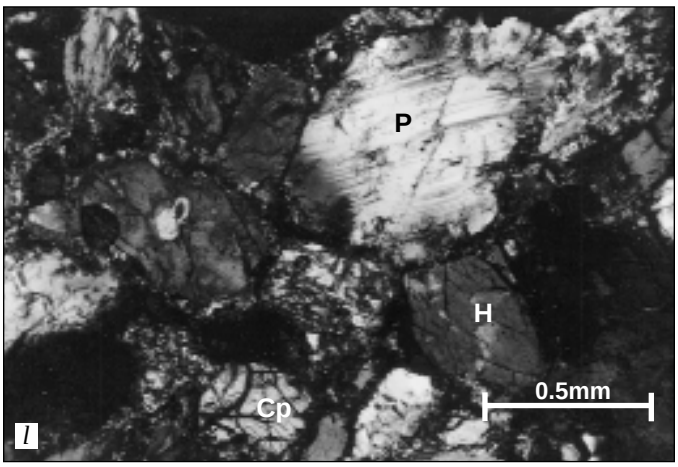

g. *Metamorphosed ultramafic rock, viewed with uncrossed Nicols, displays abundant anthophyllite and clinopyroxene. Secondary chlorite and serpentine replace orthopyroxene and olivine in upper right part of photograph.*

h. *Same view as (g) with crossed Nicols.*

i. *Hornblende-plagioclase gneiss, viewed with uncrossed Nicols, consists of partly altered plagioclase grains, hornblende with amphibole cleavage, and minor amounts of anhedral quartz.*

j. *Same view as (i) with crossed Nicols.*

k. *Biotite locally replaces hornblende in sample of hornblende-plagioclase gneiss.*

l. *Clinopyroxene grains in weakly foliated sample of hornblende-plagioclase gneiss is partly replaced by hornblende.*

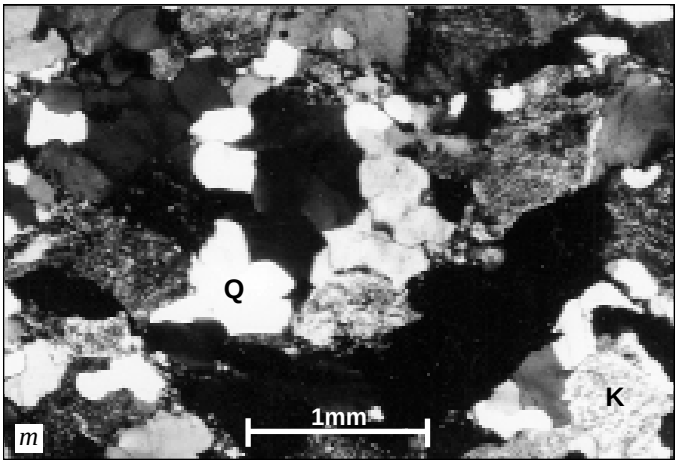

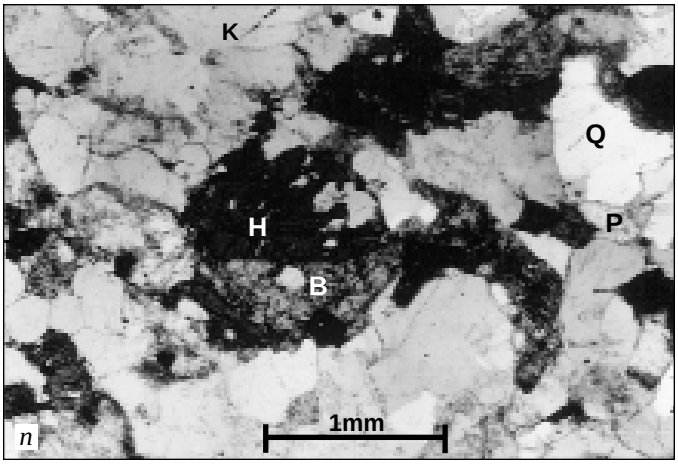

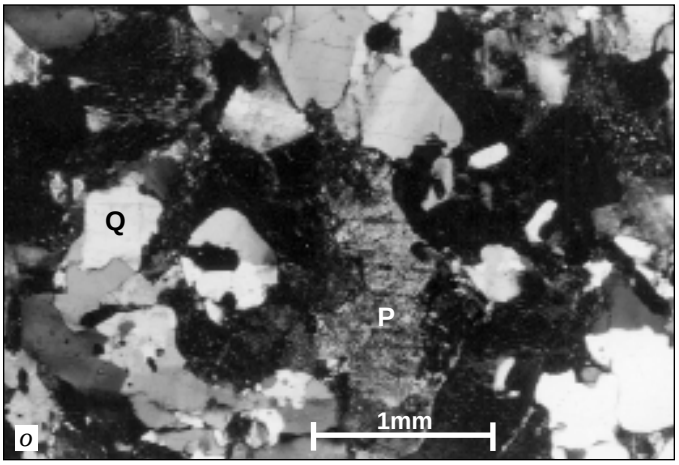

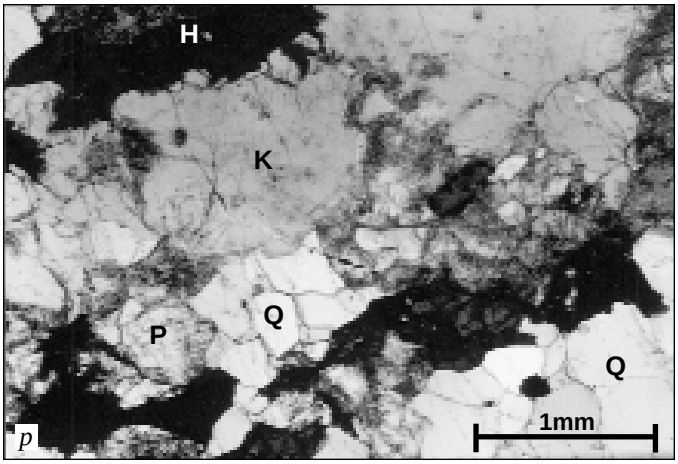

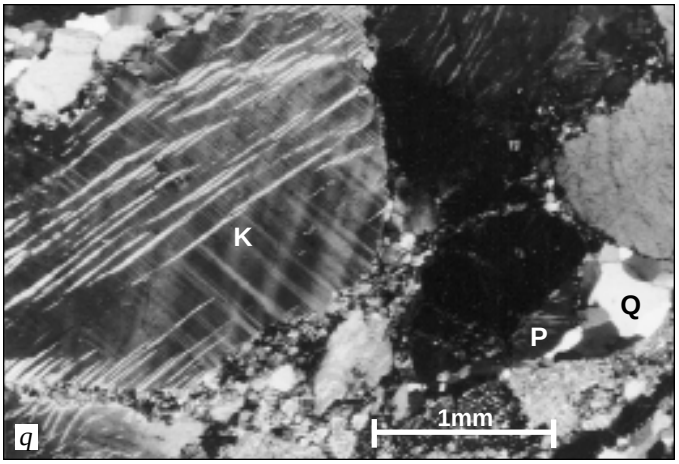

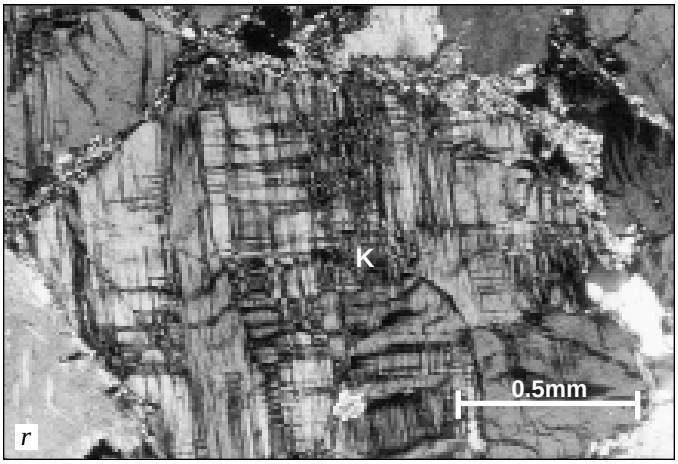

m. *Banded gneiss, viewed with crossed Nicols, displays abundant quartz, partly sericitized plagioclase, and K-feldspar with granoblastic textures.*

n. *Banded gneiss, viewed with uncrossed Nicols, displays hornblende and fine-grained biotite, stilpnomelane, and chlorite that may be replacing hornblende or pyroxene.*

o. *Granitic gneiss, viewed with crossed Nicols, displays granoblastic texture and contains abundant quartz, perthitic K-feldspar, and partly sericitized plagioclase.*

p. *Granitic gneiss, viewed with uncrossed Nicols, displays larger aggregates of polygonal quartz grains, K-feldspar, and partly altered plagioclase.*

q. *Coarse-grained, red granite consists of quartz, perthitic K-feldspar, and plagioclase. Some larger feldspar grains are recrystallized along their boundaries.*

r. *Large grain of K-feldspar in pegmatite displays well-developed tartan twinning.*

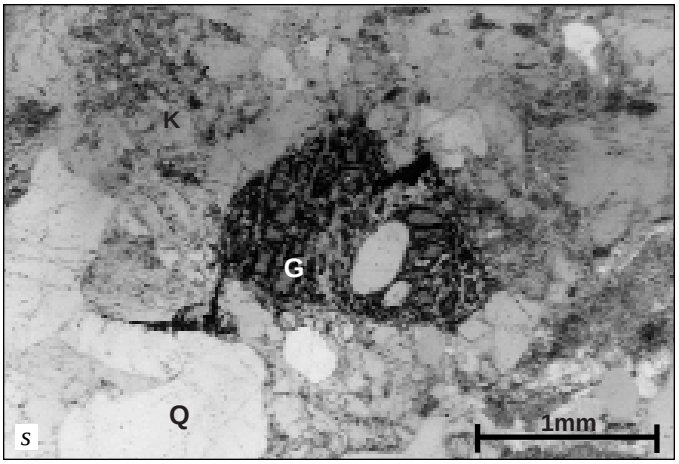

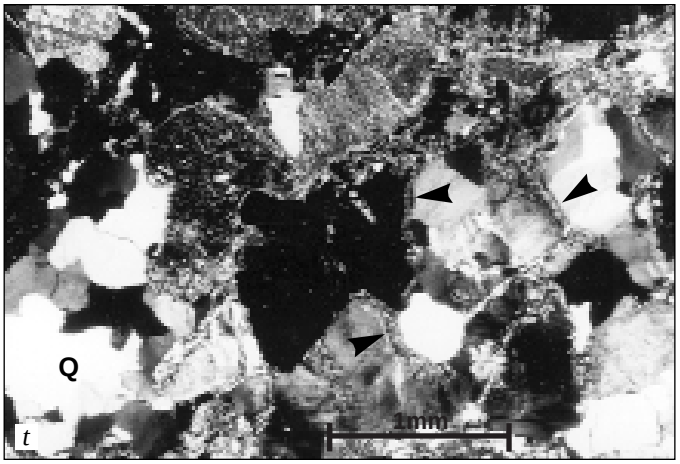

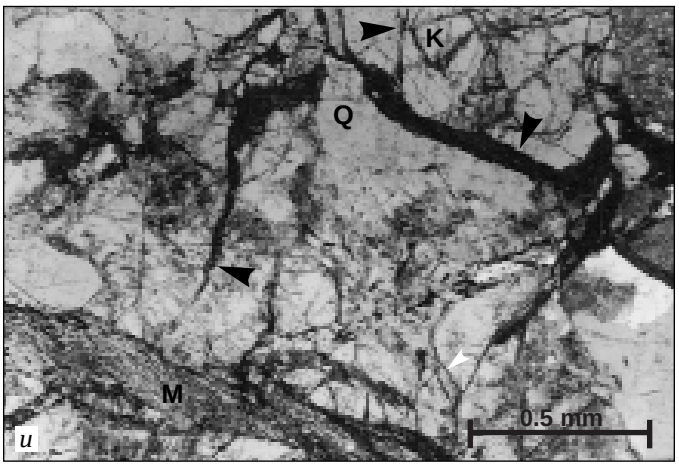

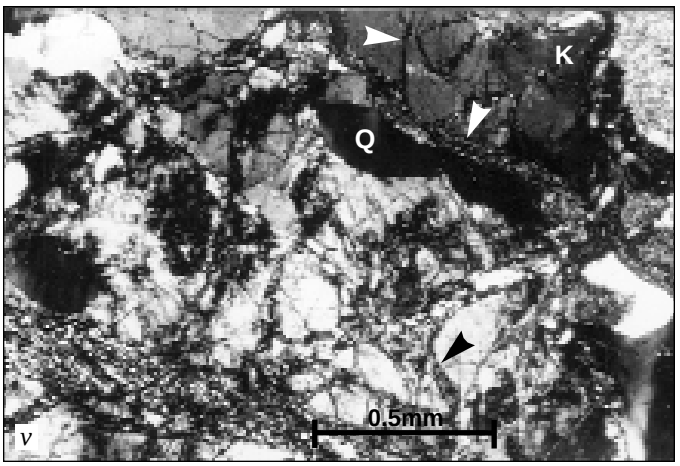

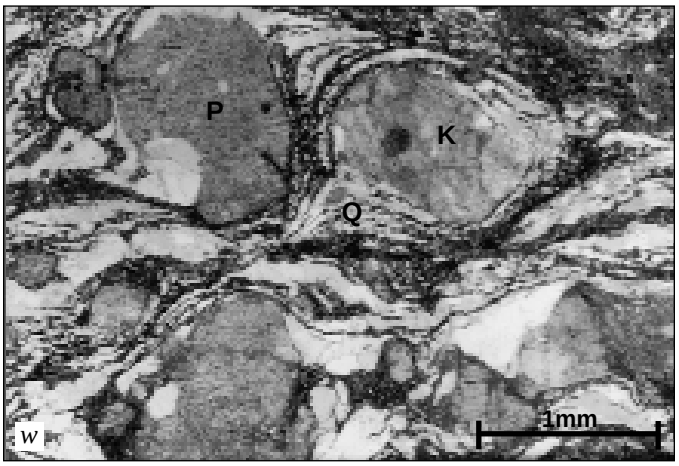

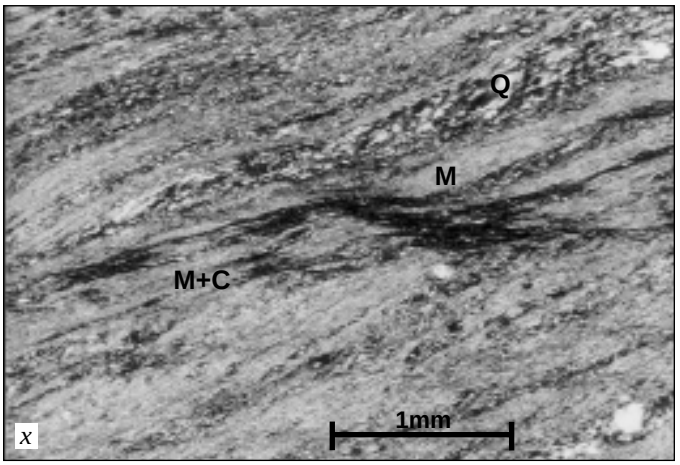

s. *Poikiloblastic grain of garnet with quartz inclusion, from sample of garnet-muscovite-bearing granite.*

t. *Fine-grained, recrystallized feldspar and mica are concentrated along grain boundaries (arrows) in chloritic gneiss, recording initial influx of fluids. Plagioclase grains display widespread alteration to sericite.*

u. *Chloritic gneiss, viewed with uncrossed Nicols, displays numerous intragranular and intergranular fractures (arrows). Microscopic shear zone contains abundant sericite at base of photograph. Fractures filled with chlorite have dark appearance.*

v. *Same view as (u) with crossed Nicols. Note recrystallization and alteration concentrated along crack network.*

w. *Mylonite, viewed with uncrossed Nicols, displays plastically deformed quartz ribbons that wrap around more equant feldspar augen. Asymmetric tails and pressure shadows around augen indicate top-to-the-right simple shear.*

x. *Phyllonite, viewed with crossed Nicols, consists of very fine-grained recrystallized quartz and foliated aggregates of muscovite and chlorite. Cleavage rakes to left and rotates toward a shear band in center part of photograph.*

Table 1. *Mineral abundances in selected samples from Antelope Island (see figure 3c for sample localities.)*

A. Layered Gneiss

Sample	540	590	620	2200	A4D	A5D	A5E	A19E	mean±s.d[1]
				Observed Abundances					
Quartz	25.4	36.2	41.3	37.9	38.3	37.3	17.7	46.0	35.0±9.1
Plagioclase	41.4	23.7	35.5	28.4	24.8	26.0	27.3	28.1	29.4±6.0
K-feldspar	3.5	14.7	12.5	11.0	13.5	7.6	6.5	2.9	9.0±4.6
Biotite	13.5	1.4	0.8	4.7	12.0	15.9	28.1	6.3	10.3±9.1
Garnet	0.5	--	--	--	1.2	3.5	8.5	6.5	2.5±3.3
Cordierite	P	--	--	--	--	0.8	P	--	P
Sillimanite	--	--	--	--	--	1.4	5.4	--	P
Opaque minerals	1.0	3.8	3.8	2.7	2.1	0.4	0.8	P	1.8±1.5
Sericite	8.2[3]	8.8	2.5	10.0	3.7	5.6[3]	5.2[3]	8.1	6.5±2.7
Chlorite	5.7	3.7	2.9	4.0	0.6	1.2	P	0.7	2.4±2.0
Epidote	0.6	6.3	0.5	0.4	3.2	--	--	1.3	1.5±2.2
				Pre-Alteration Abundances[4]					
Quartz	25.4	37.1	41.3	37.9	38.3	37.3	17.7	46.0	35.1±9.1
Plagioclase	42.5	34.8	38.0	37.9	31.2	26.8	27.9	35.1	34.3±5.4
K-feldspar	3.5	15.6	12.5	11.5	13.5	7.6	6.5	2.9	9.2±4.8
Fe-Mg silicate[5]	27.4	7.7	4.2	9.2	13.9	25.8	41.4	15.9	18.2±12.5
Al silicate[6]	--	--	--	--	--	1.8	5.4	--	P
Oxides	1.0	4.2	3.8	2.7	2.1	0.4	0.8	P	1.8±1.5

B. Other Gneiss and Schist Types

	Biotite Schist			Quartz-Rich gneiss		
Sample	560	A19C	A19D	430	A2A	A2E
			Observed Abundances			
Quartz	15.7	15.5	1.0	93.0	94.0	79.1
Plagioclase	1.0	1.9	--	5.2	4.3	4.3
K-feldspar	--	--	--	--	--	P
Biotite	54.5	38.4	49.4	P	0.4	P
Garnet	4.2	0.5	1.4	--	--	--
Muscovite[7]	4.7	6.6	3.8	1.2	0.8	3.4
Sillimanite	P	1.4	3.8	--	--	--
Opaque minerals	1.2	P	0.4	P	0.2	0.9
Carbonate	--	--	--	--	P	--
Sericite	16.7	22.8	32.0	P	0.6	8.8
Chlorite	2.1	12.9	8.5	0.6	P	3.6
Epidote	--	--	--	--	--	--

C. Ultramafic and Hornblende-Plagioclase Gneiss

	Ultramafic		Hornblende-Plagioclase Gneiss						
Sample	7290	A3B	170	190	420	510	7140	A17A	mean±s.d[1]
				Observed Abundances					
Quartz	--	--	3.6	3.1	17.2	13.6	--	7.6	7.5±6.7
Plagioclase	--	–	35.2	22.8	38.0	19.3	30.8	37.6	30.6±7.9
K-feldspar	--	–	0.8	--	1.0	--	--	0.2	0.4±0.5
Amphibole	33.3	31.0	42.5	57.2	15.5	31.7	55.2	32.3	39.1±15.8
Biotite	--	–	0.3	--	2.0	16.1	--	P	
Orthopyroxene	6.5	3.3	--	--	--	--	0.5	--	
Clinopyroxene	7.7	8.8	P	--	--	--	5.7	--	
Opaque minerals	5.4	5.0	4.7	5.9	1.8	2.5	1.0	1.5	2.9±2.0
Sericite	--	--	3.9	4.7	11.0	1.0	1.7	17.9	6.7±6.5
Chlorite	41.7[8]	47.5[8]	7.0	4.7	3.3	1.7	P	1.3	3.0±2.6
Epidote	--	--	1.3	P	10.0	12.8	5.0	1.8	5.1±5.2
Talc	5.4	4.5	--	--	--	--	--		
				Pre-Alteration Abundances[4]					
Quartz	--	--	3.6	3.1	17.2	13.6	--	7.6	7.5±6.7
Plagioclase	--	--	40.4	27.5	57.0	27.3	37.0	57.3	41.1±13.5
K-feldspar	--	--	0.8	--	1.0	--	--	0.2	0.4±0.5
Fe-Mg silicate[5]	94.6	95.0	50.3	62.7	22.8	55.3	61.9	33.6	47.8±16.2
Oxides	5.4	5.0	4.2	5.1	1.8	2.5	1.0	1.5	2.7±1.6

D. Banded Gneiss

Sample	110	140	150	160	210	220	300	A10	means±s.d[1]
					Observed Abundances				
Quartz	34.2	34.3	32.8	33.8	34.0	31.8	32.6	32.2	33.2±1.0
Plagioclase	27.1	24.2	27.8	37.2	25.0	33.5	22.9	30.6	28.5±4.9
K-feldspar	20.0	23.2	22.2	15.6	26.7	19.3	24.2	23.5	21.8±3.4
Amphibole	6.7	P	--	--	6.0	9.5	--	2.0	3.0±3.8
Biotite[2]	2.0	0.8	0.4	--	2.9	1.5	6.8	2.1	2.1±2.1
Opaque minerals	3.8	3.0	1.8	3.5	1.3	2.3	1.1	2.3	2.4±1.0
Sericite	4.1	9.2	9.0	0.5	3.5	1.5	4.3	4.3	4.6±3.1
Chlorite	0.4	3.3	1.8	4.4	P	--	7.7	1.1	2.3±2.7
Epidote	1.7	1.7	3.6	4.0	0.6	--	0.4	1.4	1.7±1.5
					Pre-Alteration Abundances[4]				
Quartz	34.2	34.3	32.8	33.8	34.0	31.8	32.6	32.2	33.2±1.0
Plagioclase	32.6	32.4	36.6	37.7	29.1	35.0	27.8	35.7	33.7±3.1
K-feldspar	20.2	23.6	22.6	16.2	26.7	19.3	24.2	23.5	22.0±3.0
Fe-Mg silicate[5]	9.1	6.4	6.0	8.0	8.9	11.0	14.0	5.8	8.6±1.9
Oxides	3.8	3.0	2.0	3.5	1.3	2.3	1.6	2.3	2.5±0.9

E. Granitic Gneiss

Sample	7110	7130	A20A	A20B	A21B	350	370	A12B	A-11[9]	A-5[9]	mean±s.d[1]
					Observed Abundances						
Quartz	33.0	30.6	31.9	33.1	32.4	33.0	32.6	34.2	36.4	32.2	32.9±1.5
Plagioclase	19.6	28.4	30.6	28.8	28.5	28.6	22.3	27.3	15.1	29.9	25.9±5.1
K-feldspar	30.0	31.7	26.7	32.4	29.0	26.5	29.9	29.3	39.3	29.6	30.3±3.8
Amphibole	1.0	1.7	1.9	2.8	0.7	3.5	2.0	2.4	--	1.4	1.7±1.0
Biotite[2]	2.9	3.8	2.6	0.6	4.2	1.8	4.6	2.1	--	0.8	2.3±1.6
Opaque minerals	2.9	1.6	3.3	1.6	2.0	2.1	2.6	2.4	2.6	3.5	2.5±0.7
Sericite	8.9	0.8	0.4	0.2	0.7	1.2	2.8	0.5	--	--	1.6±2.7
Chlorite	0.8	--	--	--	0.5	--	0.2	1.4	0.6	--	0.4±0.5
Epidote	1.0	1.4	2.3	0.4	2.1	1.9	2.8	0.2	5.8	0.1	1.8±1.7
					Pre-Alteration Abundances[4]						
Quartz	33.0	30.6	31.9	33.1	32.4	33.0	32.6	34.2	36.4	32.2	32.9±1.5
Plagioclase	28.5	29.9	32.2	29.2	29.7	30.9	27.1	28.0	18.0	29.9	28.3±3.9
K-feldspar	30.5	31.7	26.7	32.4	29.0	26.9	29.9	29.3	39.3	29.6	30.5±3.6
Fe-Mg silicate[5]	5.2	6.2	5.6	3.7	7.0	7.1	7.6	6.1	3.5	4.8	5.7±1.4
Oxides	2.9	1.6	3.3	1.6	2.0	2.1	2.6	2.4	2.6	3.5	2.5±0.7

F. Granite and Pegmatite

	Pegmatitic Granite			Garnet-Muscovite-Bearing Granite		Red Granite		Mean±s.d.[1]
Sample	1060	2180	7150	640	1250	7180	7200	for all granites
				Observed Abundances				
Quartz	32.0	38.8	33.6	32.2	31.8	26.8	30.5	32.3±3.9
Plagioclase	35.6	18.8	29.7	24.8	24.5	19.3	23.1	25.2±6.5
K-feldspar	30.0	30.0	33.6	37.0	38.5	52.7	34.2	36.5±8.5
Muscovite	0.4	--	0.5	0.8	0.7	--	0.8	0.6±0.3
Garnet	0.2	--	--	P	2.0	--	--	
Biotite	--	P	--	0.4	0.7	--	1.2	--
Opaque minerals	--	--	--	--	--	--	P	--
Sericite	1.2	11.5	2.2	2.0	1.0	0.8	5.7	3.5±4.2
Chlorite	--	--	--	2.8[10]	--	P	0.5	
Epidote	0.4	0.3	0.5	P	0.7	0.5	4.0	1.0±1.4
				Pre-Alteration Abundances[4]				
Quartz	32.0	38.8	33.6	32.2	31.8	26.8	30.5	32.3±3.9
Plagioclase	36.8	30.6	31.9	26.8	26.2	20.6	32.4	29.7±5.6
K-feldspar	30.0	30.0	33.6	37.0	38.5	52.7	34.2	36.5±8.5
Fe-Mg silicate[5]	0.2	P	--	3.2	2.7	P	2.1	0.8±1.2
Al silicate[6]	0.4	0.3	0.5	--	0.7	--	0.8	0.5±0.3
Oxides	--	--	--	--	--	--	P	--

G. Chloritic Gneiss, Phyllonite, and Mylonite

	Chloritic Gneiss			Phyllonite			Mylonite	
	F327A	F358	F379A	F355	F411	F434B	240	250
	Observed Abundances							
Quartz	35.9	39.0	38.7	40.4	51.0	42.3	28.8	39.7
Plagioclase	19.7	6.7	15.0	--	1.2	--	14.1	11.0
K-feldspar	16.1	12.9	15.0	--	--	1.3	16.8	6.3
Biotite[2]	11.6	--	3.3	--	--	2.0	--	--
Opaque minerals[11]	1.8	2.4	1.7	1.8	1.6	2.3	2.0	3.5
Sericite	6.7	26.6	17.3	35.3	24.7	30.5	6.1	15.7
Chlorite	8.1	12.4	5.0	22.5	21.4	20.2	30.5	21.7
Epidote	P	1.4	0.7	--	--	--	1.6	2.0

[1] mean±one standard deviation
[2] includes fine-grained biotite, stilpnomelane, and oxidized chlorite that may have formed from alteration of hornblende and pyroxene
[3] includes penite alteration of cordierite
[4] see text for method of calculating pre-alteration mineral abundances
[5] includes biotite, hornblende, garnet, and pyroxene
[6] includes primary sillimanite and muscovite
[7] includes muscovite grains larger than 0.1 mm (.004 in) in long dimension
[8] includes serpentine
[9] data from Bryant (1988b)
[10] produced by alteration of garnet
[11] includes sphene

P present

ples contain 18 to 46 percent quartz, 27 to 43 percent plagioclase, 3 to 16 percent K-feldspar, and 4 to 32 percent biotite, after effects of minor alteration are removed (table 1A, figure 6a). Some samples also contain garnet, sillimanite, and cordierite. Accessory minerals include zircon, allanite, and apatite. Layered gneiss has a lower average content of K-feldspar, and higher and more variable contents of plagioclase and biotite than banded and granitic gneiss. Mineral abundances for layered gneiss on Antelope Island are similar to abundances reported by Bryant (1988b) for his gneiss and schist rock unit in the Wasatch Range.

Microscopically, layered gneiss displays granoblastic textures with polygonal aggregates of quartz and feldspar (figures 5a, 5b). Anhedral quartz grains have sizes mostly between 0.1 and 2 millimeters (0.004-0.08 in), and form polycrystalline aggregates with long dimensions up to 5 millimeters (0.2 in) that enclose feldspar and biotite grains. Anhedral to subhedral plagioclase grains, with sizes generally between 0.1 and 5 millimeters (0.004-0.2 in), have compositions of An15 to An40. Many grains show patchy alteration to sericite (fine-grained muscovite), epidote, and albite. Anhedral K-feldspar grains, with sizes ranging from 0.1 to 4 millimeters (0.004-0.16 in), vary from well-developed string perthite to non-perthitic. Subhedral biotite grains, with long dimensions of 0.2 to 2 millimeters (0.008-0.08 in), are generally subparallel to macroscopic foliation. Garnet forms subhedral, locally poikiloblastic grains up to 3 millimeters (0.12 in) in diameter. Some biotite-rich layers contain elongate prisms of sillimanite (figure 5c), and cordierite that is mostly altered to pinite (figure 5d).

Biotite Schist

Biotite schist, a distinctive rock type that forms lenses up to 2 meters (6 ft) wide within the layered gneiss unit, consists of abundant biotite, variable amounts of quartz and muscovite, and minor amounts of garnet and sillimanite (figures 4c, 4d). The unit is relatively non-resistant, and weathers to form brown slopes and subdued ledges. Complex minor folds and strong foliation, defined by preferred orientation of mica, are widely developed. Intercalated thin layers and pods of granitic material may record partial melting of the schist. The schist probably represents metamorphosed pelitic material and grades into layered gneiss.

Samples contain 38 to 55 percent biotite, 1 to 16 percent quartz, and 4 to 7 percent coarser-grained muscovite, 1 to 4 percent garnet, and lesser amounts of sillimanite and highly altered cordierite(?) (table 1B). Samples also contain 17 to 33 percent sericite produced by widespread alteration.

Microscopically, samples display schistose textures defined by preferred orientation of biotite (figure 5e). Subhedral grains of biotite, with long dimensions of 0.2 to 2 mil-

limeters (0.008-0.08 in), are mostly parallel to foliation. However, some grains randomly cut foliation and may be post-kinematic, and some are kinked and rotated into minor folds. Many biotite grains are partly altered to sericite and chlorite. Anhedral quartz grains form elongate aggregates that are up to 5 millimeters (0.2 in) in long dimension. Subhedral garnet grains, up to 5 millimeters (0.2 in) in diameter, are largely altered to chlorite. Coarser-grained muscovite, with sizes of 0.1 to 0.5 millimeters (0.004-0.2 in), and minor amounts of sillimanite are intergrown with biotite in most samples. These larger muscovite grains may have formed by synmetamorphic crystallization or by retrograde mimetic growth. Small remnants of plagioclase are surrounded by sericite. Rare cordierite(?) is almost completely altered to pinite.

Quartz-Rich Gneiss

Quartz-rich gneiss, another distinctive rock type that forms concordant lenses ranging from 1 to 30 meters (3 to 100 ft) wide within the layered gneiss, consists dominantly of quartz, with lesser amounts of plagioclase, biotite, and oxides (figures 4e, 4f). The gneiss weathers to form vitreous, milky to greenish-gray, fractured and resistant outcrops. Foliation, defined by preferred orientation of minor oxides and mica, is parallel to layering in adjacent gneiss, but is difficult to discern in some outcrops. This rock type is interpreted to have formed by metamorphism of quartz-rich sedimentary rocks.

Samples consist of 79 to 94 percent quartz, 5 to 12 percent plagioclase and its alteration products (sericite), and lesser amounts of biotite and coarser-grained muscovite (table 1B, figure 6a). Accessory minerals include zircon and magnetite.

Microscopically, the gneiss consists of complex polygonal aggregates of quartz grains with dispersed grains of plagioclase, muscovite, biotite, and oxides (figure 5f). Anhedral quartz grains, with sizes mostly between 0.2 and 5 millimeters (0.008-0.2 in), have planar to curved boundaries, probably reflecting recovery after high-temperature deformation. Some grains display undulatory extinction, subgrains, and sutured boundaries, possibly reflecting younger plastic deformation. Many grains have abundant inclusions of very fine-grained oxides that produce a "dusty" appearance. Subhedral grains of plagioclase, biotite, and coarser-grained muscovite are weakly aligned parallel to macroscopic foliation.

Metamorphosed Ultramafic Rock

Metamorphosed ultramafic rock and surrounding hornblende-rich gneiss form small isolated pods within layered gneiss at the southern end of the island. Meta-ultramafic rock consists of amphibole, pyroxene, and rare olivine that are variably altered to chlorite, serpentine, and talc. This rock type has a dark green to black color and weathers to form rusty brown surfaces. Foliation varies from weak in pod cores to strong near pod margins that are bounded by hornblendite and hornblende-plagioclase gneiss. Pods of ultramafic and mafic rock may represent highly deformed and dismembered oceanic crust, komatiitic flows, or part of a deformed layered-mafic complex.

Metamorphosed ultramafic rock consists of about 30 percent anthophyllite and tremolite, 15 percent orthopyroxene and clinopyroxene, minor olivine, and alteration minerals including abundant chlorite, serpentine, and talc (table 1C). Accessory minerals include ilmenite, magnetite, and sphene. Original mineral abundances and textures are difficult to determine due to alteration.

Ultramafic rock displays complex textures that are partly related to retrograde alteration (figure 5g, 5h). Anthophyllite and tremolite grains are weakly aligned parallel to foliation. Orthopyroxene and light-green clinopyroxene grains are up to 3 millimeters (0.12 in) in size. Anhedral olivine grains are cut by irregular fractures and are largely altered to serpentine.

Hornblende-Plagioclase Gneiss

This rock type consists of varying proportions of hornblende and plagioclase, with lesser amounts of quartz, biotite, and rare pyroxene. Rock that is relatively rich in plagioclase forms gray outcrops, whereas rock that is richer in hornblende forms dark green to black, generally less resistant outcrops (figures 4g, 4h). Hornblende-plagioclase gneiss occurs in two settings, as elongate pods in other units, and within a large mafic gneiss body.

Pods of hornblende-plagioclase gneiss that cut other rock units are generally 0.1 to 3 meters (0.3 to 10 ft) thick, but a few larger pods reach 30 meters (100 ft) in width. Many pods have sharp planar boundaries that locally crosscut compositional layering in surrounding gneiss, and are interpreted to be metamorphosed mafic dikes. Foliation varies from well-developed to weak in different pods, probably recording emplacement of dikes over a protracted history. Highly deformed pods in layered gneiss are relatively old, and less deformed pods in banded and granitic gneiss are relatively young.

Hornblende-plagioclase gneiss is also abundant within a large mafic gneiss body in the central part of the island (figure 3a). The mafic body consists of strongly foliated hornblende- to plagioclase-rich gneiss interlayered with, and cut by, pods of granitic and pegmatitic gneiss. This body may represent part of a mafic pluton that was later intruded by granitic material or it may represent a metamorphosed volcanic sequence.

Samples of gneiss consist of about 20 to 60 percent hornblende, 30 to 60 percent plagioclase and its alteration products, 0 to 15 percent quartz, and minor pyroxene (table 1C). Samples vary compositionally from gabbro to diorite to tonalite (figure 6b). Accessory minerals include ilmenite, magnetite, and allanite.

Microscopically, the gneiss displays granoblastic to decussate textures with interlocking hornblende and plagioclase grains (figures 5i, 5j). Elongate, subhedral grains of hornblende, with long dimensions of about 0.5 to 4 millimeters (0.02-0.16 in), are crudely aligned parallel to foliation. Hornblende is partly altered to chlorite and partly replaced by biotite in some samples (figure 5k). Subhedral grains of plagioclase, with dimensions of about 0.3 to 2 millimeters (0.012-0.08 in), have compositions between An25 and An50. Plagioclase is variably altered to sericite and epidote. A few samples contain clinopyroxene and rare orthopyroxene (figure 5l). Most pyroxene grains appear to be in disequilibrium, being partly replaced by hornblende. Anhedral quartz grains

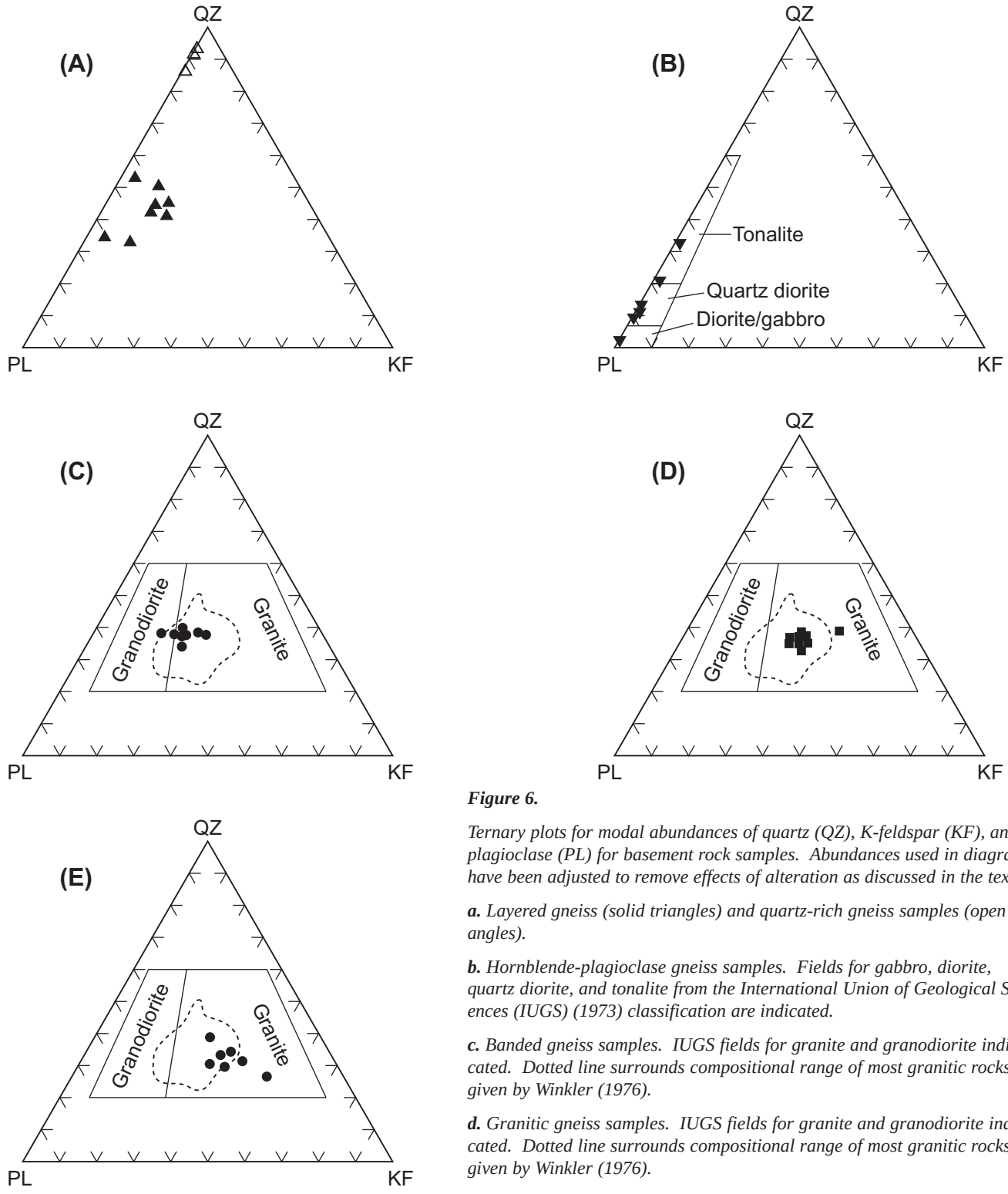

Figure 6.

Ternary plots for modal abundances of quartz (QZ), K-feldspar (KF), and plagioclase (PL) for basement rock samples. Abundances used in diagrams have been adjusted to remove effects of alteration as discussed in the text.

a. *Layered gneiss (solid triangles) and quartz-rich gneiss samples (open triangles).*

b. *Hornblende-plagioclase gneiss samples. Fields for gabbro, diorite, quartz diorite, and tonalite from the International Union of Geological Sciences (IUGS) (1973) classification are indicated.*

c. *Banded gneiss samples. IUGS fields for granite and granodiorite indicated. Dotted line surrounds compositional range of most granitic rocks as given by Winkler (1976).*

d. *Granitic gneiss samples. IUGS fields for granite and granodiorite indicated. Dotted line surrounds compositional range of most granitic rocks as given by Winkler (1976).*

e. *Granite and pegmatite samples. Dotted line surrounds compositional range of most granitic rocks as given by Winkler (1976).*

have sizes between 0.1 and 1 millimeters (0.004-0.04 in) and rarely form aggregates.

Banded Gneiss

This rock type displays well-developed compositional layering and foliation that produce a banded appearance in outcrop (figure 4i, 4j). Banded gneiss consists mostly of fine- to medium-grained quartz and feldspar, with lesser amounts of hornblende. The gneiss weathers to form overall gray to pink outcrops of varying resistance that are cut by irregular fractures. Planar to lenticular stringers of leucocratic material with widths mostly between 0.01 to 0.1 meters (0.4 in to 4 in) and variations in abundances of mafic minerals define layering. Preferred orientation of hornblende and quartz aggre-

gates define foliation that is rotated into ptygmatic folds in some outcrops. Banded gneiss is locally migmatitic, with alternating discontinuous layers of leucocratic and mafic material (figure 4k). The gneiss probably represents part of a deformed and metamorphosed granitic pluton with possible enclaves of older gneiss.

Banded gneiss samples consist of 31 to 34 percent quartz, 28 to 38 percent plagioclase, 16 to 27 percent K-feldspar, and 6 to 12 percent hornblende, possible pyroxene, and biotite, after effects of minor alteration are removed (table 1D). Accessory minerals include zircon, allanite, and apatite. The samples are granitic to granodioritic in composition (figure 6c).

In thin section, banded gneiss displays granoblastic textures with polygonal aggregates of quartz and feldspar and dispersed mafic grains (figures 5m, 5n). Veinlets of leucocratic material define layering in some samples. Anhedral quartz grains, with sizes mostly between 0.1 and 1 millimeters (0.004-0.04 in), are locally grouped into polygonal aggregates up to 3 millimeters (0.12 in) in length. Most grains have uniform extinction and smooth to curviplanar boundaries. Anhedral to subhedral plagioclase grains generally have sizes from 0.1 to 2.0 millimeters (0.004-0.08 in) and compositions of An20 to An30. Many plagioclase grains are partly altered to sericite, epidote, and albite, especially along grain margins. Anhedral K-feldspar grains, with sizes from 0.2 to 3 millimeters (0.008-0.12 in), have complex perthitic intergrowths and local "tartan" twinning. Subhedral grains of hornblende, with long dimensions up to 2 millimeters (0.08 in), are preferentially aligned parallel to foliation. Biotite, chlorite, and stilpnomelane appear to have formed by alteration of horneblende and possible pyroxene.

Granitic Gneiss

Granitic gneiss consists mostly of medium-grained quartz and feldspar, with lesser amounts of hornblende and rare pyroxene. Granitic gneiss forms homogeneous, light-gray to light-red outcrops (figures 4l, 4m, 4n), which appear to grade into outcrops of banded gneiss. Weakly to strongly developed foliation is defined by preferred orientation of quartz aggregates and mafic minerals. Discontinuous pods and stringers of leucocratic material with widths generally between 0.025 and 0.15 meters (1 and 6 in) define compositional layering in some outcrops. Leucocratic pods and stringers consist dominantly of coarse-grained feldspar and quartz with minor amounts of hornblende and biotite concentrated along their margins (figure 4l). Most pods and stringers are concordant with foliation and have gradational boundaries, but later, less-deformed pegmatitic dikes crosscut foliation. Widely spaced, generally planar fractures cut the gneiss, producing a blocky appearance in most outcrops.

Granitic gneiss samples contain 31 to 36 percent quartz, 18 to 32 percent plagioclase, 27 to 39 percent K-feldspar, 4 to 8 percent hornblende and rare pyroxene, after effects of minor alteration are removed (table 1e). Accessory minerals include apatite, zircon, allanite, and sphene. Samples have granitic compositions (figure 6d). Mineral abundances for granitic and banded gneiss overlap, but granitic gneiss has lower average abundances of plagioclase and mafic minerals, and a greater average abundance of K-feldspar.

Doelling and others (1990) divided granitic gneiss into two gradational units: a central body of weakly to moderately foliated red granitic gneiss, and a surrounding body of moderately to strongly foliated migmatitic granitic gneiss (figure 3a). Mineralogically, these two map units are indistinguishable. Foliation traces define an elliptical pattern that is subparallel to contacts of the red granitic, migmatitic granitic, and banded gneiss map units (figure 3b) (Doelling and others, 1990). These three units are interpreted to represent part of a deformed granitic pluton that underwent local partial melting and injection of leucocratic dikes. The pluton may have been zoned with slightly more mafic material, now represented by the banded gneiss, along the margin.

Microscopically, granitic gneiss displays granoblastic textures, with medium- to locally coarse-grained aggregates of quartz, feldspar, and dispersed mafic grains (figures 5o, 5p). Anhedral quartz grains have sizes mostly between 0.1 and 2 millimeters (0.004-0.08 in), and tend to form polygonal aggregates up to 6 millimeters (0.23 in) in length. Most grains have uniform extinction and smooth to curviplanar boundaries. Anhedral plagioclase and K-feldspar grains generally have sizes between 0.3 and 3 millimeters (0.012-0.12 in), but some grains are up to 10 millimeters (0.4 in) long. Samples from the red granitic gneiss map unit tend to be slightly coarser grained compared to samples from the migmatitic granitic gneiss map unit. Plagioclase composition ranges from An15 to An25 for most grains, but almost pure albite occurs along some grain margins. Some plagioclase grains include smaller K-feldspar grains and myrmekitic intergrowths of quartz. Many K-feldspar grains display "tartan" twinning, most grains are perthitic, and some grains include smaller plagioclase and quartz grains. Subhedral to anhedral hornblende grains have long dimensions up to 3 millimeters (0.12 in) and are weakly aligned parallel to foliation. Many biotite grains are randomly oriented and appear to have formed by alteration of hornblende. Textural relations of rare clinopyroxene are difficult to discern due to extensive alteration to chlorite and fine-grained amphibole. The pyroxene may be either of igneous or metamorphic origin.

Granite and Pegmatite

Granite and pegmatite consist of varying proportions of coarse-grained quartz and feldspar, with limited amounts of mafic minerals and mica (figures 4o, 4p). This general rock type includes: (1) pegmatitic granite that forms large bodies on the eastern part of the island; (2) garnet-muscovite-bearing granite that forms small pods within and near layered gneiss; (3) red granite that forms small plutons on the southern end of the island; and (4) pegmatite that forms widespread dikes and pods (generally 0.01 to 1 meter [0.4 in to 3 ft] wide) within other units. Larger outcrops of granite and pegmatite are generally white to gray to pink, variably fractured, and have a knobby appearance. The red granite and some outcrops of pegmatitic granite display patchy red coloring caused by minor amounts of dispersed hematite. Pegmatitic granite is massive to weakly foliated and is roughly concordant to banded gneiss on a large scale. Pods of garnet-muscovite-bearing granite vary from approximately concordant and

weakly foliated to crosscutting and nonfoliated, consistent with derivation from local partial melting of nearby layered gneiss late in the deformation history. Plutons of red granite are discordant, nonfoliated, have sharp boundaries, and contain enclaves of surrounding wall rock, recording intrusion after main-phase deformation. Pegmatite dikes vary from foliated and concordant to undeformed and mutually crosscutting, recording a protracted history or multiple periods of intrusion and partial melting (figures 4q, 4r). Pegmatite dikes are generally leucocratic, with minor amounts of dark mafic minerals concentrated along dike margins.

Granite and pegmatite samples consist of about 25 to 40 percent quartz, 20 to 35 percent plagioclase, and 30 to 50 percent K-feldspar, and minor muscovite, garnet, and biotite (table 1f). All samples plot in the granite field (figure 6e). Accessory minerals include zircon, apatite, and tourmaline. Samples of pegmatite are too coarse-grained for point counts in thin section, but vary from quartz-, to plagioclase-, to K-feldspar-rich.

In thin section, most varieties of granite and pegmatite display randomly oriented, coarse grains of feldspar and quartz (figure 5q). Quartz forms anhedral, equant grains with smooth to curviplanar boundaries. Anhedral to subhedral plagioclase grains are albitic and display limited alteration to sericite. K-feldspar grains are anhedral and many grains are perthitic and display "tartan" twinning (figure 5r). Garnet, up to 3 millimeters (0.12 in) in size, forms subhedral grains in some samples (figure 5s). Grain sizes of quartz and feldspar vary considerably, ranging from less than 1 millimeter (0.04 in) for some pods of garnet-muscovite-bearing granite, to between 1 and 10 millimeters (0.04-0.4 in) for the red granite, to locally greater than 1 centimeter (0.4 in) for pegmatite.

Chloritic Gneiss

Chloritic gneiss displays widespread fractures, veins, and alteration that overprint earlier high-grade structures of the previously described rock types (figures 4s, 4t). Mineral abundances of chloritic gneiss vary greatly, reflecting different protoliths and variable alteration. Most outcrops are green to black in color with widespread alteration of original minerals to sericite, fine-grained chlorite, biotite, stilpnomelane, epidote, and albite. Outcrops that contain abundant quartz veins are relatively resistant, but other areas are non-resistant. Quartz veins and pods have widths from less than 1 centimeter (0.4 in) to greater than 3 meters (10 ft), and are associated with minor shear zones (figure 4s) and net vein systems that surround fragments of less-altered basement rock (figure 4u). Variably developed cleavage, defined by flattened aggregates of quartz and preferred orientation of mica, locally obliterates earlier fabrics, but most outcrops display patches where earlier high-grade structures are preserved (figure 4v). Chloritic gneiss grades into phyllonite and mylonite with increasing deformation intensity along the margins of shear zones and near the contact between the basement and the sedimentary cover.

Samples contain 7 to 27 percent sericite produced by alteration of feldspar, and 5 to 12 percent chlorite produced by alteration of mafic minerals (table 1G). Compared to protoliths, feldspar abundances are lower and mica abundances are greater.

Alteration in chloritic gneiss is concentrated along grain boundaries and crack networks (figure 5t). Microscopically, chloritic gneiss is cut by numerous fractures, quartz- and mica-filled veinlets, and minor shear zones (figures 5u, 5v). Many quartz grains display widespread undulatory extinction, subgrains, and limited recrystallization concentrated along grain margins, recording localized plastic deformation. Widespread planar fluid inclusion trains in quartz grains are interpreted to represent healed microcracks. Plagioclase grains are partly altered to sericite, epidote, and recrystallized albite. K-feldspar grains are cut by microcracks and locally altered to sericite. Mafic minerals are altered to chlorite and to finely recrystallized biotite and stilpnomelane. Alteration and recrystallization produced grains with sizes generally less than 0.05 millimeters (0.002 in), resulting in overall grain size reduction.

Phyllonite and Mylonite

This rock type displays pervasive alteration, well-developed cleavage, and local vein networks (figures 4w, 4x). Phyllonite consists mostly of very fine-grained mica and quartz, and mylonite consists of recrystallized quartz, feldspar, and mica. Most outcrops are green to black, with areas having abundant quartz veins being relatively resistant, and mica-rich areas being relatively non-resistant. Phyllonite and mylonite are found in shear zones and in a broad region near the basement-cover contact. Flattened and ribboned quartz pods and preferred orientation of mica define cleavage. Many shear zones also contain thin shear bands with very fine grain size and high strain. Offset of sheared dikes and well-developed cleavage record concentrated strain within shear zones. Fractures and breccia zones locally offset cleavage (figure 4x), but cleavage locally overprints fractured gneiss, recording temporally overlapping alteration, plastic deformation, and cataclasis.

Phyllonite and mylonite samples contain 6 to 35 percent sericite, 21 to 31 percent chlorite, 29 to 51 percent quartz, and 0 to 30 percent total feldspar. Overall, mica contents are greater and feldspar contents are lower than for chloritic gneiss and basement protoliths. Phyllonite samples have lower feldspar, slightly higher quartz, and higher sericite contents compared to mylonite samples.

Microscopically, mylonite consists of recrystallized quartz ribbons and variably altered, fractured, and recrystallized feldspar augen (figure 5w). Phyllonite displays fine-grained, foliated aggregates of sericite and chlorite and recrystallized quartz aggregates (figure 5x). Quartz occurs as elongate ribbons, subgrains, and recrystallized grains with sizes of about 5 to 50 microns (0.0002 to 0.002 in), recording widespread plastic deformation. Quartz augen, however, are locally preserved. Some feldspar grains are cracked along cleavage planes and grain edges, and some grains have pressure shadows and recrystallized tails of quartz, mica, and albite. Elongate grains of sericite and chlorite with long dimensions of 5 to 50 microns (0.0002 to 0.002 in) are generally parallel to cleavage. Variably deformed and recrystallized quartz veins record overlapping fracturing, fluid influx, quartz precipitation, and plastic deformation.

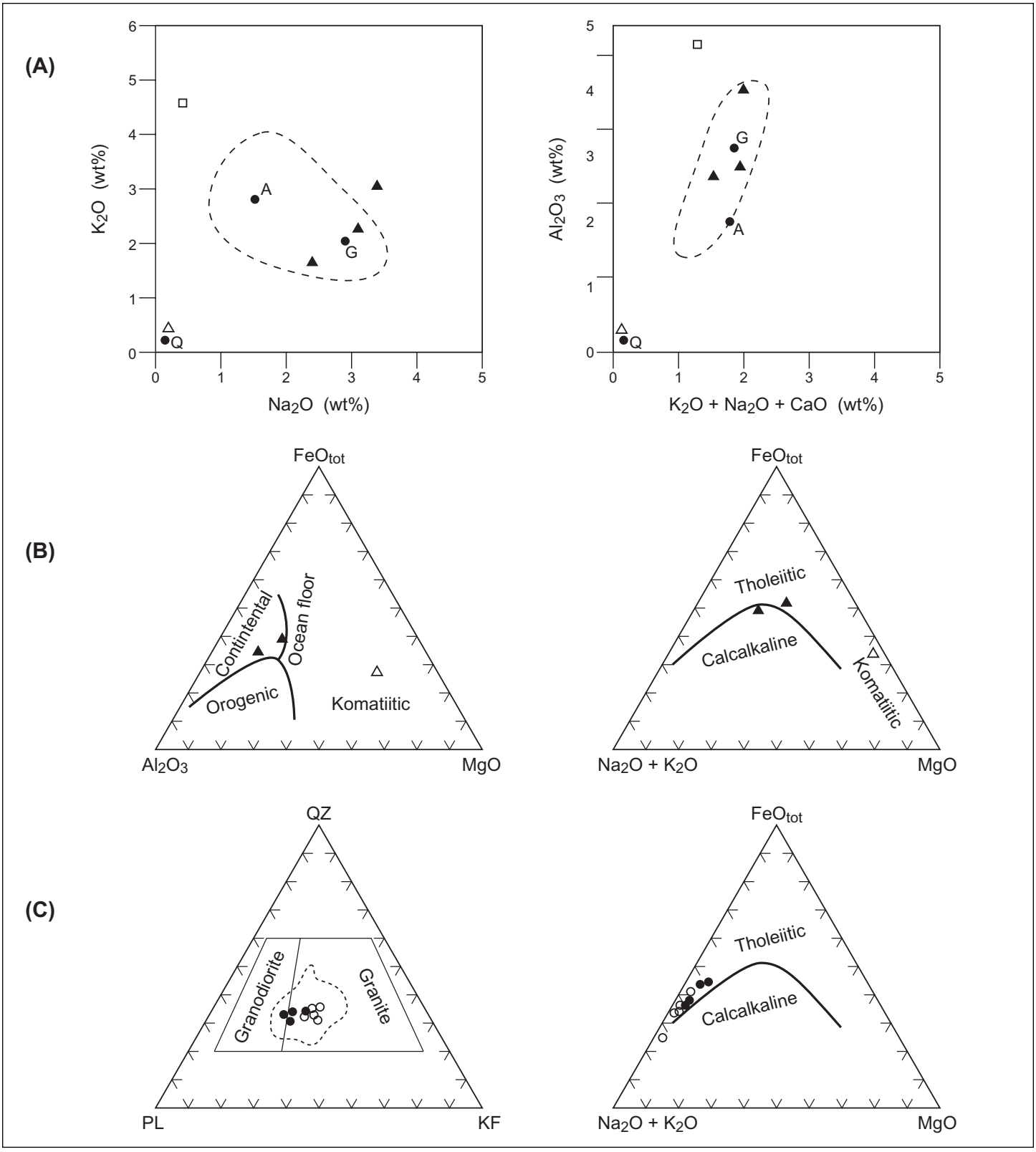

Figure 7. *Chemical characteristics of different rock types.*

a. *Chemical compositions for samples of layered gneiss (solid triangles), quartz-rich gneiss (open triangle), and biotite schist (open square). Solid circles are labeled for mean compositions of arkose (A), graywacke (G), and quartz arenite (Q), from Pettijohn and others (1973). Compositional range of paragneisses in Wasatch Range reported by Bryant (1988b) outlined by dashed line.*

b. *Chemical compositions for samples of hornblende-plagioclase gneiss (solid triangles) and ultramafic rock (open triangle). Fields for orogenic, continental, and ocean floor basalts from Pearce and others (1977). Fields for tholeiitic and calc-alkaline rocks from Irvine and Barager (1971). General compositions of peridotitic komatiites also indicated.*

c. *Normative abundances of quartz (QZ), K-feldspar (KF), and plagioclase (PL) for samples of banded gneiss (solid circles) and granitic gneiss (open circles). Abundances calculated using CIPW method (Cox and others, 1979). Corresponding chemical compositions of samples also shown. Fields for tholeiitic and calc-alkaline rocks from Irvine and Barager (1971).*

Table 2. *Whole-rock chemistry of selected samples from Antelope Island (see figure 3c for sample localities).*

	Layered Gneiss			Qtz-Rich Gneiss	Biotite Schist	Ultra-Mafic	Hornblende-Plagioclase Gneiss		Granite		Phyllonite
	590	A5D	A19E	A2A	560	A3B	7140	A17A	1250	7150	F355
SiO_2	69.1	61.3	75.1	96.4	55.7	37.7	48.7	54.4	72.9	72.1	74.4
Al_2O_3	12.3	18.1	11.9	1.3	20.7	10.4	14.5	17.3	13.8	14.9	9.4
K_2O	2.3	3.1	1.6	0.46	4.6	0.11	0.90	2.6	6.7	7.5	2.4
Na_2O	3.1	3.5	2.4	0.25	0.36	0.42	3.4	3.9	2.9	3.5	0.20
CaO	2.6	1.2	2.2	0.02	0.15	4.5	10.3	5.5	0.41	0.26	0.20
Fe_2O_3	7.8	7.8	4.4	0.37	10.0	14.0	11.8	10.1	1.8	0.43	5.0
MgO	1.0	2.8	0.62	0.07	3.0	23.1	6.6	3.1	0.18	0.15	4.0
MnO	0.09	0.10	0.16	0.01	0.07	0.14	0.20	0.13	0.22	0.01	0.04
TiO_2	0.75	0.77	0.34	0.06	1.1	0.62	1.1	1.2	0.07	0.04	0.39
P_2O_5	0.16	0.08	0.08	0.01	0.09	0.05	0.10	0.27	0.03	0.02	0.11
LOI	1.0	1.3	1.0	0.54	4.5	6.8	1.0	1.5	0.39	0.23	2.9
Total	100.4	100.2	100.2	99.5	100.3	98.2	98.6	100.1	99.5	99.3	99.1

	Banded Gneiss					Granitic Gneiss					
	110	150	220	A10	Mean	7130	350	A12B	A-11(1)	A-5(1)	Mean
SiO_2	69.6	71.4	69.0	71.7	70.4	72.2	71.3	72.5	72.3	69.2	71.5
Al_2O_3	12.2	12.8	12.3	12.2	12.4	12.6	12.0	11.4	12.1	12.1	12.1
K_2O	4.0	4.0	3.0	4.3	3.8	5.4	4.8	4.6	4.8	4.4	4.8
Na_2O	3.2	3.9	3.6	3.2	3.5	3.5	3.2	3.1	2.7	3.2	3.1
CaO	2.0	1.8	2.6	1.2	1.9	1.0	1.6	1.0	1.2	1.9	1.3
Fe_2O_3	6.8	5.1	6.8	5.4	6.0	3.4	5.3	5.0	5.0	5.6	4.9
MgO	0.47	0.36	0.70	0.42	0.49	0.14	0.41	0.41	0.21	0.42	0.32
MnO	0.14	0.07	0.12	0.11	0.11	0.08	0.14	0.12	0.09	0.15	0.11
TiO_2	0.54	0.41	0.59	0.39	0.48	0.22	0.38	0.33	0.33	0.44	0.34
P_2O_5	0.13	0.11	0.14	0.12	0.13	0.03	0.11	0.06	0.06	0.15	0.08
LOI	0.39	0.54	0.31	0.77	0.50	0.23	0.54	0.23	0.47	0.35	0.36
Ba	1700	1600	1200	1600		1900	1600	1700	ND	1498	
Nb	30	40	40	60		50	40	70	ND	30	
Rb	180	190	100	140		160	140	130	ND	140	
Sr	120	90	110	70		70	90	80	ND	80	
Zr	850	630	710	920		570	930	870	710	550	
Total	99.8	99.8		99.5	100.2		99.1	100.0	99.2	99.3	98.5

Major oxides, LOI and Total in weight percent
Minor elements in ppm (parts per million)
LOI loss on ignition
ND not determined
(1) data from Bryant (1988b)

GEOCHEMISTRY

Whole-rock chemical analyses were completed for 20 samples of basement rock from Antelope Island. Chemical compositions, in conjunction with petrographic and structural relations, are used to interpret the origin of some of the different rock types. (All percentages in the following discussion are weight percent).

Chemical compositions of layered gneiss are highly variable, with SiO_2 contents ranging from 61 to 75 percent (table 2). Samples contain abundant Al_2O_3, significant total FeO, and moderate amounts of alkalis. The broad range in compositions for samples of layered gneiss, quartz-rich gneiss, and biotite schist is similar to the range reported by Bryant (1988b) for his gneiss and schist unit in the Wasatch Range (figure 7a). Bryant (1988b) concluded that protoliths for these rocks included graywacke, arkose, quartz arenite, and shale.

Table 3. *Normative values of selected samples from Antelope Island (see figure 3c for sample localities). Calculations based on CIPW method (Cox and others, 1979).*

	Banded Gneiss					Granitic Gneiss					
Sample	110	150	220	A10	Mean	7130	350	A12B	A-11[1]	A-5[1]	Mean
Quartz	29.6	28.3	28.4	32.2	29.6	28.2	29.4	33.3	33.8	29.2	30.8
Albite	27.1	32.8	30.1	27.3	29.3	29.5	26.7	26.0	24.2	26.7	26.8
Anorthite	7.3	5.7	8.5	5.1	6.7	2.7	4.5	3.6	5.6	5.9	4.5
Orthoclase	23.3	23.7	18.2	25.2	22.6	32.0	28.3	27.4	28.5	26.0	28.4
Diopside	1.6	2.2	3.1	--	1.7	1.8	2.3	1.0	--	2.2	1.5
Hypersthene	4.9	3.4	6.0	4.4	4.7	2.4	4.6	3.1	2.2	2.3	2.9
Magnetite	3.6	2.5	2.8	3.0	3.0	1.7	2.2	3.2	3.7	4.6	3.0
Ilmenite	1.0	0.8	1.1	0.7	0.9	0.4	0.7	0.6	0.7	0.8	0.6
Corundum	--	--	--	0.4	0.1	--	--	--	0.2	--	0.1
Apatite	0.3	0.3	0.3	0.3	0.3	0.1	0.3	0.1	0.1	0.4	0.2
Quartz	29.6	28.3	28.4	32.2	29.6	28.2	29.4	33.3	33.8	29.2	30.8
Plagioclase	34.4	38.5	38.6	32.4	36.0	32.1	31.2	29.6	29.8	32.6	31.3
K-feldspar	23.3	23.7	18.2	25.2	22.6	32.0	28.3	27.4	28.5	26.0	28.4
Fe-Mg Silicates	6.5	5.6	8.8	4.4	6.4	4.2	6.9	4.1	2.2	4.5	4.4
Oxides	4.6	3.3	3.9	3.7	3.9	2.1	2.9	3.8	4.4	5.4	3.6

[1] data from Bryant (1988b)

A lone sample of metamorphosed ultramafic rock had a very low SiO_2 content (37.7 percent) and a very high MgO content (23.1 percent), consistent with a komatiitic composition (table 2; figure 7b). Komatiitic textures are absent and these ultramafic rocks have undergone metasomatism as indicated by widespread chlorite alteration.

Samples of hornblende-plagioclase gneiss have low SiO_2 contents and relatively high total FeO contents (table 2). Samples plot in or near the tholeiitic field and basalts may have been emplaced in an oceanic or continental setting (figure 7b). However, samples may have undergone metasomatism.

Banded and granitic gneiss have overlapping compositions with SiO_2 ranging from about 69 to 73 percent (table 2). Granitic gneiss samples have slightly higher average contents of SiO_2 and K_2O, and lower contents of CaO, total FeO, and MgO compared to banded gneiss. All samples have relatively low Al_2O_3 contents, moderate alkali contents, and high total FeO contents. Granitic gneiss in the Wasatch Range described by Bryant (1988b) is chemically similar to granitic gneiss on Antelope Island. Samples of granitic and banded gneiss on Antelope Island contain 28 to 34 percent normative quartz, 30 to 39 percent normative plagioclase, 18 to 32 percent normative orthoclase, and 2 to 9 percent normative Fe-Mg silicates (table 3). Normative mineral abundances plot within the granite field for granitic gneiss and within the granite and granodiorite fields for banded gneiss (figure 7c), similar to plots of observed modal abundances (figures 6c and 6d). The limited range of chemical compositions lies along the boundary between the tholeiitic and the calc-alkaline fields.

Abundances of most elements for banded and granitic gneiss vary approximately linearly with increasing SiO_2 contents (figure 8), probably reflecting a common genesis for the two rock types. Contents of K_2O increase, and contents of CaO, FeO, MgO, and TiO_2 decrease with increasing SiO_2 content, possibly reflecting fractional crystallization or magma mixing. The limited range of compositions and apparent clustering of SiO_2 contents may reflect limited sampling.

Granitic and banded gneiss on Antelope Island display chemical similarities with A-type granites as defined by White and Chappel (1983), including relatively low Al contents, high Fe contents, and enrichment in high-field-strength elements (large ionic size and high charge) such as Zr and Nb. Mineralogical similarities with A-type granites include the presence of Fe-rich biotite and amphibole. White and Chappel (1983) reported that many A-type granites were emplaced after peak deformation, and were derived from crust previously depleted by extraction of partial melts. Creaser and others (1991), however, presented arguments for derivation of A-type granites by partial melting of non-depleted tonalitic to granodioritic crust, implying that A-type granites can form during peak deformation and metamorphism. Well-developed foliation and locally gradational contacts between granitic, banded, and migmatitic layered gneiss in the Wasatch Range and on Antelope Island are consistent with igneous intrusion during peak metamorphism and deformation. These intrusions may have formed by partial melting of older gneiss (Bryant, 1988a).

Normative compositions of banded and granitic gneiss plot near the orthoclase-plagioclase-quartz cotectic line in the system quartz-albite-anorthite-orthoclase-H_2O (figure 9). The relative location of the cotectic line only changes slightly with moderate changes in total pressure and water pressure, although temperatures along the line are higher for lower water pressures (see Winkler, 1976). Two features are note-

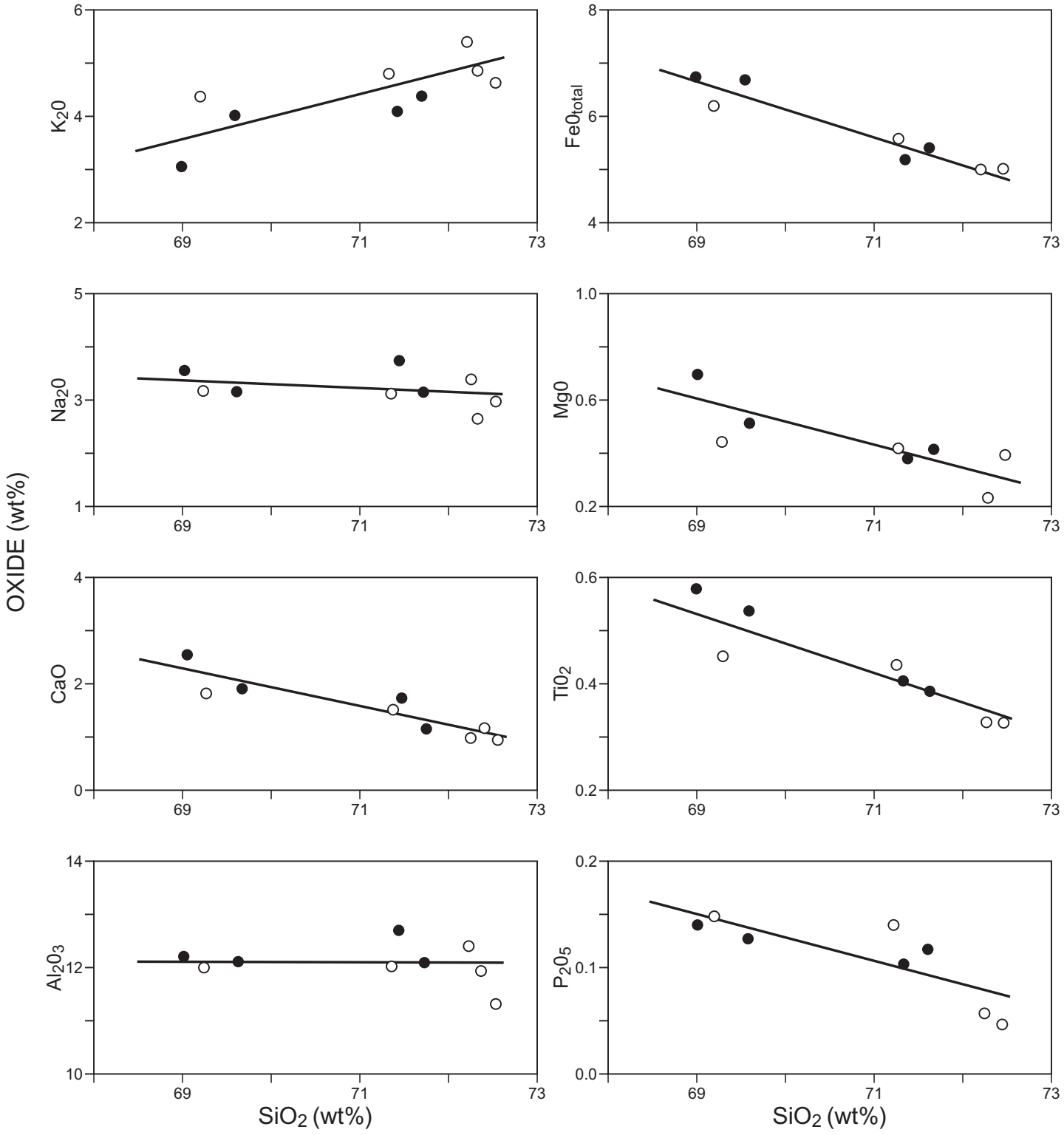

Figure 8. *Harker variation plots for whole-rock chemical data for banded gneiss samples (solid circles) and granitic gneiss samples (open circles). Major element contents vary systematically with increasing SiO_2 content as indicated by lines. Note that chemical compositions of the two rock types overlap.*

worthy: (1) The granitic gneiss probably crystallized along the cotectic line at temperatures between 650 and 800°C, depending on water pressure. This is similar to the estimated temperatures of metamorphism discussed in the next section. (2) If the granitic gneiss crystallized from a parent magma of similar composition, then this magma would also lie near the cotectic line. Such a parent magma could have been generated at depths of 15 to 20 kilometers (9-12 mi) by melting granodiorite or tonalite at temperatures of about 650 to 700°C with high water pressures, or by melting biotite-bearing granodiorite to tonalite at temperatures of about 750 to 800°C with reduced water pressures (see Winkler, 1976).

Table 4. *Locations of samples.*

Sample	Lattitude	Longitude
AI 540	40° 51' 27"	112° 10' 46"
AI 590	40° 51' 27"	112° 10' 50"
AI 620	40° 57' 55"	112° 12' 50"
AI 2200	40° 58' 06"	112° 12' 53"
AI A4D	40° 51' 06"	112° 10' 52"
AI A5D	40° 51' 21"	112° 11' 02"
AI A5E	40° 51' 21"	112° 11' 02"
AI A19E	40° 57' 06"	112° 12' 40"
AI 560	40° 51' 28"	112° 10' 50"
AI A19C	40° 57' 06"	112° 12' 40"
AI A19D	40° 57' 06"	112° 12' 40"
AI 430	40° 51' 47"	112° 10' 26"
AI A2A	40° 52' 09"	112° 10' 38"
AI A2E	40° 52' 09"	112° 10' 38"
AI 7290	40° 51' 53"	112° 10' 43"
AI A3B	40° 51' 54"	112° 10' 44"
AI 170	40° 55' 33"	112° 12' 20"
AI 190	40° 55' 33"	112° 12' 20"
AI 420	40° 56' 04"	112° 14' 03"
AI 510	40° 50' 54"	112° 10' 34"
AI 7140	40° 57' 21"	112° 14' 58"
AI A17A	40° 56' 31"	112° 12' 23"
AI 110	40° 55' 27"	112° 12' 00"
AI 140	40° 55' 33"	112° 12' 20"
AI 150	40° 55' 33"	112° 12' 20"
AI 160	40° 55' 33"	112° 12' 20"
AI 210	40° 55' 30"	112° 12' 40"
AI 220	40° 55' 30"	112° 12' 40"
AI 300	40° 55' 24"	112° 13' 14"
AI A10	40° 53' 22"	112° 11' 05"
AI 7110	40° 58' 09"	112° 14' 25"
AI 7130	40° 58' 09"	112° 14' 25"
AI A20A	40° 57' 35"	112° 13' 43"
AI A20B	40° 57' 35"	112° 13' 43"
AI A21B	40° 58' 36"	112° 14' 32"
AI 350	40° 56' 04"	112° 14' 04"
AI 370	40° 56' 04"	112° 14' 04"
AI A12B	40° 55' 57"	112° 14' 04"
AI A-11	See Bryant(1988b)	
AI A-5	See Bryant(1988b)	
AI 1060	40° 55' 18"	112° 11' 25"
AI 2180	40° 58' 06"	112° 12' 52"
AI 7150	40° 57' 06"	112° 11' 34"
AI 640	40° 57' 56"	112° 12' 54"
AI 1250	40° 58' 42"	112° 11' 31"
AI 7180	40° 51' 41"	112° 10' 52"
AI 7200	40° 51' 35"	112° 10' 50"
AI F327A	40° 59' 17"	112° 14' 22"
AI F358	41° 00' 12"	112° 12' 04"
AI F379A	40° 58' 09"	112° 14' 43"
AI F355	40° 52' 24"	112° 10' 31"
AI F411	40° 57' 56"	112° 13' 02"
AI F434B	40° 57' 18"	112° 12' 59"
AI 240	40° 55' 23"	112° 13' 15"
AI 250	40° 55' 23"	112° 13' 15"

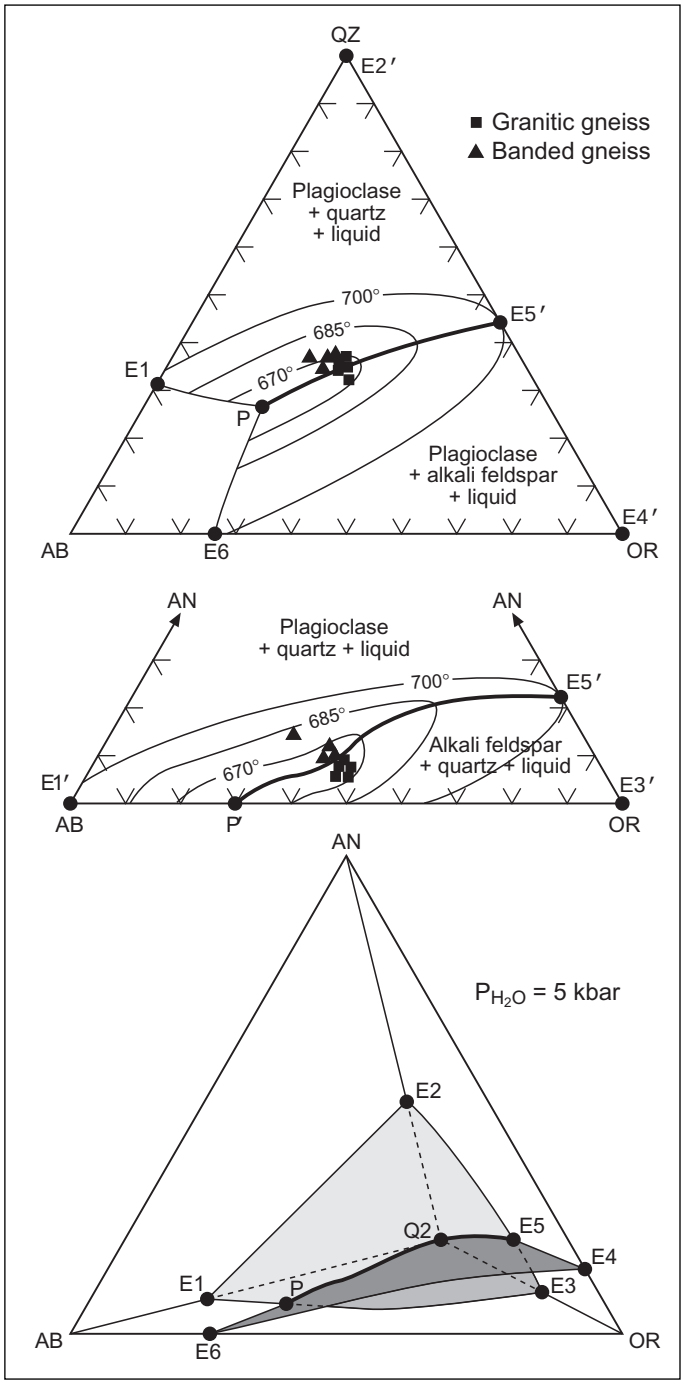

Figure 9. *Phase relations in the system quartz(QZ)-albite(AB)-anorthite(AN)-orthoclase(OR)-water for total pressure equal water pressure equal 5 kilobar. Isotherms on cotectic surfaces, cotectic line (line P-E5), and eutectic points (labeled E1 to E6) projected onto QZ-AB-OR and AN-AB-OR planes. Modified from Winkler (1976). Normative compositions of banded gneiss (triangles) and granitic gneiss (squares) indicated.*

Granite and pegmatite samples have SiO_2 contents greater than 72 percent and relatively high Al_2O_3 contents (table 2). Overall, granite and pegmatite have higher contents of Al_2O_3 and K_2O and lower contents of FeO, MgO, and TiO_2 compared to banded and granitic gneiss. Compositions do not plot on linear trends defined by samples of banded and granitic gneiss on Harker variation plots, and these granites probably had different origins than the banded

and granitic gneiss. Some granite samples have chemical and mineralogical similarities with S-type granites as defined by White and Chappel (1983), consistent with derivation by partial melting of nearby layered gneiss.

METAMORPHIC CONDITIONS

Mineral assemblages and textural relationships in layered gneiss and biotite schist, combined with geothermobarometry reported by Barnett and others (1993), and empirically and thermodynamically derived mineral reactions, constrain metamorphic conditions (figures 10a and 10b). Layered gneiss contains sillimanite, biotite, garnet, cordierite, and K-feldspar. Biotite schist contains sillimanite, biotite, garnet and possible syn-metamorphic muscovite. K-feldspar appears to be in textural equilibrium with sillimanite in layered gneiss, whereas muscovite may be in equilibrium with sillimanite in biotite schist. Cordierite is associated with biotite, garnet, and sillimanite, although textural relations of cordierite were largely obliterated during retrograde alteration. Barnett and others (1993) used compositions of coexisting biotite, garnet, and plagioclase to estimate peak metamorphic temperatures of about 650 to 750°C for samples of layered gneiss from Antelope Island and along Weber Canyon in the Wasatch Range, with a poorly constrained pressure estimate of about 4 kilobars for Antelope Island. Observed mineral assemblages and interpreted mineral reactions described below are consistent with these estimates.

The coexistence of garnet and cordierite in layered gneiss indicates that lithostatic pressures were between about 3 and 5 kilobar during metamorphism, based on stability of these minerals in other relatively iron-rich pelitic rocks (Winkler, 1976). Thermodynamic relations also indicate that cordierite will break down to garnet or biotite at pressures between about 2 kilobar for highly Fe-rich cordierite and 7 kilobar for highly Mg-rich cordierite, depending slightly on water pressure (reactions 1a to 1d in figures 10a and 10b; Holdaway and Lee, 1977).

Metamorphic temperatures and water pressures are defined by a more complicated set of reactions in the layered gneiss and biotite schist. The presence of sillimanite and cordierite require temperatures greater than 550°C (reactions 2a to 2c and 1e in figures 10a and 10b; Holdaway, 1971; Winkler, 1976). Some cordierite may have formed by the breakdown of biotite and sillimanite, which would require temperatures greater than about 650°C, even for reduced water pressures (reaction 1c in figure 10b). Muscovite is not stable in most layered gneiss samples, but may be locally stable in biotite schist, possibly reflecting varying water pressure, which partly controls the breakdown of muscovite to K-feldspar and sillimanite. Muscovite is stable at temperatures of about 650 to 700°C over a lithostatic pressure range of 3 to 5 kilobar if water pressure equals lithostatic pressure (reaction 3 in figure 10a). However, K-feldspar is stable for the same range of temperature and lithostatic pressure if water pressure is reduced (reaction 3 in figure 10b). Thus both K-feldspar and muscovite can be stable in different areas at temperatures of about 700°C if water pressure is reduced in the layered gneiss. In many high-grade gneiss terranes water

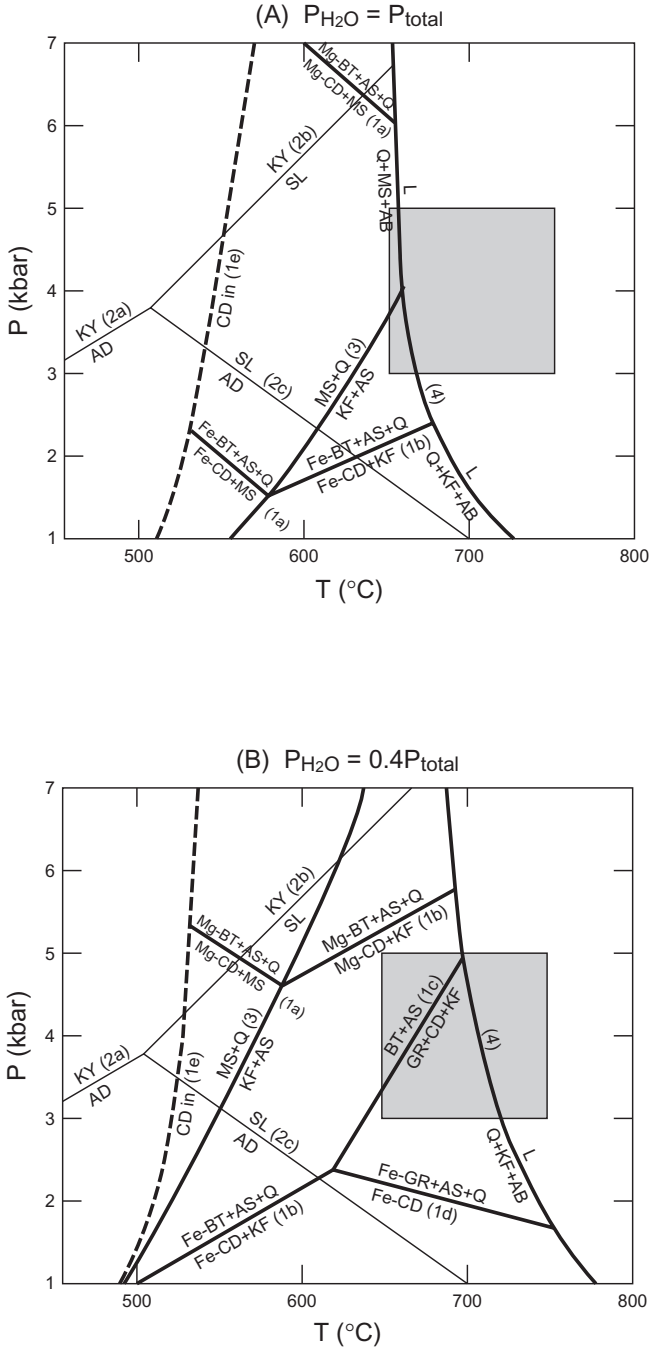

Figure 10. *Petrogenetic grids modified from Turner (1981) for P_{H_2O}=Ptotal and P_{H_2O}=0.4 Ptotal. Minerals are: AB-albite; AD-andalusite; AS-aluminosilicates; BT-biotite; CD-cordierite; GR-garnet; KF-K-feldspar; KY-kyanite; L-silicate liquid; MS-muscovite; Q-quartz; and SL-sillimanite. Continuous reactions 1a to 1d from Holdaway and Lee (1977) define breakdown of iron- and magnesium-cordierite to biotite and garnet. Reaction 1e for first appearance of cordierite from Winkler (1976). Reactions 2a to 2c for aluminosilicates from Holdaway (1971). Reaction 3 for breakdown of muscovite from Turner (1981). Reaction 4 for partial melting relations from Winkler (1976). Shaded area gives preferred range of metamorphic temperature and pressure based on results reported by Barnett and others (1993) and observed mineral assemblages.*

pressure varied with position and was less than lithostatic pressure (Winkler, 1976; Turner, 1981).

Layered gneiss and biotite schist appear to have undergone limited partial melting. Initial melting occurs at temperatures of about 650°C for lithostatic pressures between 3 and 5 kilobar if water pressure equals lithostatic pressure, and at temperatures greater than 700°C for reduced water pressures (reaction 4 in figures 10a and 10b). Water is preferentially incorporated into partial melts, and melting provides a mechanism for locally reducing water pressures in the layered gneiss (for example Turner, 1981). Biotite schist appears to have undergone less melting and contains more abundant hydrous minerals, and may thus have maintained higher water pressures.

Other terranes that contain coexisting biotite, sillimanite, cordierite, garnet, and K-feldspar also appear to have been metamorphosed at relatively high temperatures and low pressures (Schreurs and Westra, 1986; Young and others, 1989). For example, Young and others (1989) used quantitative geothermometry and geobarometry for a gneiss terrane in southern Nevada to estimate metamorphic temperatures of 590 to 750°C, lithostatic pressures of 3 to 4 kilobar, and water pressures that were less than lithostatic pressures. Metamorphism in these other terranes and on Antelope Island probably resulted from transient increases in heat flow, possibly due to large-scale igneous intrusion, crustal thickening, or increased mantle heat flow.

Clinopyroxene in granitic gneiss and clinopyroxene and rare orthopyroxene in hornblende-plagioclase gneiss may also record granulite-facies metamorphism. Textural relations are, however, ambiguous, and pyroxene grains may have formed during primary igneous crystallization.

GEOCHRONOLOGY

Limited geochronologic data from the Wasatch Range and Antelope Island broadly constrain the geologic history of the Farmington Canyon Complex. Hedge and others (1983) and Bryant (1988a, 1988b) interpreted a possible period of Archean crustal growth and metamorphism followed by a period of Early Proterozoic igneous intrusion, metamorphism, and deformation. Nd-Sm model ages (estimated crustal residency ages) of 2,740 Ma to 3,430 Ma for three samples of migmatitic gneiss and amphibolite in the Wasatch Range probably record a component of Archean crustal material (Hedge and others, 1983). Rb-Sr data for samples of layered and migmatitic gneiss from the Wasatch Range do not define an isochron (Hedge and others, 1983), but these data have been interpreted as recording partial isotopic equilibration of gneiss during late Archean metamorphism (Bryant, 1988a). Alternatively, the scatter in Rb and Sr isotopic values may reflect varying initial $^{87}Sr/^{86}Sr$ ratios in the gneiss, or mobilization of Rb and Sr during Proterozoic metamorphism, in which case a unique interpretation of the data is impossible. Protolith and metamorphic ages for lithologically similar layered gneiss on Antelope Island are currently uncertain.

Isotopic data provide evidence for early Proterozoic granitic igneous intrusions (Hedge and others, 1983). Rb-Sr data for samples from a large granitic gneiss body in the Wasatch Range define an isochron that yields a high $^{87}Sr/^{86}Sr$ initial ratio of 0.769 and an age of 1,810 Ma, interpreted as the age of synmetamorphic intrusion of a granitic pluton (Hedge and others, 1983). This initial ratio is significantly greater than values reported for most granitic plutons (Faure and Powell, 1972), and if correct, requires long crustal residence times for Rb-enriched material in the source region for the pluton. Alternatively, the high initial ratio may reflect mobilization of Rb and Sr. Discordant U-Pb ages for the granitic gneiss samples define a chord with an upper intercept of 1,790 Ma on a concordia diagram, but the scatter in data about the chord is greater than that expected from analytical error (Hedge and others, 1983).

The age of granitic gneiss on Antelope Island is less certain. Discordant U-Pb ages for two zircon fractions of granitic gneiss from Antelope Island define a chord with an upper intercept of 1,990 Ma on a concordia diagram, which was interpreted as the age of synmetamorphic intrusion of a granitic pluton (Hedge and others, 1983; Bryant, 1988a). However, the geological accuracy of this date is uncertain because only two points were used to construct the chord. Discordant U-Pb ages for zircon fractions from a sample of garnet-biotite-quartz-feldspar gneiss obtained from a drill hole located about 8 kilometers (5 mi) west of Antelope Island define a chord with an upper intercept of 2,020 Ma (Hedge and others, 1983). Further isotopic studies are needed to confirm these possible igneous ages, which are unusual for the western United States and which are different from ages of granitic gneiss in the Wasatch Range.

Barnett and others (1993 reported slightly discordant uranium lead ages of 1650 to 1700 Ma for metamorphic monazite from layered gneiss on Antelope Island and near Weber Canyon in the Wasatch Range. These ages may record cooling following peak metamorphism and intrusion of granitic plutons, or a metamorphic event slightly younger than granitic intrusion. $^{40}Ar/^{39}Ar$ plateau ages of hornblende are about 1,600 Ma and record cooling through temperatures of about 500° (Barnett and others, 1993).

CONCLUSIONS

Local Geology

Layered gneiss and lenses of biotite schist and quartz-rich gneiss exposed within the central and southern parts of Antelope Island probably represent a metamorphosed and intensely deformed sedimentary sequence. Layered gneiss is well foliated and consists mostly of quartz, plagioclase, K-feldspar, and biotite, with minor garnet, sillimanite, and cordierite. Biotite schist contains abundant biotite with lesser amounts of quartz, muscovite, garnet, and sillimanite. Quartz-rich gneiss contains abundant quartz with minor plagioclase, muscovite, and biotite. Isolated pods of metamorphosed ultramafic rock within layered gneiss consist of variably altered pyroxene, amphibole, and olivine, and may represent part of highly dismembered oceanic crust.

Hornblende-plagioclase gneiss forms thin pods within other units and is abundant within a mafic gneiss body in the central part of the island. The pods may represent mafic dikes emplaced over a protracted history and the mafic body may represent a deformed pluton or extrusive sequence.

STAGE 1. Archean(?) deposition of surpracrustal sequence

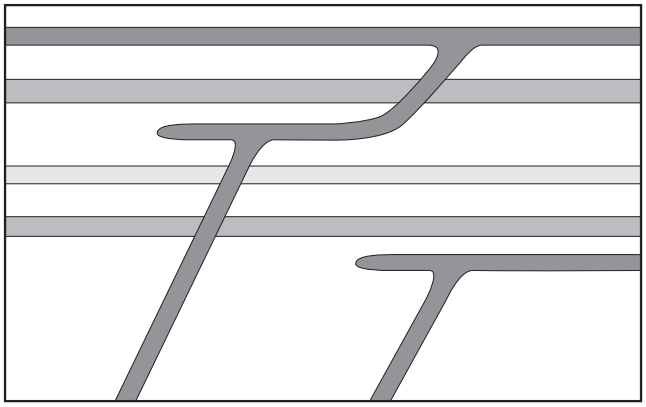

STAGE 2. Late Archean(?) metamorphism and deformation, and igneous intrusions

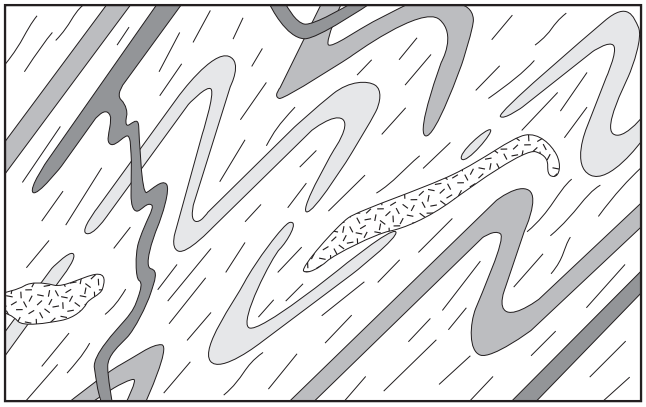

STAGE 3. Early Proterozoic igneous intrusion, and **STAGE 4.** Early Proterozoic metamorphism and deformation

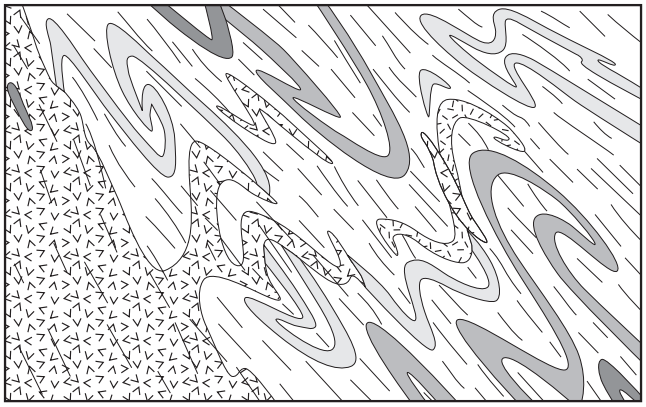

STAGE 5. Proterozoic intrusion of late-stage granites

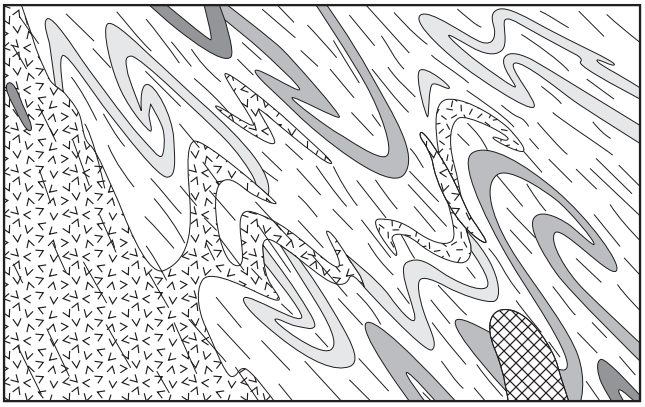

STAGE 6. Middle to Late Proterozoic erosion, and **STAGE 7.** Late Proterozoic to Mesozoic deposition of sedimentary rocks

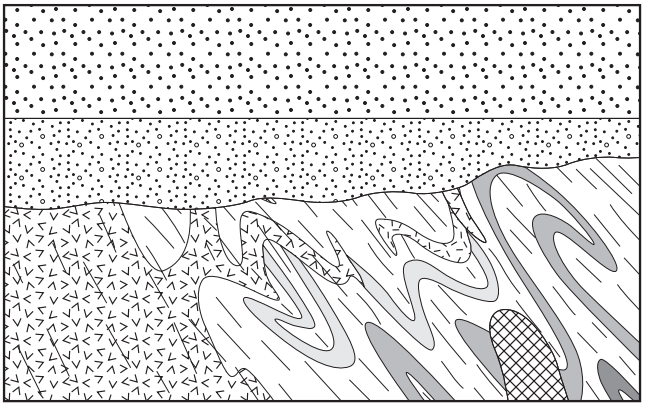

STAGE 8. Mesozoic deformation and retrograde alteration

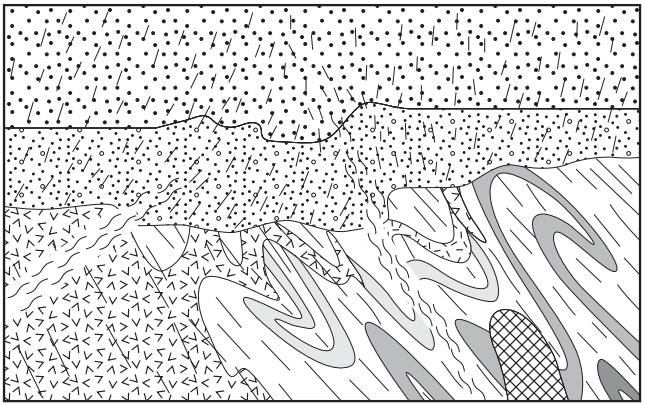

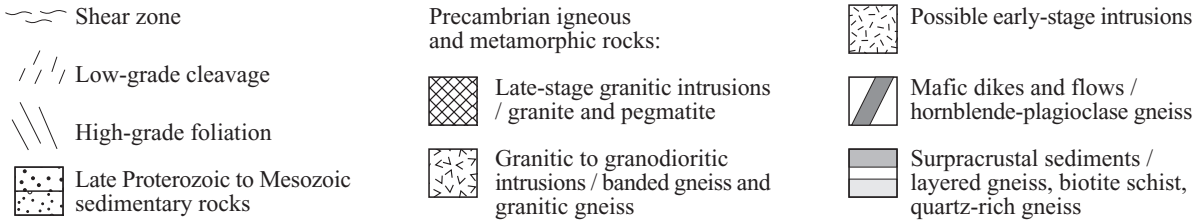

Figure 11. *Schematic diagram of interpreted geologic history of Antelope Island. Stage 1- A supracrustal sequence of sediments and mafic dikes and flows is deposited. Stage 2- The supracrustal sequence undergoes Late Archean(?) metamorphism and deformation, with possible intrusion of plutons. Stages 3 and 4- Large granitic to granodioritic plutons are intruded, approximately synchronous with Early Proterozoic main-phase metamorphism and deformation that produce strong foliation. Stage 5- Late-stage granites are intruded and locally crosscut earlier structures. Stages 6 and 7- Middle to Late Proterozoic uplift and erosion are followed by Late Proterozoic to Mesozoic deposition of sedimentary rocks. Stage 8- Mesozoic thrusting, deformation, and retrograde alteration produce shear zones and cleavage that overprint high-grade structures. Stage 9 (not illustrated)- Cenozoic extension, uplift, and erosion.*

Hornblende-plagioclase gneiss has gabbroic to tonalitic composition and consists mostly of amphibole and plagioclase, with minor quartz and biotite, and rare pyroxene.

Well-foliated banded gneiss forms a broad belt on the eastern part of the island, and surrounds the margin of weakly to well-foliated granitic gneiss on the western part of the island. These two rock types have overlapping mineralogical and chemical compositions, and may represent a granitic to granodioritic pluton. Banded and granitic gneiss consists mostly of quartz, plagioclase, and K-feldspar, with lesser amounts of hornblende. A single weak to strong foliation developed in banded and granitic gneiss during main-phase deformation and high-grade metamorphism.

Coarse-grained granite forms plutons on the eastern and central part of the island and small bodies that crosscut older structures in other rock types, recording intrusion after peak deformation. Pegmatite forms foliated concordant to non-foliated discordant dikes and lenses within most rock types, indicating a protracted history of intrusion. Granite and pegmatite consist of course-grained quartz, albitic plagioclase, and K-feldspar, with minor and variable amounts of muscovite, biotite, and garnet.

Chloritic gneiss bounds shear zones and is widespread near the basement-cover contact. It displays variable retrograde greenschist alteration and variably developed sets of fractures, veins, and minor shear zones that crosscut earlier high-grade structures. Phyllonite and mylonite occur within shear zones that display pervasive alteration and concentrated plastic deformation. Shear zones and fracture sets probably accommodated internal deformation of thrust sheets during the Sevier orogeny.

Layered gneiss contains biotite, garnet, sillimanite, K-feldspar, and cordierite, and has undergone local partial melting consistent with high metamorphic temperatures (about 700°C), relatively low lithostatic pressures (about 3 to 5 kilobar), and locally reduced fluid pressures. Rare pyroxene in granitic and hornblende-plagioclase gneiss may reflect locally preserved granulite facies metamorphism or primary igneous crystallization. Normative mineral abundances of banded and granitic gneiss are consistent with crystallization at temperatures of 650 to 700°C from a magma initially derived from partial melting of granodioritic to tonalitic gneiss. A dominant foliation that formed during main-phase deformation cuts layered, banded, and granitic gneiss and generally strikes north to northeast. However, complex fold interference patterns and multiple foliations locally preserved within layered gneiss may record an earlier period of deformation.

Regional Correlation

Rocks of the Farmington Canyon Complex display similarities with both the Archean Wyoming Province and Early Proterozoic terranes of Colorado and southern Utah (figure 2). Layered gneiss in the Farmington Canyon Complex is petrologically similar to some paragneisses in the Wyoming Province and Nd-Sm model ages of layered gneiss in the Wasatch Range probably record a component of Archean parent (Hedge and others, 1983). Bryant (1988a) thus suggested that the Farmington Canyon Complex represents a western extension of the Wyoming Province. However, layered gneiss in the Farmington Canyon Complex is also similar to some metasedimentary rocks in Colorado and was strongly deformed, metamorphosed, and remobilized during the Early Proterozoic; a pattern that is only observed along the southern margins of the Wyoming Province and farther southwest in the Mohave Province (Bennett and DePaolo, 1987). Granitic gneiss in the Wasatch Range was emplaced and metamorphosed at about 1,800 Ma, similar to ages of intrusion and metamorphism along and south of the Cheyenne belt. Thus, older basement rocks, such as layered gneiss exposed on Antelope Island, may represent part of the Wyoming Province that was remobilized during Early Proterozoic intrusion, metamorphism, and deformation. However, further isotopic data are needed to confirm this interpretation.

Geologic History

Basement rock within the Wasatch Range and on Antelope Island experienced a complex history of igneous intrusion, partial melting, high-grade metamorphism, and deformation. A simplified hypothetical model of this history is illustrated in idealized stages (figure 11).

Stage 1- Archean(?) deposition of a supracrustal sequence.

A sequence of sedimentary strata, including graywacke, quartz-rich sandstone, and shale, now represented by layered gneiss, quartz-rich gneiss, and biotite schist, was deposited. Mafic flows and dikes, now represented by pods of hornblende-plagioclase gneiss, may also have been included in this supracrustal sequence. The material upon which these rocks was deposited is uncertain, and may have been oceanic crust now represented by isolated lenses of metamorphosed mafic and ultramafic rock. Evidence for the origin of this supracrustal sequence has been largely obliterated by subsequent metamorphism and deformation.

Stage 2- Late Archean(?) metamorphism and deformation.

A period of metamorphism and deformation appears to have affected the layered gneiss prior to main-phase deformation, based on fold interference patterns and multiple foliations preserved in some fold hinges. The age and conditions of this event are uncertain, with Hedge and others (1983) and Bryant (1988a, 1988b) suggesting a period of Late Archean metamorphism. This event may have been synchronous with intrusion of igneous bodies. Pods of granitic gneiss within layered gneiss may represent early intrusion of granitic material, local partial melting, or may be related to later intrusion during stage 3.

Stage 3- Early Proterozoic granitic intrusion.

Large plutons of granitic material were probably intruded between 2,000 and 1,800 million years ago, prior to or synchronous with main-phase deformation and metamorphism. Bodies of granitic and banded gneiss on Antelope Island and granitic gneiss in the Wasatch Range may record regional intrusion of granitic plutons, based on petrologic and chemical similarities. However, limited available isotopic data indicate different ages for granitic gneiss on Antelope Island and in the Wasatch Range (Hedge and others, 1983).

Stage 4- Early Proterozoic main-phase metamorphism and

deformation.

Main-phase metamorphism and deformation, possibly synchronous with granitic intrusion, produced weak to strong foliation in banded and granitic gneiss, and tight to isoclinal folds that largely obliterated earlier structures in layered gneiss. Metamorphism was overall at upper amphibolite to granulite facies. Partial melting, injection of pegmatite dikes, and migmatization accompanied metamorphism. Estimated metamorphic conditions suggest a high geothermal gradient and locally reduced water pressures, perhaps related to heating during regional intrusion of granitic to granodioritic plutons.

Stage 5- Proterozoic intrusion of late-stage granites.

Coarse-grained granitic plutons and pegmatite dikes were emplaced after peak metamorphism and deformation. Late-stage granitic bodies are much less deformed and crosscut main-phase foliation and compositional layering. Some granite was probably derived by partial melting of surrounding layered gneiss after peak deformation.

Stage 6- Middle to Late Proterozoic uplift and erosion.

Uplift and erosion of high-grade basement rocks followed metamorphism and intrusion. Local retrograde metamorphism may have accompanied uplift, but such metamorphism would be difficult to distinguish from Mesozoic alteration.

Stage 7- Late Proterozoic to Mesozoic deposition of sedimentary rocks.

A late Proterozoic sequence of diamictite, dolomite, quartzite, and argillite was deposited over the basement. A lithologically similar but much thicker sequence of late Proterozoic rocks in the Willard thrust sheet contains basalt flows and dikes, and may record rifting along the western margin of the North American craton (Christie-Blick and others, 1989). An overlying sequence of Paleozoic to Mesozoic carbonates, sandstone, and shale was deposited on the late Proterozoic strata. This sequence is part of a westward-thickening wedge of miogeoclinal strata deposited along the western margin of North America.

Stage 8- Mesozoic deformation and retrograde alteration.

Mesozoic deformation and greenschist-facies retrograde alteration overprinted earlier Precambrian structures during the Sevier orogeny. Large thrust sheets were translated eastward and basement and sedimentary cover rocks were locally imbricated. Internal deformation of thrust sheets produced shear zones in basement rock, and cleavage and folds in the sedimentary cover.

Stage 9- Cenozoic extension.

Large-displacement normal faults developed during Cenozoic extension. Uplift and erosion of ranges between normal faults resulted in the current topography and exposures of the island.

ACKNOWLEDGMENTS

Jon King provided a detailed and thoughtful review of an earlier version of this manuscript. The Utah Division of Parks and Recreation provided logistical support and access during the field work. Mark Jensen assisted in bedrock mapping on Antelope Island that led to this study.

REFERENCES

Armstrong, R.L., 1968, Mantled gneiss domes in the Albion Range, southern Idaho: Geological Society of America Bulletin, v. 79, p. 1,295-1,314.

Barnett, Daniel, Bowman, J.R., and Smith, H.A., 1993, Petrologic and geochronologic studies in the Farmington Canyon Complex, Wasatch Mountains and Antelope Island, Utah: Utah Geological Survey Contract Report 93-5, 34 p.

Bennett, V.C., and DePaolo, D.J., 1987, Proterozoic crustal history of the western United States as determined by neodymium isotopic mapping: Geological Society of America Bulletin, v. 99, p. 674-685.

Bell, G.L., 1951, Farmington Canyon Complex of north-central Wasatch: Salt Lake City, University of Utah, Ph.D. dissertation, 101 p.

Bryant, Bruce, 1988a, Evolution and early Proterozoic history of the margin of the Archean continent in Utah, *in* Ernst, W.G., editor, Metamorphism and crustal evolution of the western United States: Englewood Cliffs, N.J., Prentice-Hall, p. 432-445.

Bryant, Bruce, 1988b, Geology of the Farmington Canyon Complex, Wasatch Mountains, Utah: U.S. Geological Survey Professional Paper 1476, 54p.

Christie-Blick, Nicholas, Mount, J.F., Levy, Marjorie, Signor, P.W., and Link, P.K., 1989, Late Proterozoic and Cambrian tectonics, sedimentation, and record of Metazoan radiation in the Western United States: 28th International Geological Congress Field Trip Guidebook T331, 113p.

Compton, R.R., Todd, V.R., Zartman, R.E., and Naeser, C.W., 1977, Oligocene and Miocene metamorphism, folding, and low-angle faulting in northwestern Utah: Geological Society of America Bulletin, v. 88, p. 1,237-1,250.

Cox, K.G., Bell, J.D., and Pankhurst, R.J., 1979, The interpretation of igneous rocks: London, George, Allen, and Unwin, 450 p.

Creaser, R.A., Price, R.C., and Wormland, R.J., 1991, A-type granites revisited: assessment of residual-source model: Geology, v. 19, p. 163-166.

Doelling, H.H., Willis, G.C., Jensen, M.E., Hecker, Suzanne, Case, W.F., and Hand, J.S., 1990, Geologic map of Antelope Island, Davis County, Utah: Utah Geological and Mineral Survey Map 127, 27 p, 1:24,000.

Duebendorfer, E.M., and Houston, R.S., 1987, Proterozoic accretionary tectonics at the southern margin of the Archean Wyoming craton: Geological Society of America Bulletin, v. 98, no. 5, p. 554-568.

Eardley, A.J., and Hatch, R.A., 1940, Precambrian crystalline rocks of north-central Utah: Journal of Geology, v. 48, p. 58-72.

Faure, Gunter, and Powell, J.L., 1972, Strontium isotope geology: New York, Springer-Verlag, 188 p.

Graff, P.J., Sears, J.W., and Holden, G.S., 1980, The Uinta arch project--investigations of uranium potential in Precambrian X and older metasedimentary rocks in the Uinta and Wasatch Ranges, Utah and Colorado: U.S. Department of Energy Open-File Report GJBX-170(80), 180 p.

Hedge, C.E., Houston, R.S., Tweto, O.L., Peterman, Z.E., Harrison, J.E., and Reid, R.R., 1986, The Precambrian of the Rocky Mountain region: U.S. Geological Survey Professional Paper 1241-D, p. 1-17.

Hedge, C.E., Stacey, J.S., and Bryant, Bruce, 1983, Geochronology of the Farmington Canyon Complex, Wasatch Mountains, Utah, *in* Miller, D.M., Todd, V.R., and Howard, K.A., editors, Tectonic and stratigraphic studies of the eastern Great Basin: Geological Society of America Memoir 157, p. 37-44.

Hintze, L.F., and Stokes, W.L., 1964, Geologic map of northwestern Utah: Utah Geological and Mineral Survey map, unnumbered, 1:250,000.

Holdaway, M.J., 1971, Stability of andalusite and the aluminum silicate phase diagram: American Journal of Science, v. 271, p. 97-131.

Holdaway, M.J., and Lee, S.M., 1977, Fe-Mg cordierite stability in high-grade pelitic rocks based on experimental, theoretical, and natural observations: Contributions to Mineralogy and Petrology, v. 63, p. 175-198.

Karlstrom, K.E., and Houston, R.S., 1984, The Cheyenne belt: analysis of a Proterozoic suture in southern Wyoming: Precambrian Research, v. 25, p. 415-446.

International Union of Geological Scientists (Subcommission on the Systematics of Igneous Rocks), 1973, Classification and nomenclature of plutonic rocks: Geotimes, v. 18, no. 10, p. 26-30.

Irvine, T.N., and Barager, W.R.A., 1971, A guide to the chemical and classification of common volcanic rocks: Canadian Journal of Earth Sciences, v. 8, p. 523-548.

Larsen, W.N., 1957, Petrology and structure of Antelope Island, Davis County, Utah: Salt Lake City, University of Utah, Ph.D. dissertation, 142 p., map scale 1:24,000.

Pearce, T.H., Gorman, B.E., and Birkett, T.C., 1977, The relationship between major element chemistry and tectonic environment of basic and intermediate volcanic rocks: Earth and Planetary Science Letters, v. 36, p. 121-132.

Pettijohn, F.J., Potter, P.E., and Siever, R., 1973, Sand and sandstone: New York, Springer-Verlag, 618 p.

Schreurs, J., and Westra, L., 1986, The thermotectonic evolution of a Proterozoic low pressure, granulite dome, West Uusimaa, Finland: Contributions to Mineralogy and Petrology, v. 93, p. 236-250.

Sears, J.W., Graff, P.J., and Holden, G.S., 1982, Tectonic evolution of lower Proterozoic rocks, Uinta Mountains, Utah and Colorado: Geological Society of America Bulletin, v. 93, p. 990-997.

Turner, F.J., 1981, Metamorphic Petrology: New York, McGraw-Hill, 524p.

Tweto, O.L., 1987, Rock units of the Precambrian basement in Colorado: U.S. Geological Survey Professional Paper 1321-A, 54 p.

White, A.R., and Chappell, B.W., 1983, Granitoid types and their distribution on the Lachlan fold belt, southeastern Australia: Geological Society of America Memoir 159, p. 21-33.

Winkler, H.G.F., 1976, Petrogenesis of metamorphic rocks: New York, Springer Verlag, 334 p.

Yonkee, W.A., 1990, Geometry and mechanics of basement and cover deformation, Farmington Canyon Complex, Wasatch Range, Utah: Salt Lake City, University of Utah, Ph.D. dissertation, 255 p.

Yonkee, W.A., 1992, Basement-cover relations, Sevier orogenic belt, northern Utah: Geological Society of America Bulletin, v. 104, no. 3, p. 280-302.

Young, E.D., Anderson, J.L., Clark, H.S., and Thomas, W.M., 1989, Petrology of biotite-cordierite-garnet gneiss of the McCullough Range, Nevada: Evidence for Proterozoic low-pressure fluid-absent granulite-grade metamorphism in the southern Cordillera: Journal of Petrology, v. 30, p. 39-60.

PROTEROZOIC AND CAMBRIAN SEDIMENTARY AND LOW-GRADE METASEDIMENTARY ROCKS ON ANTELOPE ISLAND

by
W.A. Yonkee[1], G.C. Willis, and H.H. Doelling
Utah Geological Survey

[1]now at Department of Geosciences
Weber State University, Ogden, Utah

ABSTRACT

A thin stratigraphic section of Late Proterozoic and Cambrian sedimentary and low-grade metasedimentary rocks unconformably overlies Archean(?)to Early Proterozoic high-grade metamorphic and igneous rocks on Antelope Island. The sedimentary and metasedimentary rocks are divided into three formations, the Late Proterozoic Mineral Fork and Kelley Canyon Formations, and the Cambrian Tintic Quartzite. The Mineral Fork Formation is 0 to about 200 feet (0-60 m) thick and consists mostly of dark-colored diamictite. The Kelley Canyon Formation unconformably overlies the Mineral Fork Formation, and is divided into a lower dolomite member and an upper slate member. The dolomite member is 20 to 30 feet (6-9 m) thick and consists of light-gray to pink, fine-grained crystalline dolomite with minor amounts of calcareous slate. The slate member is 50 to 250 feet (15-75 m) thick and consists of purple, greenish-gray, and reddish-brown, thin-bedded slate and argillite with minor silty dolomite and fine-grained quartzite. The Tintic Quartzite is estimated to be in excess of 800 feet (250 m) thick and consists mostly of tan to greenish-gray, fine- to coarse-grained quartzite and quartz-pebble conglomerate.

Late Proterozoic strata are generally absent in outcrops directly east of Antelope Island, are thin on Antelope Island, and are as much as 12,000 feet (3,500 m) thick in the allochthonous, structurally overlying Willard thrust sheet, which was originally located to the west prior to thrusting. When restored to their pre-thrust positions, Late Proterozoic and Paleozoic strata form a westward-thickening sedimentary wedge, and the section on Antelope Island is transitional between a thicker western section and a thinner eastern section. The configuration of this sedimentary wedge appears to have partially controlled the location of Mesozoic thrust faults.

INTRODUCTION

A thin stratigraphic section of Late Proterozoic to Cambrian sedimentary and low-grade metasedimentary rocks is preserved on Antelope Island. Lithologic and stratigraphic characteristics of this section provide an important link with sedimentary rocks of similar lithology and age exposed elsewhere in northern Utah (figures 1 and 2). In this paper we describe the outcrop and microscopic characteristics of this section, and then compare these characteristics with other sections to refine regional stratigraphic correlations and to better understand the Late Proterozoic to Cambrian geologic history of northern Utah.

Two distinctive Late Proterozoic to Paleozoic stratigraphic sections are preserved in northern Utah, a thick western section and a thin eastern section (Levy and Christie-Blick, 1989; Link and others, 1993; figure 1). The western section, preserved in the Willard thrust sheet, consists of up to 12,000 feet (3,500 m) of Late Proterozoic strata and about 25,000 feet (7,500 m) of Paleozoic strata (Hintze, 1988). The eastern section, preserved in thrust sheets to the east, includes about 10,000 feet (3000 m) of Paleozoic strata that directly overlie Archean(?) to Early Proterozoic high-grade metamorphic and igneous rocks (Hintze, 1988).

The sedimentary and low-grade metasedimentary rocks preserved on Antelope Island mark a transition from the eastern to western sections. These rocks were previously described by Larsen (1957) and Christie-Blick (1983), and were mapped in detail by Doelling and others (1990) (figure 2). These rocks consist of: (1) a lower unit of diamictite; (2) a middle unit of dolomite and interbedded slate, argillite, silty dolomite, and fine-grained quartzite; and (3) an unconformably overlying upper unit of quartzite and quartz-pebble conglomerate (figure 3). Christie-Blick (1983) and Doelling and others (1990) assigned the lower diamictite unit to the Late Proterozoic Mineral Fork Formation. Christie-Blick (1983) assigned the middle unit to the Late Proterozoic Kelley Canyon Formation, and Doelling and others (1990) subdivided this formation into a lower dolomite member and an upper slate member. Doelling and others (1990) assigned the upper unit to the Early Cambrian Tintic Quartzite, based on lithologic similarities to rocks exposed in the Wasatch Range (Eardley, 1944). A measured section of the Late Proterozoic rocks is given in the appendix and summarized in figure 4.

Middle Cambrian through Mesozoic strata are not preserved on Antelope Island, probably due to erosion, but clasts of Paleozoic rocks are preserved in unconformably overlying Tertiary conglomerates (Doelling and others, 1990; Willis and Jensen, this volume). Tertiary conglomerate at the north end of the island (figure 2) contains abundant angular clasts of shale and silty limestone that were probably eroded from the

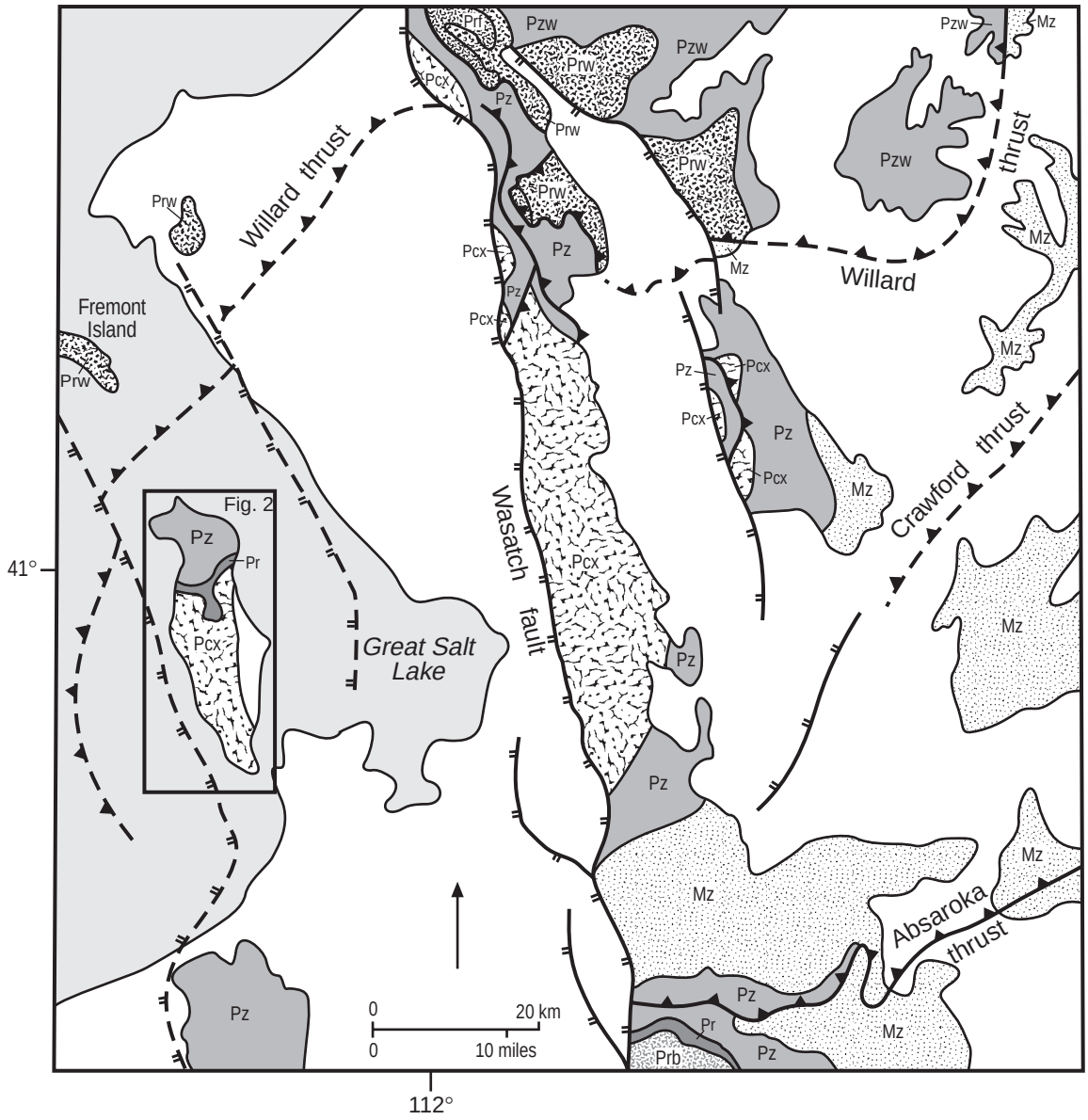

***Figure 1**. Generalized geologic index map of northern Utah showing regional setting of Antelope Island. Units in the eastern section preserved in the Crawford and Absaroka thrust sheets are Pcx- Archean(?) to Early Proterozoic basement rocks, Prb- Middle to Late Proterozoic Big Cottonwood Formation, Pr- thin stratigraphic section of Late Proterozoic strata, Pz- Paleozoic strata, and Mz- Mesozoic strata. Units in the western section preserved in the Willard thrust sheet are Prf- Early Proterozoic Facer Formation, Prw- Late Proterozoic strata, and Pzw- Paleozoic strata.*

middle Cambrian Ophir Shale and Maxfield Limestone, which overlie the Tintic Quartzite. Tertiary conglomerate on the southeastern side of the island (figure 2) contains clasts of upper Cambrian to Mississippian quartzite, dolomite, and limestone up to 11 feet (3 m) in maximum dimension. Clasts in these conglomerates were derived from nearby sources, indicating that early to middle Paleozoic rock must have overlain the Tintic Quartzite on or near the island area prior to Tertiary erosion.

Late Proterozoic and Cambrian sedimentary rocks on Antelope Island were internally deformed and metamorphosed to low grades during the Mesozoic Sevier orogeny (Yonkee, 1992). Many of these rocks display weak to strong cleavage and some intervals display minor folds and faults (Doelling and others, 1990). Yonkee (1992) reported principal strain ratios ranging mostly from about 1.5:1 to 3:1, with principal extension directions at moderate to low angles to bedding. Using this range in axial ratios and extension directions, a unit originally 10 feet (3 m) thick before deformation would range from about 6 to 12 feet (2 to 4 m) thick after deformation. Minor folding and faulting also produced local changes in thicknesses. Thus, measured thicknesses of Late Proterozoic and Cambrian strata include effects of deformation that modified original thicknesses.

OUTCROP CHARACTERISTICS OF SEDIMENTARY ROCKS

Mineral Fork Formation

The Mineral Fork Formation on Antelope Island consists mostly of massive, dark-colored diamictite, with minor amounts of interbedded argillite, quartzite, and conglomerate locally present near the top of the unit (figure 4 and appendix). Clasts constitute 20 to 60 percent of the diamictite in most areas, and sit within a micaceous, gritty matrix (figures 5a and 5b). Cobble-sized clasts are abundant, but clast size is highly variable, ranging up to boulders 7 feet (2 m) across (figure 5a). Clasts vary from angular to rounded, but many were altered and flattened during Mesozoic deformation. Clast types include quartzo-feldspathic gneiss and granite, quartzite (including rare, but distinctive, chrome-green

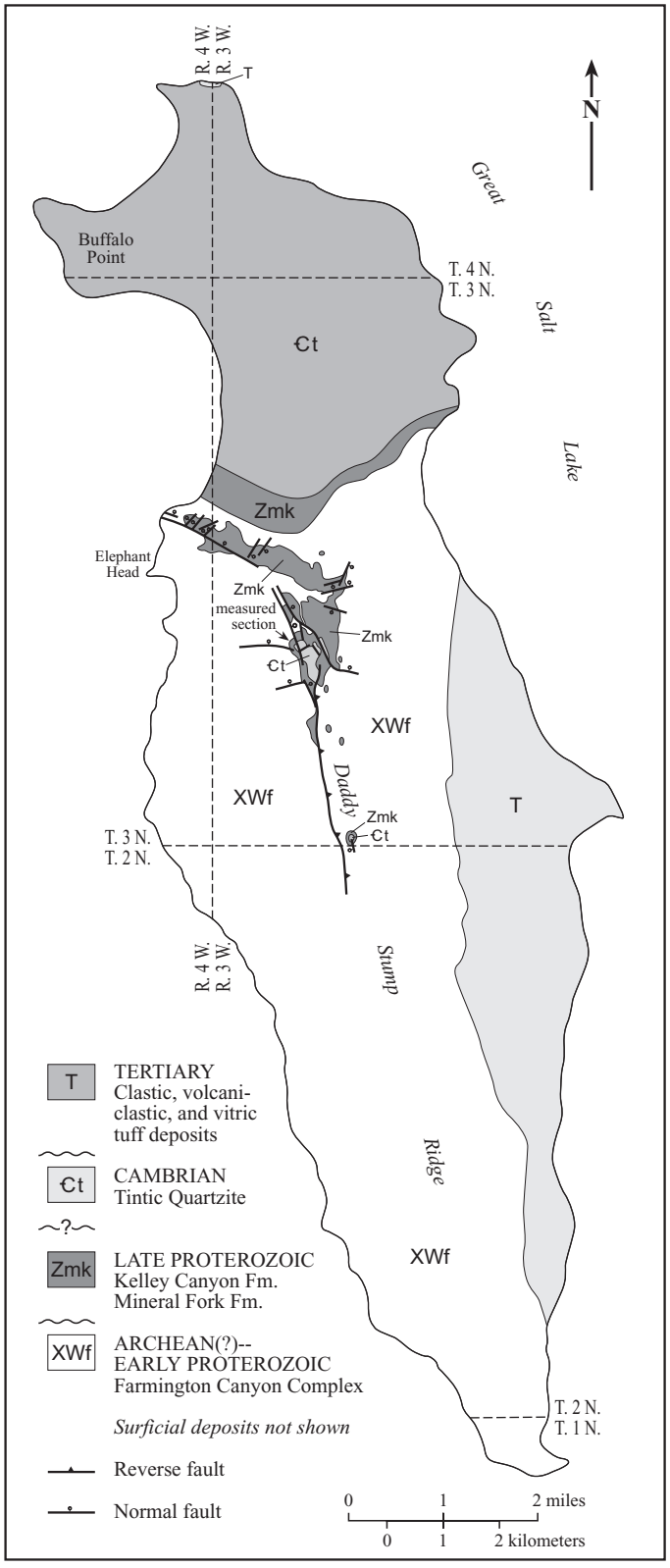

Figure 2. *Generalized geologic map of Antelope Island. Late Proterozoic strata unconformably overlie Archean(?) to Early Proterozoic basement, and are overlain by Cambrian quartzite. Tertiary clastic and volcaniclastic deposits unconformably overlie older units. Location of measured section (appendix) is indicated. Quaternary deposits are not shown. Modified from Doelling and others (1990).*

quartzite), schist, and amphibolite. Relative abundance of clast types varies between outcrops. Gneiss and granite clasts comprise 70 to 95 percent of all clasts greater than 1/2 inch (1 cm) in size; rounded to angular quartzite cobbles to boulders constitute 5 to 30 percent of the larger clasts, and amphibolite clasts are rare. The matrix is black to dark green, micaceous, and contains variable amounts of sand-sized quartz and feldspar. Most diamictite is massive and not sorted, but rare concentrations of pebbles define crude bedding locally. The diamictite has well-developed cleavage that formed during Mesozoic thrusting and is defined by subparallel partings in the matrix and flattened clasts (Yonkee, 1992).

On Antelope Island, the Mineral Fork Formation unconformably overlies Archean(?) to Early Proterozoic crystalline basement rocks, and is overlain sharply by dolomite of the Kelley Canyon Formation. The Mineral Fork Formation varies from 0 to 200 feet (60 m) thick, largely reflecting deposition on an irregular basement surface. A zone 1 to 3 feet thick (0.3-1 m), characterized by disaggregated grains of basement gneiss in a light-green chloritic matrix, is locally preserved along the basement contact and may represent a fossilweathering horizon.

Kelley Canyon Formation

The Kelley Canyon Formation on Antelope Island was informally divided into a lower dolomite member and an upper slate member by Doelling and others (1990). Total thickness of this formation is about 70 to 260 feet (20 to 80 m).

Dolomite Member

The dolomite member consists of fine-grained crystalline dolomite with interbeds of calcareous slate locally near the top of the unit (figure 4 and appendix). The dolomite is light gray to pink where fresh and weathers to form light-gray to yellowish-pink, resistant cliffs that contrast with the underlying diamictite (figure 6a). The member varies from finely laminated to thick bedded, partly reflecting recrystallization (figure 6b). Laminations are locally wavy and define domal structures. The dolomite is generally weakly deformed by fractures, thin quartz- and calcite-filled veins, and open folds. However, spaced cleavage and tight folds with inclined axial planes are locally developed where this unit is more strongly deformed. The member has a relatively uniform thickness of 20 to 30 feet (6 to 9 m) where less deformed. The lower contact with the diamictite is sharp and shows local relief up to 3 feet (1 m).

Slate Member

The slate member consists of thin-bedded, purple, greenish-gray, and reddish-brown, slate, argillite, silty dolomite, and fine-grained quartzite (appendix, figures 4 and 7). The member commonly forms smooth, covered slopes, but is locally well exposed. The lower half of the member consists of multi-colored slate with interbedded calcareous slate and silty dolomite. The upper half consists mostly of purplish to reddish slate and fine-grained quartzite. The member generally displays well-developed slaty cleavage, widespread minor

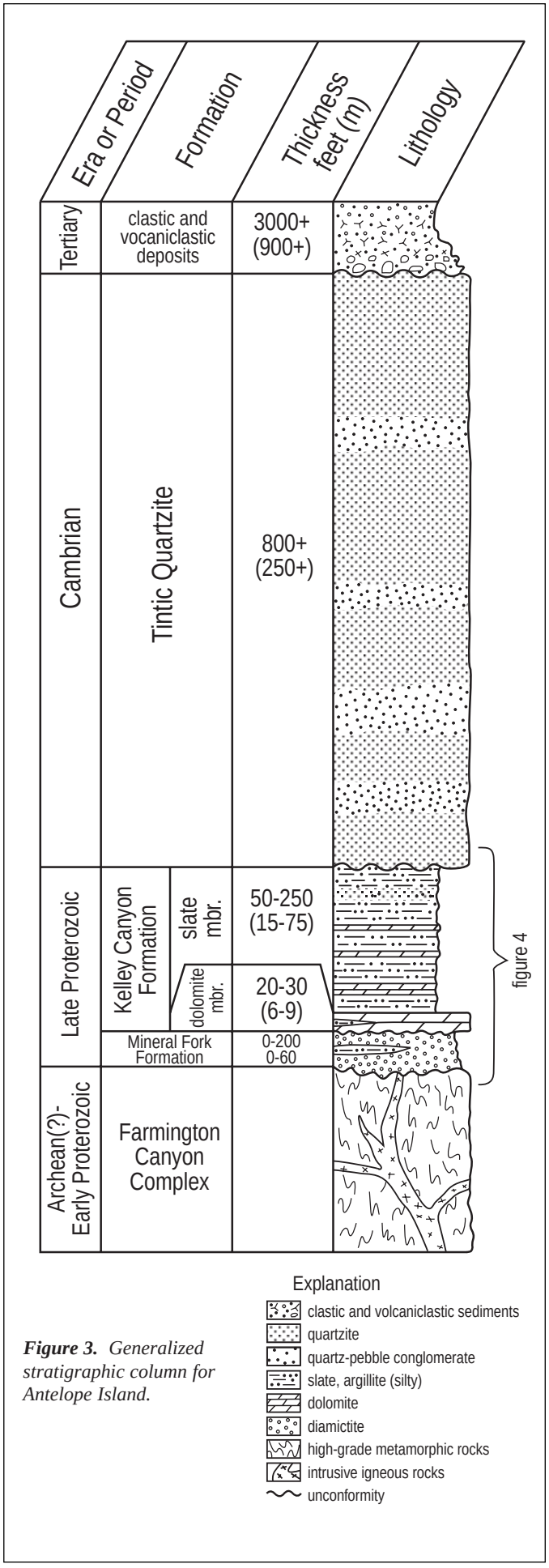

Figure 3. *Generalized stratigraphic column for Antelope Island.*

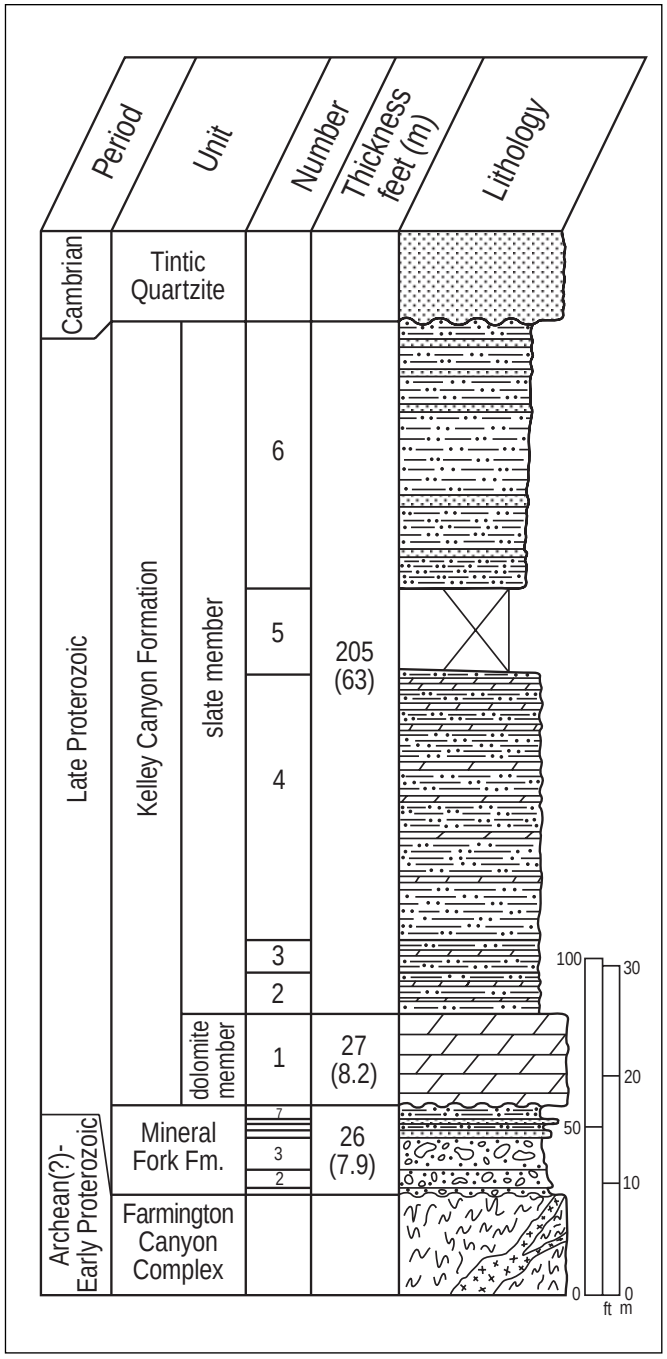

Figure 4. *Stratigraphic column of section measured through Late Proterozoic strata on Antelope Island. Measured section is described in appendix; location is shown on figure 2. See figure 3 for explanation of symbols.*

folds, and locally complex quartz-filled veins that developed during Mesozoic thrusting. Locally, such as at the measured section, cleavage is absent to weakly developed and the term argillite is used (appendix). The contact with the underlying dolomite appears conformable and gradational, with thin beds of dolomite locally interfingering with slate in the lower part of the member. The thickness of the member is difficult to determine due to widespread deformation, but is probably between 50 and 250 feet (15 and 75 m).

Tintic Quartzite

The Tintic Quartzite consists of tan to greenish-gray, fine- to coarse-grained quartzite, with interbeds of quartz-pebble conglomerate (figure 8). Quartzite layers vary from quartz rich, to micaceous, to arkosic. Some quartzite layers are pebbly and grade into conglomerate that contains more than 60 percent clasts. Clasts within conglomerate layers include tan, white, and red polycrystalline quartz, and have maximum dimensions from 0.5 to 4 inches (0.01 to 0.1 m). Fine- to medium-grained quartzite is estimated to constitute about 60 percent of the formation, pebbly quartzite about 20 percent, and conglomerate about 20 percent. The Tintic Quartzite is medium- to thick-bedded, and weathers to form ledgy slopes and blocky cliffs. The quartzite is variably deformed, with locally well-developed cleavage, quartz-filled veins, and minor folds. Cleavage is defined by stretched pebbles and micaceous partings. The contact with the underlying slate member of the Kelley Canyon Formation is sharp, locally marked by a basal conglomerate, and is probably unconformable. The top of the quartzite is not exposed. Widespread deformation and discontinuous exposures make determination of thickness difficult, but the unit is probably in excess of 800 feet (250 m) thick.

MICROSCOPIC CHARACTERISTICS OF SEDIMENTARY ROCKS

Mineral Fork Formation

The diamictite consists of variably deformed and altered polycrystalline clasts of quartzo-feldspathic gneiss and granite, quartzite, schist, and amphibolite that lie in a variably recrystallized, micaceous matrix. Feldspar grains within clasts are variably altered to fine-grained aggregates of muscovite, quartz, and chlorite. Quartz grains within clasts display undulatory extinction, subgrains, and local recrystallization. The matrix consists of fine-grained muscovite and chlorite, with dispersed, angular to rounded, variably stretched quartz and altered feldspar grains. Minor iron oxide is common in the matrix, and some samples contain minor secondary calcite and siderite. Recrystallized quartz and mica aggregates within clasts and preferred orientation of mica and stretched quartz grains in the matrix define cleavage. Shear bands, marked by very fine-grained material with high strain, occur at acute angles to cleavage in some samples, and record localized simple shear. Strain shadows filled with mica and quartz fibers occur around some clasts and larger grains in the matrix. These alteration and deformation features in the diamictite are similar to features observed within shear zones in underlying Archean(?) to Early Proterozoic crystalline basement rocks (Yonkee, 1992).

Figure 5a. *Diamictite of the Mineral Fork Formation with large boulder of quartzite supported in dark, micaceous matrix. Mesozoic cleavage deflects around relatively undeformed quartzite boulder. Granitic and gneiss clasts derived from basement rocks are flattened and altered such that they are difficult to distinguish from the matrix. Backpack (middle left) for scale. Photograph taken on Elephant Head.*

Figure 5b. *Relatively undeformed diamictite of the Mineral Fork Formation east of Elephant Head. Clasts in this photograph range to about 8 inches (20 cm) in diameter.*

Kelley Canyon Formation

Dolomite Member

This member consists of fine-grained, recrystallized dolomite with widely dispersed quartz grains. Dolomite crystals are generally subequant, have sizes from about 0.005 to 0.01 inches (0.015 to 0.3 mm), and form interlocking mosaics. Some samples contain spaced seams enriched in quartz, mica, and iron oxides that define a spaced cleavage.

Slate Member

Slate and argillite of this member are composed of a mixture of fine-grained primary quartz, mica, and feldspar that sit in a very fine-grained, partly recrystallized matrix. Bedding is defined at the microscopic scale by variations in grain size and matrix content. Cleavage crosscuts bedding and is defined microscopically by closely spaced, thin seams that are enriched in mica and iron oxides, and depleted in quartz. These cleavage seams bound less-deformed lozenges of rock. Some mica grains appear recrystallized along seams, and many quartz grains have sutured boundaries adjacent to seams that are probably related to dissolution. Within the lozenges, mica varies from undeformed to kinked, and quartz grains show limited undulatory extinction.

Figure 6a. *Dolomite member of the Kelley Canyon Formation (light-colored outcrop) overlying diamictite and argillite of the Mineral Fork Formation near Elephant Head.*

Figure 6b. *Deformation-induced wavy lamination developed in the dolomite member of the Kelley Canyon Formation near Elephant Head. The dolomite forms light-tan, hackly outcrops. Outcrop is about 5 feet (1.5 m) high.*

Tintic Quartzite

The Tintic Quartzite consists of quartz grains, polycrystalline quartz clasts, and lesser amounts of variably altered feldspar grains that sit in a fine-grained matrix of variably recrystallized quartz, muscovite, and chlorite. The quartzite also contains minor amounts of opaque minerals and detrital mica grains. Quartz grains display widespread undulatory extinction, deformation lamellae, and subgrains, with localized recrystallization concentrated near original grain and clast margins. Feldspar grains are variably fractured and extend into trains of angular fragments. Some feldspar grains are partly altered to fine-grained aggregates of muscovite, quartz, and minor chlorite. Weakly to strongly developed cleavage is defined by stretched quartz grains and clasts, and by preferred orientation of mica in the matrix. Quartz and mica fibers form strain shadows between many feldspar fragments and at ends of larger quartz clasts. Dissolution along sutured quartz grain boundaries and alteration of feldspar may have been sources for material precipitated in the strain shadows.

REGIONAL CORRELATION OF LATE PROTEROZOIC TO EARLY CAMBRIAN STRATA

Two distinct stratigraphic sections exist in northern Utah: an eastern section in which Late Proterozoic strata are generally absent and Paleozoic strata are relatively thin, and a western section containing thick Late Proterozoic and Paleozoic strata (Levy and Christie-Blick, 1989; Christie-Blick, 1997). The western section is preserved in the structurally overlying Willard thrust sheet, which has been translated at least 12 to 24 miles (20-40 km) eastward relative to its footwall (Levy and Christie-Blick, 1989). The eastern section is preserved in the more frontal Crawford and Absaroka thrust sheets, which lie beneath and to the east of the Willard sheet. Sedimentary rocks on Antelope Island have intermediate characteristics and mark a transition between the eastern and western sections (figure 9).

Crittenden and others (1971), Christie-Blick (1982), and Christie-Blick and others (1989), Link and others (1993), and Christie-Blick (1997) have presented correlations of Late Proterozoic to Early Cambrian strata in Utah and surrounding areas. Key elements in correlating stratigraphic sections are the presence of a lower diamictite and volcanic succession, the presence of an upper terrigenous detrital succession that can be divided into lower and upper parts, and the interpretation of possible sequence boundaries. Important sequence boundaries correspond to: (1) a major unconformity at the base of the diamictite succession, (Mineral Fork Formation on Antelope Island); (2) conglomeratic quartzite within incised channels in the upper Caddy Canyon Formation and at the base of the Mutual Formation, separated by distinctive argillite of the Inkom Formation (not present on Antelope Island); and (3) local channeling and conglomerates at the base of Cambrian quartzites (the Tintic Quartzite on Antelope Island).

Western Section

Late Proterozoic to Early Cambrian strata of the western section are divided into three informal intervals for this discussion: a lower interval of diamictite, meta-sandstone, argillite, and meta-volcanic rocks (corresponding to the diamictite and volcanic succession of Link and others, 1993); a middle interval of quartzite and argillite (corresponding to the lower part of the terrigenous detrital succession of Link and others, 1993); and an upper interval of dominantly quartzite (corresponding to the upper part of the terrigenous detrital succession of Link and others, 1993)(figure 9).

The lower interval contains abundant diamictite, fine-grained to conglomeratic, feldspathic to lithic meta-sandstone (or graywacke), and argillite, with some metamorphosed mafic volcanic rocks. This interval is laterally heterogenous and units in different areas include the formation of Perry Canyon, and the Pocatello, Otts Canyon, and Dutch Peak Formations (figure 9). Diamictite exposures locally contain striated clasts and dropstones, and are interpreted to be of glacial-marine origin (Crittenden and others, 1983; Link and others, 1993). Mafic intrusive and extrusive rocks in this interval have geochemical signatures consistent with rifting (Harp-

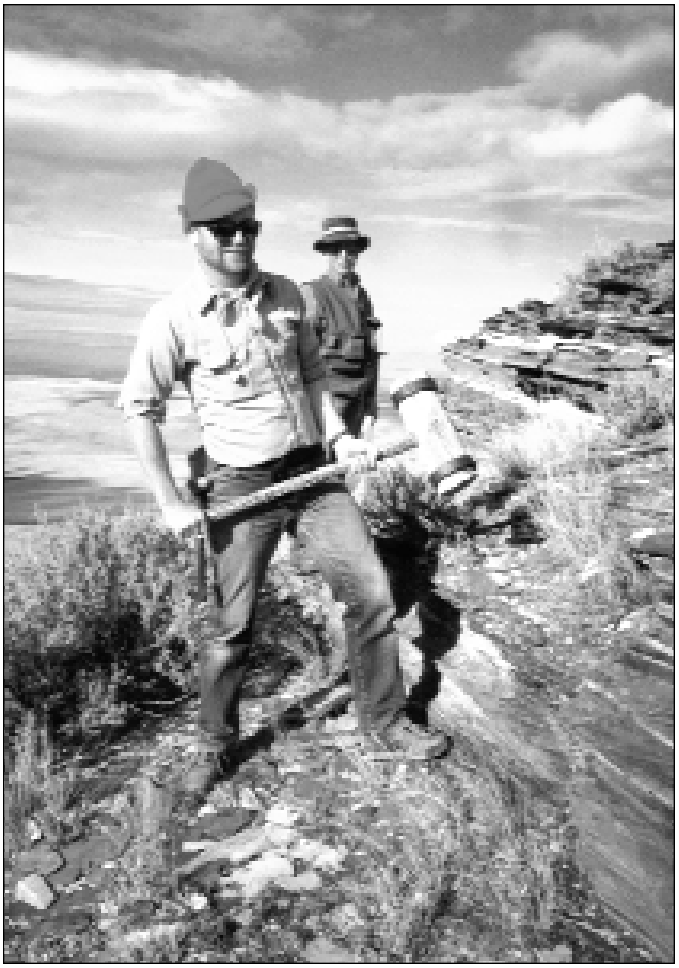

Figure 7. *Well-defined bedding within the slate member of the Kelley Canyon Formation exposed on north end of Daddy Stump Ridge. Mallet was used by early settlers to split slate for roofing and flagstone.*

er and Link, 1986). Although the Utah mafic rocks have not been dated, similar mafic rocks in other parts of the Cordillera are dated at 780 to 720 Ma (Armstrong and others, 1982; Devlin and others, 1988). The bottom of the interval is generally not exposed, but near Willard Peak, Utah, diamictite rests unconformably on metamorphic rocks of the Early Proterozoic Facer Formation. Marine argillite, carbonate, and calcareous siltstone of the Kelley Canyon Formation form the upper part of this interval, and may record sea level rise following glaciation. Overall, this interval probably records glacially influenced, dominantly marine sedimentation in subsiding, locally fault-bounded rift basins (Christie-Blick and others, 1989; Link and others, 1993), followed by glacial melting and sea level rise.

The middle interval consists of Late Proterozoic quartzite and argillite. Interbedded fluvial to shallow marine quartzite and argillite of the Caddy Canyon and Papoose Creek Formations form the lower part of the interval (Christie-Blick and others, 1989). Shallow marine argillite and micaceous, fine-grained quartzite of the Inkom Formation form a distinctive marker in the middle part of this interval, and may record a second pulse of glaciation, possibly at about 600 Ma (Christie-Blick, 1997). Distinctive gray-red to purple-red, fluvial quartzite with local channels in the Mutual Formation

Figure 8. *Pebbly horizons in Tintic Quartzite east of Buffalo Point. Quartz pebbles are flattened in the plane of cleavage.*

provide a regional marker in the upper part of the interval. The interval is locally capped by a thin sequence of sandstone and basalt flows emplaced at 580 Ma (Bond and others, 1985). This interval probably records sedimentation in rift basins, prior to final formation of a passive margin (Link and others, 1993).

The upper interval consists of latest Proterozoic(?) to Early Cambrian shallow marine to fluvial quartzite and quartz-pebble conglomerate. Units in this interval have rather uniform lithologies, but are referred to by a variety of names, including the Geertsen Canyon, Camelback Mountain, and Prospect Mountain Quartzites. Quartzite layers are generally fine- to coarse-grained, arkosic near the base of the interval, and grade into widespread pebbly conglomerate layers. Scolithus tubes occur locally within the upper part of the interval (Crittenden and others, 1971). Locally a conglomerate marks the base of the interval where it channels into the underlying Mutual Formation, corresponding to an interpreted sequence boundary (Link and others, 1993). The quartzite interval is overlain by Middle Cambrian carbonate and shale. Deposition of this quartzite interval and thick overlying Cambrian strata may mark onset of passive margin sedimentation (Link and others, 1993).

Eastern Section

The eastern section is much thinner than the western section, but similarities between the two are apparent and the eastern section can be divided into three corresponding intervals. The eastern section includes: a rarely preserved, thin, lower interval of diamictite; a rarely preserved, thin, middle interval of reddish to purplish quartzite; and a widespread upper interval of quartzite.

The lower interval is represented by the Mineral Fork Formation, which is only locally preserved in the central Wasatch Range. This formation occurs as isolated lenses, locally on striated surfaces, and appears to be of glacial origin (Christie-Blick, 1983; Christie-Blick, 1997). This interval is much thinner, but lithologically similar to the lower part of the diamictite interval in the western section.

The middle interval is locally represented by a very thin

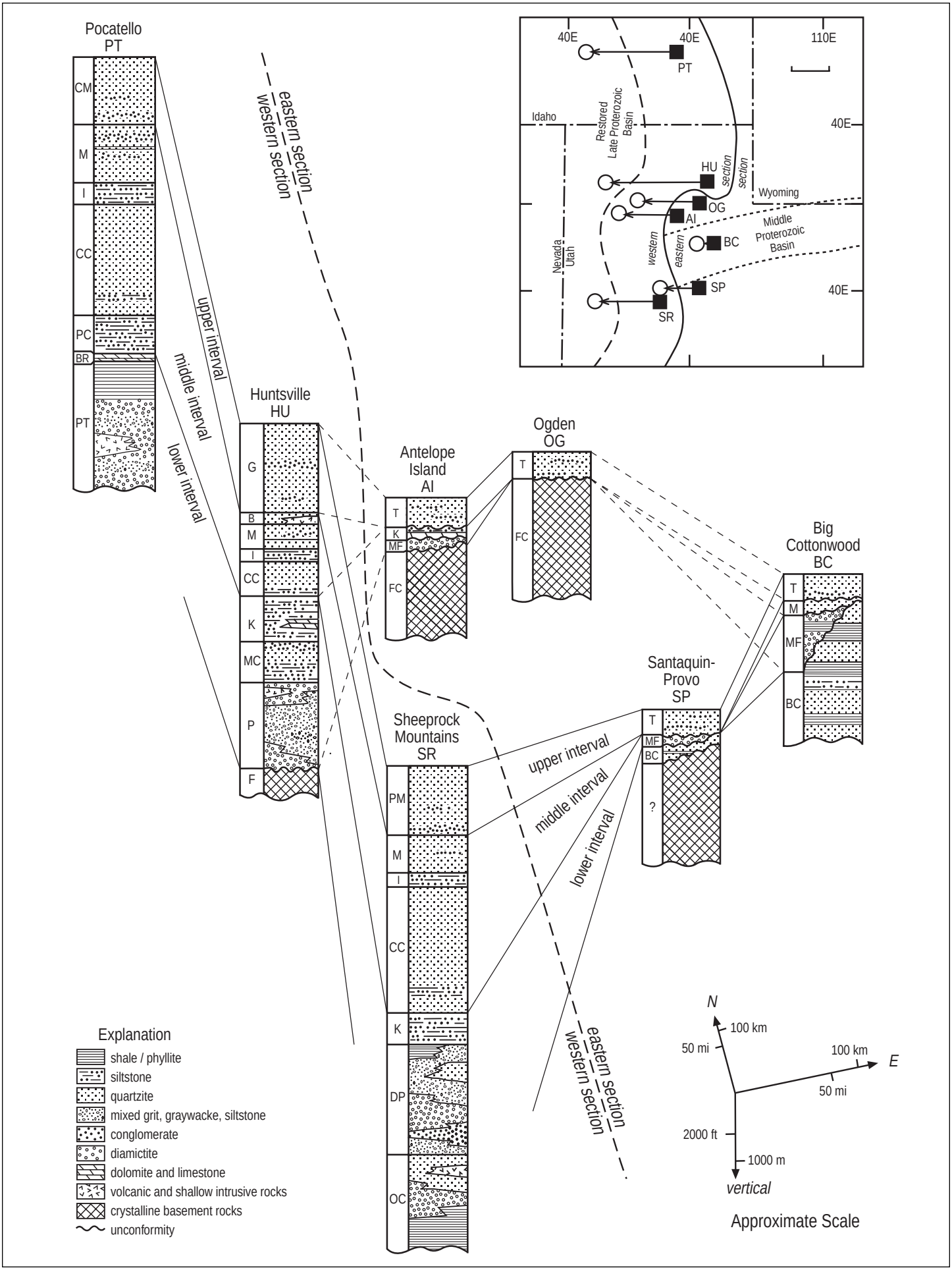

Proterozoic and Cambrian sedimentary and low-grade metasedimentary rocks - Yonkee, Willis, Doelling

stratigraphic section of red to purple quartzite, conglomerate, and variegated shale, which is restricted to the central Wasatch Range. These rocks were assigned to the Mutual Formation by Crittenden and others (1952). This interval is much thinner, but lithologically similar to part of the middle interval in the western section.

An upper interval of quartzite and quartz-pebble conglomerate is widespread in the eastern section. This interval corresponds to the Early Cambrian Tintic Quartzite and is overlain by Middle Cambrian shale and carbonate. The interval is lithologically similar to, but thinner than, the upper quartzite interval in the western section.

Correlation with Antelope Island

Metasedimentary and sedimentary rocks preserved on Antelope Island lie structurally just below the Willard thrust sheet (Yonkee, 1992). These rocks are transitional between rocks of the eastern and western sections and were assigned to the Mineral Fork Formation, Kelley Canyon Formation, and Tintic Quartzite by Doelling and others (1990).

Diamictite of the Mineral Fork Formation on Antelope Island is lithologically similar to, and regionally correlated with, the lower part of the diamictite interval preserved in the western section and locally in the eastern section. Diamictite exposed on Antelope Island and in the Willard thrust sheet (western section) contain abundant granitic and rare but distinctive chrome-green quartzite clasts, consistent with a common source area. The thickness of the diamictite interval on Antelope Island, however, is less than 200 feet (60 m), whereas the thickness of the equivalent formation of Perry Canyon in the Willard thrust sheet is locally greater than 3,300 feet (1,000 m) (figure 9) (Crittenden and others, 1983; Christie-Blick, 1985).

Dolomite, silty dolomite, slate, argillite, and fine-grained quartzite of the Kelley Canyon Formation exposed on Antelope Island are about 70 to 260 feet (20 to 80 m) thick, and probably correlate with the upper part of the lower interval of the western section, which is about 3,000 feet (900 m) thick in the Willard sheet (figure 9). Rocks of similar lithology are not exposed in the eastern section in the Wasatch Range.

Strata equivalent to the middle interval have not been identified on Antelope Island. This interval, however, is about 3,000 to 4,000 feet (900 to 1,200 m) thick in the Willard thrust sheet of the western section.

The Tintic Quartzite unconformably overlies the Kelley Canyon Formation on Antelope Island, and correlates with the previously described upper quartzite intervals of the western and eastern sections. The original thickness on Antelope Island is uncertain, but may have been intermediate between preserved thicknesses of about 4,000 feet (1,200 m) in the western section and about 1,500 feet (450 m) in the eastern section.

◀ ***Figure 9.*** *Regional correlation of Late Proterozoic and Early Cambrian stratigraphy. Inset shows: (1) current locations of areas, filled boxes: (2) restored positions after effects of Tertiary normal faulting and Mesozoic thrusting have been removed, open circles; and (3) location of Middle to early Late Proterozoic Big Cottonwood basin, dotted line. Dashed line on insert and fence diagrams shows approximate restored boundary between thin eastern section and thick western section. Units on the fence diagram are: Upper interval, CM=Camelback Mountain Quartzite, G=Geertson Canyon Quartzite, PM=Prospect Mountain Quartzite, T=Tintic Quartzite; Middle interval, B=Browns Hole Formation, M=Mutual Formation, I=Inkom Formation, CC=Caddy Canyon Quartzite, PC=Papoose Creek Formation; and Lower interval, BR=Blackrock Canyon Limestone, PT=Pocatello Formation, K=Kelley Canyon Formation, MC=Maple Canyon Formation, P=formation of Perry Canyon, MF=Mineral Fork Formation, DP=Dutch Peak Formation, OC=Otts Canyon Formation. Other units are F=Facer Formation, BC=Big Cottonwood Formation, FC=Farmington Canyon Complex. Based on data from: Pocatello, Idaho (PT) (Crittenden and others, 1971); Huntsville, Utah (HU) (Crittenden and others, 1971; Crittenden and Sorensen, 1985); Sheeprock Mountains (SR) (Christie-Blick, 1982); Antelope Island (AI) (this study; Doelling and others, 1990); Ogden, Utah (OG) (Eardley, 1944); and Big Cottonwood Canyon (BC) (Crittenden and others, 1952; Christie-Blick, 1985); Santaquin-Provo, Utah (SP) (Hintze, 1962, 1978).*

DISCUSSION

Late Proterozoic strata thicken rapidly westward between the restored positions of the Antelope Island and the Huntsville areas, and between the restored positions of the Santaquin-Provo and Sheeprock Mountain areas (figure 9). Late Proterozoic strata are absent or very thin in most of the Wasatch Range to the east, but up to 15,000 feet (4,500 m) of Late Proterozoic strata accumulated to the west. The zone of rapid westward thickening marks the eastern boundary of a regional basin that initially formed during the Late Proterozoic (Levy and Christie-Blick, 1989). Basalt flows in the lower part of the interval and fault-bounded sub-basins are consistent with subsidence and deposition following an early period of rifting, probably at about 750 Ma (Link and others, 1993). This early rift basin probably formed prior to Cambrian rifting and development of a passive margin, and had an irregular boundary with a basement promontory near the latitude of Antelope Island.

The Early Cambrian quartzite interval also thickens towards the west, but is more widespread than the Late Proterozoic units, marking an enlargement in the area of sedimentation from the Late Proterozoic to the Early Cambrian (figure 9). Basalt flows just below and a sequence boundary at the base of the quartzite interval may mark a renewed period of rifting at about 550 Ma, followed by rapid subsidence and development of a passive margin along the western margin of North America during the Cambrian (Link and others, 1993).

The restored positions of the eastern and western sections indicate a basement promontory existed at the latitude of the central Wasatch Mountains (from the Ogden to the Santaquin-Provo sections) prior to Mesozoic thrusting (figure 9). This region was the site of localized basement imbrication during the Sevier orogeny (Yonkee, 1992). The Willard thrust sheet carried the thicker western section and a major thrust ramp formed near the transition to the thinner eastern section. Antelope Island lies near this transition and experienced both basement imbrication and footwall deformation near a probable ramp in the Willard thrust. Thus the configuration of the sedimentary wedge appears to have had important effects on

development of Mesozoic thrust-related structures.

ACKNOWLEDGMENTS

Mark Jensen, John Hand, and Hellmut Doelling (co-author) measured the section described herein. Nicholas Christie-Blick, Paul Link, and Martin Sorensen provided suggestions on nomenclature for Proterozoic rocks on Antelope Island. Doug Sprinkel and Jon King reviewed this manuscript and provided many helpful suggestions.

REFERENCES

Armstrong, R.L., Eisbacher, G.H., and Evans, P.D., 1982, Age and stratigraphic-tectonic significance of Proterozoic diabase sheets, Mackenzie Mountains, northwestern Canada: Canadian Journal of Earth Sciences, v. 19, p. 316-323.

Bond, G.C., Christie-Blick, Nicholas, Kominz, M.A., and Devlin, W.J., 1985, An early Cambrian rift to post-rift transition in the Cordillera of western North America: Nature, v. 316, p. 742-745.

Christie-Blick, Nicholas, 1982, Upper Proterozoic and Lower Cambrian rocks of the Sheeprock Mountains, Utah, Regional correlation and significance: Geological Society of America Bulletin, v. 93, p. 735-750.

Christie-Blick, Nicholas, 1983, Glacial-marine and subglacial sedimentation, Upper Proterozoic Mineral Fork Formation, Utah, *in* Molnia, B.F., editor, Glacial-marine Sedimentation: New York, Plenum Press, p. 703-775.

Christie-Blick, Nicholas, 1985, Upper Proterozoic glacial-marine and subglacial deposits at Little Mountain, Utah: Brigham Young University Geology Studies, v. 32, p. 9-18.

Christie-Blick, Nicholas, 1997, Neoproterozoic sedimentation and tectonics in west-central Utah, *in* Link, P.K., and Kowallis, B.J., editors, Proterozoic to Recent stratigraphy, tectonics, and volcanology, Utah, Nevada, southern Idaho and central Mexico: Brigham Young University Geology Studies, v. 42, part 1, p. 1-30.

Christie-Blick, Nicholas, Mount, J.F., Levy, Marjorie, Signor, P.W., and Link, P.K., 1989, Late Proterozoic and Cambrian tectonics, sedimentation, and record of Metazoan radiation in the Western United States: 28th International Geological Congress Field Trip Guidebook T331, 113 p.

Crittenden, M.D., Jr., Sharp, B.J., and Calkins, F.C., 1952, Geology of the Wasatch Mountains east of Salt Lake City, Parleys Canyon to Traverse Range, *in* R.E. Marsell, editor, Geology of the Central Wasatch Mountains, Utah: Utah Geological Society Guidebook, no. 8, p. 1-37.

Crittenden, M.D., Jr., Christie-Blick, Nicholas, and Link, P.K., 1983, Evidence for two pulses of glaciation during the late Proterozoic in northern Utah and southeastern Idaho: Geological Society of America Bulletin, v. 94, p. 437-450.

Crittenden, M.D., Jr., Schaeffer F.E., Trimble, D.E., and Woodward, L.A., 1971, Nomenclature and correlation of some upper Precambrian and basal Cambrian sequences in western Utah and southeastern Idaho: Geological Society of America Bulletin, v. 82, p. 581-602.

Crittenden, M.D., Jr., and Sorensen, M.L., 1985, Geologic map of the Mantua quadrangle and part of the Willard quadrangle, Box Elder, Weber, and Cache Counties, Utah: U.S. Geological Survey Map I-1605, scale 1:24,000.

Devlin, W.J., Brueckner, H.K., and Bond, G.C., 1988, New isotopic data and a preliminary age for volcanics near the base of the Windemere Supergroup, northeastern Washington, U.S.A.: Canadian Journal of Earth Sciences, v. 25, p. 1906-1911.

Doelling, H.H., Willis, G.C., Jensen, M.E., Hecker, Suzanne, Case, W.F., and Hand, J.S., 1990, Geologic map of Antelope Island, Davis County, Utah: Utah Geological and Mineral Survey Map 127, 27 p., scale 1:24,000.

Eardley, A.J., 1944, Geology of the north-central Wasatch Mountains, Utah: Geological Society of America Bulletin, v. 55, p. 819-894.

Harper, G.D., and Link, P.K., 1986, Geochemistry of Upper Proterozoic rift-related volcanics, northern Utah and southeastern Idaho: Geology, v. 14, p. 864-867.

Hintze, L.F., 1962, Precambrian and Lower Paleozoic rocks of north central, *in* Hintze, L.F., editor, Geology of the southern Wasatch Mountains, Utah: Brigham Young University Geology Studies v. 9, part 1, p. 8-16.

Hintze, L.F., 1978, Geologic map of the Y Mountains area east of Provo, Utah: Brigham Young University Geology Studies Special Publication 5.

Hintze, L.F., 1988, Geologic history of Utah: Brigham Young University Geology Studies Special Publication 7, 202 p.

Larsen, W.N., 1957, Petrology and structure of Antelope Island, Davis County, Utah: Salt Lake City, University of Utah, Ph.D dissertation, 142 p., map scale 1:24,000.

Levy, Marjorie, and Christie-Blick, Nicholas, 1989, Pre-Mesozoic palinspastic reconstruction of the eastern Great Basin (western United States): Science, v. 245, p. 1454-1462.

Link, P.K., Christie-Blick, Nicholas, Stewart, J.M.G., Devlin, W.J., and Levy, Marjorie, 1993, Late Proterozoic strata of the United States Cordillera, *in* Reed, J.C., Bickford, M.E., Houston, R.S., Link, P.K., Rankin, D.W., Sims, P.K., and Van Schmus, W.R., editors, Precambrian: Conterminous U.S.: Geological Society of America, The Geology of North America, v. C-2, p. 537-595.

Yonkee, W.A., 1992, Basement-cover relations, Sevier orogenic belt, northern Utah: Geological Society of America Bulletin, v. 104, no. 3, p. 280-302.

APPENDIX. Measured section through Upper Proterozoic Kelley Canyon and Mineral Fork Formations on Antelope Island

Measured east of Mormon Rocks on the west-facing ridge about 0.25 mile (0.4 km) east of the peak marked 5,576 feet (SE1/4, SE1/4, section 19, T. 3 N., R. 3 W., Antelope Island 7.5' quadrangle). Measured November 2, 1987.

Tintic Quartzite (not measured)

The upper contact of the slate member of the Kelley Canyon Formation is poorly exposed; the slate member is overlain by quartzite rubble.

Kelley Canyon Formation

Unit		Thickness feet (meters)
Slate member		
	(note: the primary term argillite is used in this measured section because slaty cleavage is only weakly developed)	
6	Interbedded argillite and fine-grained quartzite; pale-green (10G6/2), very dusky red-purple (5RP2/2) and dark-gray (N3); laminated to thin-bedded; weathers to sharp, platy ledges; cleavage is N. 71° W., 25° NE.	79.0 (24.1)
5	Covered slope; float is from unit 6.	25.0 (7.5)
4	Argillite, with minor, very thin interbeds of dolomite and calcareous argillite; very dusky red-purple (5RP2/2) to grayish-red-purple (5RP4/2); yellowish-gray (5Y7/2) weathered; thinly laminated to thin-bedded; some beds contain greenish reduction spots; light-brown (5YR 6/4) dolomitic beds increase in abundance above 40 feet (12 m) from base of unit and become dominant near top of unit; cleavage is N. 67° W., 14° NE.	79.0 (23.7)
3	Interbedded silty dolomite and argillite; greenish-gray (5GY6/1) weathered; finely laminated to thin-bedded; dolomitic layers slightly more resistant and stand as thin ribs on cliff; contains hematite, malachite, and minor chalcopyrite and pyrite coating.	9.5 (2.9)
2	Interbedded dolomite and argillite; pinkish-gray (5YR8/1); weathers grayish orange (10YR7/4) to grayish red (5R4/2); thinly laminated to thin-bedded (laminations less than 0.04 inch to about 3 inches [0.1-8 cm] thick); contains hematite blebs in dolomite beds.	12.3 (3.7)
	Total thickness of slate member	**204.8 (61.4)**
Dolomite member		
1	Dolomite; pinkish-gray (5YR8/1); weathers to grayish orange (10YR7/4); very finely crystalline; thin to medium wavy bedding; forms massive cliffs; appears finely fractured; contains hematite blebs, some sandy beds, and dendritic pyrolusite; lower contact is sharp, with 2 or more feet (0.6+ m) of local relief.	27.4 (8.2)
	Total thickness of dolomite member	**27.4 (8.2)**
	Total thickness of Kelley Canyon Formation	**232.2 (69.7)**

Mineral Fork Formation

Unit		Thickness feet (meters)
7	Interbedded argillite and quartzite; yellowish-gray (5Y7/2) to moderate yellowish-green (10GY6/2); weathers grayish yellow green (5GY7/2) to medium dark gray (N4); forms recess in cliff; beds in upper part of unit are thicker and quartzitic.	3.7 (1.1)
6	Quartzite; grayish-black (N2); weathers slightly lighter; medium- to coarse-grained; fines upward; indistinctly cross-bedded; forms a resistant blocky ledge.	1.7 (0.51)
5	Argillite; dark-gray (N3) with moderate-greenish-yellow (10Y7/2) silty partings; noncalcareous; appears to contain ripple marks; platy weathering.	2.1 (0.63)
4	Quartzite; medium-dark-gray (N4) and medium-gray (N5); weathers grayish orange (10YR7/4); fine-grained; well-indurated; contains clasts mostly less than 1 inch (2.5 cm) in diameter; thick-bedded; blocky; forms a small ledge; some clasts appear flattened; may be slightly chloritic.	2.2 (0.66)
3	Diamictite; yellowish-gray (5Y7/2) weathered with random rust-colored spots on surface; matrix is very coarse grained to gritty; well-indurated; clasts mostly subangular with diameters up to 18 inches (45 cm); gneissic to granitic clasts are subangular; quartzite clasts are well rounded; gneissic clast boundaries are indistinct; some clasts appear elongated; unbedded to indistinct bedding; forms weaker ledges than underlying unit; near top this unit becomes platy and less resistant; contains manganese and iron oxide coating along fractures.	9.7 (2.9)
2	Diamictite; yellowish-gray (5Y7/2) weathered; matrix is medium grained to gritty (coarser than underlying unit); matrix supported; clasts range up to 9 inches (23 cm) in maximum dimension; clasts and matrix are very poorly sorted to unsorted and clasts and matrix grade into each other; forms resistant ledges; contains patches of reddish iron staining on surface.	5.7 (1.7)
1	Diamictite; medium-dark gray (N4) fresh; olive-black (5Y2/1) weathered; very fine- to fine-grained matrix; noncalcareous; clasts are mostly subangular and range in size from grit to 6 inches (21 cm); clasts consist of quartzite (various colors), pegmatitic granitic gneiss, and red granitic gneiss; some clasts show chloritization; well-indurated; contains rusty minerals (possibly siderite) as small blebs; rock shows evidence of shearing; lower contact is a sharp undulating surface locally showing up to 3 feet (1 m) of relief; joints noted in underlying unit pass across contact without deviation, but the gneissic foliation stops at the contact.	1.5 (.45)
	Total thickness of Mineral Fork Formation	**26.6 (8.0)**

Farmington Canyon Complex

Granitic gneiss; blackish-red (5R2/2) fresh; grayish red (5R4/2) and dark reddish brown (10R3/4) on weathered surfaces; medium-grained; moderately foliated; massive; resistant; forms craggy outcrops; has local chloritic alteration; cut by fractures with orientations: N. 2° E., 62° E; N. 10° W., 80° NE; and N. 60° E., 48° NW; contact with overlying diamictite is nonconformable.

TERTIARY ROCKS OF ANTELOPE ISLAND, DAVIS COUNTY, NORTHERN UTAH

by
Grant C. Willis and Mark E. Jensen[1]
Utah Geological Survey

[1]now at Utah Department of Environmental Quality, Division of Drinking Water
P.O. Box 144830, 150 N., 1950 W.,
Salt Lake City, Utah 84114-4830

ABSTRACT

Stratified Tertiary rocks are exposed in two areas on Antelope Island. They are more than 2,000 feet (600 m) thick along the southeast side, and are up to 760 feet (230 m) thick at the north end. In addition, a few small felsic dikes of assumed Tertiary age cut Precambrian rock near the south end of the island.

On the southeast side, Tertiary strata are divided into three units: lower and upper members of a conglomeratic unit, and the Salt Lake Formation. The lower member consists of at least 510 feet (153 m) of: (1) basal conglomerate with carbonate and quartzite clasts up to 11 feet (3.4 m) in diameter in a matrix of gritstone derived from the underlying Precambrian Farmington Canyon Complex, (2) conglomerate composed of metamorphic clasts and matrix from the Farmington Canyon, and (3) stratified bentonitic mudstone. The upper member consists of at least 140 feet (42 m) of polymictic conglomerate with carbonate, quartzite, high-grade metamorphic, and volcanic clasts interbedded with thin beds of lacustrine limestone and bentonitic mudstone. The Salt Lake Formation consists of at least 1,800 feet (550 m) of volcanic ash, tuffaceous marl, mudstone, and minor conglomerate.

The strata at the north end of the island consist of conglomerate and breccia with coarse, angular clasts of shale, limestone, dolomite, and quartzite, that are interbedded with thick beds of volcanic ash, and are mapped as Salt Lake Formation.

Regional correlation suggests that the lower conglomeratic member is late Paleocene to middle Eocene in age. Rounded volcanic clasts and stratified, biotite-bearing, bentonitic mudstone from the upper conglomerate member yielded biotite K-Ar ages of 42.9±1.7, 49.2±1.9, and 38.8±1.5 Ma (late Eocene), and were probably deposited during the late Eocene to middle Oligocene. Strata mapped as Salt Lake Formation are probably between 11 and 8 million years old based on chemical correlations of tephra samples using electron microprobe analyses. The Salt Lake Formation strata predate most structural tilting of the island.

Lithologic variations in the sedimentary clasts indicate that most were derived from the lower plate of the Willard thrust fault. The Willard thrust, which was above rocks now exposed on the island, may have formed a lateral ramp from Cambrian rocks near the north end of the island to Mississippian rocks near the south end.

INTRODUCTION

Tertiary sedimentary and volcanic outcrops are scattered throughout northern Utah (figure 1). On Antelope Island, Tertiary strata are preserved in the southeast part of the island, and on the north tip (figure 2). In addition, a few small felsic dikes of assumed Tertiary age are exposed near the south tip of the island. In this study we measured, described, and attempted to date the Tertiary rocks and place them in the context of the Tertiary geologic evolution of northern Utah.

Data presented here were gathered as part of detailed geologic mapping in 1987, 1988, and 1990 by the Utah Geological Survey (Doelling and others, 1990) to provide geologic information to the Utah Division of Parks and Recreation for developing a master plan for Antelope Island State Park.

Antelope Island is a mountain range in the south Great Salt Lake. The island is about 5 miles (8 km) wide and 15 miles (24 km) long, and 15 miles (24 km) west of the Wasatch Range of north Utah (figure 1). Exposed rocks are primarily Precambrian high-grade metamorphic and intrusive rocks of the Farmington Canyon Complex (Yonkee, Willis, and Doelling, this volume [a]), overlain by about 1,000 feet (300 m) of Late Proterozoic and Cambrian strata (Yonkee, Willis, and Doelling, this volume [b]). Low-grade metamorphism and related semi-brittle deformation associated with Cretaceous thrust faulting deformed the Precambrian and Cambrian rocks (Doelling and others, 1990; Yonkee, 1992). Locally, Tertiary strata were deposited on a major erosional surface cut across the older rocks. The island is part of a structural block that is bounded by normal faults of the Basin and Range physiographic province, and was tilted up to 45 degrees eastward during late Cenozoic extension (figure 3). Adjacent basins are filled with as much as 15,000 feet (4,600 m) of upper Tertiary and Quaternary sedimentary and volcanic rock (Bortz and others, 1985). Much of the island is mantled by late Pleistocene Lake Bonneville lacustrine deposits and post-Bonneville alluvial deposits.

Previous Work

Bywater and Barlow (1909) prepared a generalized geo-

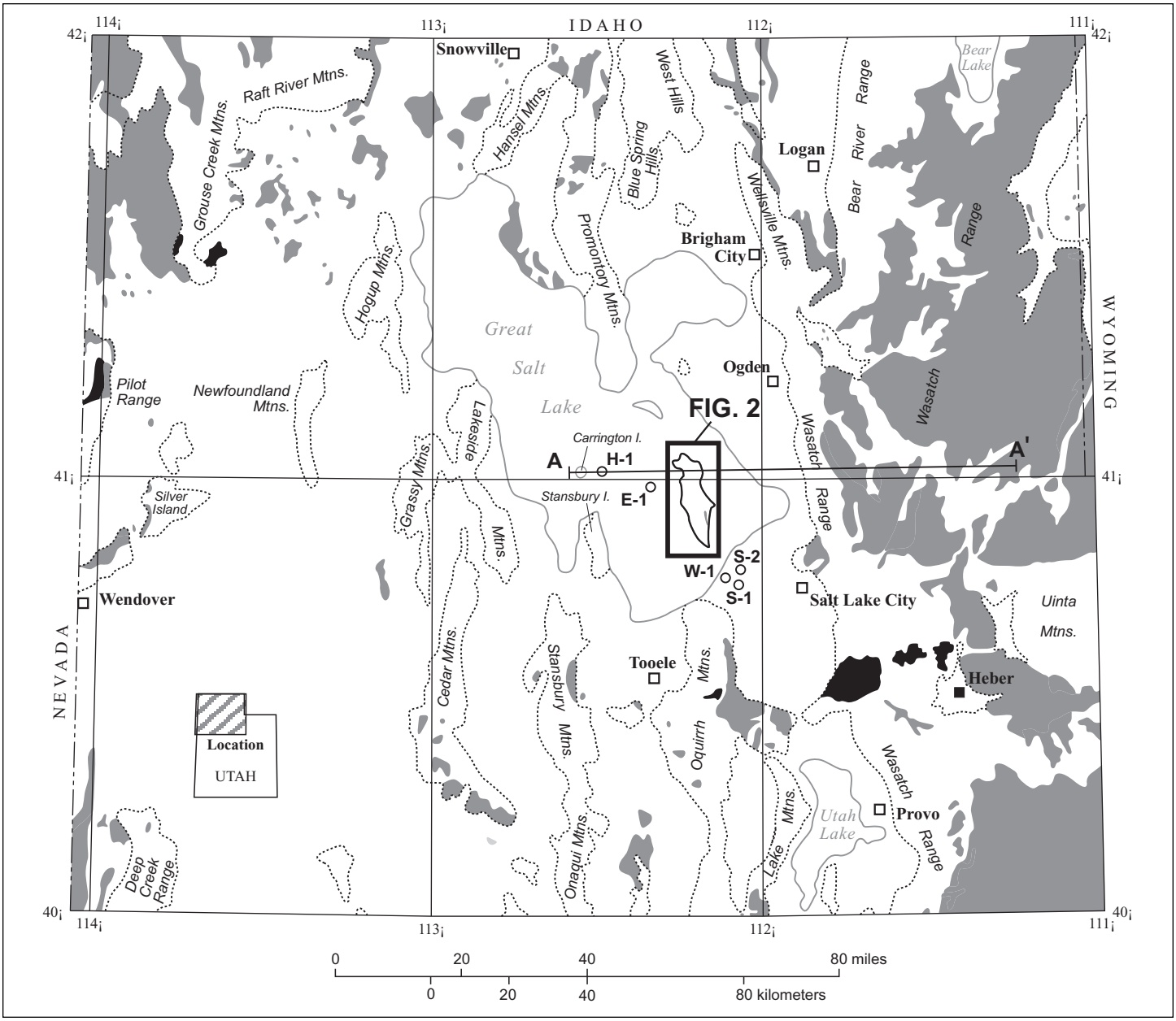

Figure 1. *Index map of northern Utah showing the location of Antelope Island, locations of geographic features and drill holes discussed in text, outcrops of Tertiary rocks (gray), and igneous intrusions (black), and location of cross section A-A' (figure 3). Modified from Hintze and Stokes, 1964.*

logic map of Antelope Island. They did not mention outcrops of Tertiary rocks, but they noted boulders of Carboniferous age, which we interpret as being eroded from Tertiary conglomerate beds. Larsen (1957) made the first detailed map of the island. He described two Tertiary rock units and concentrations of boulders, all of which he lumped into one map unit he called Wasatch Formation. Moore and Sorensen (1979) included Tertiary rocks on Antelope Island in a broadly defined unit called "siliceous conglomerate, sandstone, tuffaceous sandstone, and fresh-water limestone" that they described as Paleocene to Oligocene in age on the Tooele 1 by 2 degree quadrangle. Doelling and others (1990) mapped the island at 1:24,000 and divided Tertiary rocks into three map units: lower and upper members of a conglomeratic unit, and the Salt Lake Formation. This report is an outgrowth of that mapping.

Key studies of Tertiary strata of northern Utah include Eardley (1955), Heylmun (1965), and McDonald (1976). Bryant and others (1989a) conducted fission track and K-Ar dating of Tertiary strata from northern Utah, including one sample from Antelope Island. Miller (1990) and Miller and others (in press) summarized Mesozoic and Cenozoic tectonic evolution of the northeastern Great Basin. (This paper is based on work completed through 1991; some subsequent publications are not considered in this study).

Nomenclature

Tertiary strata in northern Utah have been referred to by many names since Hayden (1869) proposed the terms "Wasatch Group" and "Salt Lake Group" (for example, Eardley, 1955; Slentz, 1955; Heylmun, 1965; Nelson, 1971; Mann, 1974; Danzl, 1985; Miller, 1990). These names have not been consistently or accurately applied, resulting in con-

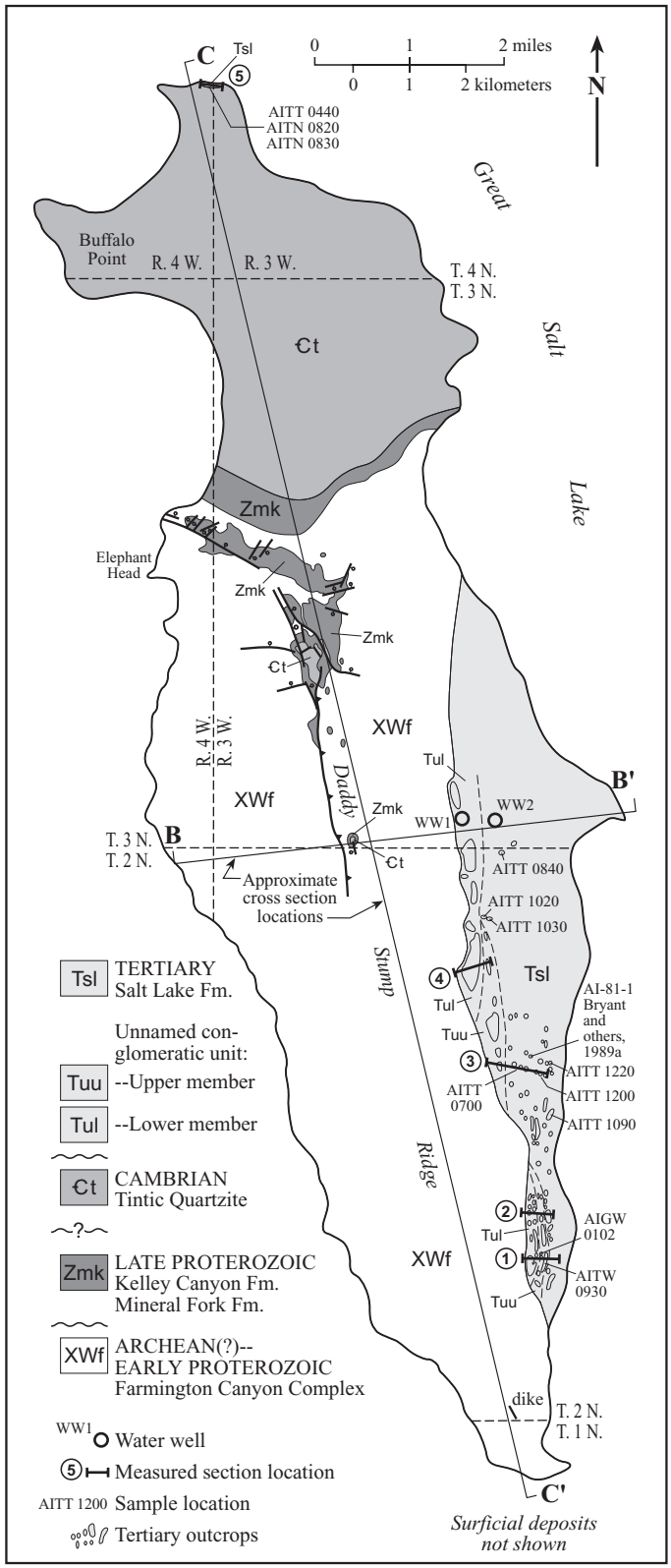

Figure 2. *Simplified bedrock geologic map of Antelope Island emphasizing Tertiary outcrops (after Doelling and others, 1990). Tertiary outcrops are outlined. Contacts between Tertiary units are shown with dashed lines. Tertiary units are: Tul-lower conglomeratic member, Tuu-upper conglomeratic member, Tsl-Salt Lake Formation. Labels S1 to S5 indicate locations of measured sections 1 to 5. WW1 and WW2 mark the location of two water wells that penetrated Tertiary strata (figure 13). K-Ar, fission track, and tephrochronology sample localities discussed in the text are labeled. Approximate locations of schematic cross sections B-B' and C-C' (figure 15) are shown.*

fusion. For this reason, many workers have chosen to use informal lithologic names rather than formal names for the strata (for example: Heylmun, 1965; Oviatt, 1986; Van Horn and Crittenden, 1987; Doelling and others, 1990; Miller and others, 1991).

The term "Wasatch Group" was first applied to variegated sandstone and clay in southwest Wyoming that Hayden (1869) considered middle Tertiary in age. The term "Wasatch Formation" (Veatch, 1907) is also used. In Utah, Wasatch Formation and Group are used interchangeably for dominantly coarse clastic strata of assumed late Paleocene to Eocene age. Typically in northwest Utah west of the Wasatch Range, the lower contact is an angular unconformity cut across Mesozoic or older strata. East of the Wasatch front, the Wasatch Formation typically conformably or disconformably overlies conglomerate and conglomeratic sandstone strata of Late Cretaceous or Paleocene age (Ryder and others, 1976; Bryant and others, 1989b; Franczyk and others, 1990; Yonkee, 1990, 1992). The upper contact is poorly defined in most parts of northern Utah.

The term “Salt Lake Group” was used by Hayden (1869) for outcrops in the Morgan Valley area of northeast Utah. The term has since been applied in northern Utah and southern Idaho to strata of variable lithology and widely ranging age (Eardley, 1944). As with the Wasatch strata, the terms “formation” and “group” have been used interchangeably. In general, the Salt Lake Formation refers to lithologically variable silicic volcanic, lacustrine, and clastic extensional basin fill of assumed Miocene and Pliocene age. Because many exposures are poorly dated, the term may have been locally applied to Eocene, Oligocene, or Pleistocene rocks.

In northern Utah, the interval between the Wasatch and Salt Lake Formations is represented by various volcanic, volcaniclastic, clastic, and lacustrine deposits, or by an unconformity. Some of these localized deposits have formal names, whereas most do not.

DESCRIPTION OF TERTIARY ROCKS ON ANTELOPE ISLAND

More than 2,000 feet (600 m) of Tertiary rocks crop out on the southeast slope of Antelope Island, and about 760 feet (230 m) crop out on the north tip of the island (figure 2; figure 4). Approximately half of the southeast exposures and all of the north exposures were created during excavation for fill during the 1970s and 1980s. In many places in the south area, excavations and later recontouring modified outcrops to the extent that interpretations are difficult. Outside the excavations, Pleistocene Lake Bonneville deposits cover much of the Tertiary strata. The following descriptions and correlations are from five sections (S1 through S5) measured across the outcrops (figures 2 and 4, and appendix).

Tertiary rocks on the island overlie the Precambrian Farmington Canyon Complex and the Cambrian Tintic Quartzite. The contact is not exposed, except in one small equivocal location on the north end. However, the contact is probably an unconformity in most areas rather than a fault since basal Tertiary conglomerates contain locally derived metamorphic clast assemblages, and because the scattered locations of Tertiary outcrops would dictate a highly irregular

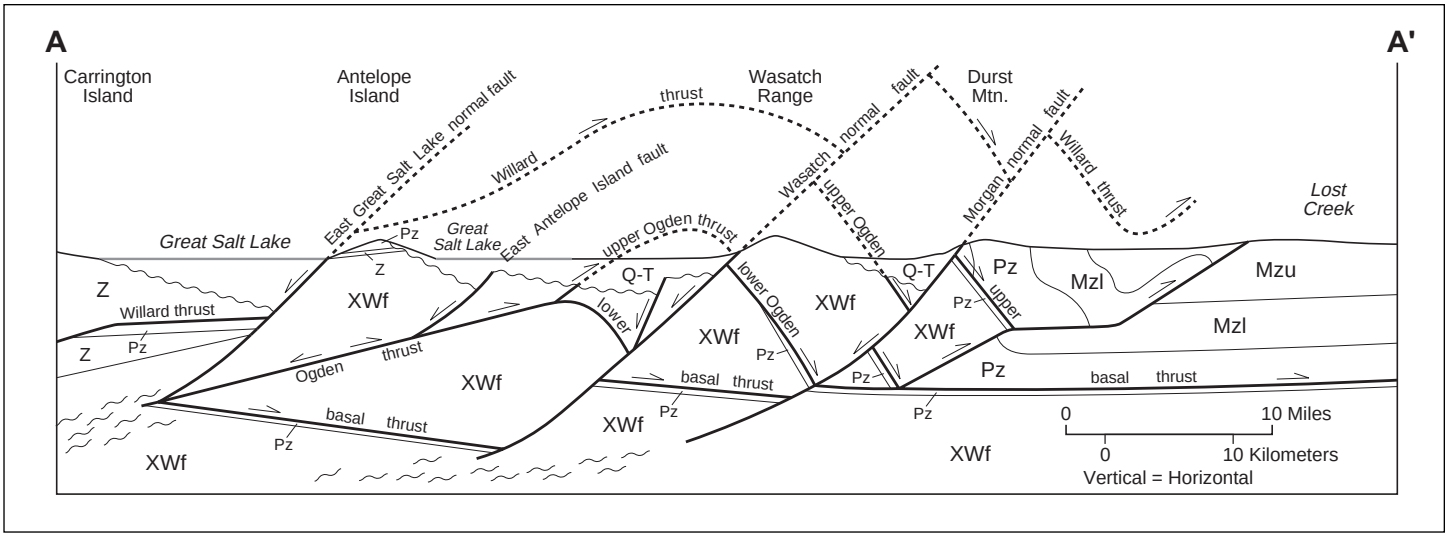

Figure 3. *Schematic regional cross section across Antelope Island from near Stansbury Island to the east flank of the Wasatch Range showing major thrust and low- and high-angle normal faults. Tertiary strata on Antelope Island dip about 35 degrees east. Antelope Island is on the west flank of the Wasatch culmination, a large anticlinal stack of thrust plates. Abbreviation: XWf - Archean? to Early Proterozoic Farmington Canyon Complex, Z - Late Proterozoic strata, Pz - Paleozoic strata, Mzl - lower Mesozoic strata, Mzu - upper Mesozoic strata, QT - Quaternary-Tertiary basin-fill deposits. From W.A. Yonkee, written communication, 2000.*

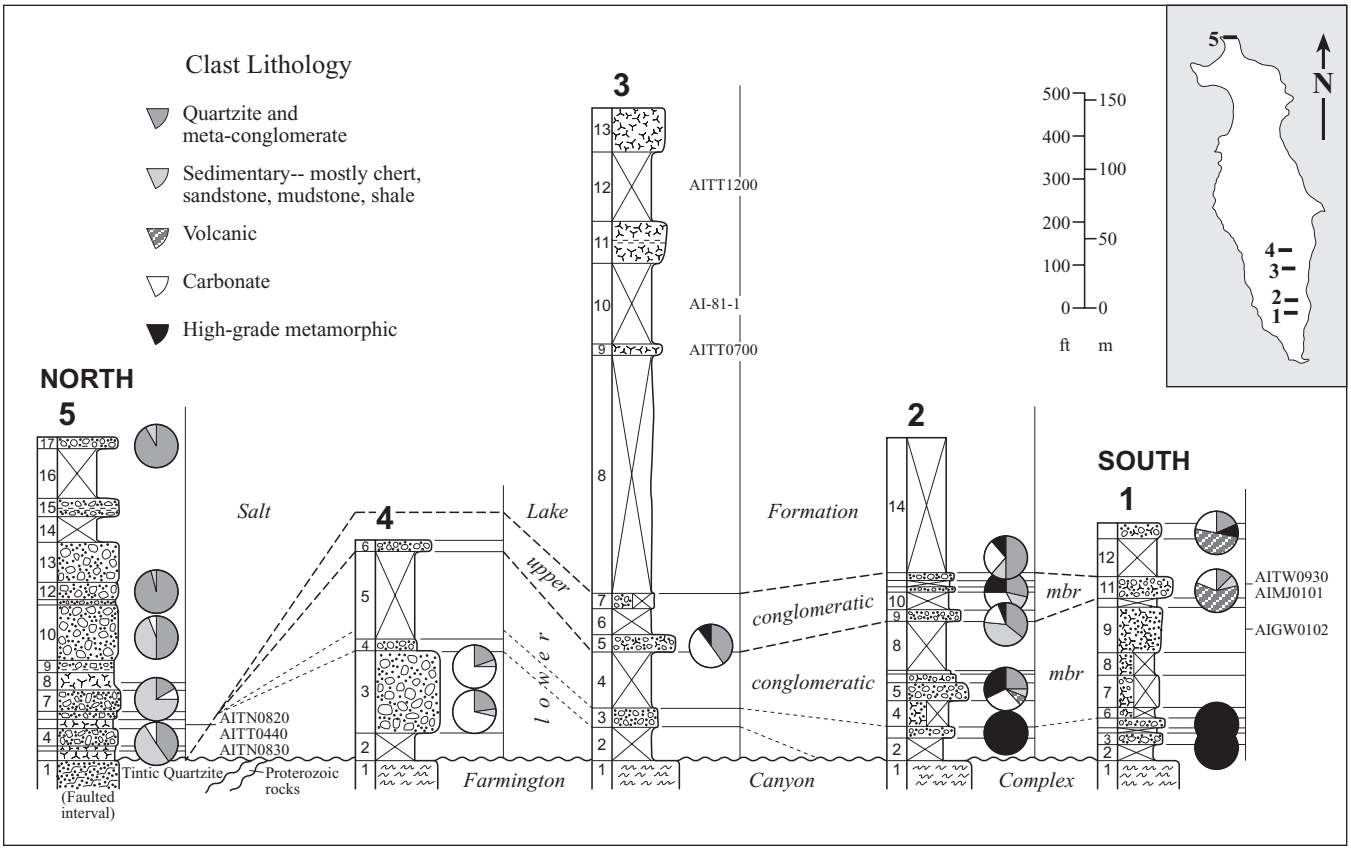

Figure 4. *Lithologic columns and correlation diagram of measured Tertiary strata on Antelope Island. The pie diagrams show the variability in clast lithology of the major conglomerate beds. Correlations were made by hiking out beds where possible and by comparing stratigraphic position and lithologic composition.*

fault trace or a near bedding-plane-parallel fault, neither of which are plausible.

SOUTHEAST EXPOSURES

Outcrops in the southeast area consist primarily of resistant conglomerate beds and small exposures of less-resistant mudstone, sandstone, and volcanic ash along gullies and washes. Doelling and others (1990) divided the southeast strata into three units: (1) conglomerate, breccia, and mudstone that comprise the lower member of an unnamed conglomeratic unit; (2) conglomerate with carbonate, quartzite, volcanic, and metamorphic clasts interbedded with mudstone, sandstone, and limestone that comprise the upper member of

the conglomeratic unit; and (3) a tuffaceous sandstone, marl, and tephra unit mapped as Salt Lake Formation. The Tertiary beds in the southeast area strike from N. 15° W. to N. 15° E. and dip from 20° to 45° to the east, averaging 35°. The Salt Lake Formation seems to be tilted slightly less overall than the older conglomeratic unit.

Lower Member of the Conglomeratic Unit

The lower member is exposed in a few isolated outcrops scattered throughout the southeast outcrop area, and is up to about 510 feet (153 m) thick. In the north part of the southeast area, the lowest exposed Tertiary rock is extremely coarse, clast-supported, boulder conglomerate with limestone, dolomite, quartzite, and rare metamorphic clasts (figure 4 and appendix, S4-unit 3). Much of the matrix is coarse gritstone composed of material eroded from the metamorphic Farmington Canyon Complex. Cement is carbonate and reddish-brown iron oxide. Exposed in situ clasts range up to about 3.5 feet (1.1 m) in diameter (figure 5); however, boulders in lag deposits eroded from this unit are commonly 4 to 5 feet (1-1.5 m) in diameter, and range up to 7 feet (2 m) long (figure 6). About 1 mile (1.6 km) north of S4, boulders in a lag deposit range up to 11 feet (3.4 m) in diameter (figure 7). The largest boulders, both in outcrop and in the boulder beach deposits, are quartzite and dolomite. However, among the smaller carbonate clasts, limestone dominates, suggesting that dolomite is more resistant to mechanical breakdown.

In the south part of the southeast area, the lowest exposed beds consist of dark-red, coarse conglomerate composed entirely of poorly sorted, angular clasts of metamorphic rocks in a coarse sandstone to gritstone matrix (figure 4 and appendix, S1-unit 3; figures 8 and 9). The clasts are lithologically similar to outcrops of Farmington Canyon Complex exposed just upslope, consistent with a local source. Identified clast types include pegmatitic granite, amphibolite, migmatitic gneiss, and quartz-plagioclase gneiss. The conglomerate varies from clast- to matrix-supported, and is crudely stratified. Clasts are up to 2.5 feet (0.75 m) in diameter, although most are 1 to 4 inches (2.5 to 10 cm). The dark-red color is from iron oxide weathered from the metamorphic clasts and matrix.

The dark-red conglomerate appears to overlie the large-boulder conglomerate where both are present, though outcrops are poor and discontinuous. S4-unit 4, a mostly covered interval with dark-red metamorphic float, may correlate with the dark-red conglomerate (figure 4).

A few small, poorly exposed outcrops of medium- to thin-bedded, gray, purple, green, and red bentonitic mudstone are stratigraphically above the red conglomerate. Some exposures are biotitic. Locally, the interval is sandy and contains a few conglomerate lenses. One such lens, S2-unit 5 (probably equivalent to the covered part of S1-unit 7) consists of mixed carbonate, quartzite, metamorphic, volcanic, and chert clasts.

Upper Member of the Conglomeratic Unit

The upper member consists of interbedded conglomerate and conglomeratic limestone with covered intervals that may be underlain by mudstone and sandstone. We measured 140

Figure 5. *Outcrop of poorly sorted, crudely stratified, large-boulder conglomerate beds of the lower conglomeratic member (outcrop is upper part of S4-unit 3). Notebook in lower right for scale.*

Figure 6. *Quartzite (lighter shades) and carbonate (darker shades) boulders eroded from the Tertiary conglomerate beds redeposited in Late Pleistocene boulder beach lag deposits (photograph taken near lower part of S4-unit 3).*

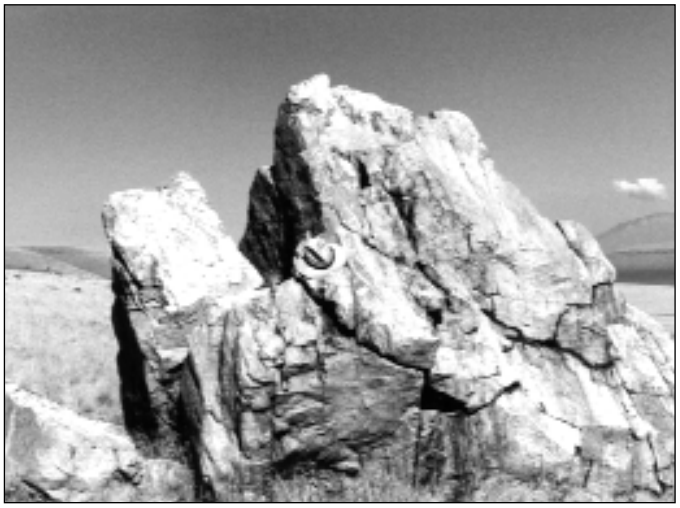

Figure 7. *Large boulder of Tintic Quartzite (now fractured by recent weathering) about 11 feet (3.4 m) in maximum diameter that eroded from Tertiary boulder-conglomerate beds (NE 1/4, sect. 4, T. 2 N., R. 3 W.). Hat for scale.*

Figure 8. *Dark-brownish-red conglomerate and breccia beds of the lower conglomeratic member consist of angular to subangular clasts of metamorphic rocks in a gritty matrix (outcrop is S1-unit 3). View to north. Hammer for scale.*

Figure 9. *Closeup of the outcrop shown in figure 8, showing size, sorting, and angularity of boulder clasts.*

feet (42 m) of upper member, but it may be considerably thicker in other areas. The contact between the lower and upper members is placed at the base of the lowest thick conglomerate beds with interstitial lacustrine carbonate and,

Figure 10. *Lacustrine conglomeratic limestone with abundant boulder clasts in the upper conglomeratic member (outcrop is S4-unit 6). Largest boulders are about 20 inches (50 cm) long. Shovel for scale.*

where present, the base of the lowest conglomerate that contains abundant volcanic clasts (figure 4 and appendix) (Doelling and others, 1990).

The upper member is present in all the measured sections; however, percentages of clast types, particularly of volcanic clasts, are highly variable between outcrops only a few hundred feet apart. Intervening beds are commonly covered. The variation may reflect different local sources, or that different beds are exposed at different sites.

The basal beds of the upper member (S3-unit 5 and S4-unit 6), form a prominent ledge that varies from conglomeratic limestone to conglomerate (figure 10). Clasts rarely exceed one foot (0.3 m) in diameter. Most clasts were derived from Paleozoic carbonates and quartzites, but a small number were derived from the Farmington Canyon Complex, the Mineral Fork Formation, and the Kelley Canyon Formation. The bed is pale gray to white with almost no iron oxide, unlike lower conglomerate beds.

The basal ledge may correlate with either unit 9, 11, or 13 of S2, and with either unit 11 or 13 of S1 (figure 4). S2-unit 9 is white, calcareous conglomerate containing subangular to subrounded quartzite and limestone cobbles that rarely exceed 3 inches (8 cm) in diameter, interbedded with tuffaceous sandstone. S2-units 11 and 13 are mostly conglomerate with metamorphic, quartzite, and carbonate clasts, mostly 1 to 6 inches (2.5-15 cm), but up to 14 inches (36 cm), in diameter. Clasts are mostly purple, green, and white quartzite cobbles derived from Proterozoic sources, with occasional sandstone, shale, and black chert. No volcanic clasts were found.

S1-unit 11 contains almost 50 percent volcanic clasts. It may correlate with S2-unit 9, which contains no volcanic clasts, with S2-unit 5, which contains about 6 percent volcanic clasts, or with the covered interval between. It may also correlate with S3-unit 5, which also does not contain volcanic clasts. Regardless of which bed is correlative, volcanic clasts decrease rapidly in abundance towards the north.

Figure 11. *Clean, planar-bedded, and cross-bedded volcanic ash in the Salt Lake Formation (outcrop is about 1/2 mile (0.8 km) northeast of S4). Shovel for scale.*

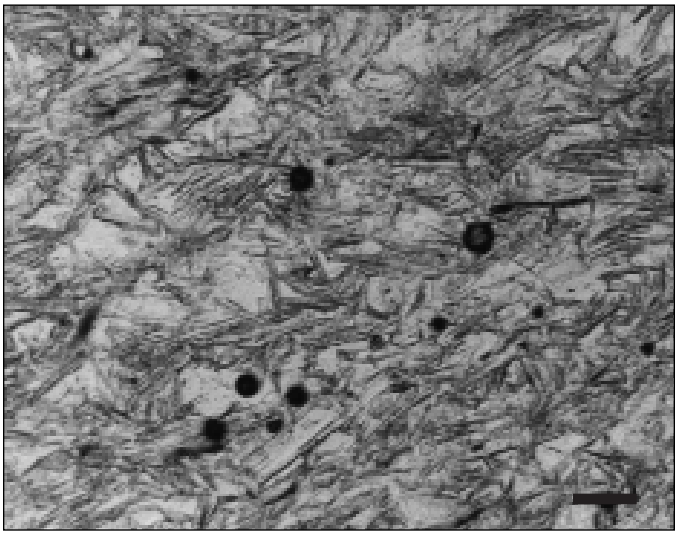

Figure 12. *Thin-section photomicrograph showing clean glass shards typical of ash beds in the Salt Lake Formation (matrix is epoxy cement). Bar in lower right equals 0.004 inches (0.1 mm).*

Salt Lake Formation

Overlying the conglomeratic sequence is a thick interval consisting of fine-grained volcanic ash with greater than 95 percent glass shards, tuffaceous sandstone, marl, mudstone, and a few thin pebble-conglomerate beds that Doelling and others (1990) mapped as Salt Lake Formation (figures 11 and 12).

The Salt Lake Formation is poorly exposed, but abundant pale-gray to white tuffaceous float and numerous small outcrops indicate that it is present under much of the Quaternary cover east of the conglomeratic outcrops. The more resistant outcrops are tuffaceous sandstone, volcanic ash, and conglomerate. Float suggests the unexposed parts of the formation are poorly cemented sandstone, siltstone, marl, and ash.

The volcanic ash beds are light- to medium-gray on fresh surfaces and weather to a lighter gray. They are generally

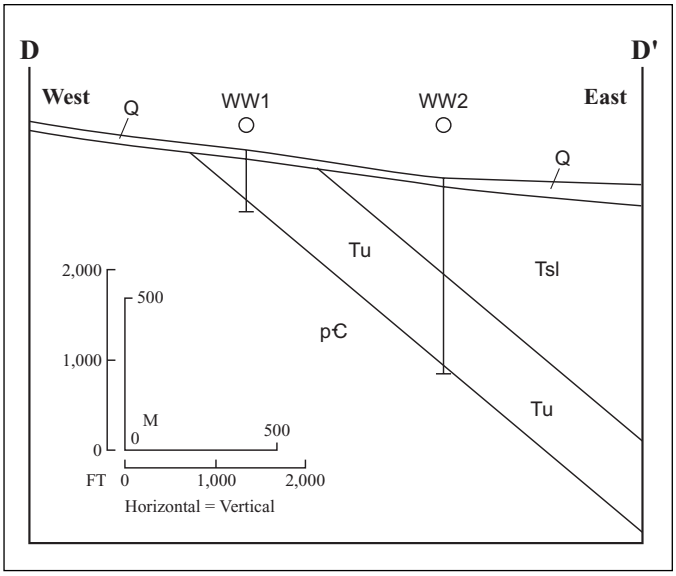

Figure 13. *Cross section through two water wells (WW1 and WW2, locations shown on figure 2). Tertiary strata dip about 35° to 45° east. Both wells penetrated bouldery Quaternary surficial deposits, then Tertiary strata, and may have bottomed in Precambrian bedrock. Q-undifferentiated Quaternary surficial deposits, Tsl-Salt Lake Formation, Tu-undivided Tertiary conglomeratic units, pC Precambrian high-grade metamorphic rock.*

very fine grained, noncalcareous, porous, moderately indurated, laminated to thick bedded, and locally exhibit cross-bedding (figure 11). Angular glass shards comprise up to 100 percent of the ash. In places the ash contains small specks of dark iron oxide.

The upper part of the Salt Lake Formation is not exposed on the island, so the total thickness cannot be measured. Assuming no structural complexities and a uniform strike and dip, the formation is at least 1,800 feet (550 m) thick.

Drill Holes in the Southeast Outcrop Area

Two water wells were drilled in the southeast outcrop area by the Antelope Island Cattle Company, Inc. (part of the Anchutz Corporation) in 1975 and 1976 (S.B. Montgomery, Utah Division of Water Resources, written memorandum, 1980). One hole located 1,650 feet (503 m) north and 100 feet (30 m) west of the SE corner of section 33, T. 3 N., R. 3 W. was drilled to a depth of 2,082 feet (635 m) (figures 2 and 13). The other hole, located about 2,200 feet (660 m) to the west approximately 1,600 feet (490 m) north and 2,300 feet (700 m) west of the same section corner, was drilled to a depth of 600 feet (180 m).

Well cutting descriptions on file with the Utah Division of Water Rights are brief. The shallower west hole penetrated "conglomerate" to 305 or 400 feet (93 or 120 m), and "black, white, and gray rock" in a small interval at the bottom of the hole (thickness was not stated); the intervening interval was not described. The description of the deeper east hole is also brief. It cut "clay, silt, sand, gravel, and boulders" to 1,213 feet (370 m) and "hardpan, conglomerate, and bedrock" from 1,213 to 2,082 feet (370 to 635 m).

We reinterpreted the penetrated intervals using the written descriptions and correlation with our surface mapping

(table 1) to construct a cross section through the site (figure 13). Late Pleistocene alluvial and lacustrine deposits are at the surface at each site, but nearby outcrops indicate that both holes primarily penetrated thick Tertiary strata. The east hole cut the tuffaceous Upper Tertiary Salt Lake Formation, then clasts of Paleozoic carbonate and quartzite contained in the unnamed Tertiary conglomeratic unit. It may have bottomed in metamorphic bedrock. The west hole penetrated surficial materials, then the conglomeratic unit, and then bottomed in metamorphic bedrock.

Table 1. *Our interpretation of rock penetrated by water wells in the southeast part of Antelope Island (all measurements are approximate). Locations are shown on figure 2. Our interpretation is shown on figure 13. Number in parentheses is stratigraphic thickness after adjusting for 40° dip.*

Interval (feet) (strat. thickness)	Lithology
	WW 1 (western)
0-100 (77)	Late Quaternary surficial alluvial and lacustrine deposits consisting of gneissic, granitic, and quartzitic boulders, sand, and silt.
100-550 (345)	Early Tertiary conglomeratic strata containing mostly Cambrian to Mississippian carbonate and quartzite clasts.
550-600 (38)	Precambrian gneissic and granitic bedrock.
	WW 2 (eastern)
0-100 (77)	Late Quaternary surficial alluvial and lacus trine deposits consisting of gneissic, granitic, and quartzitic boulders, sand, and silt.
100-1,200 (843)	Late Tertiary Salt Lake Formation tuff, tuffaceous sandstone, and conglomerate.
1,200-2,082 (676)	Early Tertiary conglomeratic unit consisting of Cambrian to Mississippian carbonate and quartzite boulder clasts. Depending on the dip used in the model, the hole may have bottomed in Precambrian metamorphic rock.

Our reconstruction shows that metamorphic rocks penetrated in the upper part of the hole are actually boulders contained in surficial and Tertiary strata, and that Paleozoic carbonate rocks in the lower part of the hole are large clasts in the Tertiary boulder conglomerate. Dip of Tertiary bedding within one mile (1.6 km) of the holes varies from 20 to 45° (Doelling and others, 1990). Near the holes the dip is probably about 40°, in which case the east hole penetrated only Tertiary strata and the west hole penetrated about 450 feet (135 m) (345 feet [105 m] when adjusted for dip) of Tertiary rock. Hansen and McCarley (this volume) present different interpretations of these holes.

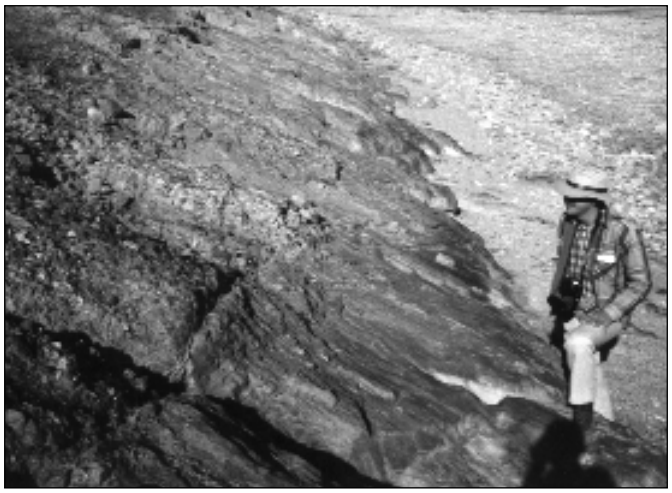

Figure 14. *Faulted volcanic ash and coarse, angular conglomerate and breccia of the Salt Lake Formation on the north end of Antelope Island. Strata are near-vertical to overturned.*

NORTH EXPOSURES

A small, narrow belt of Tertiary outcrops is exposed along the Great Salt Lake shoreline at the north tip of the island (figures 2 and 14). These outcrops were first exposed when surficial gravel deposits were removed to construct a causeway to the island in the 1970s and 1980s. The Tertiary rocks are primarily very poorly sorted sedimentary breccia and conglomerate interbedded with gray volcanic ash and pale-reddish-gray mudstone and are up to 760 feet (230 m) thick (figure 4 and appendix S5). The rocks are strongly fractured and are cut by numerous faults. Though contacts are mostly covered, the Tertiary strata appear to unconformably overlie the Cambrian Tintic Quartzite in some locations and are faulted against it in others. The Tertiary beds strike from N. 57° E. to N. 75° E. The beds apparently are part of an overturned fold; they are overturned, dipping 67° SE, near the east end of the outcrop, are vertical a short distance farther west, then gradually flatten, dipping about 15° to the NW in the westernmost exposure. The fold and faults may be indicative of a larger, unexposed fault north of the island.

The basal contact of the Tertiary beds is a 1-foot (0.3 m) thick, yellowish-brown breccia with mostly Tintic Quartzite clasts. It may be either sedimentary or fault breccia. Medium-gray, thin- to thick-bedded volcanic ash overlies the breccia (figure 14). The ash consists primarily of glass shards, although it contains a few suspended angular clasts of quartzite, shale, and small blebs of black obsidian. It is present in three intervals from 12 to 30 feet (4-9 m) thick that are interbedded with sedimentary breccia (figure 4 and appendix S5). Two or more of the intervals may be the same bed repeated by faults. The ash has been reworked and contains interbedded sedimentary breccia as clots, stringers, and irregular bodies. Contacts between the sedimentary breccia and the ash vary from sharp to gradational.

The sedimentary breccia and conglomerate (figure 4 and appendix S5 - units 4, 6, 7, 9-13, 15, and 17) are very poorly sorted, with individual clasts as large as 3 feet (1 m) in diameter. Clasts are mostly very angular, olive-green shale in the lower beds, and mostly white- to pale-gray quartzite in the middle and upper beds. Lesser amounts of silty, dolomitic

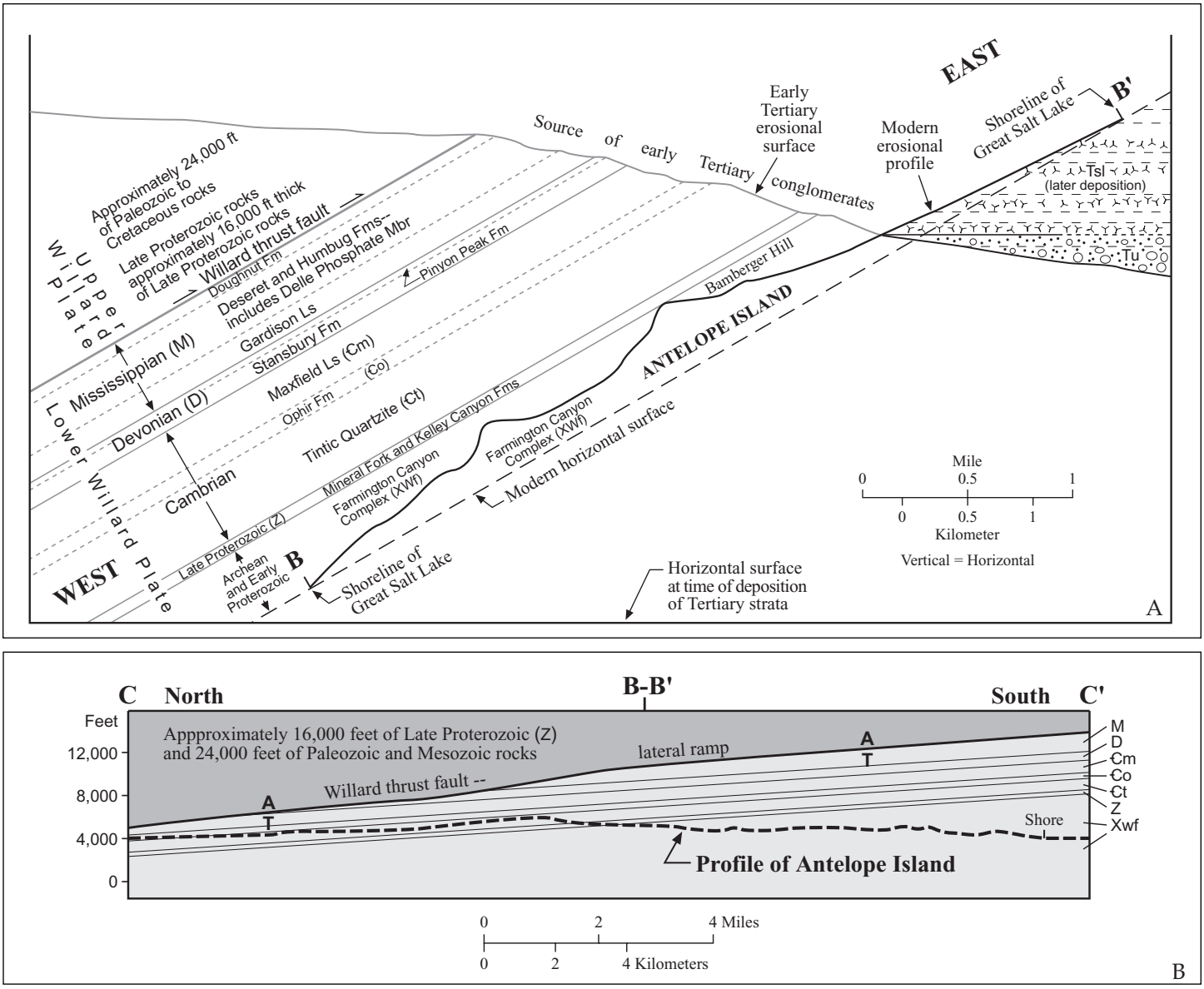

Figure 15. *Schematic cross sections showing restoration of Antelope Island to about late Eocene time (prior to Neogene tilting). Note that the cross-section scales are different. Lines of section shown on figure 2.*
(A): East-west cross section B-B' across the middle of the island. The island block is tilted 35° to the west to restore Tertiary beds to horizontal. The likely location of the Willard thrust fault and of the source of Paleozoic boulders now found in the Tertiary sediments is indicated. The Willard thrust fault rides on Mississippian strata. The lower part of the upper plate rocks consists of several thousand feet of Late Proterozoic metasedimentary strata.
(B): North-south cross section C-C' showing a postulated lateral ramp cutting up-section from Cambrian rocks near the north end of the island, to Mississippian rocks near the central or south part of the island. Fault movement: A-away, T-toward.

limestone, micaceous argillite, and dark-gray to black quartzite are also present. The angular nature, poor sorting, immature composition, and nonresistant nature of some of the clasts indicate that they were transported only a short distance from their source.

The north exposures cannot be correlated directly with Tertiary rocks on the southeast part of the island. The abundant volcanic ash does indicate that they are part of the Salt Lake Formation.

INTRUSIVE ROCKS

A few felsic dikes about 5 feet (1.5 m) wide cut Precambrian metamorphic rock in SW 1/4, SW 1/4, SW 1/4 section 34, T. 2 N., R. 3 W. Chemically, they are alkali-rich trachyte (table 2) and are not chloritized or altered by low-grade metamorphism as are the adjacent rocks. The dikes were not radiometrically dated, but they are probably late Eocene or Oligocene, based on their proximity to Eocene and Oligocene intrusions in the Oquirrh Mountains to the south (figure 1) (Tooker and Roberts, 1971; Moore and McKee, 1983), their trachyte composition, and the fact that they postdate Cretaceous chlorite-grade metamorphism that affected the host rocks (W.A. Yonkee, verbal communication, 1991).

AGE AND CORRELATION

The Tertiary rocks of Antelope Island have proven

Table 2. *Geochemical X-ray fluorescence analysis and normative calculation of mineral content of Tertiary igneous dike in the south part of Antelope Island. Analyses in percent [no symbol] or parts per million [.ppm] Sample collected in SW1/4, SW1/4, SW1/4 section 34, T. 2 N., R. 3 W.*

SiO_2	63.96	K_2O	4.49	P_2O_5	0.06	Sr	20.ppm
Al_2O_3	19.45	Fe_2O_3	2.94	LOI	0.54	Y	40.ppm
CaO	0.18	MnO	0.03	Ba	240.ppm	Zr	430.ppm
MgO	0.57	Cr_2O_3	<0.01	Nb	180.ppm		
Na_2O	8.09	TiO_2	0.33	Rb	110.ppm	**TOT**	**100.4**

CIPW Weight Normative Calculations*

Orthoclase	26.48	Olivine	2.49
Albite	65.08	Ilmenite	0.63
Anorthite	0.50	Magnetite	1.41
Nepheline	1.74	Apatite	0.14
Corundum	1.09		

*Normalized on a 100% water-free basis and with the total iron corrected according to Irvine and Barager (1971).

difficult to date. We attempted to determine the ages of the rocks using palynomorph identification, field constraints, radioisotopic dating, tephrochronology, and correlation with surrounding areas. No indicative megafossils were found. Fred May of Palynex International examined five samples for palynomorphs, but all were barren (written communication, 1990).

Field Constraints

Field relationships, combined with the geologic history of the area, provide some constraints on the timing of Tertiary deposition. The Tertiary rocks overlie Precambrian and Cambrian strata that were involved in intense structural and low-grade metamorphic changes during the Cretaceous Sevier orogeny (Doelling and others, 1990; Yonkee, 1992; Yonkee, Willis, and Doelling, this volume [b]). The conglomeratic strata do not exhibit this deformation, but contain clasts that were deformed. Thus, the conglomerate postdates both the deformation and the vast erosion necessary to denude the deformed rocks. We estimate that at least 40,000 feet (13,000 m) of rock must have been structurally and erosionally removed from what is now Antelope Island in order to expose the source of some of the clasts and the Precambrian rocks on which they are deposited (figure 15). This denudation was probably not completed before late Paleocene or early Eocene time.

Both the older unnamed rocks and the Salt Lake Formation deposits are tilted as much as 45° on the southeast side of the island and are steeply dipping on the north end (figures 11 and 14). No major angular unconformities exist within the Tertiary strata. Thus, the exposed Tertiary strata predate most of the faulting that tilted the island block during the late Cenozoic.

Radioisotopic Dating and Tephrochronology

Several bentonitic clay beds in the lower part of the upper conglomerate member contain biotite amenable to radiometric potassium-argon (K-Ar) dating. In addition, some of the conglomerate beds near S1 and S2 contain abundant volcanic clasts with biotite and other datable minerals. We selected one sample from the bentonitic clay and two volcanic clasts for K-Ar dating. They yielded ages of 42.9±1.9 Ma, 38.8±1.5 Ma, and 49.2±1.7 Ma, respectively (table 3; fig-

Table 3. *Analytical data on potassium-argon age determinations for samples collected on Antelope Island. Ages reported in millions of years.*

Sample: AIGW-0102
Unit: Conglomeratic unit, lower member (volcanic clast)
Location: 40°52'52"N., 112°10'25"W.
Material Analyzed: Biotite concentrate, -80/+200 mesh
DATE ANALYZED: Nov. 13, 1987
AGE: 42.9+-1.7
^{40}*Ar/40K = 0.002523
^{40}*Ar (ppm) = 0.01991; 0.01983 Average = 0.01987
^{40}*Ar/Total ^{40}Ar = 0.575; 0.512
%K = 6.549; 6.654 Average = 6.602
^{40}K (ppm) = 7.876

Sample: AIMJ-0101
Unit: Conglomeratic unit, upper member (bentonite)
Location: 40°52'51"N., 112°10'28"W.
Material Analyzed: Biotite concentrate, -80/+200 mesh
DATE ANALYZED: Oct. 28, 1988
AGE: 49.2+-1.9
^{40}*Ar/^{40}K = 0.002897
^{40}*Ar (ppm) = 0.02014; 0.02024 Average = 0.02019
^{40}*Ar/Total 40Ar = 0.434; 0.347
%K = 5.879; 5.806 Average = 5.843
^{40}K (ppm) = 6.970

Sample: AITW-0930
Unit: conglomeratic unit, upper member (volcanic clast)
Location: 40°52'48"N., 112°10'22"W.
Material Analyzed: Phlogopite concentrate, -80/+200 mesh
DATE ANALYZED: Oct. 28, 1988
AGE: 38.8+-1.5
^{40}*Ar/^{40}K = 0.002279
^{40}*Ar (ppm) = 0.01966; 0.01906 Average = 0.01936
^{40}*Ar/Total 40Ar = 0.586; 0.392
%K = 7.094; 7.147 Average = 7.121
^{40}K (ppm) = 8.495

Constants Used:
$\lambda_\beta = 4.962 \times 10^{-10}$/year
$(\lambda_e+\lambda'_e) = 0.581 \times 10^{-10}$/year
^{40}K/K = 1.193x10-4g/g

Laboratory:Krueger Enterprises, Inc., Geochron Laboratories Division, Cambridge, MA

ure 2), similar to reported ages from Eocene volcanic rocks in a belt to the south and west (Moore and McKee, 1983; Bryant and others, 1989a). The wide range in ages may be due to dating of clasts from different sources, low radiogenic argon (table 3), or both. The dated materials were collected from water-lain beds reworked from the primary volcanic rocks, so the dated materials were deposited later than the K-Ar ages, probably during the late Eocene or Oligocene (see "Regional Correlation").

The volcanic ash beds in the Salt Lake Formation are composed of clean glass shards (vitric tuff) with minor amounts of incorporated chert and other sedimentary sand grains (figure 12). We examined several samples but found no minerals datable by standard K-Ar methods. Bryant and others (1989a) dated a sample collected from approximately the middle of the Salt Lake Formation in the NW1/4, section 15, T. 2 N., R. 3 W., in the southeast part of the island, by fission track on zircon at 6.1±1.1 Ma (figure 2).

Michael E. Perkins and William P. Nash of the University of Utah conducted electron microprobe analyses on ten samples of gray vitric tuffs from the Salt Lake Formation on Antelope Island (figure 2; table 4). They did the analyses with a Cameca SX-50 electron microprobe using methods Perkins and others (1995) described. They compared the chemical analyses of these samples with similar analyses of about 2,200 samples of vitric tuffs from Neogene basins of the western U.S. in the University of Utah database. Comparisons were based on titanium, iron, manganese, magnesium, calcium, barium, and chlorine using the distance function (Perkins and others, 1995; 1998).

Comparisons of electron microprobe analyses provide useful preliminary correlations of tuffs (tephrochronology) and also provide information on the source of the tuffs. It is important to note, however, that high precision, trace-element analyses of the glass shard fraction of these tuffs are needed to confirm specific correlations discussed below. Using the classification of Perkins and others (1998), the Antelope Island tuffs are gray metaluminous rhyolite tuffs and are within the glass shard compositional field of Snake River Plain-type tuffs. The available evidence firmly indicates that the tuffs are from sources in the Snake River Plain volcanic province (Yellowstone hotspot track) and are 11 to 8 million years old (late Miocene). Future analyses may prove some of the suggested correlations are in error, but they are unlikely to alter the overall age range now estimated for these tuffs. Preliminary (electron microprobe) correlations for nine of the ten samples are as follows (Michael Perkins written communication, 1998, shown in table 4):

Table 4. *Results of electron microprobe analyses of volcanic tuff samples from Antelope Island. All amounts are in weight percent of oxides.*

	AITT-0440	AITT-0700	AITT-0820	AITT-0830	AITT-0840	AITT-1200	AITT-1020	AITT-1030	AITT-1090	AITT-1220
SiO_2	72.9	72.5	72.8	72.6	73.3	72.7	72.1	71.0	70.8	72.3
TiO_2	0.22	0.21	0.20	0.25	0.16	0.17	0.26	0.40	0.37	0.28
Al_2O_3	11.6	11.6	11.6	11.6	11.5	11.4	11.6	11.9	11.7	11.5
Fe_2O_3	2.14	2.13	2.07	2.10	1.77	1.73	2.17	2.53	2.82	2.31
MnO	.035	.039	.026	.044	.030	.031	.041	.041	.046	.036
MgO	.051	.043	.049	.084	.064	.062	.111	.202	.182	.107
CaO	0.66	0.66	0.65	0.62	0.51	0.53	0.70	0.93	1.01	0.74
BaO	0.05	0.04	0.05	0.04	0.02	0.02	0.06	0.06	0.06	0.07
Na_2O	2.5	1.8	2.5	2.5	2.7	1.7	1.8	2.0	1.7	2.3
K_2O	5.5	5.6	5.6	5.6	5.3	6.4	6.2	5.9	5.1	5.5
Cl	.040	.043	.042	.033	.050	.054	.033	.026	.024	.038
F	0.27	0.25	0.29	0.24	0.24	0.25	0.22	0.22	0.25	0.23
H_2O	4.7	6.4	4.9	4.5	5.5	5.6	5.6	5.5	6.8	5.4
ĐO	0.12	0.12	0.13	0.11	0.11	0.12	0.10	0.10	0.11	0.11
Total	100.5	101.2	100.6	100.1	101.0	100.5	100.8	100.6	100.8	100.7

Note: Correlative samples grouped together. Comparisons based on contents of TiO_2, Fe_2O_3, MnO, MgO, CaO, BaO, and Cl.

Locations: Sample	Latitude	Longitude
AITT-0440	41° 03' 35"	112° 14' 20"
AITT-0700	40° 55' 36"	112° 10' 35"
AITT-0820	41° 03' 35"	112° 14' 20"
AITT-0830	41° 03' 35"	112° 14' 19"
AITT-0840	40° 56' 36"	112° 10' 52"
AITT-1200	40° 54' 32"	112° 10' 20"
AITT-1020	40° 56' 00"	112° 11' 05"
AITT-1030	40° 55' 59"	112° 11' 02"
AITT-1090	40° 54' 08"	112° 10' 16"
AITT-1220	40° 54' 38"	112° 10' 18"

(1) Samples AITT-0440, AITT-0700, and AITT-0820 are from the same tuff. This tuff is likely the 10.94 ± 0.03 Ma Cougar Point Tuff (CPT) XIII ash bed of Perkins and others (1995; 1998). This ash bed can generally be identified with confidence using electron microprobe analyses. The CPT XIII ash bed is present in sections across the Basin and Range. In particular it is in the South Willow Creek section of the Salt Lake Formation on the east flank of the Stansbury Range, Utah (Perkins and others, 1998) to the south of Antelope Island.
(2) Sample AITT-0830 possibly matches a fallout tuff at the base of the 8.6 ± 0.20 Ma uppermost unit (unit 4?) of the tuff of McMullen Creek at the top of the Trapper Creek section in southern Idaho (Perkins and others, 1995).
(3) Samples AITT-0840 and AITT-1200 are likely from the same ash bed. They have a unimodal glass shard composition and likely match either the 7.9 ± 0.5 Ma Rush Valley, Utah ash bed of Perkins and others (1998) or an unnamed ash bed about 9.2 Ma. The 7.9 Ma Rush Valley ash bed and the unnamed 9.2 Ma ash bed cannot be confidently differentiated using electron microprobe analyses, hence the correlation uncertainty.
(4) Sample AITT-1030 has glass shards with two compositional modes. It appears to match an about 9.8 Ma bimodal ash bed in southwest Montana.
(5) Sample AITT-1090 has glass shards with four discrete compositional modes. This distinctive tuff is a good match with an unnamed about 9.8 Ma tuff just above the 9.8 ± 0.20 Ma Hazen ash bed in western Nevada of Perkins and others (1998).
(6) Sample AITT-1220 contains glass shards with two distinct compositional modes. It appears to match an about 10.5 to 9.5 Ma bimodal tuff from the Mink Creek area of southeast Idaho.

Only sample AITT-1020 is not matched to a specific tuff in the University of Utah database. However, sample AITT-1020 is in the compositional field of the group A tuffs of the Trapper Creek section (Perkins and others, 1995). Group A tuffs are mostly 10.5 to 8.6 Ma in age and none are known that are younger than about 8.0 Ma. The possibility of tuffs as young as about 6 Ma (fission track) on Antelope Island, as reported by Bryant and others (1989a), cannot be completely ruled out. However, several 11 to 8 Ma samples were collected in the general area of the Bryant and others (1989a) sample. This suggests that the 6.1 ± 1.1 Ma zircon fission track date reported by these workers may err on the young side.

Regional Correlation

Tertiary rocks are exposed in several ranges and valleys, and were penetrated by several drill holes in northwest Utah (figure 16A-C). Most are also poorly dated, but comparison with the Antelope Island outcrops provide some constraints on the Tertiary history.

Salt Lake Salient

The Salt Lake salient contains one of the thickest and most complete sequences of Tertiary rocks in northern Utah (figure 16A-C). However, the rocks are mostly coarse clastics that have yielded little datable material. Van Horn (1981) and Van Horn and Crittenden (1987) mapped six Tertiary units in the salient area: (1) a basal conglomerate (their "conglomerate no. 1"), with limestone and quartzite clasts, which they correlate with the Wasatch Formation; (2) an overlying sequence of tuffaceous siltstone, sandstone, and limestone dated at about 37 Ma, which they correlate with the Norwood Tuff; (3) andesite breccia dated at about 37 Ma, which they correlate with the Keetley Volcanics; (4) a sequence of over 8,500 feet (2,650 m) of conglomerate (their "conglomerate no. 2") with clasts reworked from conglomerate no. 1 and metamorphic clasts derived from the Farmington Canyon Complex; and (5) and (6) two upper units of probable Pliocene age that consist of poorly consolidated conglomerate that unconformably overlies the previously described units.

Their conglomerate no. 1 may correspond in age to the lower part of the lower conglomeratic member on Antelope Island. Their overlying tuffaceous and andesitic units and their conglomerate no. 2 may correspond with the bentonitic beds or the upper conglomeratic member on the island. Their upper two units probably do not correlate with strata exposed on Antelope Island.

Oquirrh Mountains

Tooker and Roberts (1961, 1971) mapped a small exposure of coarse conglomerate overlain by a remnant of andesite breccia in the north Oquirrh Mountains (figure 16A, B). The conglomerate is poorly sorted, is stained reddish brown, and contains boulders of limestone and quartzite, some of which were derived from exposures outside the Oquirrh Mountains. The overlying andesite breccia is comparable to rocks to the south that are about 38 million years old (Moore, 1973; using revised decay constants according to Dalrymple, 1979). The conglomerate is similar to the lower conglomeratic sequence on Antelope Island and the andesite may roughly correlate with the bentonitic mudstone beds.

Slentz (1955) described outcrops of clastic, volcanic ash, and volcaniclastic deposits exposed in gravel pits and road and railroad cuts in the foothills east of the Oquirrh Mountains, which he assigned to the Salt Lake Group (figure 16C). These outcrops form a key area for attempts to correlate vitric tuffs around the northeast Great Basin (see “Radiometric Dating and Tephrochronology”) (Smith and Nash, 1976; Perkins and others, 1998).

Stansbury Mountains

Rigby (1958) mapped reddish-brown pebble conglomerate up to 400 feet (120 m) thick on the east flank of the Stansbury Mountains (figure 16A). The conglomerate overlies an unconformity cut across upper Paleozoic strata and is overlain by volcanic strata that Moore and McKee (1983) dated at about 39 million years (figure 16B). The conglomerate contains locally derived boulders up to 2.5 feet (0.76 m) in diameter composed mostly of upper Paleozoic rocks. The volcanic sequence consists of interbedded latite flows, breccias, tuffs, and pebble conglomerate up to 1,800 feet (550 m) thick. Overlying the volcanic sequence is up to 1,300 feet (400 m) of interbedded tuffaceous sandstone and gritty pebble to cobble conglomerate that may correlate with the Salt Lake Formation (figure 16C).

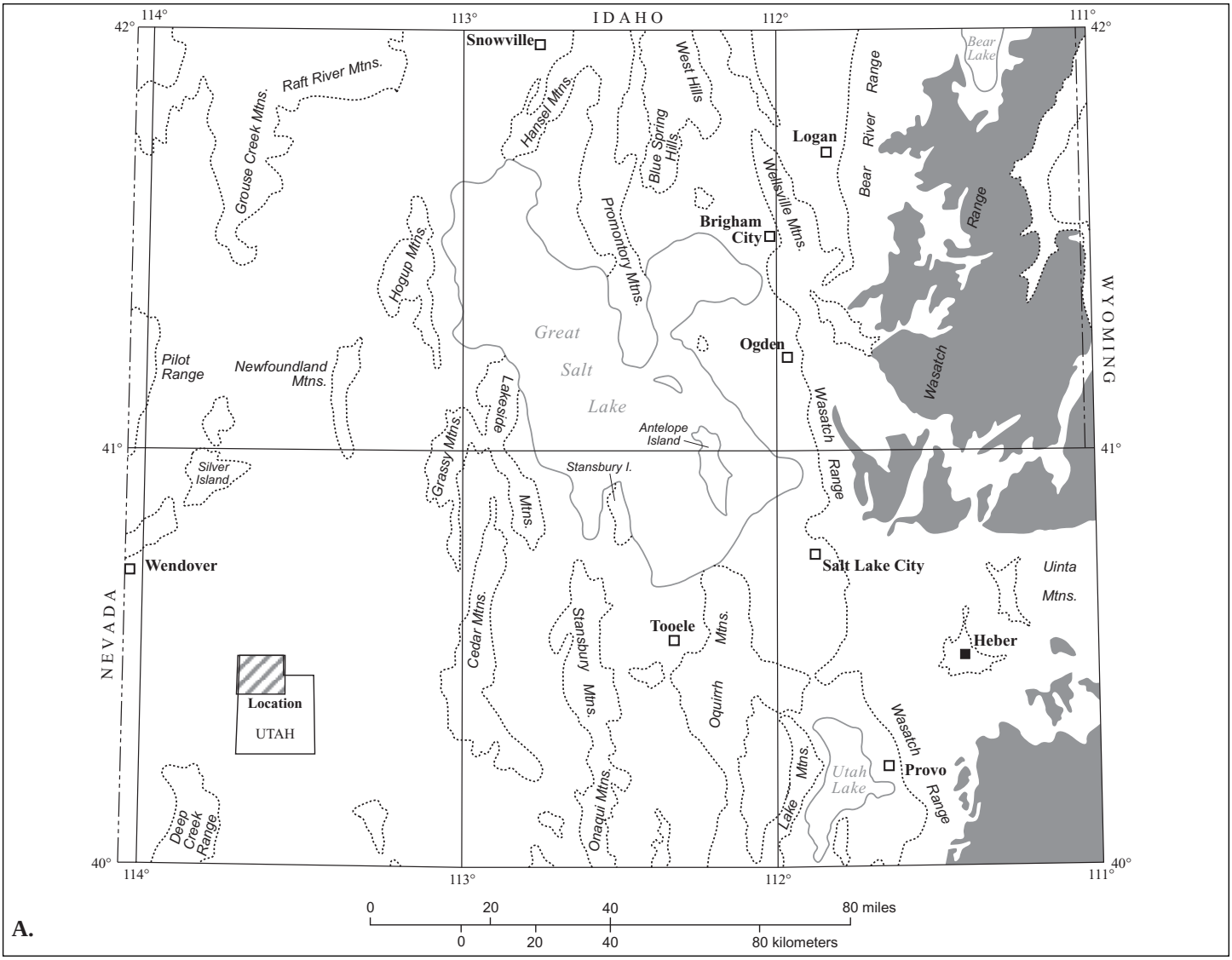

Figure 16A. *Maps showing outcrops of Tertiary rocks in northern Utah divided into three groups (16A, B, C) by age (modified from Hintze and Stokes, 1964): Paleocene to middle Eocene sedimentary strata that predate major volcanism in the area (primarily Wasatch Formation and related rocks). The Paleocene to Eocene highland in northwest Utah and associated deposition to the east is apparent.*

Cedar Mountains

Maurer (1970) described several hundred feet of sandstone to conglomerate with clasts up to 1.5 feet (0.56 m) in diameter on the west side of the Cedar Mountains (figure 16A-C). The clasts were locally derived from the upper Paleozoic Oquirrh and younger formations. He also described outcrops of clayey and tuffaceous sandstone on the east side of the range. Age control is limited, though he does report fossils that are "...certainly Cenozoic, most probably late Paleocene or Eocene."

North Promontory Mountains

Miller and others (1991) and Miller and Schneyer (1994) mapped "tuff and associated fine-grained sedimentary deposits" that unconformably overlie the Pennsylvanian-Permian Oquirrh Formation in the North Promontory Mountains (figure 16C). Using experimental K-Ar methods, they obtained radiometric ages on glass shards from near the base of the unit of 17 to 18 Ma and about 9.6 Ma from near the erosionally truncated top. They indicated that the 17 to 18 Ma ages were from experimental methods and are probably too old (Miller and others, in press). Discordantly overlying the tuff are loess and alluvium older than 4.8 Ma (Nelson and Miller, 1990).

Other areas

Tertiary strata are exposed in numerous other areas throughout northern Utah (figure 16A-C). The Grouse Creek - Raft River Mountains area is particularly important because of thick, well-exposed sections and better age control (Williams and others, 1982; Compton, 1983; Todd, 1983). Williams and others reported ages ranging from 11 to 7 Ma for the Salt Lake Group strata in that area. Also important are outcrops in the Pilot Range (Miller, 1985; Miller and Schneyer, 1985; Miller, 1993), the Silver Island Mountains (Schaeffer, 1960), the Gold Hill area (north end of the Deep Creek Mountains) (Nolan, 1935; Dubiel and others, 1996), the north Wellsville Mountains (Adamson and others, 1955; Oviatt, 1986), and the northern Cache Valley area in southern Idaho (Danzl, 1985). Perkins and others (1998) and Miller

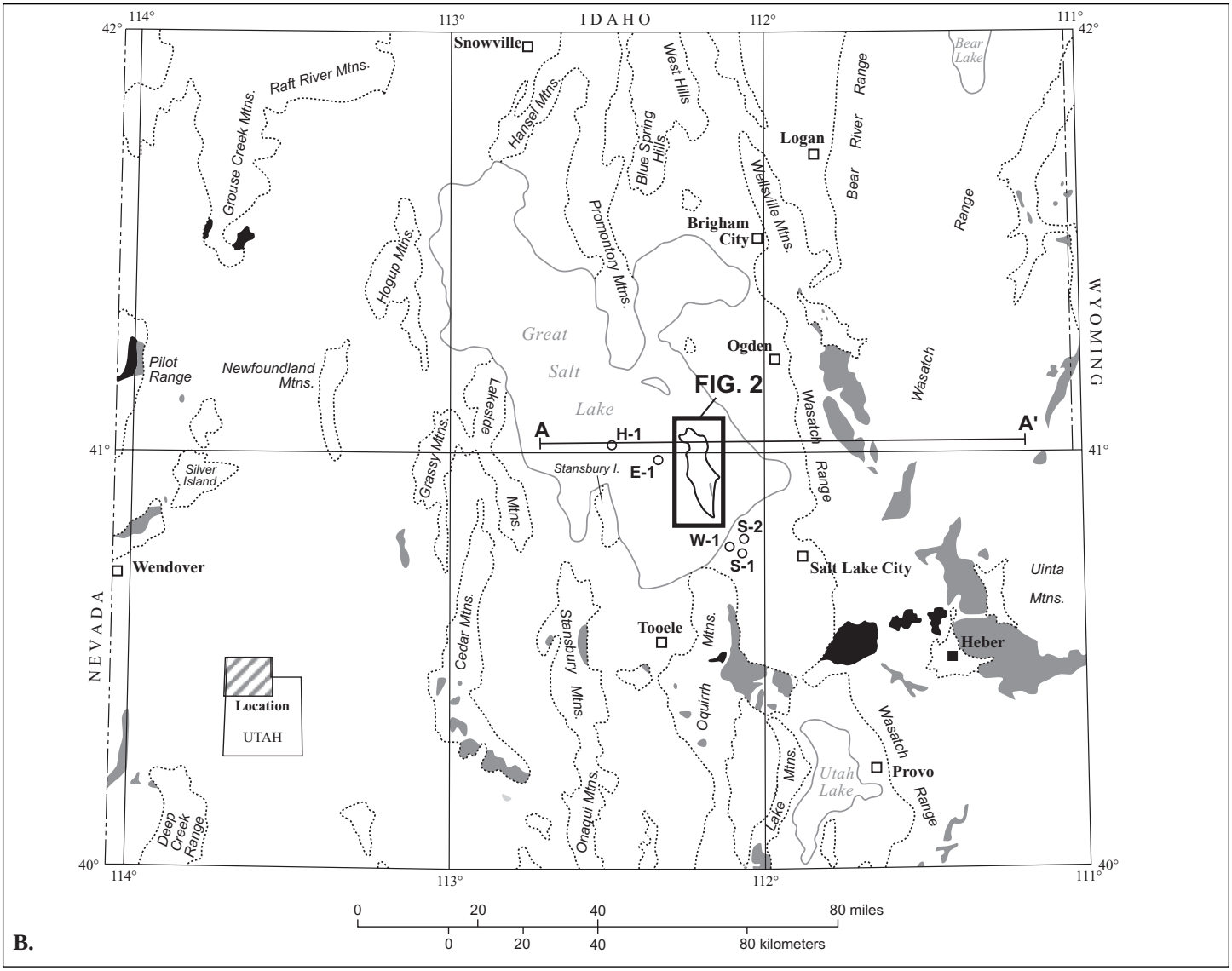

Figure 16B. *Middle Eocene to middle Oligocene volcanic and volcaniclastic deposits (mostly of intermediate composition) and related rocks (grey); and intrusive igneous rocks (black). Note the belt of igneous activity south of Antelope Island.*

and others (in press) summarized chronologic data and correlations of these and other Tertiary outcrops in northern Utah.

Drill holes in the Great Salt Lake basin

Several drill holes in Great Salt Lake west and northwest of Antelope Island penetrated upper Tertiary sections up to 15,000 feet (4,600 m) thick (figure 1) (Bortz and others, 1985). The oldest Tertiary rock is Miocene in most wells, though one well (State L-1, section 12, T. 5 N., R. 7 W.) penetrated volcanic tuff near the bottom that Bortz and others (1985) dated at 29.0 ±1.3 Ma (late Oligocene). In nine wells, the Tertiary strata rest unconformably on Paleozoic rock. In the two wells closest to Antelope Island, the State E-1 (section 19, T. 3 N., R. 4 W., about 1 mile [1.6 km] west of the island), and the State H-1 (section 11, T. 3 N., R. 6 W.), about 7 miles [11 km] west of the island), Tertiary rocks rest on probable Precambrian Farmington Canyon Complex rocks (figure 1). In the State E-1, the Tertiary-Precambrian contact may be a fault (W.A. Yonkee, verbal communication, 1991). Four wells bottomed in upper Tertiary strata.

Several other wells were drilled in the valley floor 3 to 8 miles (5-13 km) southeast of the south tip of the island. Of these, three are particularly interesting. The Whitlock-Morton 1 (W-1 on figure 1) (section 24, T. 1 N., R. 3 W.) encountered the top of the Tertiary at about 1,430 feet (436 m), and the top of the Precambrian (high-grade metamorphic rocks) at about 3,650 feet (1,110 m), based on geophysical logs. The 2,300 to 2,800 foot (700-850 m) interval cut volcanic rocks that were dated at about 34 and 37 Ma (adjusted using new decay constants according to Dalrymple, 1979) (Howard Ritzma, unpublished data, 1975). These ages are slightly younger than the ages we obtained on Antelope Island, but are still within the period of late Eocene to early Oligocene volcanism. The 2,800 to 3,650 foot (850-1,110 m) interval probably consists of early Tertiary clastic deposits.

The Saltair 1 well (S-1 on figure 1) (section 29, T. 1 N., R. 2 W.) encountered the Quaternary/Tertiary contact at 1,328 feet (405 m) and the Tertiary/Precambrian contact at 3,070 feet (936 m) (Howard Ritzma, unpublished notes, 1975).

The Saltair 2 well (S-2 on figure 1) (section 16, T. 1 N.,

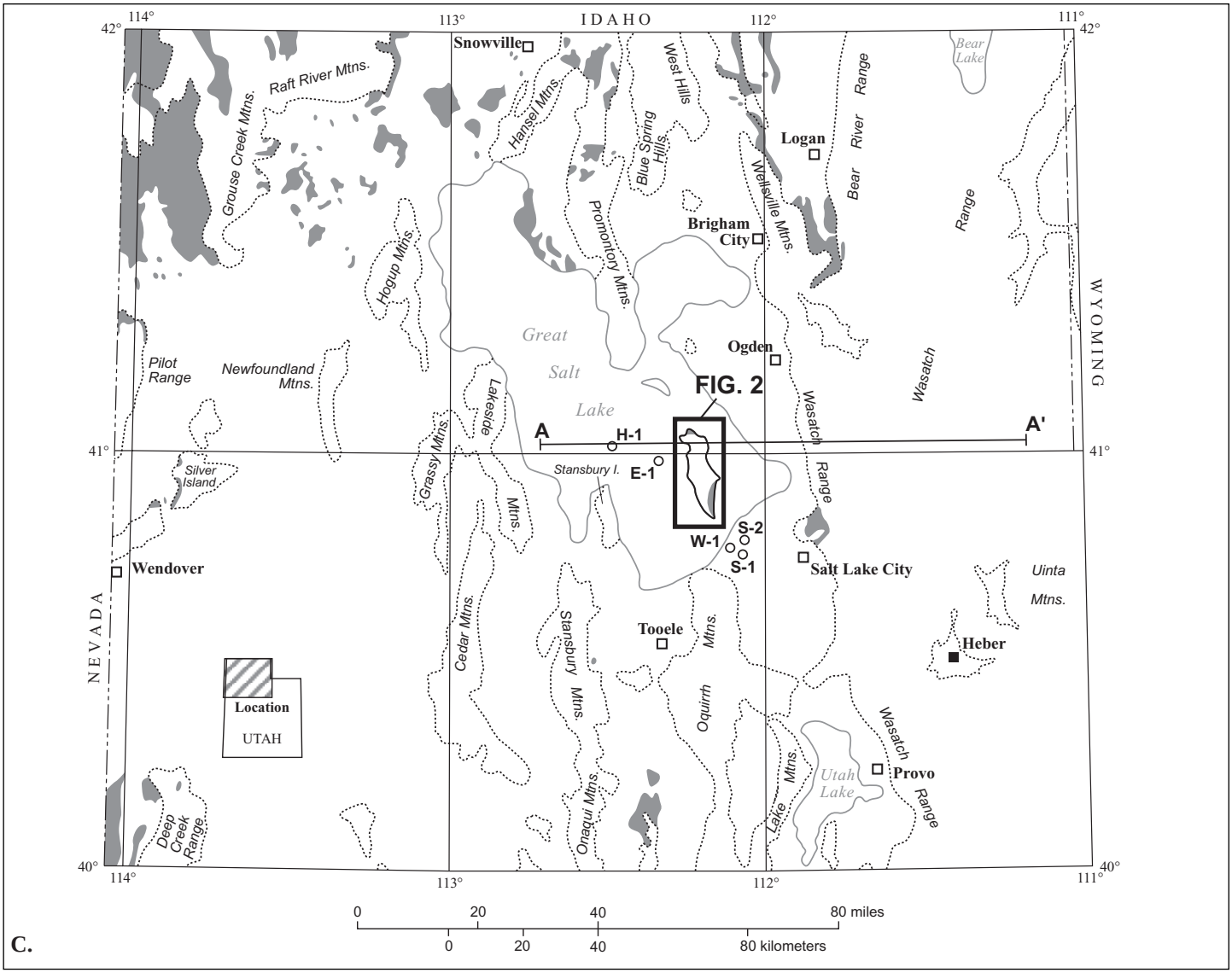

Figure 16C. *Miocene through Pliocene (and possibly some early Pleistocene) fluvial, lacustrine, and volcaniclastic strata, tuff and volcanic ash (mostly rhyolitic), and basalt. These rocks are commonly assigned to the Salt Lake Formation. Though not shown because of Quaternary cover, thousands of feet of rocks of this age also fill the basins between the faulted ranges. The outcrops shown on the map are relatively small remnants of these "basin-fill" rocks preserved on the flanks of upthrown blocks.*

R. 2 W.) bottomed at 3,207 feet (978 m), but the information on the well is unreliable. The Utah Geological Survey sample library holds two boxes of core from the Saltair 2 well, one labeled as the 1,721-1,740 foot (525-530 m) interval and the other as the 3,200-3,207 foot (975-978 m) interval. Both boxes contain only high-grade metamorphic rock. Based on our interpretation of the basin configuration, an examination of geophysical well logs, and the description of the geology penetrated in the nearby Saltair 1 well, we estimate the Tertiary-Precambrian contact is below the 3,000 foot (910 m) interval. We believe that the samples in the higher-interval box are mislabeled and are part of the lower-interval samples. Alternatively, the well may have penetrated a displaced section such as a slump block.

Summary of Regional Correlation

Tertiary deposits on Antelope Island have a lithologic sequence similar to other Tertiary deposits in north Utah (figure 16A-C) (Miller, 1990; Miller and others, in press). This sequence consists of: (1) basal clastic, generally conglomeratic strata, commonly with red coloration, of probable late Paleocene to Eocene age that unconformably overlie Paleozoic or Precambrian rocks; (2) locally overlying and interfingering lacustrine beds in north Utah and east Nevada of late Paleocene to late Eocene age; (3) intermediate-composition volcanic and volcaniclastic deposits of mostly middle and late Eocene age interlayered with, and overlying the lacustrine beds, or overlying the conglomeratic beds where lacustrine beds are absent; (4) generally limited or missing strata of known or assumed Oligocene age; and (5) overlying coarse fluvial to fine-grained lacustrine deposits, vitric tuffs, rhyolite, and locally, basalt, that range from Miocene to Pleistocene in age. The Tertiary section on Antelope Island conforms to this basic sequence.

CONSTRAINTS ON THE WILLARD THRUST FAULT

The large-boulder conglomerate on the southeast part of the island and the breccia on the north end of the island are significant in reconstructing the structural geology of the area. The fractured, easily broken, angular nature of some of the boulders and shale clasts, along with their size of up to 11 feet (3.4 m) in diameter, dictate that they could only have been transported a short distance from their bedrock source.

Boulders in the southeast outcrops eroded from Cambrian, Devonian, and Mississippian strata. Fossiliferous and phosphatic, oolitic limestone clasts from the Mississippian Lodgepole and Deseret Formations are particularly conspicuous. The identifiable boulder and cobble clasts on the north end of the island are from Cambrian or older formations, including olive-green shale derived from the Cambrian Ophir Formation. None of these Paleozoic formations except the Tintic Quartzite are now preserved on the island. A comparison with outcrops along the Wasatch Front suggests that the boulders in both areas came from the footwall of the Willard thrust rather than from the upper plate (figure 3; figure 15) (W.A. Yonkee, verbal communication, 1991). Current direction indicators are not apparent in the deposits, however, the most likely sources for clasts were beds once present on the island block.

We postulate that the Willard thrust cut through Cambrian strata near what is now the north end of the island, and ramped up-section to the Mississippian (probably the Manning Canyon Shale), near the south part of Antelope Island (figure 15). This is similar to exposures in the Wasatch Mountains near Ogden, in which the Willard thrust fault cuts up-section to the south from Cambrian to Mississippian rocks along a lateral ramp (Yonkee, 1992).

The north outcrops contain a small percentage of black argillic quartzite clasts that are most similar to rocks of the Huntsville Group present just above the Willard thrust along the Wasatch Front (Crittenden, 1972). If these are from the hanging wall of the Willard thrust, it also supports a Cambrian position for the thrust near the north end of the island.

SUMMARY AND CONCLUSIONS

More than 2,000 feet (600 m) of Tertiary strata are exposed on Antelope Island. They are divided into lower and upper members of an unnamed conglomeratic unit that are at least 510 feet (153 m) and 140 feet (42 m) thick, respectively; and the Salt Lake Formation, which is over 1,800 feet (550 m) thick. Conglomerate beds of the lower member contain Paleozoic boulders up to 11 feet (3.3 m) in diameter and locally abundant metamorphic clasts and matrix from the Farmington Canyon Complex. The upper conglomerate member contains Paleozoic carbonate and quartzite, Tertiary volcanic, and Precambrian metamorphic clasts and is interbedded with bentonitic mudstone and lacustrine limestone beds. The Salt Lake Formation consists of interbedded volcanic ash, marl, tuffaceous mudstone, conglomerate, and breccia.

The lower conglomeratic member is probably late Paleocene to middle Eocene in age, and probably correlative with the Wasatch Formation to the east and with other Tertiary basal conglomeratic sequences in ranges to the south and west. The coarse nature of the conglomerates suggests that local uplift contributed to their deposition. The uplift may be related to movement on thrust faults of the Sevier orogenic belt, which were in their waning stages in the early Eocene (Bruhn and others, 1983).

The upper conglomerate member may be contemporaneous with an east-west belt of middle Eocene to Oligocene intermediate volcanism south of Antelope Island that blanketed the area with tuff, lavas, and volcaniclastic deposits. Bentonitic mudstone in the member yielded a K-Ar age of 42.9±1.7 Ma, and welded tuff clasts yielded ages of 49.2±1.9 and 38.8±1.5 Ma. Small dikes on the south part of the island may be the only direct record of this igneous event on Antelope Island.

No strata of late Oligocene through middle Miocene age are recognized on Antelope Island, though some of the upper conglomeratic unit could be of this age.

Thick silicic volcanic ash of the Salt Lake Formation, mostly derived from eruptions in the Snake River Plain along the track of the Yellowstone hotspot in southwest Idaho, blanketed northern Utah during the Miocene and Pliocene (Miller, 1990; Perkins and others, 1998; Miller and others, in press). Volcanic ash beds on the island are probably between 11 and 8 million years old. Interbedded, angular to subrounded, poorly sorted clasts indicate local topographic relief.

The older and younger Tertiary deposits on Antelope Island are tilted up to 45 degrees eastward as a unit. Strata of the Salt Lake Formation are parallel to, or are tilted slightly less than older Tertiary rock, indicating that most fault-induced rotation of the island occurred after about eight million years ago. Structural deformation during the Oligocene to middle Miocene was limited to broad warping (Miller and others, in press).

Pre-Tertiary rocks exposed on Antelope Island were part of thick thrust sheets emplaced in a generally eastward-younging sequence across northern Utah (Armstrong, 1968; Royse and others, 1975; Doelling and others, 1990; Miller, 1990; Yonkee, 1990; 1992). The Willard thrust sheet, in excess of 40,000 feet (13,000 m) thick (Crittenden, 1972), passed just above rocks now exposed on Antelope Island (figure 3) (Doelling and others, 1990; Yonkee, 1992). The island rocks in turn were transported eastward on the Ogden thrust, which cuts rocks beneath the island. A later and even lower thrust, the Absaroka, probably formed the basal detachment (figure 3). Most clasts in the conglomerate beds were derived from the lower plate of the Willard thrust, which is now completely eroded from the island. Distinctive suites of clasts on the north and southeast parts of the island suggest that the Willard thrust was in Cambrian strata near the north end of the island, and ramped up to the Mississippian near the south part of the island.

ACKNOWLEDGMENTS

The cooperation and logistical support of the Utah Department of Natural Resources, Division of Parks and Recreation made the field work for this study possible. Michael E. Perkins and William P. Nash of the University of

Utah and Andrei Sarna-Wojcicki of the U.S. Geological Survey analyzed tephra samples and aided in the interpretation of results. David M. Miller of the U.S. Geological Survey and W. Adolph Yonkee of Weber State University provided constructive reviews and made many helpful comments and suggestions based on their extensive studies of the geology of northwest Utah. This study benefitted from many conversations with Hellmut H. Doelling of the Utah Geological Survey.

REFERENCES

Adamson, R.D., Hardy, C.T., and Williams, J.S., 1955, Tertiary rocks of Cache Valley, Utah and Idaho *in* Eardley, A.J., editor, Tertiary and Quaternary geology of the eastern Bonneville Basin: Utah Geological Society Guidebook to the Geology of Utah 10, p. 1-22.

Armstrong, R.L., 1968, Sevier orogenic belt in Nevada and Utah: Geological Society of America Bulletin, v. 19, p. 429-458.

Bortz, L.C., Cook, S.A., and Morrison, O.J., 1985, Great Salt Lake area, Utah, *in* Gries, R.R., and Dyer, R.C., editors, Seismic exploration of the Rocky Mountain region: Rocky Mountain Association of Geologists and Denver Geophysical Society, p. 275-281.

Bruhn, R.L., Picard, M.D., and Beck, S.L., 1983, Mesozoic and early Tertiary structure and sedimentology of the central Wasatch Mountains, Uinta Mountains, and Uinta Basin, *in* Nash, W.P., and Gurgel, K.D., editors, Geologic excursions in the overthrust belt and metamorphic core complexes of the intermountain region, Guidebook, Part I: Utah Geological and Mineral Survey Special Studies 59, p. 63-105.

Bryant, Bruce, 1988, Evolution and early Proterozic history of the margin of the Archean continent in Utah, *in* Ernst, W.G., editor, Metamorphism and crustal evolution of the western United States, Rubey volume 7: Englewood Cliffs, N.J., Prentice Hall, p. 431-445.

Bryant, Bruce, Naeser, C.W., Marvin, R.F., and Mehnert, H.H., 1989a, Ages of late Paleogene and Neogene tuffs and the beginning of rapid regional extension, eastern boundary of the Basin and Range Province near Salt Lake City, Utah: U.S. Geological Survey Bulletin 1787-K, 11 p.

Bryant, Bruce, Naeser, C.W., Marvin, R.F., and Mehnert, H.H., 1989b, Upper Cretaceous and Paleogene sedimentary rocks and isotopic ages of Paleogene Tuffs, Uinta Basin, Utah: U.S. Geological Survey Bulletin 1787-J, 22 p.

Bywater, G.G. and Barlow, J.A., 1909, Antelope Island, Great Salt Lake: Salt Lake City, University of Utah, B.S. thesis, 21 p.

Compton, R.R., 1983, Displaced Miocene rocks on the west flank of the Raft River-Grouse Creek core complex, Utah, *in* Miller, D.M., Todd, V.R., and Howard, K.A., editors, Structural and stratigraphic studies in the eastern Great Basin: Geological Society of America Memoir 157, p. 271-279.

Crittenden, M.D., Jr., 1972, Willard thrust and the Cache allochthon, Utah: Geological Society of America Bulletin, v. 83, p. 2,871-2,880.

Dalrymple, G.B., 1979, Critical tables for conversion of K-Ar ages from old to new constants: Geology, v. 7, no. 11, p. 558-560.

Danzl, R.B., 1985, Depositional and diagenetic environments of the Salt Lake Group at Oneida Narrows, southeastern Idaho: Pocatello, Idaho State University, M.S. thesis, 177 p.

Doelling, H.H., Willis, G.C., Jensen, M.E., Hecker, Suzanne, Case, W.F., and Hand, J.S., 1990, Geologic map of Antelope Island, Davis County, Utah: Utah Geological and Mineral Survey Map 127, 27 p., scale 1:24,000.

Dubiel, R.F., Potter, C.J., Good, S.C., and Snee, L.W., 1996, Reconstructing an Eocene extensional basin - The White Sage Formation, eastern Great Basin, *in* Beratan, K.K., editor, Reconstructing the history of basin and range extension using sedimentology and stratigraphy: Geological Society of America Special Paper 303, p. 1-14.

Eardley, A.J., 1944, Geology of the north-central Wasatch mountains, Utah: Geological Society of America Bulletin, v. 55, no. 7, p. 819-849.

Eardley, A.J., 1955, Tertiary history of north-central Utah, *in* Eardley, A.J., editor, Tertiary and Quaternary geology of the eastern Bonneville Basin: Utah Geological Society Guidebook to the Geology of Utah 10, p. 37-44.

Franczyk, K.J., Pitman, J.K., and Nichols, D.J., 1990, Sedimentology, mineralogy, palynology, and depositional history of some uppermost Cretaceous and lowermost Tertiary rocks along the Utah Book and Roan Cliffs east of the Green River: U.S. Geological Survey Bulletin 1787-N, 27 p.

Hayden, F.V., 1869, Preliminary field report of the U.S. Geological Survey of Colorado and New Mexico: U.S. Geological and Geographical Survey of the Territory, 3rd Annual Field Report, 155 p.

Heylmun, E.B., 1965, Reconnaissance of the Tertiary sedimentary rocks in western Utah: Utah Geological and Mineralogical Survey Bulletin 75, 38 p.

Hintze, L.F. and Stokes, W.L., 1964, Geologic map of northwestern Utah: Utah Geological and Mineralogical Survey, scale 1:250,000.

Irvine, T.N., and Barager, W.R.A., 1971, A guide to the chemical classification of the common volcanic rocks: Canadian Journal of Earth Science, v. 8, p. 523-548.

Larsen, W.N., 1957, Petrology and structure of Antelope Island, Davis County, Utah: Salt Lake City, University of Utah, Ph.D. dissertation, 142 p., scale 1:24,000.

Mann, D.C., 1974, Clastic Laramide sediments of the Wasatch hinterland, northeastern Utah: Salt Lake City, University of Utah, M.S. thesis, 112 p.

Maurer, R.E., 1970, Geology of the Cedar Mountains, Tooele County, Utah: Salt Lake City, University of Utah, Ph.D. dissertation, 184 p.

McDonald, R.E., 1976, Tertiary tectonics and sedimentary rocks along the transition-Basin and Range province to

plateau and thrust belt province, Utah, *in* Hill, J. G. editor, Geology of the Cordilleran hingeline: Rocky Mountain Association of Geologists Symposium, p. 281-317.

Miller, D.M., 1985, Geologic map of the Lucin quadrangle, Box Elder County, Utah: Utah Geological and Mineral Survey Map 78, 10 p., scale 1:24,000.

Miller, D.M., 1990, Mesozoic and Cenozoic tectonic evolution of the northeastern Great Basin, *in* Shaddrick, D.R., Kizis, J.A., Jr., and Hunsaker, E.L., III, editors, Geology and ore deposits of the northeastern Great Basin: Geological Society of Nevada, p. 43-73.

Miller, D.M., 1993, Geologic map of the Crater Island NW quadrangle, Box Elder County, Utah: Utah Geological Survey Map 145, 13 p., scale 1:24,000.

Miller, D.M., Crittenden, M.D., Jr., and Jordan, T.E., 1991, Geologic map of the Lampo Junction quadrangle, Box Elder County, Utah: Utah Geological Survey Map 136, 17 p., scale 1:24,000.

Miller, D.M., Nakata, J.K., Hillhouse, W.C., and Hamachi, Bette, in press, New K-Ar ages for Cenozoic volcanic rocks in the northeastern Great Basin and implications for Cenozoic tectonics: U.S. Geological Survey Bulletin.

Miller, D.M. and Schneyer, J.D., 1985, Geologic map of the Tecoma quadrangle, Box Elder County, Utah and Elko County, Nevada: Utah Geological and Mineral Survey Map 77, 8 p., scale 1:24,000.

Miller, D.M., and Schneyer, J.D., 1994, Geologic map of the Sunset Pass quadrangle, Box Elder County, Utah: Utah Geological Survey Map 154, 14 p., scale 1:24,000.

Moore, W.J., 1973, Summary of radiometric ages of igneous rocks in the Oquirrh Mountains, north-central Utah: Economic Geology v. 68, p. 97-101.

Moore, W.J., and McKee, E.H., 1983, Phanerozoic magmatism and mineralization in the Tooele 1- by 2-degree quadrangle, Utah, *in* Miller, D.M., Todd, V.R. and Howard, K.A., editors, Tectonic and stratigraphic studies in the eastern Great Basin: Geological Society of America Memoir 157, p. 183-190.

Moore, W.J. and Sorensen, M.L., 1979, Geologic map of the Tooele 1- by 2-degree quadrangle, Utah: U.S. Geological Survey Miscellaneous Investigations Map I-1132, scale 1:250,000.

Nelson, M.E., 1971, Stratigraphy and paleontology of the Norwood Tuff and Fowkes Formation, northeastern Utah and southwestern Wyoming: Salt Lake City, University of Utah, Ph.D. dissertation, 181 p.

Nelson, M.G., and Miller, D.M., 1990, A Tertiary record of the giant marmot *Paenemarmota sawrockensis*, in northern Utah: University of Wyoming, Contributions to Geology, v. 28, p. 31-37.

Nolan, T.B., 1935, The Gold Hill mining district, Utah: U.S. Geological Survey Professional Paper 177, 172 p., scale 1:62,500.

Oviatt, C.G., 1986, Geologic map of the Cutler Dam quadrangle, Box Elder and Cache Counties, Utah: Utah Geological and Mineral Survey Map 91, 7 p., scale 1:24,000.

Perkins, M.E., Brown, F.H., Nash, W.P., and Fleck, R.J., 1995, Fallout tuffs of Trapper Creek, Idaho--A record of Miocene explosive volcanism in the Snake River plain volcanic province: Geological Society of America Bulletin, v. 107, no. 12, p. 1,484-1,506.

Perkins, M.E., Brown, F.H., Nash, W.P., McIntosh, William, and Williams, S.K., 1998, Sequence, age and source of silicic fallout tuffs in middle to late Miocene basins of the northern Basin and Range province: Geological Society of America Bulletin v. 110, no. 3, p. 344-360.

Rigby, J.K., 1958, Geology of the Stansbury Mountains, *in* Rigby, J.K., editor, Geology of the Stansbury Mountains, Tooele County, Utah: Utah Geological Society Guidebook 13, p. 1-34.

Royse, Frank, Jr., Warner, M.A., and Reese, D.L., 1975, Thrust belt geometry and related stratigraphic problems, Wyoming, Idaho, northern Utah: Rocky Mountain Association of Geologists Symposium, p. 41-54.

Ryder, R.T., Fouch, T.D., and Elison, J.H., 1976, Early Tertiary sedimentation in the western Uinta basin, Utah: Geological Society of America Bulletin, v. 87, no. 4, p. 496-512.

Schaeffer, F.E., 1960, Stratigraphy of the Silver Island Mountains, *in* Schaeffer, F.E., editor, Guidebook to the Geology of Utah: Utah Geological Society Guidebook 15, p. 15-113.

Slentz, L.W., 1955, Tertiary Salt Lake Group in the Great Salt Lake Basin: Salt Lake City, University of Utah, Ph.D. dissertation, 58 p.

Smith, R.P. and Nash, W.P., 1976, Chemical correlation of volcanic ash deposits in the Salt Lake Group, Utah, Idaho, and Nevada: Journal of Sedimentary Petrology, v. 46, p. 930-939.

Smith, R.B., and Bruhn, R.L., 1984, Intraplate extensional tectonics of the eastern Basin-Range: Inferences on structural style from seismic reflection data, regional tectonics, and thermal-mechanical models of brittle-ductile deformation: Journal of Geophysical Research, v. 89, no. B7, p. 5,733-5,762.

Todd, V.R., 1983, Late Miocene displacement of pre-Tertiary and Tertiary rocks in the Matlin Mountains, northwestern Utah: Geological Society of America Memoir 157, p. 239-270.

Tooker, E.W., and Roberts, R.J., 1961, Preliminary geologic map and sections of the north end of the Oquirrh Range, Tooele and Salt Lake Counties, Utah: U.S. Geological Survey Mineral Investigations Field Map MF-240, scale 1:24,000.

Tooker, E.W., and Roberts, R.J., 1971, Geologic map of the Garfield quadrangle, Salt Lake and Tooele Counties, Utah: U.S. Geological Survey Geologic Quadrangle Map GQ-922, scale 1:24,000.

Van Horn, Richard, 1981, Geologic map of pre-Quaternary rocks of the Salt Lake City North quadrangle, Davis and Salt Lake Counties, Utah: U.S. Geological Survey Miscellaneous Investigations Map I-1330, scale 1:24,000.

Van Horn, Richard, and Crittenden, M.D., Jr., 1987, Maps showing surficial units and bedrock geology of the Fort Douglas quadrangle and parts of the Mountain Dell and Salt Lake City North quadrangles, Davis, Salt Lake, and Morgan Counties, Utah: U.S. Geological Survey Miscellaneous Investigations Map I-1762, scale 1:24,000.

Veatch, A.C.,1907, Geography and geology of a portion of southwestern Wyoming: U.S. Geological Survey Professional Paper 56, scale 1:125,000.

Viveiros, J.J., 1986, Cenozoic tectonics of the Great Salt Lake from seismic reflection data: Salt Lake City, University of Utah, M.S. thesis, 81 p.

Williams, P.L., Covington, H.R., and Pierce, K.L., 1982, Cenozoic stratigraphy and tectonic evolution of the Raft River Basin, Idaho: Idaho Bureau of Mines and Geology Bulletin 26, p. 491-504.

Wilson, E.A., Saugy, Luc, and Zimmermann, M.A., 1986, Cenozoic tectonics and sedimentation of the eastern Great Salt Lake area, Utah: Bulletin de Societe Geologique Francaise, v. 2, no. 5, p. 777-782.

Yonkee, W.A., 1990, Geometry and mechanics of basement and cover deformation, Farmington Canyon Complex, Wasatch Range, Utah: Salt Lake City, University of Utah, Ph.D. dissertation, 255 p.

Yonkee, W.A., 1992, Basement-cover relations, Sevier orogenic belt, northern Utah: Geological Society of America Bulletin, v. 104, p. 280-302.

Yonkee, W.A., Willis, G.C., and Doelling, H.H., this volume (a), Petrology and geologic history of the Precambrian Farmington Canyon Complex, Antelope Island, Utah.

Yonkee, W.A., Willis, G.C., and Doelling, H.H., this volume (b), Proterozoic and Cambrian sedimentary and low-grade metasedimentary rocks on Antelope Island, Utah.

APPENDIX

Measured section S1

Start approximately 1,100 feet east and 2,100 feet south of the northwest corner of section 27, T. 2 N., R. 3 W. Strike and dip at start: N. 20° E., 33° E.

Unit no.	Thickness (feet) unit	cumulative	
Salt Lake Formation			
13	33	123+	Poorly exposed, white, volcanic ash, sandstone, and conglomerate.
12	45	90	Covered.
Upper member of unnamed conglomeratic unit			
11	45	45	Conglomerate with limestone, chert, quartzite, and volcanic clasts; interbedded with thin, conglomeratic, fresh-water limestone and bentonitic mudstone; carbonate clasts are from Cambrian to Mississippian strata; some phosphatic clasts are from the Mississippian Deseret Limestone; moderately to well-rounded clasts; most clasts are 1 to 4 inches, but some are 10 to 14 inches in diameter; at least three lithologic varieties of volcanic clasts; aragonite and calcite cement; poorly sorted, coarse sandstone and gritstone matrix; limestone is micritic, algal, and contains suspended clasts; clast count (202 clasts): volcanic 55%, carbonate 21%, quartzite 15%, chert 9%; (Samples AIMJ-0101 and AITW-0930 were collected from this unit.)
Lower member of unnamed conglomeratic unit			
10	20	390	Covered.
9	105	370	Reddish-purple to pale-gray, bentonitic mudstone; exposed in small gully; locally biotite-bearing; (Sample AIGW-0102 was collected from an outcrop on strike with this unit).
8	55	265	Covered; mudstone float.
7	75	210	Covered; has a few small patches of purple and gray bentonitic mudstone; top of unit is a low rise that may be a buried conglomerate.
6	25	135	Covered; float suggests either more breccia or a reddish mudstone.
5	25	110	Conglomerate and breccia like unit 3; metamorphic clasts; poorly exposed in a few scattered outcrops; clasts become subrounded in upper part; diameters of largest measured clasts: 30 inches, 4 inches, 5 1/2 inches, 18 inches, and 13 inches.
4	15	85	Covered.
3	28	70	Covered intervals (1/2) and grayish-red to dark-reddish-brown conglomerate and breccia (1/2); very poorly sorted; grit matrix; most clasts are angular, a few are moderately rounded; most are 1/2 inch to 6 inches in diameter, but range up to 48 inches long; all clasts are gneiss, schist, pegmatite, and chlorite schist eroded from the Farmington Canyon Complex; clasts are angular to very angular; densely cemented; ledges 2 to 5 feet thick.
2	42	42	Covered.
Farmington Canyon Complex			
1	--	--	Gneiss and migmatite.

Measured Section S2

Start at approximately 850 feet east and 700 feet north of the southwest corner of section 22, T. 2 N., R. 3 W. Strike and dip at start: N.10° E., 30° E.

Unit no.	Thickness (feet) unit	cumulative	
Salt Lake Formation			
14	305+	305+	Covered; end section at road.
Upper member of unnamed conglomeratic unit			
13	15	115	White, calcareous, pebbly sandstone and conglomerate; subangular to subrounded; clast supported; sandy matrix; bedding is 6 inches to 5 feet thick; clasts to 5 inches near base, to 14 inches higher in bed (one notable large clast is a purple metaconglomerate, another is a limestone with crinoids); clast estimate: metaconglomerate and quartzite 50%, metamorphic (gneiss, schist, pegmatite) 10%, carbonate 30%, sandstone 5%, and other 5%.
12	15	100	Covered.
11	5	85	Conglomerate; subangular to subrounded clasts; poorly sorted; from sand-size to 6 inches, most are 1 inch to 3 inches; clast estimate: quartzite 30%, carbonate 30%, metamorphic 25%, chert 10%, sandstone 5%, and other trace.
10	55	80	Covered.
9	25	25	Very pale, grayish-orange conglomerate and gritstone; calcareous matrix; most clasts less than 1 inch; a few up to 3 inches; poorly sorted; immature; many flat shale and mudstone clasts; clast estimate: quartzite 35%, metamorphic 5%, carbonate 20%, and pale mudstone, sandstone and chert 40%.
Lower member of unnamed conglomeratic unit			
8	120	233	Covered.
7	3	213	Pale-gray, bentonitic mudstone; biotitic; plastic.
6	25	210	Conglomerate like unit 5; interbedded with variegated purple and gray bentonitic mudstone.
5	40	185	Medium-gray to pinkish-gray conglomerate in a coarse grit to fine pebble matrix that comprises 50% of the rock; clasts to 16 inches in diameter; clast count (108 counted): carbonate 32%, metamorphic 29%, quartzite 27%, chert 7%, and volcanic 6%.
4	60	145	Covered; float suggests bentonitic mudstone.
3	20	85	Mostly covered; small areas of poorly exposed, dark-brownish-red breccia of metamorphic clasts from the Farmington Canyon Complex.
2	65	65	Covered.
Farmington Canyon Complex			
1	--	--	Gneiss and migmatite.

Measured Section S3

Start approximately 900 feet west and 1500 feet south of the northeast corner of section 16, T. 2 N., R. 3 W. No strike and dip available near start. Strike and dip on unit 5 is N. 5° W., 43° E.

Unit no.	Thickness (feet) unit	cumulative	
Salt Lake Formation			
13	98	1135+	Interbedded, pale-gray to white marl and volcanic ash; mostly stratified; locally ash is nonstratified.
12	170	1037	Covered.
11	85	867	Interbedded, pale-gray to white marl and volcanic ash; locally sandy; stratified; ash is mostly reworked; poorly exposed; nonresistant.
10	197	782	Covered.
9	25	585	Volcanic ash; pale-gray; slightly stratified; poorly exposed in small gully.
8	560	560	Covered; scattered poor exposures of volcanic ash.
Upper member of unnamed conglomeratic unit			
7	30	140	Covered; forms a small topographic rise covered with gravel float that was disturbed by gravel quarrying, then recontoured; may be a conglomerate bed.
6	75	110	Covered.
Offset south along cuesta about 300 feet.			
5	35	35	Very pale-red, pebble and cobble con-

			glomerate interbedded with pale-pinkish-gray limestone; forms a prominent, resistant cuesta for about a mile along strike; clasts are angular to subangular; most less than 6 inches but largest to 20 inches; largest clasts are quartzite and carbonate; gritstone and limestone matrix; smaller clasts and gritstone matrix are mostly from the Farmington Canyon Complex; limestone cement and bedded limestone are sandy, finely crystalline to micritic, and contain some algal structures; interbedded limestone is about 2 feet thick; estimate of composition: matrix 50% (metamorphic 50%, dolomite 20%, other 10%, limestone cement 20%) and clasts 50% (dolomite 45%, limestone 5%, quartzite 40%, metamorphic 10%); clasts are notable for the variety of lithologies (no volcanic clasts were found in spite of a thorough search).
Lower member of unnamed conglomeratic unit			
4	135	270	Covered.
3	45	135	Moderate- to dark-reddish-brown, muddy sandstone and conglomerate with metamorphic clasts; very poorly exposed; forms a few patches of reddish float throughout interval.
2	90	90	Covered; topography suggests Tertiary beneath cover.
Farmington Canyon Complex			
1	--	--	Gneiss and migmatite.

Measured Section S4

Start at approximately 2,500 feet west and 1,600 feet south of the northeast corner of section 9, T. 2 N., R. 3 W. Strike and dip near start: N. 5° E. 37° E.

Unit no.	Thickness (feet) unit	cumulative	
Upper member of unnamed conglomeratic unit			
6	20	530+	Limestone and conglomerate; poorly exposed; forms a small knoll; (this outcrop is the same as unit 5 of measured section S3).
Lower member of unnamed conglomeratic unit			
5	220	510	Covered.
4	20	290	Poorly exposed; dark-reddish-brown slope with metamorphic grit mixed with Paleozoic carbonate and quartzite clasts; float is silty and has abundant metamorphic materials.
3	190	270	Pale-gray conglomerate; very poorly sorted; subangular to subrounded clasts; up to 2-foot-diameter clasts common in lower part; sandy to gritty matrix with some metamorphic gneiss and pegmatite; bedding is poor to absent; no imbrication could be found; clasts with corals, crinoids, and brachiopods are present, but most clasts are nonfossiliferous; clast count near base (102 counted): carbonate 74%, quartzite 20%, chert 4%, metamorphic 1%, and other 1%; clast count near top (125 counted): carbonate 78%, quartzite 17%, chert 2%, metamorphic 2%, and other 1%; limestone dominates over dolomite among the smaller clasts, but all the larger carbonate clasts are dolomite; largest boulders (those over 18 inches in diameter) are dolomite and quartzite; measured in-place boulders: 40 inches, 15 inches, and 43 inches; boulders up to 7 feet in diameter are present in wash and on a boulder-covered beach platform about a hundred feet to the south that are believed to have eroded from this unit.
2	80	80	Covered; float is mostly gravel and boulders deposited by Lake Bonneville that were reworked from Tertiary outcrops.
Farmington Canyon Complex			
1	--	--	Gneiss and migmatite.

Measured Section S5

North tip of Ladyfinger. Start approximately 200 feet north and 500 feet east of the southwest corner of section 19, T. 4 N., R. 3 W. Outcrops form narrow strip along shoreline. Stated thicknesses are questionable because the outcrops are folded, units may be duplicated by several faults, and bedding is poorly defined.

Unit no.	Thickness (feet) unit	cumulative	
Salt Lake Formation			
18	--	--	Covered; top of exposed section.
17	37	760+	Interbedded mudstone and sedimentary breccia; pale-brown where wet, pale-orange-pink to light-brown where dry; crudely bedded; angular clasts; poorly sorted from clay to 1 foot diameter clasts; clasts are estimated at 90% light-colored quartzite, 10% other,

			including micaceous shale, argillite, and dark quartzite; fine-grained intervals have abundant matrix-supported angular clasts.
16	120	723	Covered.
15	45	603	Interbedded mudstone and breccia; pale-pinkish-gray; poorly sorted; mudstone has scattered clasts to 6 inches; breccia has clasts to 18 inches.
14	60	558	Covered.
13	90	498	Sedimentary breccia like unit 10 with a few poorly sorted sandstone beds; quartzite clasts to 2.5 feet in diameter; clasts composition varies but averages about 90% quartzite, 5% limestone, 3% olive gray shale, and 2% dark gray to black argillic quartzite.
strike and dip			N. 45° E., 25° NW.
12	40	408	Sedimentary breccia like unit 10; white- to light-gray; clasts: quartzite 95%, olive-gray shale 4%, dark quartzite, and other 1-2%; quartzite boulders to 2.75 feet in diameter.
11	15	368	Sandstone and breccia; poorly sorted; clasts to 3 inches, medium-gray; minor volcanic ash; grades upward to a breccia with mostly quartzite clasts.
10	140	353	Sedimentary breccia; poorly sorted; clasts to 2 feet in diameter; similar to breccia units below but has higher percentage of quartzite clasts; clasts: quartzite 50%, shale 35%, limestone 10%, and other 5%, in some beds quartzite up to 90%; in this unit quartzite clasts are mostly white to pale-gray, whereas in lower units some are dark gray, brownish gray, and reddish gray.
9	28	213	Reddish-gray mudstone and siltstone with interbedded sedimentary breccia; breccia has olive-gray shale, quartzite, and limestone clasts similar to units below.
8	42	185	Same as units 2 and 5; gray quartzite clasts dispersed throughout.
7	54	143	Coarse, brown breccia with silt and sandy matrix; similar to unit 6 but with fewer fine- bedded layers; clasts are angular to very angular and are up to two feet in diameter; clasts are about 70% olive-colored shale, 20% quartzite, and 10% other; crude bedding.
6	12	89	Similar to unit 4; brown breccia (50%) interbedded with fine-grained siltstone and sandstone (50%); most clasts in the breccia are angular shale up to 8 inches in diameter similar to those described in unit 3; the fine-grained part of the unit has a few clasts up to 2 inches in diameter that make up about 5% of the total volume, and a few stringer and isolated "clots" similar to the coarser part of the unit; the contact with unit 5 is gradational.
5	29	77	Same as unit 3.
4	35	48	Sedimentary breccia; very poorly sorted, pale- to medium-brown mudstone with silt and fine-grained sand matrix; clasts range up to 12 inches in diameter; clasts consist of very angular, light- to moderate-olive-gray, dusky-yellow, and light-olive-brown shale; silty, dolomitic limestone; and quartzite; shale clasts, which are dominant, are platy and nonresistant; unit has crude bedding; clast estimate: shale 50%, quartzite 40%, limestone 8%, and black argillic quartzite—less than 2%; unit is cut by numerous faults with displacements of up to a few feet.
3	12	13	Medium-gray, very fine-grained, reworked volcanic ash interbedded and interfaulted with brown sedimentary breccia; laminated but no partings; ash has some layers that are medium to coarse grained with a few angular clasts up to 2 inches in diameter; most of unit is glass shards; has suspended obsidian grains; breccia clasts are angular, brown to grayish-green shale, quartzite, argillite, and micaceous shale; quartzite clasts are up to 15 inches in diameter; shale are up to about 3 inches; cut by numerous faults, thus actual thickness is uncertain.
2	1	1	Breccia, pale-reddish-brown, sandy matrix, clasts mostly quartzite with minor greenish- gray shale.
Tintic Quartzite			
1	--	--	Intensely fractured and brecciated; locally conglomeratic.

ANTELOPE ISLAND, NEW EVIDENCE FOR THRUSTING

by
Alan R. Hansen[1] and Lon A. McCarley[2]

[1]Consulting Geologist, Lakewood, Colorado
[2]Consulting Geophysicist, Englewood, Colorado

ABSTRACT

The logs and sample cuttings from the Anschutz #1 Orchard well, NW1/4 SW1/4 section 34, T. 3 N., R. 3 W., on Antelope Island and seismic reflection data across the island may indicate the presence of Paleozoic rocks below a thrust fault at a depth of 1,354 feet (410 m). Recently released data are presented as evidence and brief arguments are given.

INTRODUCTION

Antelope Island, probably the best known island in the state of Utah, is in the southeast part of Great Salt Lake. The island is 15 miles (24 km) long, and about 5 miles (8 km) wide with its highest peak reaching 6,597 feet (2,010 m), or about 2,400 feet (730 m) above the lake level. The geology of Antelope Island was first investigated in 1850 by Howard Stansbury (1852) and later by others. Comprehensive geologic maps were prepared by Larsen (1957) of the University of Utah, and Doelling and others (1990) of the Utah Geological Survey. These investigations described metamorphosed and deformed Precambrian rocks that are disconformably overlain by Late Proterozoic and Cambrian metasedimentary rocks, which in turn are unconformably overlain by early Tertiary rocks.

Antelope Island was previously shown in cross section with high-angle normal faults (Larsen, 1957; Doelling and others, 1990) devoid of thrusting. Recent data show that thrusting is present at Antelope Island, with Precambrian and Cambrian metamorphic rocks overlying a thick section of Paleozoic and possibly Mesozoic sedimentary rocks.

During 1971 through 1983, the writer Hansen consulted with The Anschutz Corporation of Denver, Colorado, coordinating various geological and geophysical work on the island. In 1981 the surface estate of the island was acquired by the State of Utah from Anschutz.

Appreciation is expressed to The Anschutz Corporation for permission to publish this information, to Frank Owings and Floyd Moulton who encouraged this study, and to anonymous reviewers.

GEOPHYSICAL DATA

Forty miles (64 km) of heliportable shothole seismic was completed on Antelope Island in 1980. Record quality was good and reflection events were imaged to 6.0 seconds after 24-fold common-depth-point processing. We interpreted thrust planes between discordant reflectors, including a 3 to 4 second “thick” sedimentary section. Magnetotelluric and magnetic data were integrated with the seismic interpretation. We concluded that the depth to magnetic basement is nearly 40,000 feet (12 km), and that Precambrian and Paleozoic rocks at the surface, near the #1 Orchard well, appear to be underlain by a thick interval of low-resistivity rocks that could be Mesozoic in age.

In 1992, some of the seismic records were reprocessed using Dip Moveout (DMO) and Wave Equation Migration techniques. A reinterpreted east-west DMO final stack section is shown in figure 1a and an unmarked version is provided as figure 1b. Our geophysical interpretation shows imbricate east and southeast thrusting followed by low-angle extension and normal faulting, as shown in figure 2 cross section A-A'. The seismic-line location is shown on the index map.

GEOLOGIC DATA

In 1976, a water well on Antelope Island, the Anschutz #1 Orchard, NW1/4 SW1/4 section 34, T. 3 N., R. 3 W. (see index map in figure 2), was drilled and logged to a depth of 2,077 feet (629 m). The well spudded in Cenozoic valley fill, consisting of granitic debris, quartzite, clay, black shale, volcanic tuff, sand, and mica. This material was logged to a depth of 1,220 feet (370 m), where a granite or granite gneiss and some tuffaceous rock were encountered. Beginning at 1,354 feet (410 m), a limestone and dolomitic interval was drilled to the total depth. Figure 3 shows the electrical and gamma ray logs from the well.

The carbonate cuttings were examined in 1978 by micropaleontologist Morris S. Petersen of Brigham Young University. Dr. Petersen reported, "It is my opinion that these rocks represent the Mississippian section in central Utah." The writers concur with this interpretation.

Doelling and others (1990) noted large boulders of Mississippian carbonate rock 10 feet (3 m) or more in diameter on the east side of the island. In 1994 the writer McCarley was directed by Doelling to an outcrop above Mushroom Springs (figure 2) where carbonate boulders and abundant quartzite clasts were noted. The carbonates contain abundant

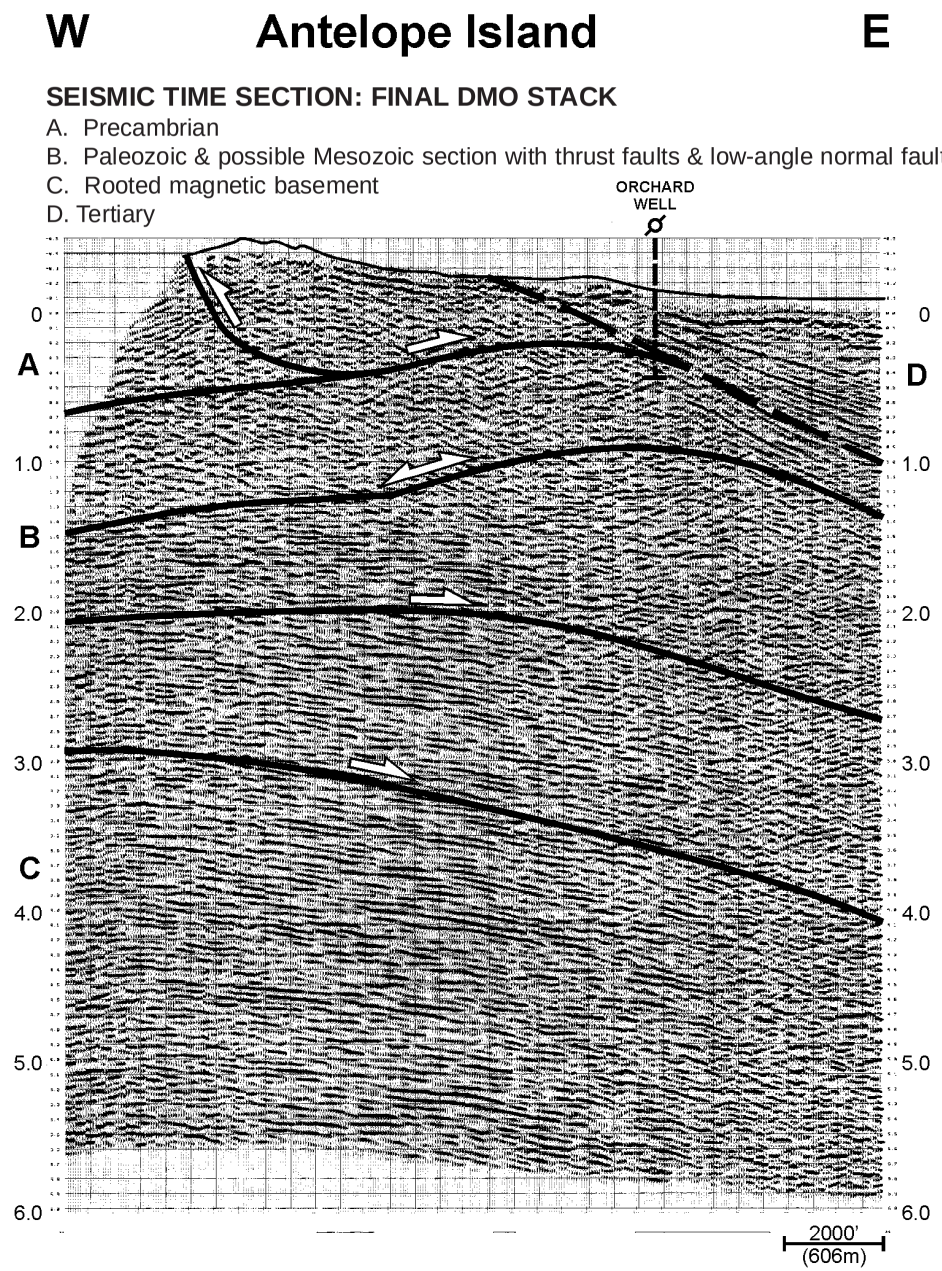

Figure 1a

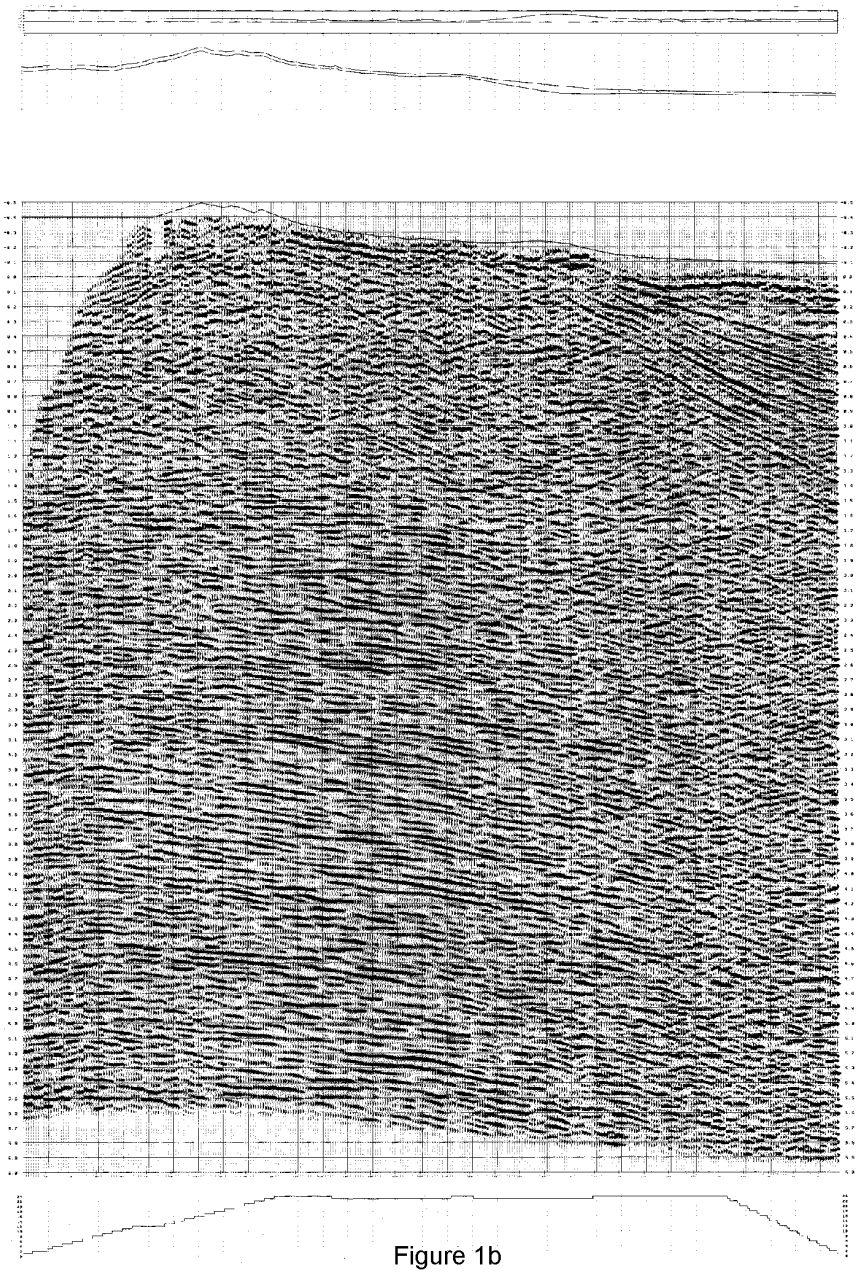

Figure 1b

Figure 1. *East-west seismic section across Antelope Island to the eastern shoreline of the Great Salt Lake. Both the interpreted version and the unmarked section are given.*

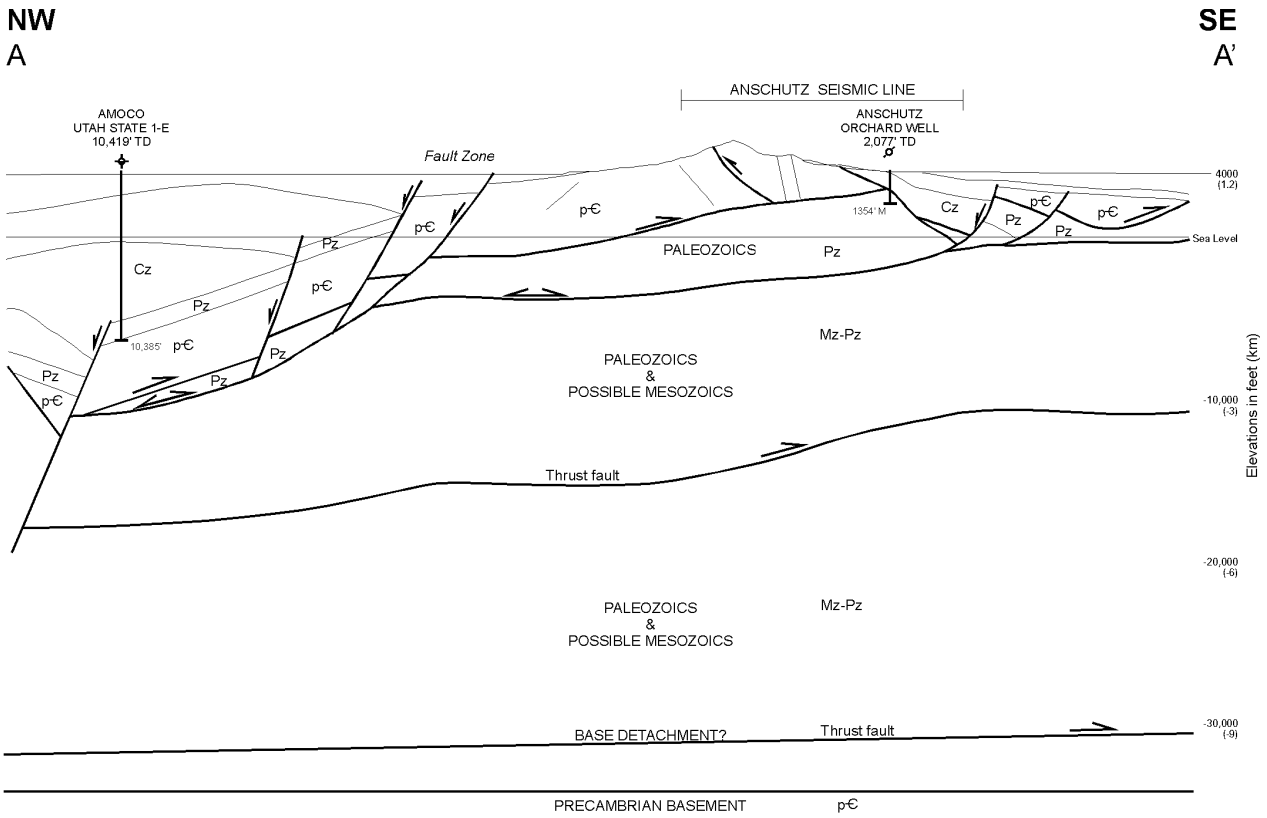

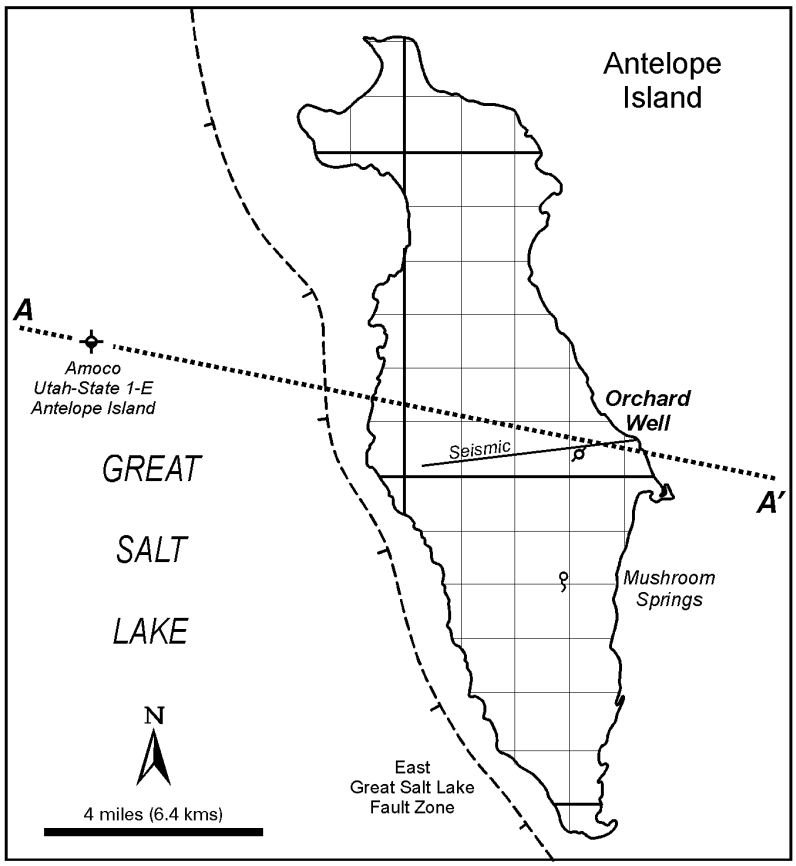

Figure 2. *East-west geologic cross section A-A' and index map showing the seismic line, Anschutz #1 Orchard well, the Amoco Utah State #1-E well, and major faulting. Cz = post-thrusting Cenozoic rocks and deposits, Mz-Pz = possible Mesozoic and Paleozoic sedimentary rocks, M = Mississippian rocks, Pz = Paleozoic sedimentary rocks, p€ = Upper Proterozoic and Archean to Lower Proterozoic Farmington Canyon Complex.*

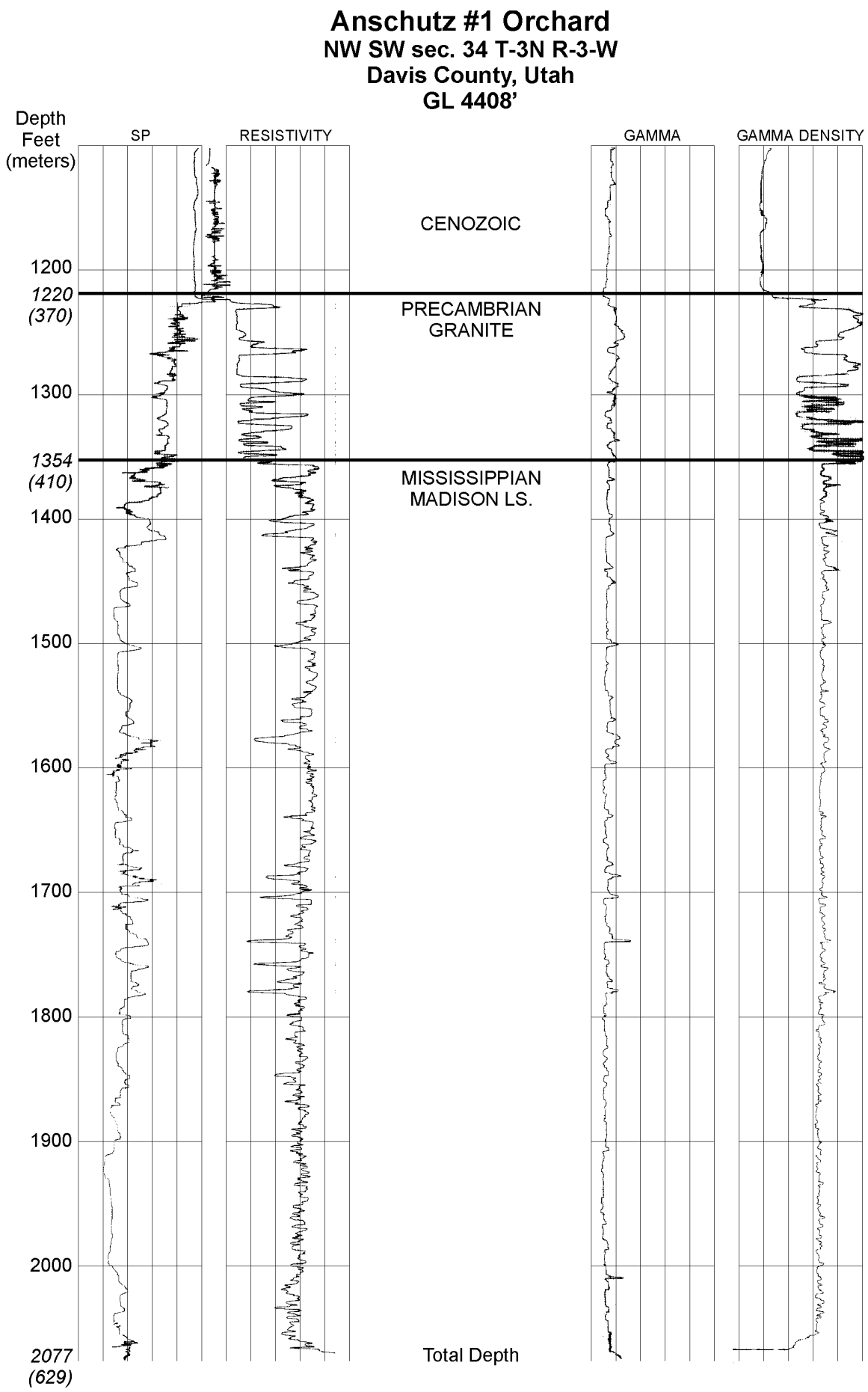

Figure 3. *Electrical resistivity and gamma-ray logs of the Anschutz #1 Orchard well, NW1/4 SW1/4 section 34, T. 3 N., R. 3 W.*

crinoid debris and have been identified by Norman Silberling (Consulting Geologist, Lakewood, Colorado) and Peter Sheehan (Geologist of the Milwaukee Public Museum, Milwaukee, Wisconsin) as being from the upper Ordovician Fish Haven Dolomite. The quartzite is tentatively identified as being from the Ordovician Swan Peak Quartzite. This boulder/clast material is probably erosional debris from an earlier thrust underlying the Precambrian granite.

CONCLUSIONS

Antelope Island is a topographic and structural high that has been affected by multiple episodes of thrusting. Mississippian and older Paleozoic-age rocks underlie the allocthonous Precambrian section. Our geologic interpretation in figure 2 shows that sedimentary rocks at least 30,000 feet (9.1 km) thick may exist beneath the island.

REFERENCES

Doelling, H.H., 1989, Antelope Island State Park--The history, the geology, and wise planning for future development: Utah Geological and Mineral Survey, Survey Notes v. 23, no. 1, p. 2-14.

Doelling, H.H., Willis, G.C., Jensen, M.E., Hecker, Suzanne, Case, W.F., and Hand, J.S., 1990, Geologic map of Antelope Island, Davis County, Utah: Utah Geological and Mineral Survey Map 127, scale 1:24,000.

Larsen, W.N., 1957, Petrology and structure of Antelope Island, Davis County, Utah: Salt Lake City, University of Utah, Ph.D. dissertation, 142 p.

Stansbury, Howard, 1852 (reprinted in 1988), Exploration and survey of the valley of the Great Salt Lake, including a reconnaissance of a new route through the Rocky Mountains: Philadelphia, Lippincott, Grambo & Co., 487 p. [U.S. 32nd Congress, Special Session, Senate Executive Document 3](reprinted with the title “Exploration of the valley of the Great Salt Lake” by Smithsonian Institution Press, Washington D.C. 421 p.).

LATE PLEISTOCENE AND HOLOCENE SHORELINE STRATIGRAPHY ON ANTELOPE ISLAND

by
Stuart B. Murchison[1] and William E. Mulvey[2]

[1]formerly Department of Geography, University of Utah
[2]formerly Utah Geological Survey
now at 4408 Surry Ridge Circle
Apex, NC 27502

INTRODUCTION

The late Pleistocene and Holocene stratigraphy of Great Salt Lake and the Great Salt Lake Desert is preserved at various lake-margin localities, including cored or trenched basin depositional sites, archeological sites, and islands (Murchison, 1989a). Antelope Island has been isolated during parts of this century due to lake rises, and has thus not been studied in detail. The historic high level 4,211.85 feet (1,283.77 m), reached during the 1986-1987 lake rise, produced littoral deposits and new exposures that were investigated between October 1 and December 6, 1987, as part of the Utah Geological Survey (UGS) Antelope Island Project. Our part of the study concerned Holocene geologic history, processes, and geomorphology.

Age control on the stratigraphy of late Pleistocene and Holocene Great Salt Lake units was limited before researchers obtained numerous radiocarbon age estimates on samples collected at Antelope Island between 1986 and 1988. A new chronology of the hydrographic history of Great Salt Lake was under investigation at the inception of the UGS Antelope Island project, and Antelope Island offered a unique opportunity for geographers and geologists to study semi-pristine littoral units. A wealth of chronostratigraphic information was extracted from three localities on the island (figure 1).

The Island's conspicuous Lake Bonneville shorelines (Stansbury, Bonneville, and Provo Levels) have been, and continue to be studied, but relatively few researchers have concentrated on the post-Pleistocene (Holocene) history of the lake (see for examples Gilbert, 1890; Eardley and others, 1957; Crittenden, 1963; Morrison, 1965; Scott and others, 1983). Ross (1973) made some morphostratigraphic studies of post-Bonneville lacustrine deposits at Lady Finger Point, White Rock Bay, and Bridger Bay (see figure 1), often erroneously incorporating shorelines of earlier Lake Bonneville fluctuations. Spencer (1983) conducted geochemical and McKenzie and Eberli (1987) conducted isotope chronostratigraphic studies on cores taken west of Antelope Island at 41° N., 112° 20' W. The geomorphic evidence and the geochemical and isotope chronostratigraphic data from cores were utilized to estimate the timing of the late Holocene high lake level of 4,221 feet (1,286.5 m) (Currey and others, 1988a).

Atwood and Mabey (1988 and this volume) studied shoreline features around Antelope Island produced by the 1986-1987 lake rise, revealing littoral deposits and erosional cuts up to about 6 feet above the static water line of 4,211.85 ft (1,283.7 m).

LATE PLEISTOCENE AND EARLY HOLOCENE UNITS

Seagull Point contains a sequence of sediments which range in age from post-Provo (<14,200 ^{14}C yr B.P.) (Currey and Burr, 1988) to late Holocene (figure 2). Pre-Gilbert red beds discussed by Currey and others (1988b) lie unconformably over a groundwater(?)-stained boulder unit of the Bonneville Alloformation. The red beds are calcareous muds (clays) and minor sands that were reddened off-site and deposited basinward on newly exposed flats about 13,000 ^{14}C yr B.P. (Currey and others, 1988b). The red beds range in thickness from 3 to 5 feet (0.9 to 1.5 m) with a 6.5 degree eastward dip. This red-bed unit contains an oxidized ostracode-rich red sand horizon averaging 0.75 inch (1.9 cm) that is consistent and traceable throughout the exposure. This sand is overlain by more red beds and the top of the red-bed unit is overlain unconformably by an ostracode-rich fine-sand layer that is up to 0.3 inch (0.76 cm) thick (Murchison, 1989a). It is assumed (Murchison, 1989a) that both of these ostracode-rich assemblages were probably deposited during a hiatus when the lake was lower than Seagull Point and salinities were higher, killing the ostracodes.

A Gilbert transgressive green sand unit 1 to 2 feet thick (0.3 to 0.6 m) overlies the pre-Gilbert red beds. The sand exhibits alternating color bands composed of fine, well-sorted quartz grains with rare silt and clay stringers. Some layers have been stained orange and brown, probably due to groundwater(?) oxidation. This green sand contains an assemblage of gastropods in the upper portion. It is therefore similar to, and correlated with, a green sand unit deposited at the Public Shooting Grounds, near Corrine, Utah, between 11,000 and 10,000 ^{14}C yr B.P. (Murchison, 1989a). Both units contain similar sand texture, color, and gastropod death assemblages. A Gilbert regressive sand unit unconformably overlies the Gilbert transgressive green sands locally at Seagull Point. This regressive unit is composed of wave-rippled beds of well-sorted carbonate sands of coarse to medium texture,

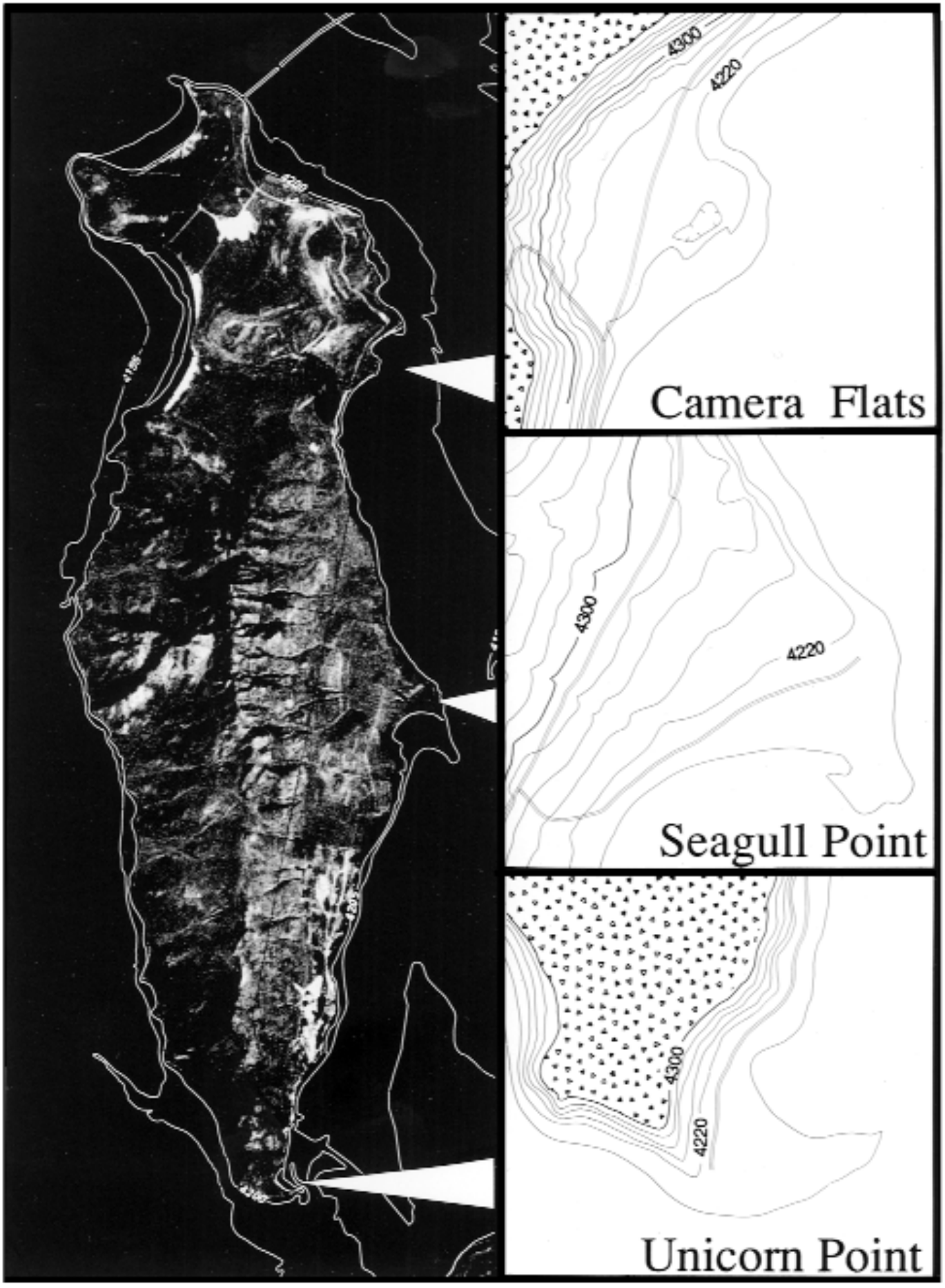

Figure 1. *Aerial photograph of Antelope Island showing sites discussed in this paper and inserts of the sites.*

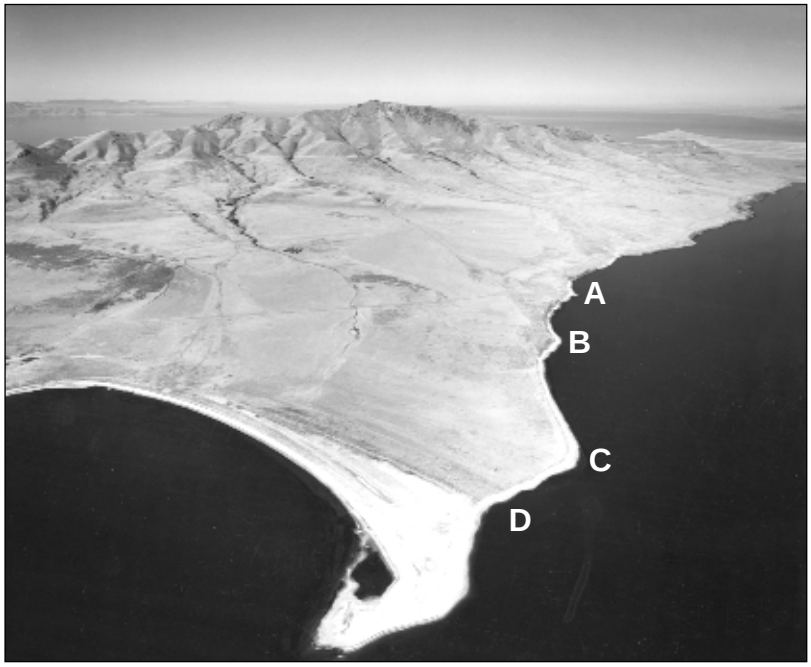

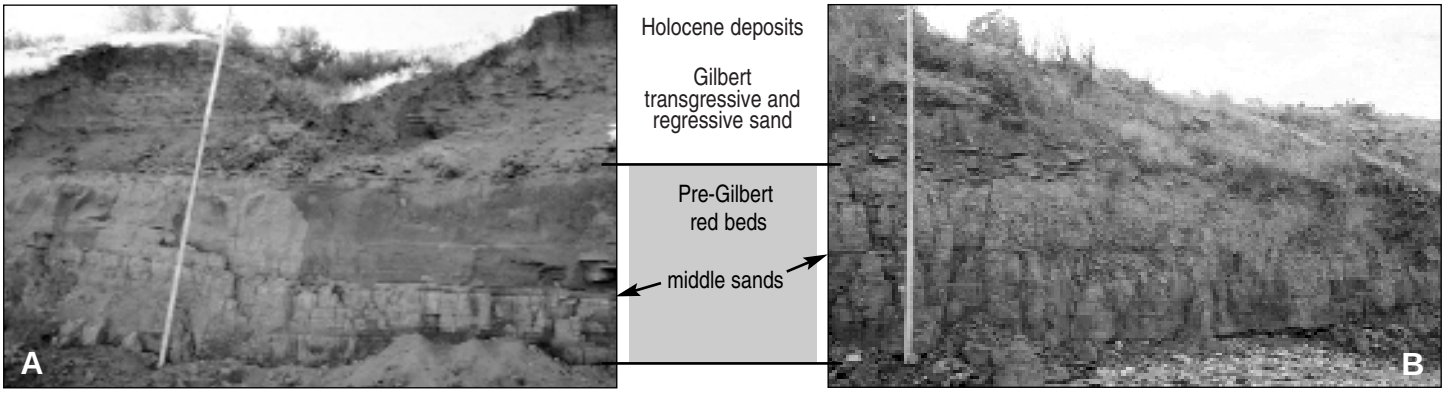

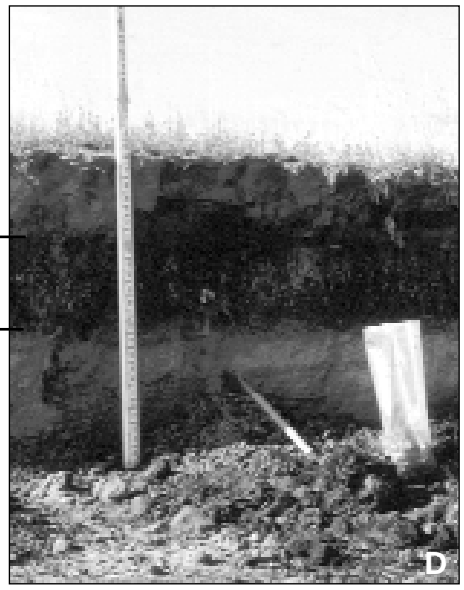

Figure 2. *Shoreline stratigraphy at Seagull Point exposure showing pre-Gilbert red beds, Gilbert transgressive beds overlain by Gilbert regressive beds, and middle to late Holocene deposits. Letters on the oblique aerial photograph correspond to photographs of exposures below. (Labels on A through D were added by editors and may vary slightly from authors' interpretations.) A. Bluff is approximately 14 feet (4 m) high. B. Bluff is approximately 10 feet (3 m) high. C. View looking northwest showing resistant nature and uniform bedding of shoreline deposits. Photographer is approximately 6 feet (2 m) tall. D. Middle Holocene deposits. Bluff is approximately 4 feet (1.2 m) high. Compare with figure 3.*

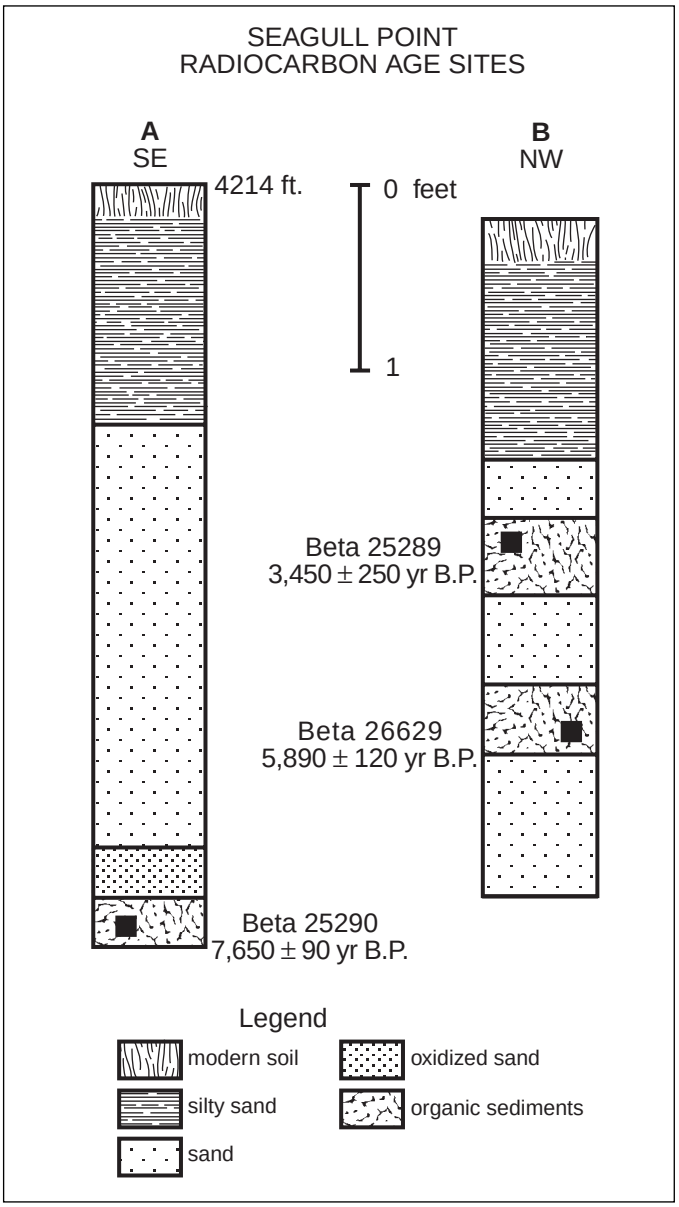

Figure 3*. Stratigraphic columns on the eastern part of the Seagull Point exposure (near figure 2D), with an explanation of symbols and patterns (modified from Murchison, 1989a).*

which are interlaminated with clays and silts (Murchison, 1989a).

The sand unit that overlies the Gilbert regressive rippled beds is fine to medium grained and lacks defined bedding. The 6 feet thickness (1.8 m), texture, and relatively low ripple index suggests that this sand unit was deposited as a dune complex after the Gilbert regression sometime after 10,000 ^{14}C yr B.P. (Murchison, 1989a).

A late Gilbert episode, documented by Rubin and Alexander's (1958) 9,730 ± 350 yr B.P. age estimation at Hooper, Utah, is probably expressed as transgressive pebbles and cobbles that overlie the dune sand unit between 4,225 and 4,228 feet (1,287 and 1,288 m). The pebbles and cobbles grade into cemented sands lakeward as low as 4,224 feet (1,287 m). This coarse-grained material is interpreted as a post-Gilbert transgression to the 4,230 foot (1,289.3 m) level seen as beach crests and berms around the lake (Murchison, 1989a).

Figure 4. *Aerial photograph of Unicorn Point showing surveyed shoreline features (from Murchison, 1989a).*

MIDDLE HOLOCENE UNITS

The middle Holocene, sometimes referred to as the Altithermal, has been described as a period of reduced moisture effectiveness and low lake levels in the western and southwestern United States (Antevs, 1955; Morrison, 1966; Currey 1980; Madsen, 1980; Currey and James, 1982; Mehringer, 1985). This arid environment was assumed to have been prevalent at Great Salt Lake, although no direct corroborating radiometric evidence of lacustrine deposition has been recovered. At Seagull Point, chronostratigraphic evidence supports and documents lower lake levels (Murchison, 1989a).

On the eastern end of Seagull Point, middle Holocene marsh deposits crop out as wedge-shaped bodies of organic sediments. The organic sediments probably accumulated behind berms or barrier beaches and are thought to continue laterally along strike throughout the length of the Point (Murchison, 1989a).

The oldest and most organic sediment sample (8.0 gm of humates) was taken from a 2-inch-thick (5 cm) bed at an elevation of 4,210 feet (1,283 m)(figure 3A). The sample was overlain by a 6-inch-thick (15 cm) oxidized coarse sand unit and a white-gray calcareous, medium-grained sand unit with a modern soil developed on it. The sample has a radiocarbon age of 7,650 ± 90 yr B.P. (- 26.4 ‰ ^{13}C; Beta 25290). The high organic content suggests accumulation on a lagoon floor during a protracted lake rise and stabilization level. The presence of oxidized coarse sands overlying the organic sediment infers a drop in lake level and subaerial exposure after deposition (Murchison, 1989a), supporting the theory of Currey (1980) and Currey and James (1982) for partial desiccation in post-Bonneville times.

West of the Beta 25290 sample, a 6-inch (15 cm) wedge-shaped organic bed is found at 4,211 feet (1,283 m)(figure 3B). The radiocarbon age of a sample (2.5 gm of humates) of the organic marshy material is 5,890 ± 120 yr B.P. (-26.1 ‰ ^{13}C; Beta 26629). This organic stratum overlies a coarse sand unit 10 inches (25 cm) thick and is conformably overlain by a graded, white to gray, medium clean sand unit 4 inches (10

cm) thick. This clean sand unit indicates eolian conditions after organic deposition, implying lake regression after 5,900 yr B.P. to at least a mean level of 4,200 feet (1,280 m) or lower (Murchison, 1989a).

LATE HOLOCENE UNITS

Marsh sediment located 1 foot (30 cm) above sample Beta 26629 at Seagull Point (figure 3B) indicates that the next identifiable lake rise at this site took place about 3,450 ± 250 yr B.P. (-25.5 ‰ ^{13}C; Beta 25289). The sample (1.7 gm of humates) was dug from an 8-inch-thick (20 cm) wedge-shaped bed exposed in a bluff at 4,212 feet (1,283 m). Conformably overlying the marsh sediment is a calcareous medium to fine sand and modern soil. This marshy sediment is probably the precursor, and its age is the maximum limiting age, of the lake rise to 4,221 feet (1,286 m) (Murchison, 1989a) discussed in Currey and others (1988a) and Merola and others (1989).

Farther west in the Seagull Point exposure is a cemented gravel layer at 4,219 feet (1,285 m). These transgressive gravels and the 4,221 feet (1,286 m) grass-covered berm on the surface mark the Holocene high water level at this site (Murchison, 1989a).

A lagoonal depression behind the 4,221 foot (1,286 m) berm at Camera Flats (figure 1) is thought to be a washover marsh from the late Holocene lake high water level. A sample (1.9 gm of humates) was taken from a 16-inch-deep (40 cm) pit below the modern soil. An accelerator mass spectrometer (AMS) age estimate of 1,400 ± 75 yr B.P. (Beta 25580 and AMS ETH 3999, ^{13}C adjustment by Beta Analytic Inc.) was reported for this sample. This radiocarbon age estimate represents a minimum limiting age for the late Holocene high and supports previous hypotheses for the geochronology of the lake (Murchison, 1989a) presented in Currey (1987), and McKenzie and Eberli (1987).

Late Holocene Geomorphology

Chronometric data inferred for Great Salt Lake after 1,400 ± 75 yr B.P. consist of archeologic radiocarbon age estimates at various temporary and permanent lakeshore camps near the Bear and Weber River deltas (Aikens, 1966,1967; Shields and Dalley, 1968; Fry and Dalley, 1979). The lack of geomorphic or stratigraphic radiocarbon age estimates between 1,400 yr B.P. and the historical record are partially addressed by the qualitative analysis of shoreline berms and surficial material at Unicorn Point (figure 4).

A paleogeographic reconstruction of the features at Unicorn Point was produced from 50 Electronic Distance Measuring (EDM) theodolite survey points and surficial textural analysis, revealing four major beach-building events. Late Holocene beach berms were mapped at 4,217 feet (1,285.3 m), 4,214 feet (1,284.5 m), 4,214 feet (1,284.4 m), and 4,212 feet (1,283.7 m). As seen on figure 4, the post-Gilbert 4,230 foot (1,289.3 m) and late Holocene 4,221 foot (1,286.5 m) beaches seem to be wave-cut notches with little or no accumulation of nearshore material. These beaches were eroded by a high-energy regime, producing pebbles and cobbles within a matrix of weathered ooids and sand, probably deposited by swash (Murchison, 1989a).

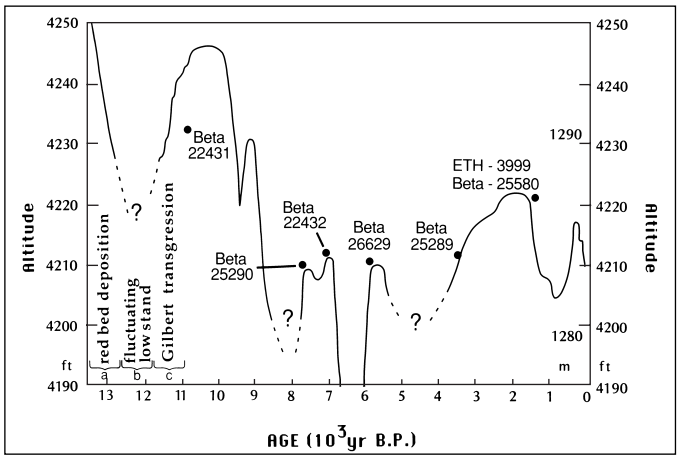

Figure 5. *Fluctuation history of Great Salt Lake 13,000 yr B.P. to present (from Murchison, 1989a).*

The next highest berm is found at 4,217 feet (1,284.3 m) and is composed of pebbles and ooids deposited by littoral progradation from the northwest and the north-northeast. This beach-building event was responsible for the first small spit developed at Unicorn Point and probably occurred between 300 and 400 yr B.P.; see Mehringer (1985) for supporting climatic data and dates. Two berms at 4,214 feet (1,284.5 and 1,284.4 m) seem to have been deposited during different lake-rise episodes which occurred very close temporally, most likely beginning around 1,700 A.D. (McKenzie and Eberli, 1987). The higher level (figure 4, 1-4,214 feet) added beach sediment (88% ooids) on the southeast shore while curving the previous spit tip toward the northwest, probably forming the unicorn's horn, much like King and McCullaghs' (1971) simulation of spit recurvature. The lower 4,214 foot (1,284.4 m) shoreline (figure 4, 2-4,214 feet) “encapsulated” the older feature with cobble and gravel berms. This last depositional event is thought to be the last major lake rise of the 1700s A.D. (Murchison, 1989a) as reported by Currey and James (1982). The 4,212-foot-high (1,283.7 m) water line of 1986-1987 can be seen as a small ridge of gravel and debris hummocks.

SUMMARY

Three localities on Antelope Island have provided data for estimating the fluctuation history of Great Salt Lake during the past 13,000 years (figure 5). The late Pleistocene and early Holocene history is best seen at Seagull Point. The regression from the post-Provo shoreline to well below 4,220 feet (1,286.2 m) produced the deposition of oxidized sediment (red beds) that overlie Bonneville Alloformation units (boulders). Red bed deposition was probably episodic, as evidenced by ostracode death assemblages within and unconformably overlying the oxidized sands (ostracode-rich layers). Sometime after 12,000 yr B.P., the lake began a fluctuating rise to the Gilbert shoreline, best shown by layers of well-sorted green nearshore sands (transgressive green sands) and gastropod death assemblages dated elsewhere near 11,000 yr B.P. A post-Gilbert regression (wave-rippled beds) to a probable 4,225 feet level (1,287.7 m) is thought to have occurred after 10,000 yr B.P., followed by a minor transgression (peb-

bles and cobbles overlying a dune unit) to 4,230 feet(1,289.2 m) between 9,700 and 9,450 yr B.P.

It is believed that the lake lowered significantly during the Altithermal period to near a mean level of 4,200 feet (1,283.2 m) or lower. A minor transgression (organic sediment) to 4,210 feet (1,283.2 m) and probable regression (oxidized coarse sand) occurred near 7,650 ± 90 yr B.P. (Beta-25290). The lake began to rise to a 4,211 foot (1,283.5 m) level (organic sediment) around 5,890 ± 120 yr B.P. (Beta-26629), then dropped to lower levels (medium clean sand). The dry period continued until about 3,450 ± 250 yr B.P. (Beta-25289) when the lake began to rise (organic sediment) to an eventual 4,221 feet (1,286.5 m) level. The lake probably fluctuated at this high level until 1,400 ± 75 yr B.P. (Beta-25580 and ETH-3999), then dropped to lower levels (organic washover marsh). It is believed that "Little Ice Age" climatic influences caused the lake to rise to the 4,217 feet (1,285.7 m) level around 400 to 300 yr B.P. (1600 to 1700 A.D.) Subsequent fluctuations after 250 yr B.P. (1750 A.D.) probably built the remaining shoreline berms seen on Unicorn Point.

REFERENCES

Aikens, C.M., 1966, Fremont-Promontory-Plains relationships in northern Utah: University of Utah Anthropological Papers no. 82, p. 11-73.

---1967, Excavations at Snake Rock Village and the Bear River no. 2 site: University of Utah Anthropological Papers no. 87, p. 33-55.

Antevs, Ernst, 1955, Geologic-climate dating in the West U.S.: American Antiquity, v. 20, no. 4, p. 317-335.

Atwood, Genevieve and Mabey, D.R., 1988, Elevations of shoreline features produced by the 1986-87 high level of Great Salt Lake: Geological Society of America Abstracts with Programs, v. 20, no. 6, p. 404

Crittenden, M.D., Jr., 1963, New data on the isostatic deformation of Lake Bonneville: U.S. Geological Survey Professional Paper 454-E, 31 p.

Currey, D.R., 1980, Coastal geomorphology of Great Salt Lake and vicinity, *in* Gwynn, J.W., editor, Great Salt Lake - A scientific, historical, and economic overview: Utah Geological and Mineral Survey Bulletin 116, p. 69-82.

---1987, Great Salt Lake levels - Holocene geomorphic development and hydrographic history, *in* Laboratory for Terrestrial Physics, third annual Landsat workshop: NASA Goddard Space Flight Center, Greenbelt, Maryland, p. 127-132.

Currey, D.R. and James, S.R., 1982, Paleoenvironments of the northeastern Great Basin and northeastern Basin rim region - A review of geological and biological evidence, *in* Madsen, D.B. and O'Connell, J.F., editors, Man and environment in the Great Basin: Society for American Archeology Papers no. 2, p. 27-52.

Currey, D.R., Berry, M.S., Douglass, G.E., Merola, J.A., Murchison, S.B., Ridd, M.K., Atwood, Genevieve, Bills, B.G., and Lambrechts, J.R., 1988a, The highest Holocene stage of Great Salt Lake: Geological Society of America Abstracts with Programs, v. 20, no. 6, p. 411.

Currey, D.R., Berry, M.S., Green, S.A., and Murchison, S.B., 1988b, Very late Pleistocene red beds in the Bonneville basin, Utah and Nevada: Geological Society of America Abstracts with Programs, v. 20, no. 6, p. 411.

Currey, D.R. and Burr, T.N., 1988, Linear models of threshhold controlled shorelines of Lake Bonneville *in* Machette, N.M., editor, In the footsteps of G.K. Gilbert-Lake Bonneville and neotectonics of the eastern Basin and Range Province: Utah Geological and Mineral Survey Miscellaneous Publication 88-1, p. 104-110.

Eardley, A.J., Gvosdetsky, Vasyl, and Marsell, R.E., 1957, Hydrology of Lake Bonneville and sediments and soils of its basin: Geological Society of America Bulletin, v. 68, p. 1141-1202.

Fry, G.F. and Dalley, G.F., 1979, The Levee site and the Knoll site: University of Utah Anthropological Papers no. 100, p. 3-68.

Gilbert, G.K., 1890, Lake Bonneville: U.S. Geological Survey Monograph 1, 438 p.

King, C.A.M. and McCullagh, M.J., 1971, A simulation model of a complex recurved spit: Journal of Geology, v. 79, p. 22-37.

MacKenzie, J.A. and Eberli, G.P., 1987, Indications for abrupt Holocene climatic change - Late Holocene oxygen isotope stratigraphy of the Great Salt Lake, Utah, *in* Berger, W.H., and Labeyrie, L.D., editors, Abrupt climatic change: Dordrecht, Germany, D. Reidel Publishing Co., p. 127-136.

Madsen, D.B., 1980, The human prehistory of the Great Salt Lake region, *in* Gwynn, J.W., editor, the Great Salt Lake - A scientific, historical, and economic overview: Utah Geological and Mineral Survey Bulletin 116, p. 19-31.

Mehringer, P.J., 1985, Late-Quaternary pollen records from the interior Pacific Northwest and northern Great Basin of the United States, *in* Bryant, V.M., Jr., and Holloway, R.G., editors, Pollen records of Late-Quaternary North American sediments: Dallas, American Association of Stratigraphic Palynologists Foundation, p. 167-189.

Merola, J.A., Currey, D.R., and Ridd, M.K., 1989, Thematic Mapper laser profile resolution of Holocene lake limit, Great Salt Lake Desert, Utah: Remote Sensing of Environment, v. 28, p. 233-244.

Morrison, R.B., 1965, New evidence on Lake Bonneville stratigraphy and history from southern Promontory Point, Utah: U.S. Geological Survey Professional Paper 525-C, p. 110-119

---1966, Predecessors of Great Salt Lake, *in* Stokes, W.L., editor, The Great Salt Lake: Salt Lake City, Utah Geological Society, p. 75-104.

Murchison, S.B., 1989a, Fluctuation history of Great Salt Lake, Utah, during the last 13,000 years: Salt Lake City, University of Utah, Ph.D. dissertation, 137 p.

Murchison, S.B., 1989b, Utah chub (*Gila atraria*) from the latest Pleistocene Gilbert shoreline, west of Corrine, Utah: Great Basin Naturalist, v. 49, no. 1, p. 131-133.

Ross, D.S., 1973, Holocene fluctuations of Great Salt Lake with special reference to evidence from the eastern shore: Salt lake City, University of Utah, M.S. thesis, 111 p.

Rubin, Meyer, and Alexander, Corrine, 1958, U.S. Geological Survey radiocarbon dates IV: Science, v. 127, p. 1,476-1,487.

Scott, W.E., McCoy, W.D., Shroba, R.R., and Rubin, Meyer, 1983, Reinterpretation of the exposed record of the last two cycles of Lake Bonneville, western United States: Quaternary Research, v. 20, p. 261-285.

Shields, W.F. and Dalley, G.F., 1968, Excavations at Bear River no. 3: University of Utah Anthropological Papers no. 22, p. 60-65.

Spencer, R.J., 1983, The geochemical evolution of Great Salt Lake, Utah: Baltimore, MD, John Hopkins University, Ph.D. dissertation, 308 p.

SHORELINES OF ANTELOPE ISLAND AS EVIDENCE OF FLUCTUATIONS OF THE LEVEL OF GREAT SALT LAKE

by
Genevieve Atwood and Don R. Mabey
Earth Science Education
30 U Street
Salt Lake City, UT 84103

ABSTRACT

Well-preserved shorelines on Antelope Island record fluctuations of the level of Great Salt Lake over the past 10,000 years. In 1986 and again in 1987 the seasonal high static level of Great Salt Lake was about 4,212 feet (1,283.8 m) above sea level (asl), the same level as the earlier historic high in the 1860s-70s. Elevations of 1986-87 and older shorelines were measured along profiles at 19 locations distributed around Antelope Island. The shorelines of 1986-87 on Antelope Island range from approximately 0.5 feet (0.15 m) to over 6 feet (1.8 m) above maximum static lake level. The exposure of shores to storms and the geometry of the lakebed affect shoreline development. Older shorelines indicate earlier static lake levels of 4,214; 4,215, 4,217; and 4,220 feet (1,284.4; 1,284.7; 1,285.3; 1,286.3 m) asl. Wet periods, such as those that caused the lake to rise to 4,212 feet (1,285.3 m) asl in the 1860s-70s and again in 1986-87, are normal for the climate of the region, appear to occur on average about once every 100 years, and can drive the lake to 4,217 feet (1,283.8 m) asl. The level to which the lake will rise in a particular wet period depends on the lake level at the start of the cycle and the magnitude and duration of the wet period. With present climate, the static level of the lake will not rise above 4,217 feet (1,285.3 m) asl. In response to wetter and/or cooler climate approximately 2,500 years before present, the lake reached its highest level in the past 10,000 years, a static lake level of 4,220 feet (1,286.3 m) asl. Planners and engineers can use information concerning the frequency and magnitude of lake-level fluctuations and wind set-up and wave run-up to mitigate damage from inundation and waves associated with high lake levels.

INTRODUCTION AND ACKNOWLEDGMENTS

The prominent shoreline patterns that ring Antelope Island range in elevation from 1 to 2 feet (0.3-0.6 m) above the surface of Great Salt Lake to elevations over 1,000 feet (300 m) above the lake. The higher and older features record the history of Lake Bonneville. The lowest shorelines record the fluctuations of Great Salt Lake and are the subject of this report.

Great Salt Lake influences many activities in northwestern Utah. The inflow into the lake responds dramatically to climatic conditions over this basin with resulting changes in lake volume, surface area, lake level, and salinity. Because the lakebed is nearly flat, changes in lake level result in extensive changes in the lake's surface area and dramatic migrations of its shorelines. Fluctuations of the lake affect development in and around the lake and affect strategies for water-resource development in the drainage basin. The extraction of minerals from Great Salt Lake is an important industry, which is impacted by fluctuations in lake level and salinity. Lake-level rises threaten interstate railroads and highways, wastewater treatment facilities, low-lying residential, recreational, and commercial development, and wildlife refuges. Lake-level fluctuations caused hundreds of millions of dollars of damage during the 1980s and have the potential to cause even greater damage in the future.

Historical records of lake level fluctuations began in the mid-1800s. A longer prehistoric record will improve our ability to predict the magnitude and frequency of future fluctuations. Prehistoric lake levels recorded by shorelines on Antelope Island can then be used to infer the magnitude and frequency of high lake levels over the past several thousand years. The historical and prehistoric data on the lake level can then be used to develop generalized predictions on future lake-level fluctuations for use by developers, planners, and politicians in making decisions relative to developments in and around the lake.

This study of Antelope Island's shorelines was one of several geologic investigations of Antelope Island undertaken by the Utah Geological Survey (UGS) in cooperation with the Utah Division of Parks and Recreation. Hellmut H. Doelling coordinated the program and his assistance as well as that of employees of the Division of Parks and Recreation in arranging the field work is gratefully acknowledged. Bill D. Black (UGS) computed curves illustrating the relationship between volume, surface area, and elevation of Great Salt Lake. The authors have benefitted both before and during this study from many discussions with Donald R. Currey who generously shared his extensive knowledge of Lake Bonneville and Great Salt Lake with us. While we worked on Antelope Island, Stuart Murchison (1989) was engaged in a more extensive study of Great Salt Lake shore features (Murchison and Mulvey, this volume). Our study benefitted from infor-

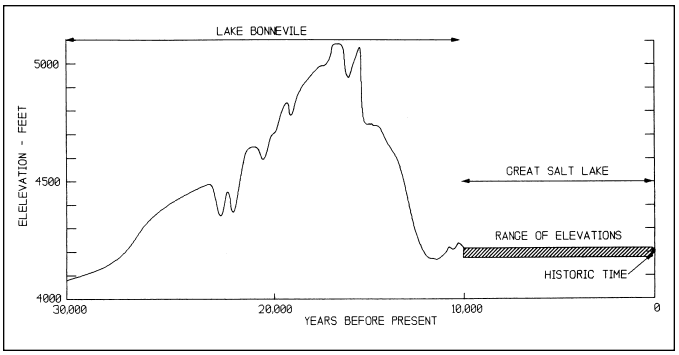

Figure 1. *Fluctuations in the level of Lake Bonneville and Great Salt Lake. Sources: Bonneville fluctuations from Oviatt (1997); Holocene fluctuations from Murchison (1989) and Currey and others, (1984); historical fluctuations from U.S. Geological Survey data.*

mation he made available to us. Technical reviews in 1990 by Donald R. Currey, Suzanne Hecker, and Charles G. (Jack) Oviatt significantly improved the quality of this report. We also appreciate the persistence of the Utah Geological Survey staff in completing this volume, specifically Grant Willis and Jon King.

The research reported in this paper was the basis for two technical papers published in the interim: Atwood (1994) and Atwood and Mabey (1995). Both publications reference this publication. The research reported on in this publication was completed in 1989. We have not rewritten this paper to include 1990s research by the senior author but we have modified the paper slightly to reflect presently accepted chronologies of Lake Bonneville and Great Salt Lake.

The lake-elevation data in this paper are the measurements of the elevation of Great Salt Lake gauged by the U.S. Geological Survey and the State of Utah during the 1980s. Since then, the datum for 1984-94 has been adjusted. These adjustments are now included in official data compilations for Great Salt Lake available from the U.S. Geological Survey. During the field seasons reported on in this paper, 1986-89, the adjustment is a consistent -0.25 feet (-7.6 cm) (David V. Allen, Data Base Administrator, U.S. Geological Survey Water Resources Division, Salt Lake City, personal communication 12/1/97 and 2/1/96 memo to files concerning revised records of lake surface elevations). This adjustment affects lake-level records used in this paper and the absolute elevation of the datums of our surveyed profiles. The adjustment does not change relative elevations and elevation differences among the shorelines, the subject of this paper.

FACTORS CONTROLLING THE LEVEL OF GREAT SALT LAKE

Magnitude of Lake Level Fluctuations

Great Salt Lake is the largest terminal lake in the Western Hemisphere. It occupies the lowest area of a 23,000-square mile (60,000 km^2) drainage basin. Wetter and colder climates cause the lake in the basin to rise to levels much higher than the historical levels of Great Salt Lake (figure 1). The most recent of these dramatically higher level lakes, called Lake Bonneville, began its rise about 28,000 years ago according to Oviatt (1997) (all references to “years ago” and “years before present” are radiocarbon years before present - “present” by convention is the year A.D. 1950). About 15,000 years ago Lake Bonneville reached a maximum depth of over 1,000 feet (300 m). At that level, lake water flowed over the rim of the Great Basin just north of Red Rock Pass in southern Idaho into the Portneuf River drainage and from there into the Snake River, the Columbia River, and on to the Pacific Ocean. At this lake level, the Bonneville level, the lake covered approximately 20,000 square miles (52,000 km^2), including all but about 4 square miles (10 km^2) of Antelope Island.

The decline of Lake Bonneville began about 14,500 years ago with a catastrophic failure of the lake's outlet. Lake waters raced through the breach, cutting through the sediments that had formed the divide. The lake dropped abruptly about 350 feet (107 m) from the Bonneville level to the Provo level with its overflow threshold at Red Rock Pass, Idaho. Lake Bonneville remained near this level for about 500 years until the climate changed. By 12,000 years before present the lake had declined to levels as low or lower than historical levels (Currey, 1990). Between 12,000 and 10,000 years before present the lake in the basin rose to the Gilbert level, formed shorelines up to about 50 feet (15 m) above the historic high level of Great Salt Lake, and then declined to historical levels. This marks the beginning of the consistently low-level lake of the Holocene epoch, Great Salt Lake. The climate of the region during the Holocene epoch (<10,000 years) has controlled the level of Great Salt Lake to no higher than 4,221 feet (1,286.6 m) asl (Murchison, 1989; Murchison and Mulvey, this volume). In historic time (1847 to present) the lake has fluctuated from a high of 4,212 feet (1,284.4 m) asl to a low of 4,191 feet (1,277.4 m) asl, with an average lake level of about 4,202 feet (1,280.8 m) asl (figure 2). Minimum lake levels during the Holocene epoch are more difficult to identify, but have been lower than the historical minimum of 4,191 feet (1,277.4 m) asl. Desiccation features suggesting lake levels of 4,180 feet (1,274.1 m) asl or lower described by Currey (1980) have not been dated.

Climate

The level of Great Salt Lake fluctuates in response to variations of precipitation and evaporation across its drainage basin. Increased precipitation drives the level of Great Salt Lake up. Inflow is about two-thirds from streams, one-third from precipitation directly on the lake, and a small contribution from ground-water discharge into the lake (Arnow and Stephens, 1990). The typical annual cycle of the lake begins during the winter when the lake rises gradually in response to moderate precipitation and low evaporation. The lake level rises more rapidly during spring when precipitation, snowmelt, and stream flows are high and evaporation is moderate. During the summer, lake level declines rapidly when evaporation is high and precipitation is low. As evaporation declines during the cooler and wetter fall months the lake declines more slowly. Yearly seasonal fluctuations average about 1.5 feet (0.46 m) but have varied in historical time between no rise to a maximum rise of about 5 feet (1.5 m), and from no decline to a maximum decline of about 3 feet

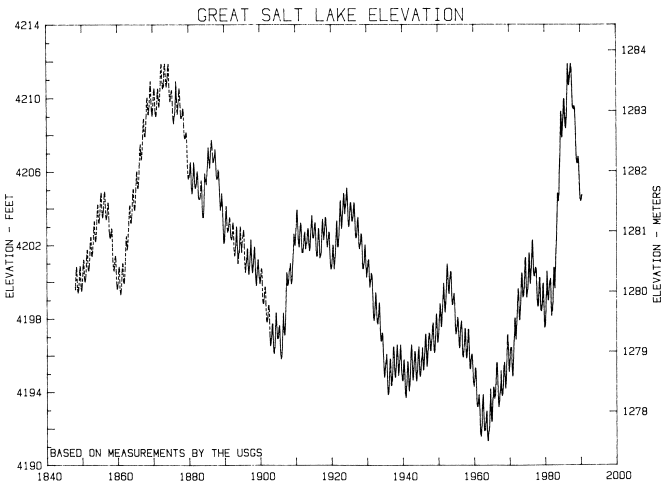

Figure 2. *Hydrograph of the historical fluctuations of Great Salt Lake. The pre-1875 portion is based on traditional data compiled by Gilbert (1890). The post-1875 portion is based on measurements by the U.S. Geological Survey.*

(0.9 m) (Arnow and Stephens, 1990).

Annual inflow to the lake is determined primarily by precipitation across the drainage basin and outgo by evaporation from the lake. Evaporation is primarily a function of the surface area of the lake, although it is also influenced by the weather over the lake, and the temperature and salinity of the lake. When annual precipitation increases, inflow to the lake increases, and the level and surface area of the lake increase. The lake level stabilizes when the surface area of the lake is at a size that evaporation from the lake equals inflow to the lake.

Over the Great Salt Lake drainage basin, annual precipitation ranges from fewer than 10 inches (25 cm) in desert areas to more than 40 inches (100 cm) in the western Uinta Mountains and the Wasatch Range. No long-term precipitation records are available for stations on the lake. The National Weather Service record at the Salt Lake City International Airport, located 12 miles (19 km) east-southeast of the southern end of Antelope Island and a few miles from the lake begins in 1929. Annual precipitation at the airport averages about 15 inches (38 cm) and ranged from 8 to 25 inches (20-64 cm) from 1929 to 1990. In the mountainous areas to the east, where most of the surface inflow into the lake originates, the variation from average increases and much of the precipitation falls as snow. The annual percentage variation in stream flow into the lake is considerably greater than that of the precipitation, ranging from 40 to 350 percent of average (Arnow and Stephens, 1990).

Geometry of the Lakebed

In historical time, the surface area of the lake has ranged from 50 to 135 percent of average and the volume of water in the lake from 50 to 175 percent of average. The lake level tends to stabilize at elevations where the nearly flat topography of the lakebed results in large increases in the lake's surface area for small increases in lake level, greatly increasing evaporation per unit increase in elevation. Between 4,200 (1,280.2 m) and 4,214 feet (1,284.4 m) asl the average increase in surface area for each two-foot rise in lake level is 120 square miles (310 km^2). At a lake level of approximately 4,215 feet (1,284.7 m) asl, the lake expands across a series of thresholds and shallow basins south of the Newfoundland Range into the Great Salt Lake Desert. In rising from 4,214.5 (1,284.6 m) to 4,216.5 feet (1,285.19 m) asl the surface area of the lake increases by 600 square miles (1,600 km^2), dramatically accelerating potential evaporation from the lake.

Human Activities on the Lake

Human activities artificially affect the level of Great Salt Lake. The construction of causeways and dikes has restricted the movement of water in the lake and limited access to portions of the natural lakebed. Consumptive use of basin water, water diversions into or from the basin, removal of water from the lake by pumping, and construction of in-lake obstructions affect lake levels. The U.S. Geological Survey calculated that by 1963 the consumptive use of water in the drainage basin of Great Salt Lake had lowered the level of the lake 5 feet (1.5 m) below what it would have otherwise been (Whitaker, 1971). This translates into a volume deficit of about 3.8 million acre-feet (4.7 billion m^3), about twice the average annual inflow from surface streams. The completion of the Southern Pacific Railroad causeway in 1960 restricted the movement of water between the main body of the lake and Gunnison Bay north of the causeway. By 1984, the water-level south of the causeway was almost four feet (1.2 m) higher and the water much less saline than the water to the north. Opening a 300-foot (91-m) breach in the causeway in 1984 reduced the water-level difference to less than 1 foot (0.3 m) (data from U.S. Geological Survey monitoring records). Construction of evaporation ponds on the lakebed has affected the level of Gunnison, Gilbert, and Bear River Bays. Diking projects proposed to stabilize shoreline levels around certain areas of the lake, such as the Lake Wasatch proposal of the 1980s, would increase fluctuations in the level of the remaining lake (Gwynn, this volume).

The Central Utah Project (which transfers water from the Colorado River drainage basin into the Great Salt Lake drainage basin through a series of dams and tunnels) imports comparatively minor volumes of water into the Great Salt Lake basin. Upon completion, it will import 100,000 to 150,000 acre-feet (123 million-185 million m^3) of water annually into the lake's drainage basin, the equivalent of the volume of the uppermost 1 inch (2.5 cm) of Great Salt Lake at a lake level of 4,202 feet (1,280.8 m) asl. The West Desert pumping project, which pumped water from Great Salt Lake into an evaporation pond west of the Newfoundland Range to increase total evaporation of lake water, could impact future fluctuations of Great Salt Lake. Put into operation April 10, 1987 after the lake had peaked April 1-15, 1987, it had no significant effect on the 1986-87 historic high levels of Great Salt Lake.

Wind, Seiches, and Surges

Diurnal ocean tides and earth tides have no measurable effect on Great Salt Lake. However winds and earthquakes may significantly disturb the lake surface, producing wind set-up, wave run-up, surges of water and seiches that raise or lower the level of the water along segments of the lake shore.

Wind set-up is the wedge of water pushed above the static elevation of the lake surface by sustained strong winds. When the winds die down suddenly, wind seiches can cause oscillations of water level. Surges of water are masses of water described as waves or walls of water. Storms and accompanying winds frequently impact the lake surface. The U.S. Army Corps of Engineers computed the combined wind set-up and wave run-up against hypothetical dikes north and south of Antelope Island as input into the design for a proposed Great Salt Lake Inter-Island Diking Project (Rollins, Brown and Gunnell, Inc. and Creamer & Noble, Engineers, 1987). The values that they computed for sustained wind velocities of 33 to 44 miles (53-70 km) per hour, at lake levels of 4,212 (1,283.8 m) to 4,216 feet (1,285.0 m) asl, and for dikes with a 1:1 slope, ranged from 4 to 8 feet (1.2-2.4 m).

Lin and Wang (1978) analyzed one wind-seiche event in January 1969, recorded at two gaging stations on the lake. For about 12 hours the wind blew from the south at an average velocity of about 25 knots (29 miles [46 km] per hour). The lake level declined 1.0 foot (0.3 m) at Black Rock at the south end of the lake and rose 0.8 feet (0.24 m) at Promontory Point about 30 miles (78 km) to the north. When the velocity of the wind dropped to less than 10 knots (11 miles [18 km] per hour) seiching started. On the first cycle the lake level at Black Rock rose about 2.5 feet (0.76 m) to a level about 1.5 feet (0.46 m) above the static lake level. At Promontory Point the level dropped 1.8 feet (0.55 m) to 1.0 feet (0.3 m) below the static lake level. Oscillations continued for two days with a period of six hours and decreasing amplitude. The geometry of the lake determines the seiche period of the lake. Lin and Wang estimate the construction of the Southern Pacific Railroad causeway reduced the seiche period of Great Salt Lake from nine hours to six hours.

Earthquakes can produce sudden temporary or permanent changes in the water level of Great Salt Lake. These earthquake-induced changes can initiate seiching. An earthquake near the northern end of the lake in 1909 reportedly produced a surge that sent water over the Southern Pacific Railroad causeway and the bath-house pier at Saltair (Deseret News, October 6, 1909). Movement on one of several active faults in or near the lake, including the Brigham City, Weber, and Salt Lake segments of the Wasatch fault zone, and the east Great Salt Lake fault, could permanently deform the lakebed, causing abrupt inundation of sections of the shore. The tectonic deformation that occurred during the Hebgen Lake earthquake in Montana in 1959, when one shore of Hebgen Lake dropped 8 feet (2.4 m) below the water level, has been used as a model for similar deformation of Great Salt Lake (Smith and Richins, 1984).

HISTORICAL FLUCTUATIONS OF GREAT SALT LAKE

Early Observations and the 1860s-70s Highstand

John C. Fremont made the first measurements of the level of Great Salt Lake in 1843 when he recorded several observations of the barometric pressure on the shores of the lake. He wrote: "From a discussion of the barometrical observations made during our stay on the shores of the lake, we have adopted 4,200 feet (1,280.2 m) for its elevation above the Gulf of Mexico," (Jackson and Spence, 1970). Fremont's barometric observations cover a considerable range of values and cannot be used to determine the exact level of the lake at that time. In 1845 he made a more useful observation when he recorded that as he rode his horse across the ford on the bar that connects Antelope Island to the mainland, the water nowhere reached above the saddle girths (Gilbert, 1890). The elevation of the low point along the ford to the island is about 4,200 feet (1,280.2 m) asl. Thus Fremont's observation suggests a lake level of about 4,202 (1,280.8 m) or 4,203 feet (1,281.1 m) asl.

In 1875-78, G.K. Gilbert, as part of his study of Lake Bonneville, interviewed ranchers who had moved animals to and from the mainland to Stansbury and Antelope Islands to determine their recollection of water depths during the period from 1847 to 1875. Gilbert (1890) constructed a hydrograph for this period from these data.

Early U.S. Geological Survey published hydrographs of the lake for the 1850-1913 period differ significantly from Gilbert's hydrograph for the period before 1875 (Mabey, 1986). These publications credit Marcus E. Jones for information for this early period. The exact year and elevation of the highstand in the 1860s-70s is not known. Gilbert stated that the lake reached its highstand in the summers of 1872, 1873, and 1874. Today the U.S. Geological Survey and most others use hydrographs based on Gilbert's early data. These hydrographs generally show the highstand in 1873 at about 4,211.5 feet (1,283.7 m) asl. Our compilation shows an elevation of 4,211.85 feet (1,283.77 m) asl for each of the three high-stand years (figure 2).

In 1877, Gilbert measured the elevation of the debris line formed on the eastern side of Antelope Island during the highstand of the 1860s-70s wet period and related it to the gauged lake level. Adjusting Gilbert's observations to a sea level datum provides an elevation of 4,213.5 feet (1,284.3 m) asl for the debris line (Mabey, 1986). This was the only direct measurement Gilbert recorded of the elevation of the 1860s-70s wet-cycle shorelines.

Recorded Lake-Level Measurements and the 1986-87 Highstand

Recorded lake-level measurements began in 1875 with the installation of a gauge at Black Rock. Since then the lake level has fluctuated over a range of 18.5 feet (5.64 m), requiring several relocations of lake gauges. In 1877, Gilbert acquired from Brigham Young a block of the granite being used to construct the Salt Lake Temple and set it near Black Rock as a benchmark. By leveling, he determined the elevation of the early, post-1875, gauges relative to this benchmark. Later surveys by the U.S. Geological Survey tied Gilbert's benchmark and early gauges to a sea-level reference (Mabey, 1986).

For about 90 years following the high lake levels of the 1860s-70s, the level of the lake generally trended downward until it reached its historic low of 4,191.35 feet (1,277.52 m) asl in 1963 (figure 2). Gilbert and others thought that con-

sumptive use of water and natural evaporation processes would prevent the lake from rising again to the high lake levels of the 1860s-70s. The decline in lake level until 1963 appeared to support this conclusion and a popular concern was that the lake would dry up. During these years, numerous kinds of public and private construction, including residential, industrial, recreational, and transportation, located on the lakebed at elevations below the historic highstand. Students of the lake did not warn the public that another wet period similar to the period that produced the rapid lake-level rise in the 1860s-70s should be expected and would produce a similar rise in the level of the lake.

From 1963 until 1976 the lake level rose until it had reached its historical average of 4,202 feet (1,280.8 m) asl. For the next six years, the lake level fluctuated a little below this level. A major wet period began in September 1982, heralded by the wettest month in the history of observations at the Salt Lake City International Airport (figure 3). From September 1982 through June 1983, the lake rose a record 5.2 feet (1.6 m) and increased in volume by 6 million acre-feet (7.4 billion m^3), more than compensating for over 136 years of basin-wide consumptive use of water. During the succeeding four years, above-average precipitation occurred over most of the Great Salt Lake drainage basin, with the Salt Lake International Airport recording about 32 inches (81 cm) of excess precipitation above average or about 50 percent above the average (weather data are from National Weather Service data files located at State Climatologist's Office, Utah State University). The level of Great Salt Lake rose rapidly in response to this above-average precipitation and in the spring of 1986 reached its highest level, 4,211.85 feet (1,283.77 m) asl, since the first gauge was established in 1875. The lake level peaked at this same elevation in 1987 and then declined rapidly in response to lower than average precipitation across its drainage basin and the pumping of water from the lake into the Great Salt Lake Desert.

1986-88 FIELD WORK AND INTERPRETATIONS

During 1986, 1987, and 1988 the authors studied the low-lying shorelines of Antelope Island. The purpose of the study was to better understand the recurrence intervals of flooding of Great Salt Lake. By documenting the depositional and erosional evidence of the highstands of the 1980s we hoped to better identify previous highstands of the lake. Documentation of previous highstands, particularly if these events could be dated, could provide a context by which to evaluate the frequency of wet cycles affecting Great Salt Lake. In 1986, we compared shoreline evidence of the 1986 highstand with that of the 1860s-70s. In 1987, our field work expanded to document the variety of geomorphic evidence produced by the 1986-87 highstands of the lake at different locations around the island. It included surveying elevations of shorelines formed during 1986-87 and surveying older, higher shorelines. We limited the study to those shorelines at or below the Holocene highstand of Murchison (1989).

Antelope Island proved to be a superb field area for such observations. Discontinuous shorelines ring the island and reflect wave action from all directions. Relatively extensive

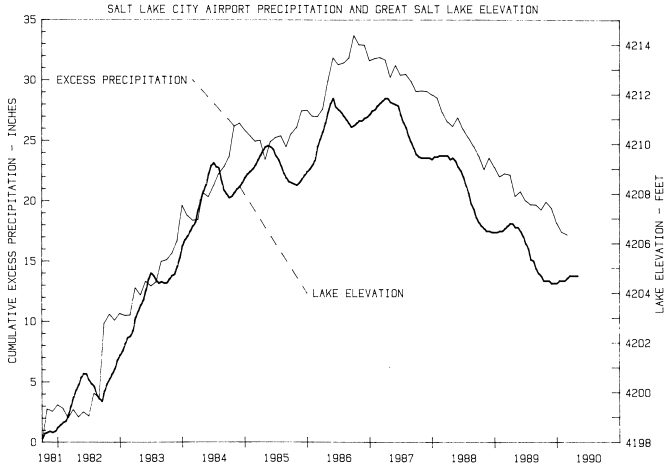

Figure 3. *Level of Great Salt Lake compared to cumulative excess precipitation measured at Salt Lake City International Airport 1975-1994. Data are from the U.S. Geological Survey and the National Weather Service.*

(longer than one-half mile [0.8 km]) beaches, unevenly distributed around the entire island, represent a variety of beach conditions. Antelope Island's undisturbed shorelines provided relatively easy identification of 1986-87 shorelines and excellent chances for recognizing older shorelines.

Field Observations

In the summer of 1986, after the lake had receded from the recorded high of 4,211.85 feet (1,283.77 m) asl, the authors and Donald R. Currey measured the elevation of the 1986 debris and gravel line at three locations on the eastern side of Antelope Island. The research objective was to compare the 1986 shoreline and highstand with the 1860s-70s shoreline and highstand as documented by Gilbert (1890). Gilbert had made his measurement relative to the lake level in 1877 somewhere on the eastern side of Antelope Island, a few years after the lake crested in the 1860s-70s. The average elevation of the 1986 debris line and gravel ridge was 4,213.5 feet (1,284.3 m) asl, the same as indicated by Gilbert's measurement of the 1860s-70s shoreline. The agreement of our measurements with his suggests that the highstands of the lake in the two historic high lake cycles were approximately the same.

In November of 1987, we began documenting the 1980s and pre-1980s shorelines and surveying shoreline elevations. We surveyed shoreline profiles at 11 locations around Antelope Island. Three were surveyed with a hand level, the others with an electronic distance measuring device (EDM). Only the data determined by EDM measurements are included in this report. In August of 1989, we surveyed an additional 11 profiles using the EDM equipment. Figure 4 shows the locations of the surveyed profiles.

The level of Great Salt Lake as recorded at the U.S. Geological Survey continuously recording lake gauge at the Saltair Marina eight miles (13 km) south of Antelope Island provided our survey datum. We were fortunate that on all except two days of surveying with the EDM equipment the lake surface was calm. Repeat measurements under these conditions indicated that the lake surface provided a datum

accurate to 0.1 feet (0.03 m). On the two days when wind disturbed the lake surface, the uncertainty of the elevation readings was estimated to be about 0.5 feet (0.15 m).

Constructional shorelines formed during the 1986-87 highstand were easily recognized in 1987 and 1988 by debris such as tires, lumber, and plastics. We measured profiles within longer, straighter stretches of shorelines and deliberately avoided small pocket beaches where slope and shoreline geometry magnifies wave run-up and builds super-elevated shorelines. Erosional shorelines were easily distinguished in 1987, but by 1988, vegetation reestablished itself on the more protected, finer grained, lower wave-energy shorelines and on shorelines where spring waters supported vegetation. In some of the latter areas, only the presence of tires, railroad ties, and other large wooden debris provided visible evidence of the 1986-87 shoreline.

Because the lake fluctuates seasonally, highstands of the lake are relatively short-term events of late spring and early summer and may or may not be documented by shorelines constructed by storms. The effects of individual storms are unevenly distributed around the island. Thus, although the lake provides a static water-level datum, the elevation of wave-constructed shorelines depends on the level of the lake at the time of the storm, the direction of storm winds, shoreline configuration (such as the shape and slope), and roughness of the shore.

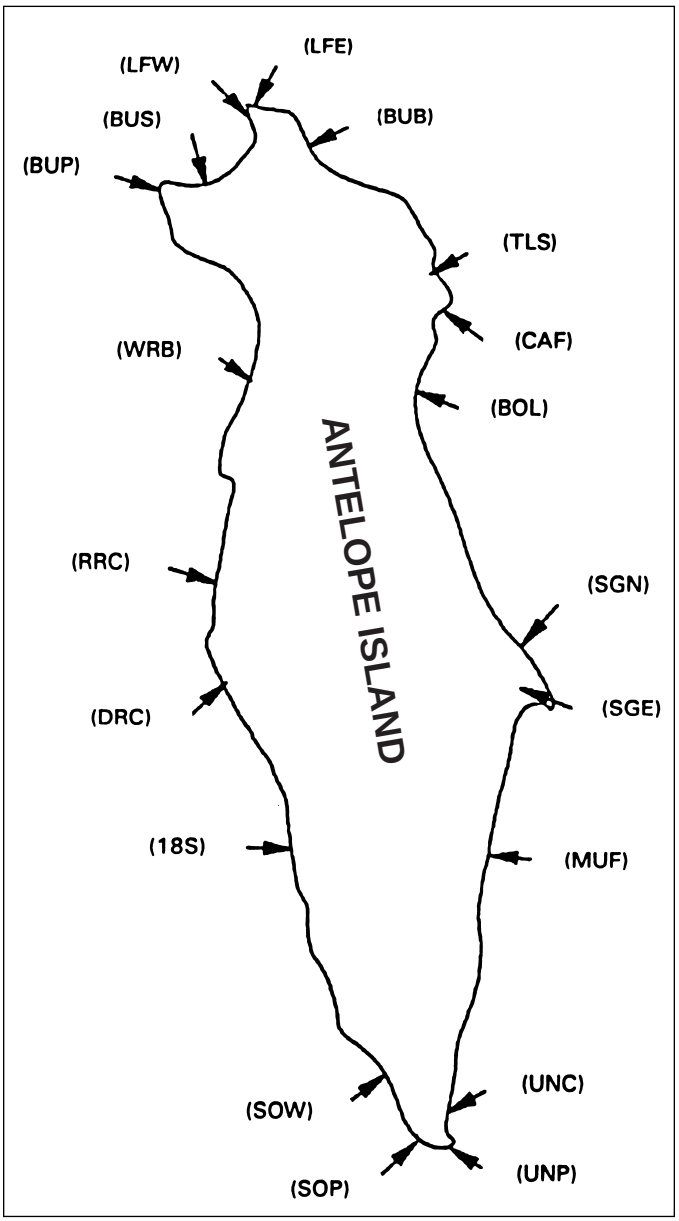

Figure 4. *Antelope Island showing the location of measured shoreline profiles of table 1. Letter designations are those used in table 1 and figure 5.*

Description of Shorelines

Shorelines on Antelope Island formed during 1986-87 can be classified into four general types. Commonly two or more of these features occur together:

1) debris lines,

2) gravel ridges and beaches,

3) erosional steps,

4) vegetation lines.

Debris Lines

The high shorelines formed in 1986-87 are nearly everywhere marked by debris consisting mostly of wood but including considerable non-wood manufactured material, much of it made of plastic. Most of the debris clearly postdates the 1870s but the possibility that some of the old wood was deposited by the 1860s-70s highstand could not be ruled out. Some of the lighter debris could have been moved by wind as well as wave action. The debris lines are generally located upslope from the gravel ridges and beaches. No debris lines associated with older shorelines were identified at elevations higher than those of 1986-87 in the 1980s field work. Debris lines formed after 1987 consist mostly of the remains of dead insects, with minor amounts of wood and other material.

Gravel Ridges and Beaches

Wave-constructed gravel ridges served as our primary markers for shoreline elevations. These shorelines resemble the geomorphic evidence of older highstands at the same locations. We surveyed the crest of the gravel ridges relative to the lake-level datum. These gravel ridges are generally well sorted. In some areas, the 1986-87 shoreline consists entirely of gravel, and in other areas almost entirely of cobbles or sand. The 1986-87 shoreline gravels are bleached with no observable surface staining in contrast to older, higher shoreline gravels. Lower, younger gravels are all bleached. At several locations, two or more gravel ridges of equal elevation formed a few to tens of feet apart. Initially we expected that these repeated ridges might represent 1860s-70s and older shorelines. We observed during storms of 1987 that waves broke across and modified several ridges and lagoons concurrently. Therefore, we determined that we could not distinguish relative ages of ridges on the basis of elevation and spacial distribution alone.

Erosional Steps

Where waves or long-shore currents erode a shoreline in relatively soft sediments, the shoreline level is marked by a

nearly vertical step. Debris or gravel has been deposited at the base of some of these steps. The steps range in height up to more than 10 feet (3 m). The vertical faces formed in 1986-87 in most areas began to slump and erode immediately. Step shorelines above the 1986-87 shorelines have been modified to gentle slopes. Only in one area of no constructional shorelines did we use erosional shoreline evidence. At that location, MUF (figure 4), we measured the 1986-87 shoreline level at the debris line at the base of the erosional step.

Vegetation Lines

Vegetation changes mark some shorelines by zones of distinctive vegetation, or changes in vegetation density or type. Some shorelines appear to be marked only by subtle vegetation zones. The lake's saline water killed most plants it inundated and some shorelines of 1986-87 are marked by the upper limit of kill zones. A notable exception to the kill-zone phenomenon is where springs discharged fresh water at or below lake level and maintained plants that were partly or completely submerged by lake water.

Gilbert noted similar vegetative changes (Gilbert, 1890). A few years after the 1860s-70s highstand he noted a kill zone below which he observed no sagebrush. He conjectured that it would take perhaps several hundred years for sagebrush to reestablish communities in the inundated zones. However the vegetation in the 1860s-70s inundation zone appeared to have fully recovered in the period between 1877 when Gilbert made his observations and the next high level in 1986.

Some of the wave-constructed gravel ridges both at the 1986-87 lake level and above are marked by plants such as sunflowers that grow well in disturbed areas or areas with coarse sediments. We did not consider vegetation alone as sufficient evidence for identifying the 1986-87 shoreline.

Elevations of 1986-87 and Older Shorelines

Table 1 summarizes, and figures 5 and 6 illustrate, the Great Salt Lake shoreline data collected on Antelope Island during 1987-88. Data are grouped into a sequence of highstands. Elevation alone did not define shoreline groupings. Modern debris allowed easy identification of 1986-87 shorelines (historic shoreline). The Holocene high studied by Murchison (1989) provided an upper limit for our surveys. Between these two features, intermediate shorelines indicate at least three additional highstands, perhaps more. We group these data into shorelines B, C, and D based on spatial relationships to the 1986-87 shoreline and geomorphic evidence such as cross-cutting erosional features. Further work, such as trenching lagoon deposits, could better define the number and age of the events represented by these shoreline features.

Historical Shorelines

The elevations of the gravel ridges formed during 1986-87 range from 4,212.4 feet (1,283.9 m) asl (0.6 feet [0.18 m] above the highest static lake level) to 4,218.1 feet (1,285.7 m) asl (6.3 feet [1.9 m] above the highest static lake level). The average elevation for 19 shoreline locations is 4,214.6 feet (1,284.6 m) asl. The elevations are generally higher on the

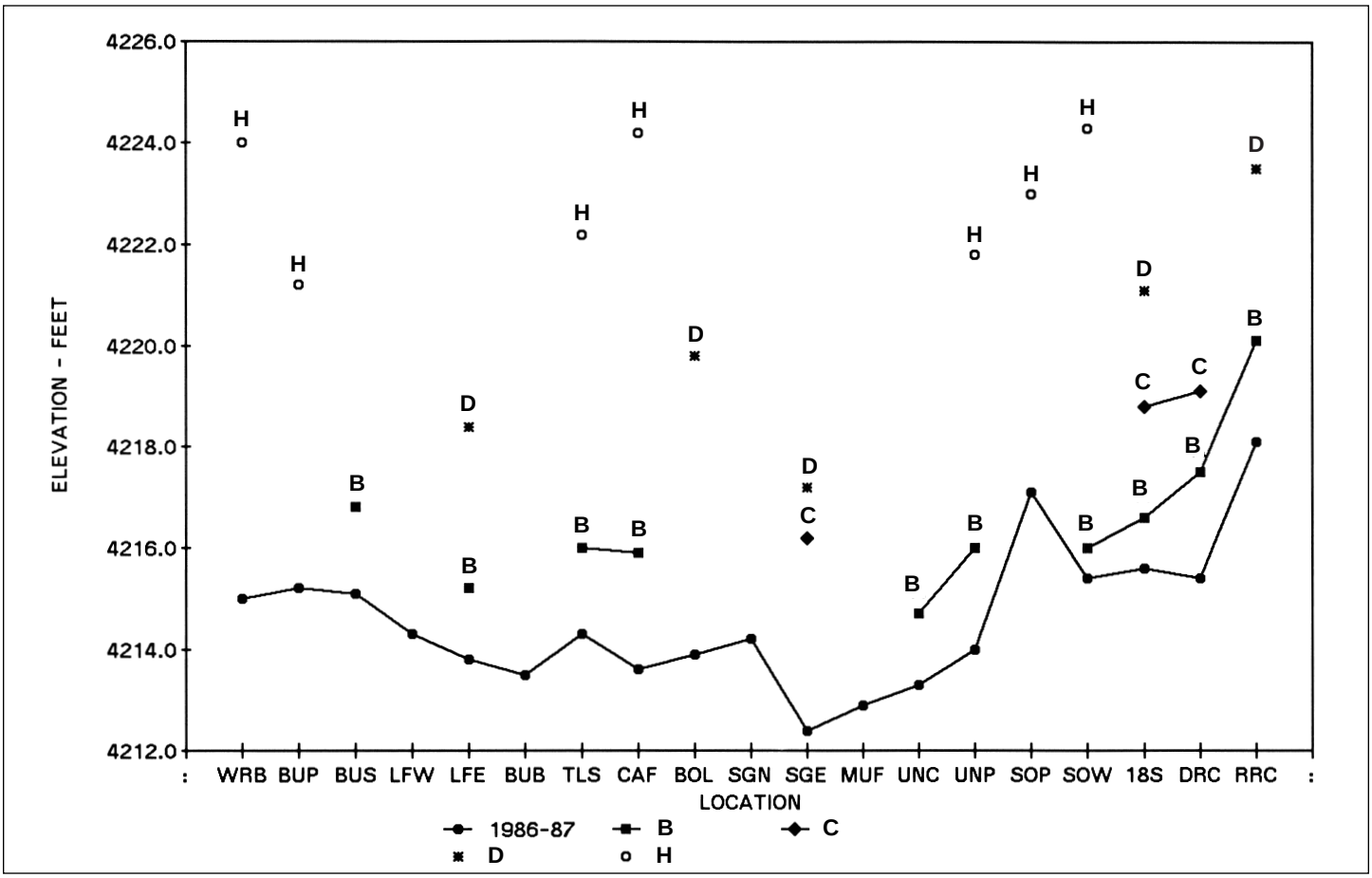

Figure 5. *Elevations of shorelines of Great Salt Lake on Antelope Island. Letter designations for locations are those used in table 1 and figure 4. Letter designations for shorelines are those used in text and table 1. Lines between locations indicate lateral correlations of shorelines.*

Table 1. *Elevations of shorelines of Great Salt Lake surveyed on Antelope Island. Profile locations are shown in figure 4 and letter designations for locations are those used in figures 4 and 5. Height above 4,212.0 feet (1,283.8 m) refers to the elevation difference of the 1986-87 shoreline versus the gauged static lake level. Relative height designations are L (low), M (moderate), and H (high). Height above 4,212.0 feet (1,283.8 m) and relative height are illustrated in figure 6. We estimate the following ages for the shorelines (present is defined as A.D. 1950):*

Historic high shoreline: *A.D. 1860s-70s and 1986-87*
Shoreline B: *250 years before present*
Shoreline C: *250 - 300 years before present*
Shoreline D: *300 - 400 years before present*
Holocene-high shoreline (H): *2,300 – 2,500 years before present*

Age estimates are based on Murchison (1989), Currey and others (1988), and Oviatt (1988).

SHORELINE ELEVATIONS - ANTELOPE ISLAND
(in feet above sea level)

Location	Historic Shoreline	Height above 4212.0	Relative height H, M, L	Shoreline B	Shoreline C	Shoreline D	Shoreline H Holocene High
WRB	4215.0	3.0	M				4224.0
BUP	4215.2	3.2	M				4221.2
BUS	4215.1	3.1	M	4216.8			
LFW	4214.3	2.3	M				
LFE	4213.8	1.8	L	4215.2		4218.4	
BUB	4213.5	1.5	L				
TLS	4214.3	2.3	L	4216.0			4222.2
CAF	4213.6	1.6	L	4215.9			4224.2
BOL	4213.9	1.9	L			4219.8	
SGN	4214.2	2.2	L				
SGE	4212.4	0.4	L		4216.2	4217.2	
MUF	4212.9	0.9	L				
UNC	4213.3	1.3	L	4214.7			
UNP	4214.0	2.0	L	4216.0			4221.8
SOP	4217.1	5.1	H				4223.0
SOW	4215.4	3.4	H	4216.0			4224.3
18S	4215.6	3.6	H	4216.6	4218.8	4221.1	
DRC	4215.4	3.4	H	4217.5	4219.1		
RRC	4218.1	6.1	H	4220.1			4223.5
Static Water Elevation Feet	4212			4214	4215	4217	4220
Static Water Elevation Meters	1238.8			1284.4	1284.7	1285.3	1286.3

southwestern shore of the island than on the eastern shore (figure 6). This is consistent with the U.S. Army Corps of Engineers calculations of wind set-up and wave-run up for proposed dikes near Antelope Island (Rollins, Brown, and Gunnell, Inc., and Creamer & Noble, Engineers, 1987). Their calculations predicted that some site conditions on the western side of Antelope Island could produce shoreline features at even higher elevations than we measured. Our data suggest that inundation and wave action can be expected 6.5 feet (2.0 m) above the static lake level at some locations depending on exposure and configuration of the lakebed and may be further amplified in pocket beaches. The 1986-87 shorelines provide a datum for recognizing potential wave damage on Antelope Island associated with a static lake level of about 4,212 feet (1,283.8 m) asl. The range in elevations indicates the need to exercise caution when using elevations of prehistoric shorelines to determine prehistoric static lake elevations.

The highstands of the 1860s-70s and 1986-87 were approximately 4,212 feet (1,283.8 m) asl. Most shoreline features produced on Antelope Island in the 1860s-70s were reactivated or masked by 1986-87 events. Theoretically, older shorelines might be recognized after later highstands if the older shorelines contained prominent markers or datable material, but the primarily gravel shorelines associated with the single- or multiple-storm events of recent highstands of Great Salt Lake are easily reactivated or masked. Under unusual circumstances, storm events of one lake highstand can construct gravel ridges that are not reactivated by storms of a subsequent highstand. At Ladyfinger Point (LFE) two gravel ridges, separated spatially but constructed at the same elevation, differed in composition and staining. The one formed in 1986-87 included trash and consisted of bleached pebbles. The other consisted of stained pebbles and lacked modern debris. We interpret the second feature as a possible 1860s-70s shoreline. At the southernmost tip of the island (SOP) a stained gravel ridge lies inches above the 1986-87 ridge and could be a 1860s-70s shoreline. But, with few exceptions, the 1986-87 storms reactivated, masked, or destroyed the surface expression of older and lower shorelines including those of the 1860s-70s.

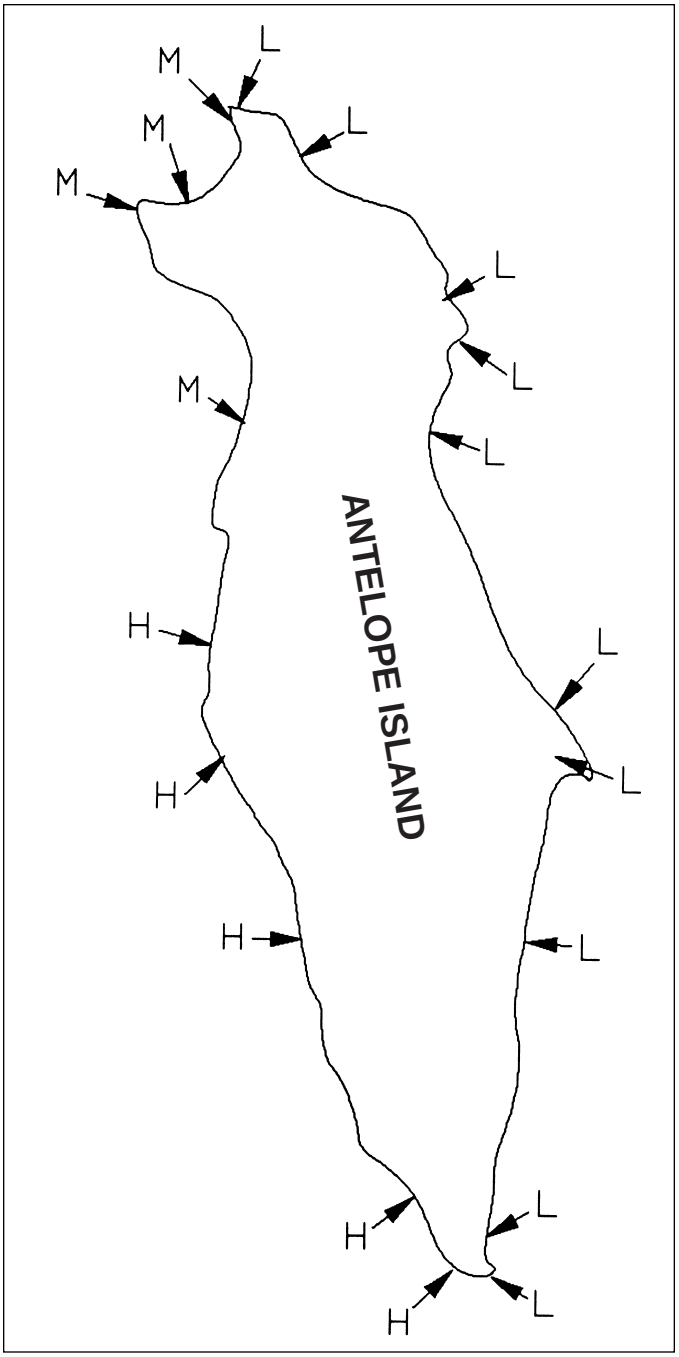

Figure 6. *Antelope Island showing profile locations, the height in feet of the 1986-87 shoreline above the static high level of the lake, and relative height of the shorelines, designated as L (low), M (moderate), and H (high). Also see table 1.*

Intermediate Shorelines

The next higher shoreline (shoreline B) above the historic high shorelines was measured at ten locations. The elevation of these features ranges from 4,214.7 (1,284.6 m) to 4,220.1 feet (1,286.3 m) asl and averages 4,216.5 feet (1,285.2 m) asl, 1.9 feet (0.58 m) higher than the historic high shorelines. We assign a static lake level of 4,214 feet (1,284.4 m) asl to this high cycle. The shoreline gravels are stained. The gravel ridges are distinct and little modified by erosion. This shoreline must be older than the approximately 150-year historical record, but its lack of modification suggests that it is no more than a few hundred years old. Murchison (1989) identified a dual-beach-forming highstand at 4,214 feet (1,284.4 m) asl, which he dated at roughly 250 years before present, and we assume this is the age of shoreline B.

At three sites a shoreline slightly above shoreline B was identified. The average elevation of this feature, which is designated shoreline C, is 3.4 feet (1.04 m) above the average historical shoreline on the island. It is assigned a static lake level of 4,215 feet (1,284.7 m) asl. This feature is more modified than shoreline B, but is not dissected by debris-flow or stream channels. The age of this shoreline is not known but, based on spatial relationships, lies between the ages of shorelines B and D.

At four locations, a third intermediate shoreline, designated shoreline D, was surveyed. The gravels on this shoreline are stained. Drainage channels, including debris-flow channels, cut this shoreline and do not cut lower shorelines. Therefore it is older than shorelines B and C. The elevation of this feature ranges from 4,217.2 (1,285.4 m) to 4,221.1 feet (1,286.6 m) asl which averages 4.5 feet (1.37 m) above the 1986-87 shoreline and indicates a static lake elevation of about 4,217 feet (1,285.3 m) asl. Murchison (1989) identified a shoreline at this elevation, which he roughly dated between 400 and 300 years before present.

Holocene-High Shoreline

The Holocene-high shoreline was identified at seven locations. An eighth location (RRC) with an elevation of 4223.5 (1,287.3 m) could be an exceptionally high shoreline D or a Holocene-high shoreline. We have grouped it with the Holocene-high shoreline set based on its elevation. The Holocene-high shoreline is considerably more modified than the lower shorelines. Its elevation averaged 8.4 feet (2.56 m) above the 1986-87 shoreline with a range of 3.1 feet (0.94 m). The wide range in elevation may be in part due to tectonic deformation and the degree of difficulty in recognizing the shoreline as well as shoreline processes. Our measurements, corrected for wind set-up and wave run-up (figure 6), indicate a static lake level of 4,220 feet (1,286.3 m) asl for the Holocene highstand of Great Salt Lake. We correlate this shoreline with Murchison's Holocene high, which he assigned an age range of 3,440 to 1,440 years before present (Murchison, 1989). Currey and others (1988) described evidence for a 2,000 to 2,500 year age for a shoreline at this elevation. Work by Oviatt (1988) suggested that 2,300 to 2,500 years before present age for a similar event of Lake Gunnison in the Sevier River drainage basin.

IMPLICATIONS OF SHORELINE EVIDENCE

Shorelines provide evidence about elevations of high lake levels, recurrence intervals of high lake levels, and geomorphic processes associated with storms. Therefore, shorelines of Antelope Island provide information for determining hazards of flooding and storm damage.

Inundation Levels

Shorelines are excellent indicators of the elevation of inundation associated with a specific static lake level. Our profiles substantiated the theoretical predictions of higher ele-

vations of wave action on the southwestern and western shores of the island as a result of regional storm directions, intensity, and duration. Local conditions, such as the geometry and roughness of the lakebed and shore, affect wave run-up. Based upon our profiles, combined wind set-up and wave run-up for Antelope Island result in construction of gravel-ridge shorelines that are 0.6 feet to over 6 feet (0.18-1.8 m) above static water level.

Shoreline elevations can be excellent indicators of high static lake levels when corrections are made for wind set-up and wave run-up caused by storms and local conditions (figure 6). Our profiles identified five highstand shorelines of Great Salt Lake with static lake levels of: 4,212; 4,214; 4,215; 4,217; and 4,220 feet (1,283.8; 1,284.4; 1,284.7; 1,285.3; and 1,286.6 m) asl.

Recurrence Intervals

Shoreline elevation data alone do not indicate the recurrence interval of high lake levels. With few exceptions, the wave action of each highstand masks or destroys the surface expression of older, lower shorelines. Thus, the record of lake-level fluctuations preserved along a shore is restricted to successively higher, older events. Thus, the number of shorelines indicates only a minimum number of high lake cycles. For example, the 4,212-foot (1,283.8 m) level records at least two highstands.

Additional stratigraphic, geochemical and climatologic data can supplement shoreline data to provide recurrence information. Sediments deposited in the lagoons associated with high lake cycles may record multiple inundations. If the sediments contain organic material, radiocarbon dating may provide a chronology of the lake cycles (Murchison, 1989). Analysis of the chemistry of lake sediments obtained from cores and trenches in the lakebed can provide an indication of the salinity of the lake when the sediment was deposited, and the salinity can be used to calculate relative levels of the lake (McKenzie and Eberli, 1985). Because lake cycles occur in response to changes in precipitation over the lake's drainage basin, statistical analyses of historic precipitation

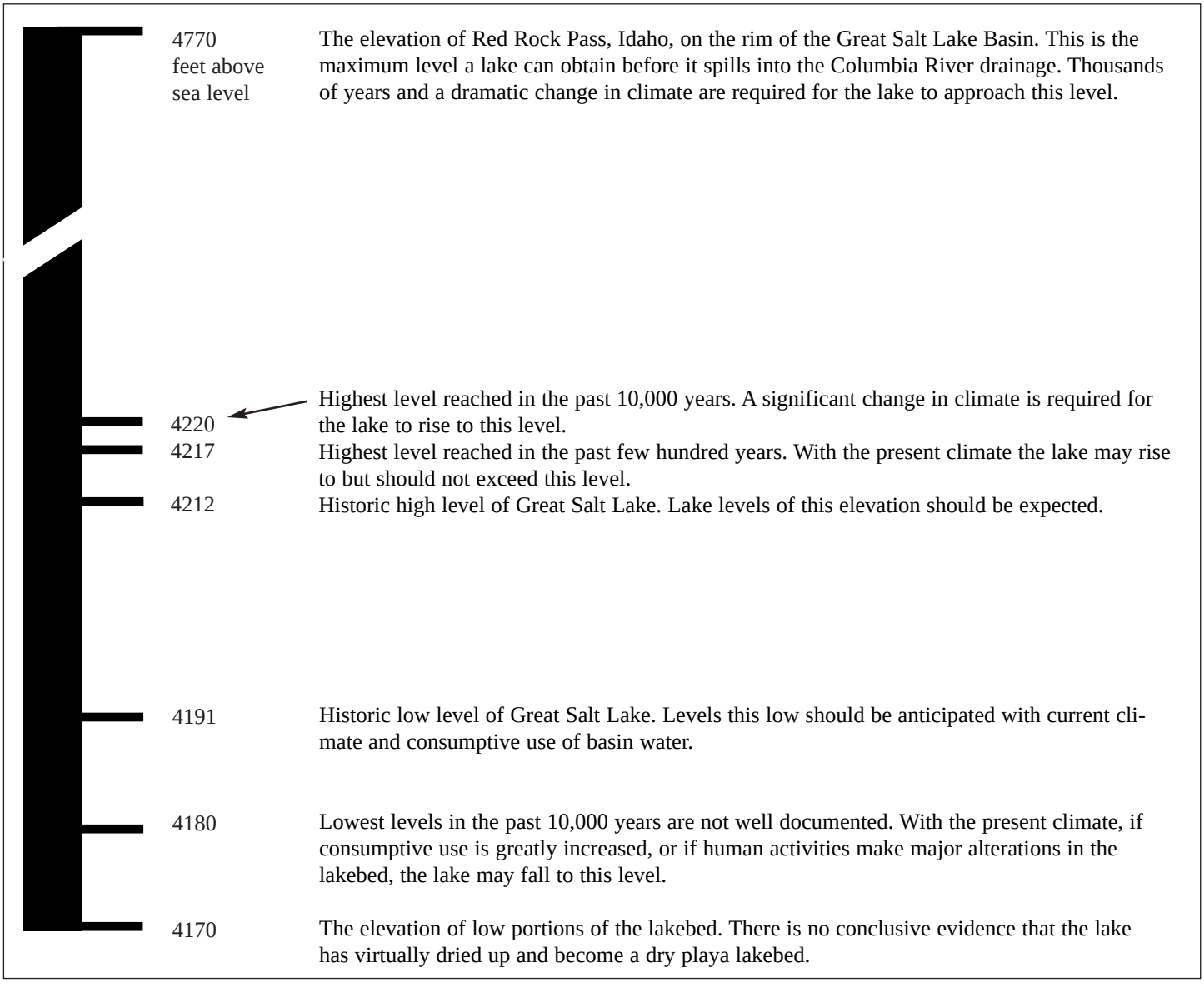

Figure 7. *Expected levels of Great Salt Lake and inferred relationship to climate.*

data provide an indication of the frequency with which precipitation events affecting lake cycles are likely to occur (Karl and Young, 1986). Tree-ring studies may provide information on prehistorical precipitation cycles in the Great Salt Lake drainage basin.

The shoreline data obtained on Antelope Island combined with the age estimates of Murchison (1989) were used to construct figure 7. Historical data show two lake highstands of approximately 4,212 feet (1283.8 m) asl separated by about 120 years. Our shoreline data indicate these two stands, plus a minimum of at least three additional, higher stands, have occurred since the Holocene high approximately 2,500 years before present.

Based on statistical analyses of historical weather data, Karl and Young (1986) determined that wet cycles have occurred about every 100 years. The two historic highstands of Great Salt Lake resulted from a series of years of significantly above-average precipitation that caused the lake to rise abruptly. The level that the lake reaches in response to a wet period depends upon the lake level at the start of the precipitation cycle and the magnitude and duration of the event. The 10-foot (3-m) rise of the lake from 4,202 to 4,212 feet (1,280.8-1,283.8 m) asl during 1982 to 1986 was a net increase of 13 million acre-feet (16 billion m^3) water. Without the effect of 140 years of consumptive use of water the level of the lake would have been significantly higher; we estimate about 2 feet (0.6 m) higher (4,214 feet [1,284.4 m] asl). If the wet period had begun 20 years earlier when the lake level was lower, the highstand would have been about 4,208 feet (1,282.6 m) asl. The highstand that the lake will reach during wet periods is also controlled by the geometry of the lakebed. Before the lake reaches an elevation of 4,217 feet (1,285.3 m) asl it expands over a large area of the Great Salt Lake Desert, greatly increasing its surface with a resulting increase in evaporation from the lake surface. With the climate that has existed for the past few hundred years the lake is not likely to exceed this elevation.

According to Murchison (1989), only once in the Holocene epoch (past 10,000 years) does the lake appear to have reached a level of approximately 4,220 feet (1,286.3 m) asl. Such a high lake level requires a different climate from that of the past several hundred years to reduce the per-acre evaporation from the vastly expanded surface area of the lake, and/or to supply sufficient volumes of precipitation and runoff to counter the increased evaporation. A rise of Great Salt Lake to levels associated with Lake Bonneville (for example to about 4,750 feet [1,447.8 m] asl at Red Rock Pass, Idaho) requires a dramatic change in climate.

Low levels of Great Salt Lake do not pose the same threat as highstands, but they affect development in and around the lake. Shorelines preserve evidence of high levels of Great Salt Lake, but water and sediments cover evidence of low lake levels. The historic low lake level of 4,191 feet (1,277.4 m) asl resulted from a long period that included many drier-than-average years. Similar dry-weather conditions, typical for the climate of Great Salt Lake drainage basin in the past several hundred years, and consumptive use of water can lower the lake to this level again. The desiccation features on the lakebed possibly associated with lake levels at least 10 feet (3 m) have not been dated. Such low lake levels require unusual, sustained changes in basin weather.

Effect of Human Activities

In our analysis, we have not attempted to compute the impact of future human activities on lake level. Nor have we attempted to estimate the effect of human activities on local, regional, and global climate that affect lake level indirectly. Past human activities have had significant and complicated impacts on the level of Great Salt Lake. Consumptive use of drainage basin water has lowered lake level but has not altered the basic pattern of lake fluctuations. Consumptive use makes low stands of the lake considerably lower than they would be naturally and highstands somewhat lower than they would be naturally. Diking and pumping brines into evaporation ponds may raise or lower the level of the remaining portions of the lake. Lake pumping to an evaporation pond on the Great Salt Lake Desert provides the possibility of limited control over fluctuations of the lake. Neither consumptive use nor pumping can prevent future highstands of the lake.

LAKE-LEVEL FLUCTUATIONS RELATED TO DEVELOPMENT OF ANTELOPE ISLAND

Shoreline Facilities

Lake-level rises occur relatively slowly and are not life-threatening. Therefore, decisions concerning shoreline development of Antelope Island primarily concern property loss rather than life loss. Two exceptions are important: inundation caused by earthquake-related waves or tectonic tilt, and flood hazards associated with failures of large diking projects. The danger from either of these phenomena is greatest when the lake level is high. Lake-level rises presently pose threats to property; some proposed lake-level control dikes could make high lake levels a threat to lives.

Access to Antelope Island

Land access to Antelope Island depends upon roadways built on the lakebed. Until the 1960s when the first road was built from the mainland near Syracuse to the north end of the island, the only land access had been along the Antelope Island bar at the south end of the island. The bar is above water at lake elevations below 4,200 feet (1,280.2 m) asl. Over the past 100 plus years, the bar has been above lake level approximately 40 percent of the time. From about 1900 to 1983 the island could be reached from the south by maintaining the road bed a few feet above the crest of the bar. By lake-bed standards the bar provides a relatively firm foundation for a roadbed and there is no requirement to maintain a passage for lake water to move through the roadway. A road that would provide access to the south end of the island even during high lake periods would be relatively easy to construct.

The causeway from Syracuse to the north end of the island encounters more difficult conditions. The minimum elevation of the lakebed along the route of the causeway is

about 4,190 feet (1,277.1 m) asl. Over the past 100 years, a portion of the route has been below water 100 percent of the time. Soft sediments underlie much of the route. The causeway must provide a passageway for a considerable volume of lake water and accommodate density and salinity differences of the water on the two sides of the causeway. A roadway maintained at the level of the causeway in use before 1984 would have been usable for over 90 percent of this century. A causeway that would be usable 100 percent of the time up to lake levels of 4,217 feet (1,285.3 m) asl would need to be about 12 feet (4 m) higher. Due to adverse foundation conditions, costs of construction along the present route increases substantially with each foot of increased elevation of the causeway.

Conclusions for Planners

Fluctuations of the level of Great Salt Lake are controlled primarily by long-term weather that we do not presently have the ability to predict accurately or control. Nevertheless, our understanding of past lake fluctuations based on shoreline and other evidence provides sufficient information to be used in determining the costs and benefits of development alternatives of Antelope Island and can minimize losses due to future high lake levels.

Recurrence of High Lake Levels

Lake-level fluctuations that have occurred in the past few hundred years can be expected in the next few hundred years. High lake cycles have occurred on average about once every hundred years. The high lake levels of the 1860s-70s and 1986-87 both reached approximately 4,212 feet (1,283.8 m) asl, but weather patterns normal for the Great Salt Lake drainage basin can drive the level of the lake as high as 4,217 feet (1,285.3 m) asl. Highstands at the 4,212 feet (1,283.8 m) asl level can be expected more frequently than highstands at higher lake levels such as at 4,214 feet (1,284.4 m) asl. The 4,217 feet (1,285.3 m) asl lake level represents the highest static lake level associated with normal weather conditions. The last highstand of the lake at about 4,217 feet (1,285.3 m) asl occurred as recently as 400 to 300 years before present.

Low Lake Levels

Less information is available about the amplitude and frequencies of extreme dry-weather periods. Evidence shows that the lake has fallen to levels well below the historic low of 4,191 feet (1,277.4 m) asl; to perhaps as low as 4,180 feet (1,274.1 m) asl.

Levels of Damage from Inundation and Wave Action

The elevation of damage from inundation or wave action at a particular site depends primarily on the static level of the lake and secondarily on the site's exposure, the geometry of the lakebed, and the geometry and roughness of the shore area. The shorelines of 1986-87 on Antelope Island range from approximately one-half foot to over 6 feet (0.15-1.8 m) static lake level. The 1986-87 shoreline elevation of a particular site compared to the 1986-87 static high water level of approximately 4,212 feet (1,283.8 m) asl provides a rough approximation of wind set-up and wave run-up for a given site caused by storms.

REFERENCES

Arnow, Ted, and Stephens, Doyle, 1990, Hydrologic characteristics of the Great Salt Lake, Utah: 1847-1986: U.S. Geological Survey Water Supply Paper 2332, 32 p.

Atwood, Genevieve and Mabey, D.R., 1995, Flooding hazards associated with Great Salt Lake, *in* Lund, W.R., Environmental and engineering geology of the Wasatch front region: Utah Geological Association Publication 24, p. 483-494.

Atwood, Genevieve, 1994, Geomorphology applied to flooding problems of closed-basin lakes… specifically great Salt Lake, Utah, *in* Geomorphology and Natural Hazards, 25th Binghamton Symposium in Geomorphology: Geomorphology, v. 10, p. 197-219.

Currey, D.R., 1980, Coastal geomorphology of Great Salt Lake and vicinity, *in* Gwynn, J.W. editor, Great Salt Lake - A scientific, historical and economic overview: Utah Geology and Mineral Survey Bulletin 116, p. 69-82.

---1990, Quaternary palaeolakes in the evolution of semi-desert basins, with special emphasis on Lake Bonneville and the Great Basin, U.S.A.: Palaeogeography, Palaeoclimatology, Palaeoecology, v. 78, p. 198-214.

Currey, D.R., Atwood, Genevieve, and Mabey, D.R., 1984, Major levels of Great Salt Lake and Lake Bonneville: Utah Geological and Mineral Survey Map 73, scale 1:750,000.

Currey, D.R., Berry, M.S., Douglass, G.S., Merola, J.A., Murchison, S.B., Ridd, M.K., Atwood, Genevieve, Bills, B.G., and Lambrechts, J.R., 1988, The highest Holocene stage of Great Salt Lake: Geological Society of America Abstracts with Programs, v. 20, p. 411.

Gilbert, G.K., 1890, Lake Bonneville: U.S. Geological Survey Monograph 1, 438 p.

Jackson, Donald, and Spence, M.L., 1970, The Expeditions of John Charles Fremont, Volume I, travels from 1838 to 1843: University of Illinois Press, 854 p.

Karl, T.R., and Young, P.J., 1986, Recent heavy precipitation in the vicinity of Great Salt Lake; just how unusual?: Journal of Climate and Applied Meteorology, v. 25, p. 353-363.

Lin, Anching, and Wang, Po, 1978, Wind tides of the Great Salt Lake: Utah Geological and Mineral Survey, Utah Geology, v. 5, no. 1, p. 17-35

Mabey, D.R., 1986, Notes on the historic high level of Great Salt Lake: Utah Geological and Mineral Survey, Survey Notes, v. 20, no. 2, p. 13-15.

McKenzie, J.A., and Eberli, G.P., 1985, Late Holocene lake-level fluctuations of Great Salt Lake as deduced from oxygen-isotope and carbonate contents of cored sediments, *in* Kay P.A. and Diaz, H.F. editors, Problems of and prospects for predicting Great Salt Lake levels: Center for Public Affairs and Administration, University of Utah, p. 25-39.

Murchison, S.B., 1989, Fluctuation history of Great Salt Lake, Utah, during the last 13,000 years: University of Utah, Ph.D. dissertation, 137 p.

Oviatt, C.G., 1988, Late Pleistocene and Holocene lake fluctuations in the Sevier Lake Basin, Utah, USA: Journal of Paleolimnology, v. 1, p. 9-21.

---1997, Lake Bonneville fluctuations and global climate: Geology, v. 25, no. 2, p. 155-158.

Rollins, Brown and Gunnell, Inc. and Creamer & Noble Engineers, 1987, Great Salt Lake inter-island diking project - final design report: prepared for the Utah Division of Water Resources, v. 1 and 2, variously paginated.

Smith, R.B., and Richins, W.D., 1984, Seismicity and earthquake hazard of Utah and the Wasatch front - paradigm and paradox, *in* Hays, W.W., and Gori, P.L., editors, Evaluation of regional and urban earthquake hazards and risk in Utah: U.S. Geological Survey Open-File Report 84-763, p. 73-112.

Whitaker, G.L., 1971, Changes in the elevation of Great Salt Lake caused by man's activities in the drainage basin, *in* Geological Survey Research, 1971: U.S. Geological Survey Professional Paper 750-D, p. D187-189.

ARAGONITE CEMENTATION AND RELATED SEDIMENTARY STRUCTURES IN QUATERNARY LACUSTRINE DEPOSITS, GREAT SALT LAKE, UTAH

by
R. B. Burke
North Dakota Geological Survey
600 East Boulevard, Bismarck ND 58505-0840

and L. C. Gerhard
Kansas Geological Survey
1930 Constant Ave., Lawrence KS 66047

ABSTRACT

Cementation of Quaternary lacustrine shoreline sediments around Great Salt Lake has modified the stratigraphy and produced a variety of interesting sedimentary features. Aragonite is precipitated as cements and laminar coatings in a variety of crystal morphologies that range in size from less than 1 micron to about 44 microns. Sediments are cemented to form very thin peloidal crusts, laterally extensive layers of thin ooid grainstone beds, and vertically stacked thin beds that dip toward the lake to form beachrock. Early precipitation of cement contributed to the formation of a number of sedimentary particles and structures including granules, clasts, flat pebble conglomerates, laminated crusts, and more interestingly, fossil bubbles and gas-eruption structures. Relict and actively forming gas-eruption structures are characterized by raised circular rims composed of flat clasts derived from broken cemented layers. Cemented layers are broken not only by over-pressured gas trapped underneath them but also by mechanical processes including wave action. Occurrence of most cements appears to be related to extremes of salinity locally mediated by soluble organic matter, organic activity and gases within the sediment.

INTRODUCTION

Recognition of early precipitation of cement in sediments and the distribution and character of those cements is fundamental to understanding the process of cementation and also has significant economic implications. Early precipitation of minor amounts of cement between grains can prevent collapse of primary porosity during burial and provide potential reservoir rocks for hydrocarbons. Alternatively, extensive early cementation of shoreline sediments can seal strata sufficiently to trap fluids or gases that later migrate up-dip from the depocenter of a sedimentary basin. Lacustrine deposits are known to be both hydrocarbon source and reservoir rocks in China, the United States and South America where they produce economic quantities of hydrocarbons (Lomando and others, 1994; Dean and Fouch, 1983). Recognition of early cementation in lacustrine rocks can thus be very helpful in many aspects of hydrocarbon exploration and production. Furthermore, knowledge about the characteristics of early shoreline cements and about the sedimentary structures resulting from the cementation process is useful in distinguishing lacustrine deposits from their marine counterparts.

Synsedimentary carbonate cementation in lacustrine shoreline sediments has not been discussed in as much detail for hypersaline lakes (Picard and High, 1972; Dean and Fouch, 1983) as it has for marginal-marine hypersaline settings in the Persian Gulf (Taylor and Illing, 1969), in Australia (Davies, 1970), in the Red Sea (Friedman and others, 1973), and in Texas (Freeman, 1962; Frishman and Behrens, 1969). Most studies of hypersaline lakes focus on precipitation of evaporites (Eugester and Hardie, 1978), on marls in temperate alkaline lakes (Muller and others, 1972; Kelts and Hsu, 1978), on the formation of ooids (for example, Eardley, 1966; Kahle, 1974; Sandberg, 1975; Halley, 1977; Reitner and others, 1997), or stromatolites (Halley, 1976). More recently significant advances in our understanding of the chemistry of precipitation of the carbonate cements in biofilms have been made (Neuweiler, 1997) although others emphasize the role of nannobacteria (Pedone and Folk, 1996).

Most of our knowledge about penecontemporaneous cementation of shoreline and shallow water sediments comes from studies of normal marine environments. Lithification of tropical marine beach sediments has been studied by many researchers (for example, Ginsburg, 1953; Multer and Hoffmeister, 1971; Moore, 1973; Hanor, 1978), but there are few reports of submarine cementation of extensive layers of sand (Taft, 1968; Shinn, 1969). Reports of contemporaneous lithification of beach sediments in lacustrine environments or of subaqueous cementation of extensive layers of lake sediments also are sparse. Binkley and others (1980) reported low-magnesium calcite cementing pisolites into beds about 25 cm (10 inches) thick to form beachrock in Ore Lake, Michigan, but there was little discussion about the extent of subaqueous cementation or of other sedimentary features associated with the cementation process.

Cements precipitating in the form of radial fibrous ooids have received the greatest attention from researchers working on cementation in Great Salt Lake (for example, Eardley, 1938; Carozzi, 1962; see others mentioned above). Cementation of ooids along some Great Salt Lake beaches to form "hydrogenic shingle" and granule sand was recognized by Eardley (1938) but he placed little emphasis on its occurrence

or petrography. Reitner and others (1997) referred to hydrogenic shingle at Antelope Island as "ooid microbiolite chips" and attributed their cementation to cyanobacterial biofilms. In that paper they also distinguished another form of cemented sediments as "microbial crusts." Descriptions of Reitner and others' microbial crusts sounds similar to the stromatolites described by Pedone and Folk (1996) which they used to illustrate the role of nannobacteria in cementation.

We observed early cementation of sediment in March, 1980 along the eastern and southern shoreline of Great Salt Lake at four locations (figure 1). This was during early spring runoff and a rise in lake level following an extended period of particularly low lake levels. This paper discusses the occurrences and petrography of these cemented sediments and some related sedimentary features including granules, intraclasts, cemented layers, beachrock, gas-eruption structures, and the formation of flat pebble conglomerates.

Setting

Great Salt Lake is an evaporated remnant of Pleistocene Lake Bonneville. Today it is about 125 km (80 miles) long and 55 km (35 miles) wide with a maximum water depth less than 15 m (50 feet). The position of the shoreline shifts great distances with the slightest variation in water level because the lake is so shallow and has extremely low-gradient shorelines. Salinity is tied directly to the level of the lake because it is a closed hydrologic system becoming more saline during extended periods of evaporation and rising solely from river influx (Eardley, 1938; Eugester and Hardie, 1978). Dissolved solids in the Great Salt Lake are more than seven times that of sea water although ions are present in similar proportions. Lake water is slightly alkaline, but highly saline with Na^+ and Cl^- as major ions. The northern part of the lake has increased salinity in comparison to the southern end where the majority of freshwater enters the lake. Air temperatures range from below freezing in the winter to over 100°F in the summer.

Sediments around the shoreline during our sampling were primarily ooids with minor amounts of clays and siliciclastic detritus. Ooids dominated at all the locations visited by the authors except for the sandy (ooids) mud flats on the west side of Stansbury Island. Radiocarbon dating of ooids indicates they are less than 4,557 ± 133 years old (Halley, 1977). Speculation by Neuweiler (1997) suggested cementation occurred within the last few years and their histochemical data suggest cementation is no older than the recent biofilms. We are unaware of any C^{14} dating of these cements.

Study Area

Cementation was found at four of the six locations examined; the exceptions were the beaches at Magna and White Rock Bay, and the backshore dunes at both locations on Antelope Island (figure 1). Cemented sediments were collected at four locations: Promontory Point (location 1), Bridger Bay north of Buffalo Point on Antelope Island (location 2), and two locations (4 and 5) on the western side of Stansbury Island. Bridger Bay is named on Utah Geological Survey geologic maps, but is unnamed on the US Geological Survey 7.5-minute quadrangle topographic map. No cementation

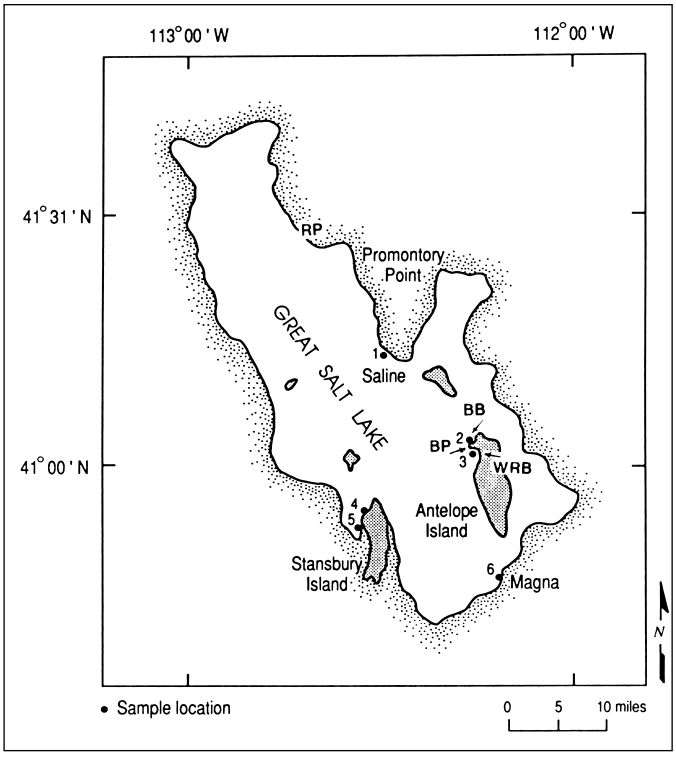

Figure 1. *Generalized map of Great Salt Lake, Utah, showing locations referred to in text. BB = Bridger Bay; BP = Buffalo Point; RP = Rozel Point; WRB = White Rock Bay.*

was encountered on Antelope Island dune or interdune surfaces, or by shallow probing (approximately 0.5 meters [1.7 feet]) into them. These aeolian dunes are composed primarily of fine-grained ooids and occupy the backshore zone of the beaches in both bays north and south of Buffalo Point. Although the ooid-dominated beach sediments at White Rock Bay appear identical with those north of Buffalo Point where cementation was pervasive, no cementation was seen in the surface sediments nor in several shallow cores (less than 0.5 m [1.7 feet]) taken in the beach. The only difference between these bays appears to be lower salinity in White Rock Bay because of unrestricted circulation of lake waters.

CEMENTED SEDIMENTS AND SEDIMENTARY STRUCTURES

Promontory Point

Cemented sediments at Promontory Point were collected from the bottom of an evaporator pond northwest of Saline (figure 1, location 1). Pond waters were hypersaline because inflow into the pond was manually controlled to concentrate hypersaline brines sufficiently to precipitate economic quantities of halite for mining.

Platy, pebble to cobble-size fragments of cemented oolitic sand (figure 2) were common around the evaporator ponds but no continuous layer of cemented sediment was observed. Fragments were relatively smooth on top and bottom and were subrounded to subangular in plan view. Their size ranged from 1 to 2 cm (0.4 to 0.8 inches) in thickness by 5 to 20 cm (2 to 7.8 inches) in long dimension. It was near

here on the southwest coast of Promontory Point that Eardley (1938) noted several miles of shoreline, up to 0.8 km (0.5 mile) wide, paved with these fragments of cemented sediments, which he termed “hydrogenic shingle”. The mineral cementing the shingle was reported by Eardley (1938) to be carbonate, either aragonite or calcite.

Antelope Island

Shoreline sediments were examined at two locations on the northwest corner of Antelope Island (figure 1, locations 2 and 3). Fine-grained ooids are the primary type of sediment forming the dunes and beaches in both bays. Significant occurrences of cemented sediment were found only along the foreshore of Bridger Bay. No cementation was found in the foreshore sediments of White Rock Bay south of Buffalo Point, nor in the backshore aeolian dunes of either bay.

Bridger Bay appeared to have restricted water circulation when viewed from Buffalo Point. A bar form parallel to the shore was present well offshore but within the confines of the headlands of the bay. Several bar forms were dimly visible through the water extending shoreward. White Rock Bay exhibited none of these structures, appearing to have unrestricted circulation. Cementation occurred in Bridger Bay which had restricted water circulation that caused increased salinity.

The areal extent of cemented sediments at Bridger Bay (figure 1, locations 2) seemed larger than that at Promontory Point and so was the size of many of the clasts (figure 3). Here layers of cemented sediment dipping toward the lake were stacked so that the lowest layers were shoreward of upper layers and formed a slightly submerged beachrock. The top of the cemented layers was relatively smooth and, where undisturbed, induration decreased downward culminating in a blackened, irregular friable base. Black, hydrogen sulfide-rich, sandy sediments were often encountered below the cemented zone. The beachrock was locally broken into large polygons up to 45 cm (18 inches) in diameter and generally less than 7 cm (2.8 inches) thick. Clasts derived from broken cemented layers were strewn over most of the lower beach face and extended some undetermined distance offshore (figure 4). Generally, where the clasts had been rolled over, many were completely encased in a relatively smooth, glossy coating. Cemented layers around the beachrock were recognized by probing into the sediment but their extent was not determined.

A variety of circular structures with raised margins were observed along the strandline and on a shoal about 2 meters (6 feet) from shore in the Bridger Bay (figure 4). An actively bubbling froth was present in some of the recent structures (figure 5). The structures ranged in size from 3 cm up to 140 cm (1.2 inches to 4.6 feet) in diameter. Although circular, their shapes were preserved in cemented sediments and expressed in a variety of forms from small domes to platy clasts arranged in somewhat imbricated concentric circles (figure 6). The structures were observed in different stages of development and degradation ranging from relatively large, meter-sized circular structures filled with gas froth, to smaller relict structures or fossil bubbles. Fossil gas-bubble structures were most commonly preserved as circular upturned

Figure 2. *Cemented oolite crust fragments on beach at Promontory Point. Marker for scale is 13 cm (5 inches) long (see also figures 14 and 16).*

Figure 3. *Relict eruption crater in high supra-strandline deposits at Bridger Bay, Antelope Island, defined by large, polygonal fragments of ruptured cemented layers. Dotted outline roughly indicates perimeter of structure which is filled with organic debris.*

Figure 4. *Panoramic view showing four gas-eruption craters (arrows) at Bridger Bay, Antelope Island, including froth-filled structure in right corner, foreground (figure 5). Note small waves breaking, indicating a shoal on the lake side of the gas-eruption structures.*

Figure 5. *Gas expulsion structure observed shortly after eruption as indicated by bubbling froth. Structure is approximately 40 cm (16 inches) in diameter (13 cm marker for scale) and was seen at Bridger Bay, Antelope Island. This structure is indicated in figure 4 by the lower right arrow.*

Figure 6. *Gas expulsion structure approximately 130 cm (4.3 feet) in diameter (13 cm marker in center for scale). Note concentric rings of semi-vertical, inward-leaning broken plates of layers of cemented sediment. At least two different layers were ruptured from a minimum depth of 13 cm (5 inches). This structure is indicated in figure 4 by the left arrow.*

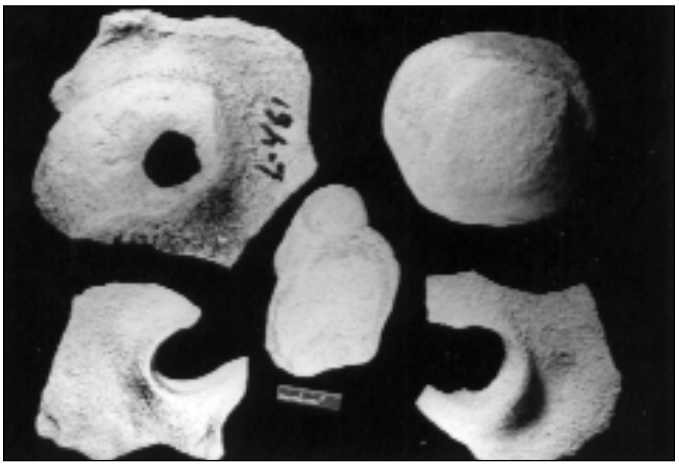

Figure 7. *Gas-formed structures showing the variety of forms from domes (upper three samples) to upturned collars. Note the apical hole in the upper left sample indicating rupture whereas the other upper two domes did not experience rupture. Scale is 2.7 cm (1.1 in).*

collars of cemented oolite grainstone, but sometimes occurred as round to oval, domed structures, often with an apical hole (figure 7). The cemented bubble structures ranged in size from 3 to 9 cm (1.2 to 3.5 inches) in diameter and 1 to 2 cm (0.3 to 0.8 inches) in height. Larger, 40 to 140 cm wide (1.3 to 4.6 foot wide), relict eruption craters occurred as circular depressions defined by broken cemented sediment layers filled with debris (figure 3). More recent gas-eruption structures consisted of upturned cobble-size platy fragments of the ruptured cemented layers that formed crude concentric rings of roughly imbricated fragments (figure 6). The structures were infilled with the surrounding sand and mud in addition to sediments carried up with the gas from below. Four recently active eruption craters and one large crater from a much older eruption (figure 3) were observed within a few tens of meters (around 65 feet) of each other (figures 3 and 4). Gas was actively forming a bubbly froth in one structure. Eruption structures known to have been formed by this process were only observed on Antelope Island, although large 1 to 2 meter (3.3 to 6.6 foot) circular structures at Stansbury Island (discussed below) are possibly of similar origin.

Stansbury Island

Cemented sediments were examined at two locations on the west side of Stansbury Island (locations 4 and 5, figure 1). The hydrologic setting of the west side of Stansbury Island is restricted during low lake levels, like those during our study. High salinities are indicated by the precipitation of halite and other evaporites in isolated pools along the strandline (figures 8 and 9).

The characteristics of the cemented sediment at each location were significantly different from each other. The two types of cemented sediment included different grain types and different proportions of cement: 1) grainstone clasts, and 2) peloid cementstone (primarily cement with few grains). At the northern location (figure 1, location 4) grainstone intraclasts similar to those found at Antelope Island were abundant and strewn about the surface. They were composed primarily of cemented ooids with a thin laminated crust around most of the clasts. In addition, a cemented oolite bed 40 cm (15.7 inches) thick with several underlying thinner beds of cemented oolites was exposed in a trench previously dug during construction (figure 10). These beds were about a meter (3.3 feet) above lake level and the ground-water table, and may represent beachrock cemented at previous high lake levels.

Another form of cemented sediment collected at Stansbury Island was granular sediment, or grapestone, ranging from 1 to 5 mm (0.04-0.2 in) in diameter (figure 11, location 4). Granules were well rounded and irregular in shape having low sphericity with glossy smooth surfaces. Broken surfaces of most granules were opaque, although a few ooids and peloids (1 to 4 grains) were seen in hand specimens of some granules.

Farther south along the western shoreline of Stansbury Island (figure 1, location 5), fragments of peloid cementstone were collected from the perimeter of large circular structures (figure 12 and 13). This second type of cemented sediment at Stansbury Island was fragmented into polygons less than 3

Figure 8. *Unidentified evaporite minerals effloresce on the sandy (ooid) mud flats of central Stansbury Island (location 5, figure 1). Photo is about 15 cm (6 in) across.*

Figure 11. *Granules, or grapestones, covered some of the surface at location 4 on northern Stansbury Island.*

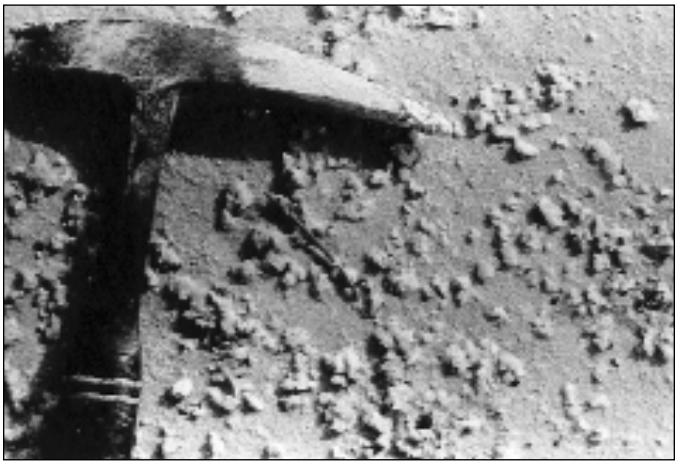

Figure 9. *Halite crystals on the surface of the sandy (ooid) mud flats of central Stansbury Island (location 5, figure 1).*

Figure 12. *Close up of raised perimeter of ring structure with fragments of macro-laminated crust or peloid cementstone. See figures 15 and 19 for photographs of thin sections of crusts and cementstone.*

Figure 10. *Cemented oolite bed approximately 31 cm (1 foot) thick with several thinner cemented zones below (arrow). Exposure is in trench at northwestern corner of Stansbury Island. See figures 24 and 26 for photographs of thin sections of cemented oolites.*

Figure 13. *Domed circular structures approximately 2.8 meters (6 ft) in diameter observed on west-central shoreline of Stansbury Island. Arrows indicate a few of the structures and one is outlined by dots.*

cm (1.2 inches) in longest dimension by less than 1 cm (0.4 inch) thick. Few grains were visible in these fragments. In hand specimens the cemented sediment generally consisted of three thick laminae with two darker outer laminae sandwiching a very dense, opaque creamy-white lamina. The contact of the outer laminae with the inner lamina was irregular and the thickness of outer laminae ranged from 1.2 to 2.5 mm (0.05-0.10 inch).

Numerous circular structures were observed at several locations on the central-western side of Stansbury (figure 13). They were 1 to 2 meters (3.3 to 6.6 feet) in diameter and distinguished by raised rims with cementstone clasts. The centers of the circles were either slightly domed or depressed. Relief from the center to the raised rims was on the order of 2 cm (0.8 inches), which appeared to be the same order of relief of the rim above the surrounding sediment surface. Some with depressed centers were filled with water.

CEMENT PETROGRAPHY

Aragonite is the only mineral found in the samples, precipitating as cement in voids, between grains, and as coatings. Cementation occurs in a variety of fabrics including meniscus, pendant, rinds, peloidal (clotted), epitaxial overgrowths, and laminated crusts. Two types of laminated crusts are distinguished petrographically: a micro-laminated crust (figure 14) common on beachrock, cemented layers, and intraclasts; and a macro-laminated crust (figure 15) forming the peloid cementstones of central Stansbury Island. Micro-laminated crusts average 211 microns in thickness with a range of 80 to 480 microns and are comprised of individual laminae ranging between a few microns up to a few tens of microns in thickness (figure 16). Macro-laminated crusts are about 1 cm (0.4 inch) in thickness and are comprised of laminae averaging 1.9 mm (0.07 inch) thick with a range from 1.2 to 2.5 mm (0.05-0.10 inch). The different cement fabrics are comprised by various crystal forms of aragonite, including: 1) subequant, anhedral submicrocrystalline grains and microcrystals; 2) bundles of subhedral prisms to blades; 3) subequant, rounded stubby-blades; 4) equant, euhedral microcrystalline-prisms; and 5) needles. End members of these five forms are very distinct although there is some gradation between the anhedral, submicrocrystalline grains and microcrystals.

Subequant, anhedral cements appear to have a bimodal size distribution with submicrocrystalline grains less than 2 microns as one size, and the other as microcrystals in the 10 to 20 micron size range. The submicrocrystalline grains occur as rounded to subrounded particles in a variety of irregular shapes (figures 17 and 18). In transmitted light they appear clear or translucent golden brown (figure 16). The term “grain” is used following the reasoning of Loreau and Purser (1973) and Halley (1977) that some microcrystalline aragonite does not have the well-defined crystal faces of euhedral aragonite, rather it takes the shape of rods, blades, needles, or rounded particles and should not be confused with sedimentary grains. Submicrocrystalline grain cement is the most common type of cement in all of our samples occurring as individual grains, grain aggregates, rinds, peloids, and in meniscus and laminated fabrics.

Individual anhedral microcrystalline grains and grain aggregates occur in all of our sample types. Partial or complete rinds of variable to uniform thickness form on sedimentary grains in most of our samples but are rare or difficult to distinguish from the matrix of the outer laminae in the peloid cementstone crusts of Stansbury Island (figure 15). The outer laminae of the macro-laminated crusts from Stansbury are comprised mostly by these subequant, anhedral submicrocrystalline grains where they define algal filaments (figure 19) and form the nucleus of most peloids. Peloids are most common in these cementstones (figure 15). Meniscus cements are most common in beachrock samples but are also present

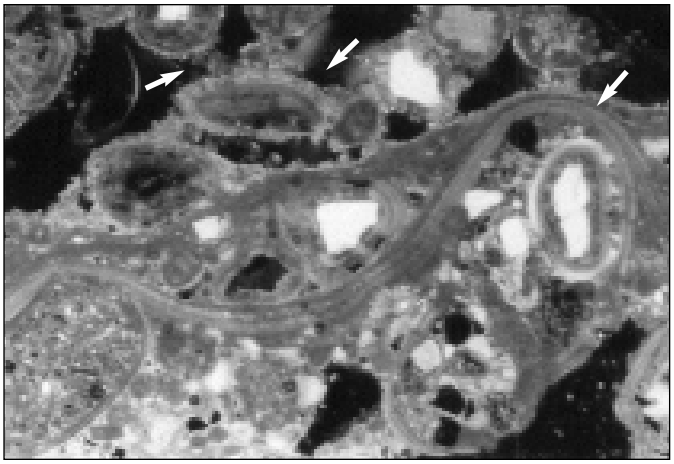

Figure 14. *Thin section of cemented oolite layer from Antelope Island. Two styles of aragonite cementation are present: laminated (right arrows) and meniscus (left arrow). Cements are dominantly two crystal forms: (1) subequant, anhedral, submicrocrystalline grains, and (2) bundles of subequant prisms that provide the radial fabric. Ooids range in size from 0.9 mm to 1.9 mm (0.04 to 0.07 inches). Note coated, broken grain (upper center arrow) in this modern sample and compare with that of Mississippian-age example in figure 30.*

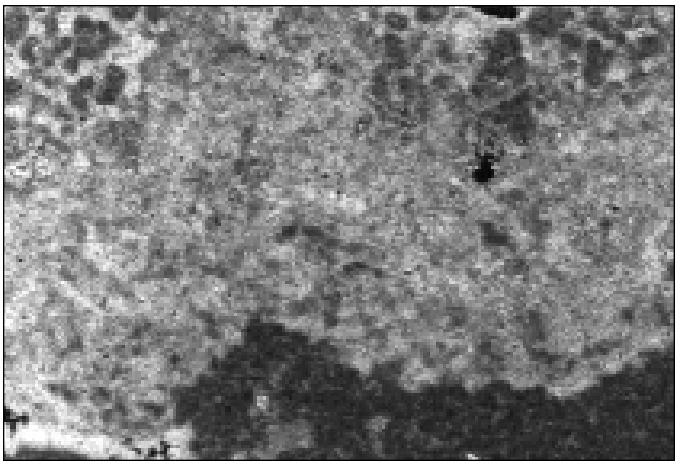

Figure 15. *Thin section of cements in macro-laminated crust or peloid cementstone from west-central Stansbury Island. Cement morphologies dominated by subequant, anhedral submicrocrystalline grains (bottom; less than 2 microns), grading into subequant, anhedral microcrystals (10 to 20 microns) in the upper left. Aragonite needle meshes of both random and spherulitic textures are visible in brighter portion of photo. Peloidal cements (dark subspherical objects) give the clotted texture. Peloids are approximately 40 microns (0.0016 inches) in diameter.*

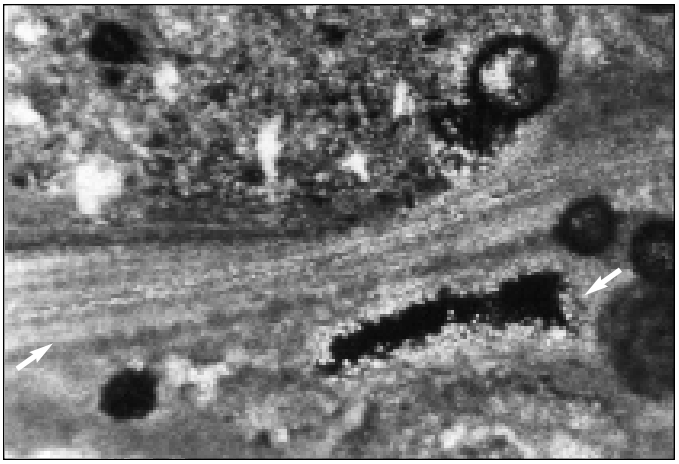

Figure 16. *Thin section of radial fibrous fabric of aragonite cement seen forming laminae (left arrow). Submicrocrystalline aragonite precipitated in vug of Antelope Island intraclast (right arrow). Photograph is about 4 mm (in) across.*

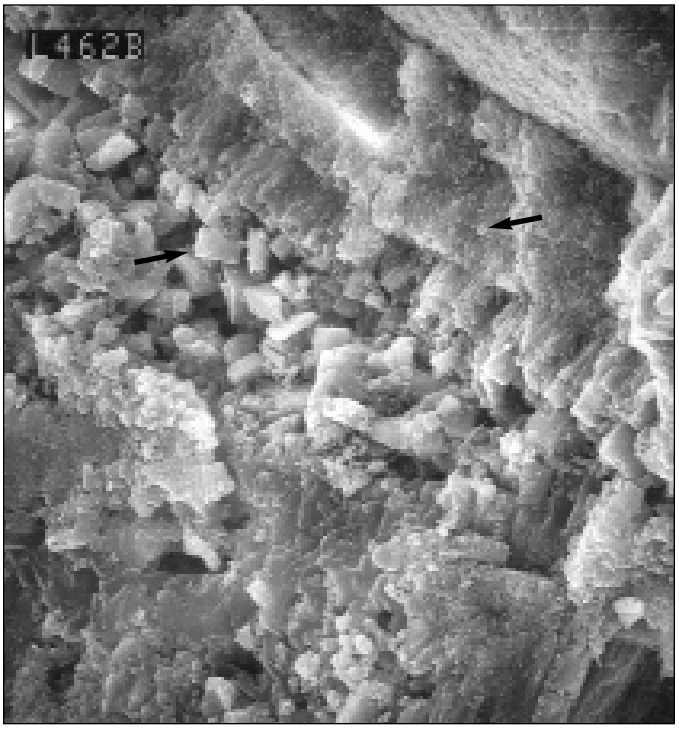

Figure 17. *SEM photomicrograph of cemented ooids shown with less magnification in figure 23. Equant, euhedral microcrystalline prisms (rhombs; left arrow), submicrocrystalline grains (right arrow) of aragonite, and bundles of subhedral prism cements bind ooids; a few clay flakes fill in void space (x1,500).*

in some intraclasts (figures 14 and 20). These cements also occur in the micro-laminated crusts as laminations and in laminae separating radial-fibrous bundles of prismatic crystals from other laminae (figure 16). Some individual lamina are continuous around much of their substrate whereas others are laterally discontinuous, possibly indicating distinct episodes of precipitation (figures 14 and 16). The micro-laminated crusts commonly drape between grain surfaces where they form coatings on clasts and beachrock (figure 14). The cements in the granules, or grapestones, of Stansbury Island are dominated by subequant, anhedral submicrocrystalline

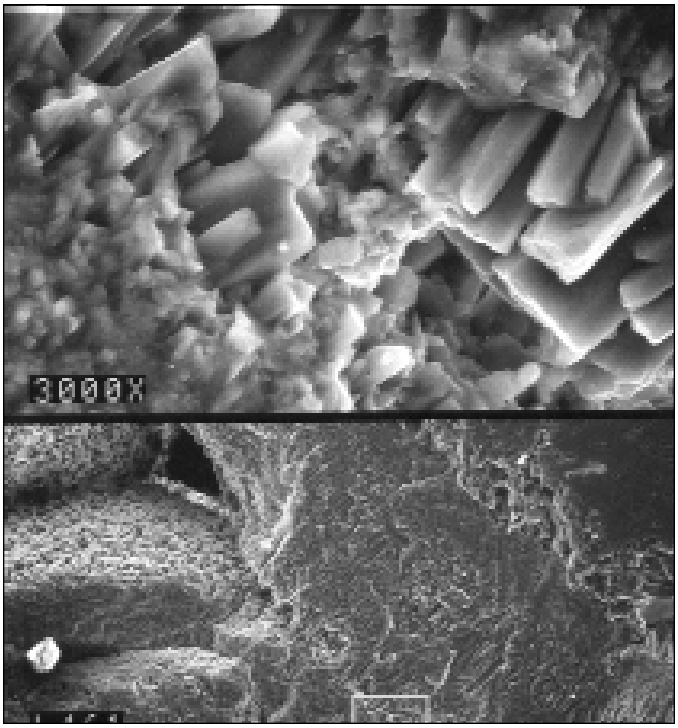

Figure 18. *SEM photomicrograph of cemented ooids in an intraclast from Bridger Bay, Antelope Island. Meniscus cement comprised of subhedral prisms and subequant, anhedral submicrocrystalline aragonite grains that infill space between prisms and provide a foundation for the prisms. Prisms range from 3 to 10 microns in length. Box on lower image (x300) shows area of detail of upper image (x3,000).*

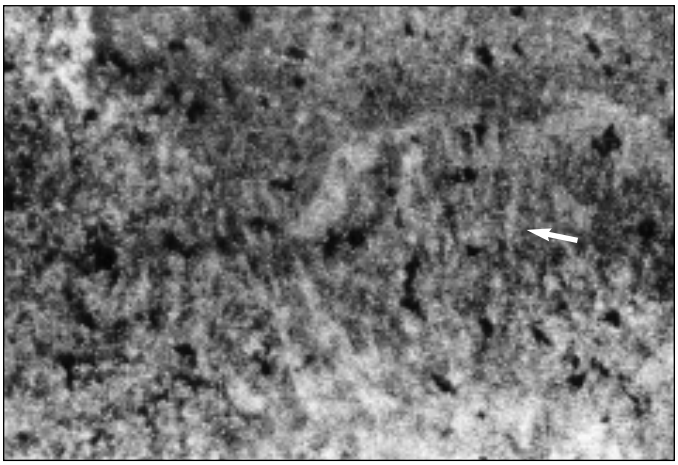

Figure 19. *Thin section of algal filaments (arrow; probably* Gloeocapsa*) defined by subequant, anhedral, submicrocrystalline aragonite grains grading into microcrystals at the bottom. Sample from macro-laminated crust from central Stansbury Island (location 5, figure 1). Note darker scattered clays and peloids. Photograph is about 1 cm (0.4 inch) across.*

grains (figure 21) although needle cements occur in some voids, and peloids may have outer laminae of radial fibrous bundles of prisms or blades (figure 15).

Microcrystals of subequant, anhedral cements (figures 15 and 19) were observed in the macro-laminated crusts of Stansbury Island where they occur in the inner lamina between the darker submicrocrystalline cements forming laminae on both sides. The contact between the two sizes of

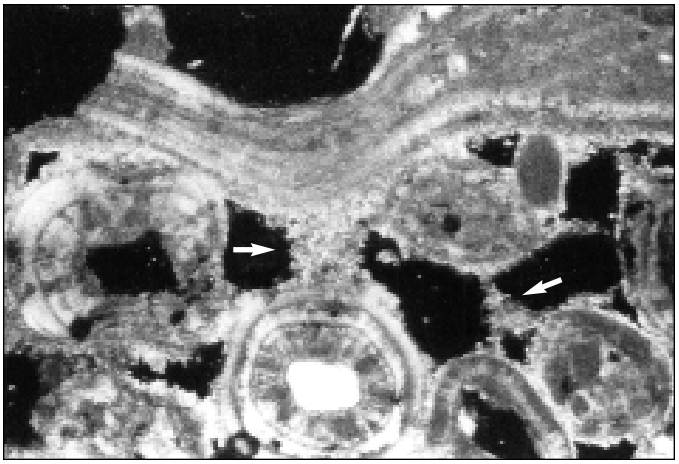

Figure 20. *Thin section of meniscus cement (right arrow) beneath micro-laminated crust on intraclast collected at Bridger Bay. Note how crust drapes between grains and pendant gravity cement (left arrow) forms between crust and underlying ooid. Pendant and meniscus cements are characteristic of cementation in a vadose environment. Photograph is about 2 mm (0.8 inches) across.*

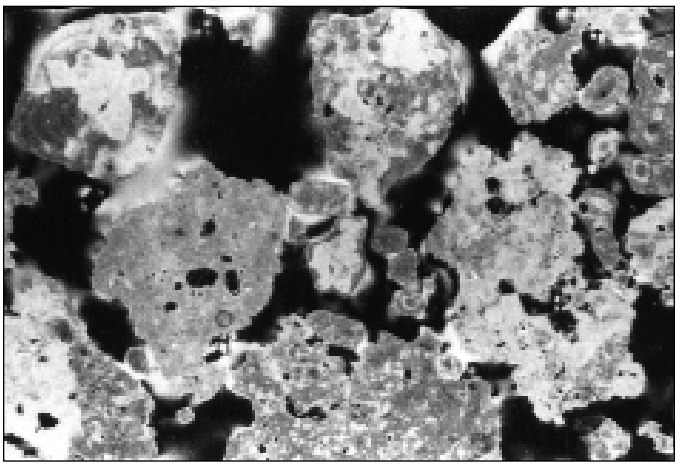

Figure 21. *Granules 1 to 5 mm (0.04-0.2 inches) across in thin section viewed with polarized light show they are dominated by peloids, pellets, and submicrocrystalline aragonite with a few ooids (see figure 29).*

anhedral crystals appears gradational and irregular (figures 15 and 19). The microcrystal cements appear brighter and more clear than the submicrocrystalline grains not only because they are larger, but also because they appear to contain fewer clay or algal impurities than the submicrocrystalline cements.

Bundles of subhedral prisms to bladed crystals range in size from 2 to 19 microns in length and from 1 to 2.5 microns in width (figures 22 and 23). Prism-to-bladed aragonite occurs as microcrystalline prisms to stubby blades with an average width to length ratio of 1:1.6 microns with a range of 1.1:1 to 1:2.7 microns. They grow perpendicular to their foundation in single layers of palisades of bundles or multiple layers of prism to bladed bundles of epitaxial overgrowths (figure 22). Determining the length of longer single crystals can be difficult because most have discontinuities perpendicular to their c-axis (figure 22). The vertical position of the discontinuities is at a similar height in the crystals and contributes a vaguely laminated or layered appearance to the cements. These discontinuities are irregular in shape and

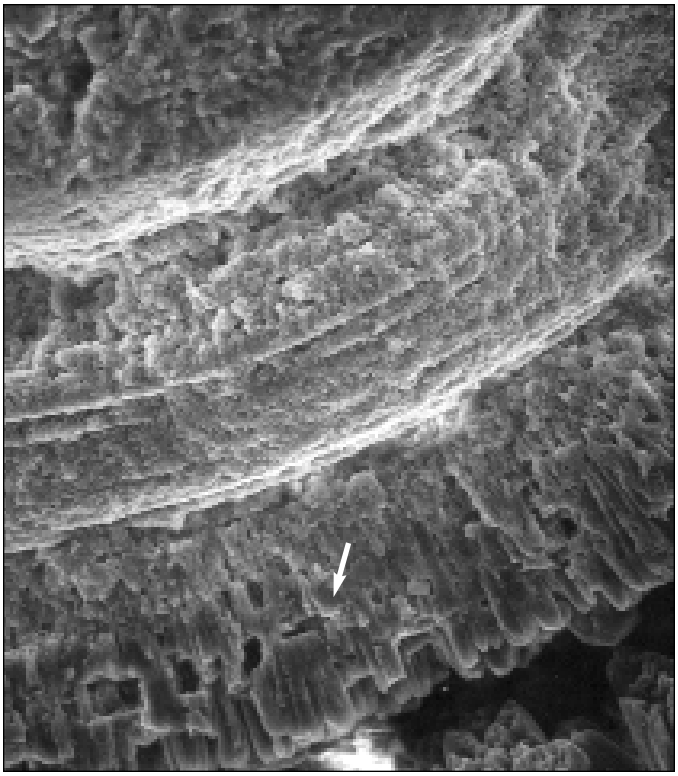

Figure 22. *SEM photomicrograph of cements binding ooids in an intraclast from northern Stansbury Island, showing thick rim of laminations of subequant, anhedral microcrystalline grains overlain by palisaded bundles of epitaxial overgrowths of subhedral, prismatic aragonite. Note the discontinuities (arrow) in the prisms that suggest laminations. We interpret these as dissolution features that may support the process of cementation proposed by Reitner and others (1997). Adjoining cements on ooid surface at bottom of micrograph show the terminations on the bundles of subhedral prisms of aragonite (x1,200).*

appear to be dissolution features. These longer crystals generally have rounded to subrounded terminations (figure 22) whereas shorter crystals in the range of 2 to 4 microns in length have sharp straight terminations perpendicular to the c-axis of growth (figures17 and 18). The small size of the crystals and their occurrence in palisaded bundles result in a radial fibrous texture (figures 16 and 20). These cements occur in clasts and in the beachrock as coatings, meniscus, and isopachous fabrics. Prismatic cements represent the second most common crystal form of aragonite in our samples.

Subequant rounded stubby blades have average width to length ratios of 1:1.5 microns and a range of 1:1.1 to 1:2 microns (figure 24). Crystal size ranges from 16 to 32 microns in height. They do not have crystal faces in SEM images (figure 25) but in thin sections sharp boundaries between crystals are apparent and they grossly resemble bladed magnesium-calcite (figure 24). In transmitted light they appear bright and clear. Subequant bladed aragonite occurs as spectacular isopachous cements rimming ooid and peloid grains in intraclasts (figure 26). Partial isopachous rims or isolated crystals are more common within intraclast pores and vugs between grains as very fine subequant crystals (figures 27 and 16). These cements are most common in submerged samples of clasts and cemented layers from Bridger Bay, but were also found in samples of cemented layers from the

Figure 23. *SEM photomicrograph of cemented ooids, middle of Stansbury Island, showing submicrocrystalline rim cements binding ooid laminae of large radial fibrous bundles of prisms (x300).*

trench about a meter above the lake at the northern Stansbury Island site (figure 10, location 4).

Equant euhedral rhombs and prisms are about 4 microns with sharp crystal faces (figure 17) that appear sharp and bright in transmitted light. They occur associated with the anhedral submicrocrystalline grains in meniscus and rim cements and in laminated crusts in spaces between prismatic crystals binding ooids and other grains.

Needles have an average width-to-length ratio of 1:8.2 microns and occur as meshes, radiating spherulites (figure 15) and solitary crystals (figure 27). Individual needles range in length from 8 to 28 microns and in width from about 1 to 4 microns. Meshes consist of randomly oriented tangles of needles, whereas spherulites are more organized clusters of needles radiating from a central point. In transmitted light solitary crystals appear clear and bright, meshes appear as small, bright, irregular areas with diffuse boundaries, and spherulites appear as bright circular-spots. Needles are most common in pores in granules and macro-laminated crusts (peloid cementstones) of central Stansbury Island, and more rarely in pores in intraclasts. Aragonite needles are seen together with aragonite blades in a few samples (figure 27). In general, needle cements represent a small portion of all the cement morphologies in our samples.

Crusts, or coatings, consist of stacks of laminae of different crystal types. Laminae of microcrystalline aragonite intermittently alternate with laminae of palisades of bundles of microcrystalline prismatic aragonite to form laminated crusts (figures 16 and 18). Some laminations in depressions thin laterally indicating different episodes of precipitation (figure 16). The prismatic aragonite crystals generally show multiple events of epitaxial overgrowth. Anhedral subequant

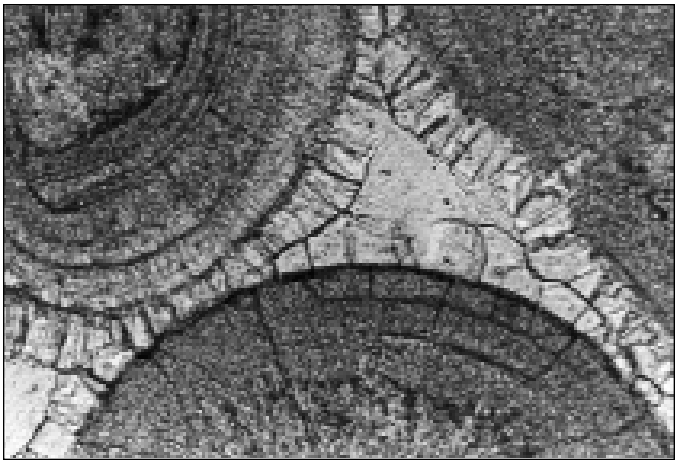

Figure 24. *Thin section of aragonite isopachous cements (16 to 32 microns thick) shown in figure 26. Note stubby-bladed habit of cement with distinct crystal boundaries and the similarity of fabrics in the ooid cortexes with fabrics in the laminated cements in figure 14 and 16.*

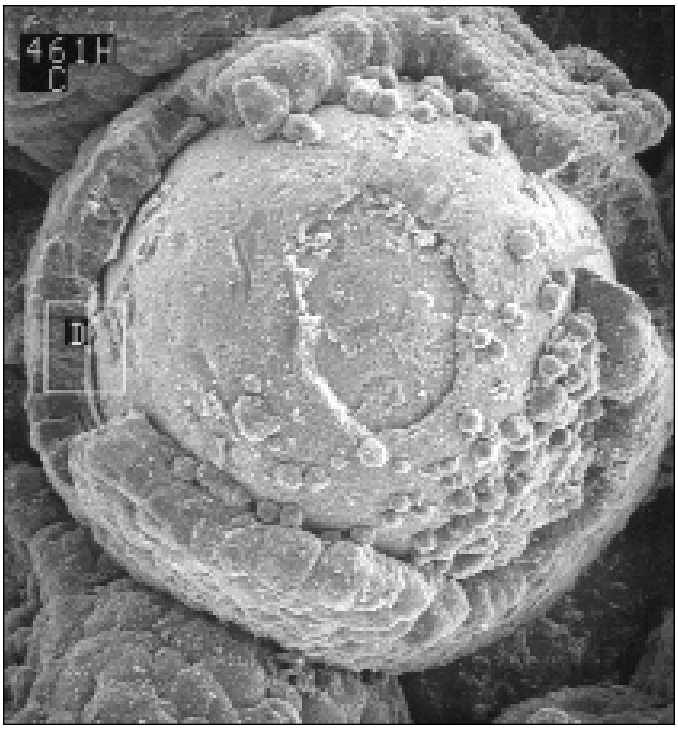

Figure 25. *SEM photomicrograph of ooid in an intraclast from Bridger Bay, Antelope Island, showing submicrocrystalline laminae on broken ooid surface and rounded, stubby-bladed isopachous cements binding ooids together (x300). Figures 24 and 26 show these cements in thin section.*

and equant submicrocrystalline grains occupy spaces between prismatic crystals and also form laminations (figure 17). Physical evidence of algae influencing the formation of the micro-laminated crusts is generally lacking among the uniform laminations (figures 16 and 20) of our samples. However, recent biogeochemical studies of the Antelope Island clasts have documented that biofilms on their surface cause calcification (Neuweiler, 1997). The biofilms were dominated by the cyanobacteria *Gloeocapsa*. Those coatings are distinctively different than our peloid cementstones of central

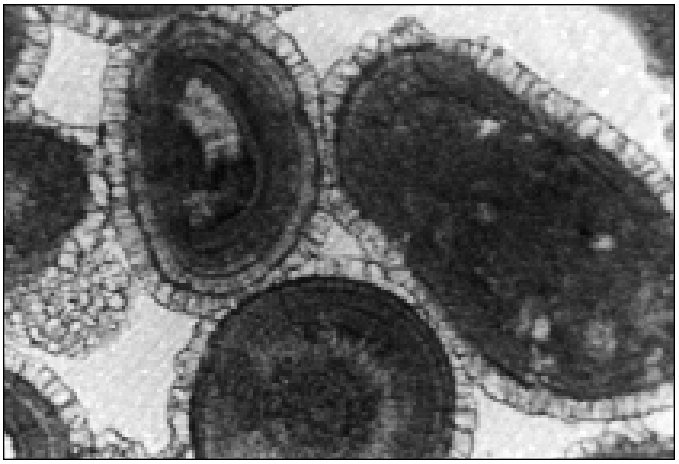

Figure 26. *Thin section of isopachous rim cements of blocky to stubby-bladed aragonite around ooid grains. Ooids are about 1.4 mm (0.06 inch) in diameter.*

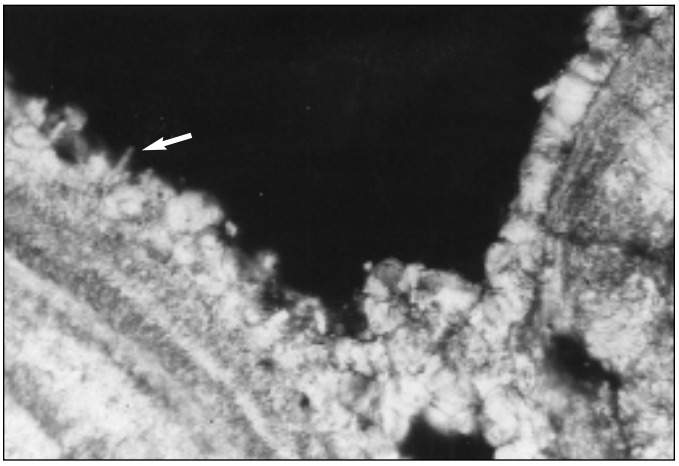

Figure 27. *Thin section of co-occurrence needle cement (arrow) and subequant, rounded, stubby bladed aragonite on outer margin of ooid on left. An aggregate of subequant, anhedral, microcrystals round-off the pore at the contact of the two ooids. Crystals are about 16 microns long.*

Stansbury Island which show clear evidence of algal filaments (figure 19) and cements are composed of thick outer laminations of anhedral submicrocrystalline grains with an inner lamination of 10 to 20 micron anherdral microcrystals (figure 15).

DISCUSSION

Cementation along the shoreline of Great Salt Lake is occurring in a rigorous physical and chemical environment that is further stressed by great lateral fluctuations in the strandline as lake levels change. The strandline is the center of the shoreline which is comprised of several facies including subaqueous foreshore, beach, and subaerial backshore. The period and frequency of lake level fluctuations vary on different scales: seasonal, historical, and geologic. With seasonal changes of lake levels as much as 0.9 m (3 feet) and over 7 m (23 feet) historically, shoreline facies have migrated miles back and forth in recent times. Beachrock provides a temporal marker of a shoreline. Because of the low dip of the shoreline and strong seasonality, sediments are exposed to a wide range of combinations of vadose and phreatic water chemistries over a wide range of periods of time and frequencies. The conditions existing at the time samples are collected may not be representative of the conditions under which they formed. Shorelines are dynamic environments with ephemeral water levels, so with each fluctuation large volumes of sediment are mobilized over vast areas. The cemented layers we sampled and observed have not always been exposed at the sediment surface as they were during our sampling. To assign a particular cement morphology to a particular environment of deposition based on where we collected the samples could be misleading in this case, but the cement morphologies and fabrics can help identify the conditions at the time they precipitated. Cement morphologies and fabrics in conjunction with sedimentary structures like beachrock provide a frame of reference for environmental reconstructions of shorelines.

Cementation

The widespread distribution of cementation around Great Salt Lake and the wide array of sedimentary structures and crystal forms of cement provide insight not only for interpreting depositional environments in ancient rocks but also for understanding the complexity and variety of the cementation processes. The occurrence of beachrock is a particularly useful feature to recognize because its presence in ancient rocks establishes the position of a shoreline. Knowing the position of the shoreline is useful in discriminating between backshore ooid dunes and offshore ooid shoals. Cementation of the shoreline indicates that conditions conducive for precipitation of cements existed for an adequate period to allow for formation and preservation of beachrock. In marine systems, Hanor (1978) determined that CO_2 degassing from groundwater at the marine phreatic contact in the beach resulted in rapid cementation and formation of beachrock in tropical environments. Binkley and others (1980) favored a similar mechanism of degassing for formation of beachrock along a marl lake in Michigan. Degassing of phreatic waters may be contributing to cementation along Great Salt Lake shorelines but other mechanisms such as hypersalinity (Shinn, 1969; Friedman and others, 1973; Halley, 1977), organomineralization (Reitner and others, 1997; Neuweiler, 1997), and interstitial gases (Cloud, 1960; Reitner and others, 1997) are also known to contribute to the precipitation of abundant cements.

The only place we found beachrock was in Bridger Bay on the northwestern shore of Antelope Island, just north of Buffalo Point. In this bay cementation was extensive and present in a variety of forms. Also present were intraclasts, layers of cemented sediment, and fossilized gas structures. This locality, compared with the small bay just to the south of Buffalo Point, illustrates the probable influence of extreme hypersalinity on cementation rates.

South of this locality, in White Rock Bay, no cementation was found. Several shallow cores (less than 0.5 m [<1.7 ft]) were taken in the beach and no cementation was encountered, although the sediments were identical with those in the bay to the north where massive cementation has taken place. Another locality where no cementation has apparently taken place is at Magna, a public beach.

Dunes flanking the beaches in both bays by Buffalo Point are composed primarily of wind blown ooids from the beach. No cementation was encountered on the dune surfaces, in the interdune areas, or by shallow probes (0.5 m [1.7 ft]) into the dunes.

The absence of cemented sediments at White Rock Bay is particularly interesting because of its proximity to cemented sediments in a geographic setting that suggests no major natural differences of sediments between the two bays. Although no apparent differences in setting seemed to exist, observations of both bays from Buffalo Point suggest that the cementation occurs in a bay that has been barred so as to increase salinity. Several bar forms confine circulation in the northerly bay whereas White Rock Bay to the south appears to have totally open circulation.

Regularity of the bar forms suggests that the northerly bay was made into a salt harvest pan and later abandoned. It is possible that the bar forms are remains of former offshore bars, but their semi-grid like pattern suggests that they are man-made. Extreme hypersalinity within the probable salt pan is the distinguishing feature between the cement-occurring and non-cement occurring bays. If groundwater degassing was the sole cause of cementation one might expect it in both bays because of their similar topography and recharge areas. Comparison of the other localities where cemented sediments are located, such as the salt evaporator at Promontory Point, shows an apparent relationship of hypersalinity and cement occurrence, leading us to suggest that extreme hypersalinity is one control for cementation in Great Salt Lake.

Three cement fabrics are characteristic of Great Salt Lake beachrock: meniscus, pendant (figure 20), and laminated. Meniscus and pedant cements indicate deposition in a vadose environment when pores are subject to filling with various amounts of air during periods alternating between wet and dry (Moore, 1973; Longman, 1980). Subequant, anhedral submicrocrystalline aragonite is the dominant crystal form in these different fabrics.

Organic Mediation of Cementation

Two groups of authors have recently proposed organic mediated mechanisms for the precipitation of laminated cements in Great Salt Lake, Pedone and Folk (1996), and Reitner and others (1997). Pedone and Folk (1996) studied samples of stromatolites from the southwestern side of Stansbury Island and proposed an elegant explanation for the different crystal forms. Based on physical evidence they proposed that consumption of brine shrimp egg cases by nannobacteria in the sediment alter the microchemical environment to precipitate laminae of anhedral microcrystals. After the organic matter has been consumed by bacterial respiration, the microcrystal laminae are overlain by inorganically precipitated bundles of prismatic aragonite. This explains one pair of laminae but not multiple pairs of stacked laminations like those in our crusts, or in ooids with nonorganic nuclei. Laminated cements on our beachrock are similar to those found on intraclasts at Antelope and northern Stansbury islands, and at Promontory Point.

Reitner and others' (1997) description of laminated cements on "ooid microbiolite chips" is similar to our micro-laminated crusts on beachrock and the coated intraclasts at three of our locations. They reported two types of clasts from Bridger Bay, Antelope Island. One they referred to as "ooid microbiolite chips," and the other as "microbiolite crusts." Their descriptions of microbiolite crusts are similar to our macro-laminated crusts from middle Stansbury Island that are discussed below. The micro-laminated crusts are comprised by laminae of anhedral microcrystalline grains intermittently alternating with a few laminae of bundles of anhedral prisms that cause the fibrous texture. Using sophisticated biogeochemical analytical techniques, Reitner and others (1997) concluded that the veneers of laminated cement on the "chips" occurred at the base of thin biofilms dominated by the cyanobacteria *Gloeocapsa*. They noted that the fabric of the laminated cements were "strikingly similar" to that of the ooids and the cements between the ooids within the chips.

This is interesting because the focus of their work was on ooids from which they concluded, via hydrocarbon analysis, that cyanobacteria played no role in the precipitation of cements forming the ooids. Yet the fabric of the laminated cements forming the ooids is "strikingly similar" to that of the chips. This may indicate that different organically mediated mechanisms produce similar crystal morphologies and fabrics. Ooid cements have fabrics similar to the micro-laminated crusts on the beachrock and intraclasts (Reitner and others, 1997), and they proposed a process for the precipitation of ooid lamina within an organic-rich mucus that explains ooid fabrics and their different crystal morphologies. The mucus is a solution of organic macromolecules containing few living organisms and dominated by waxy organic compounds derived from insects and from terrestrial plants.

The cements and the process they describe for ooids is compatible with the cements and fabrics of our laminated cements except they do not adequately explain the multiple laminations of prismatic bundles. Laminae of bundles of prismatic crystal were rare in their chips. Reitner and others, (1997) proposed that an organic mucus covers most Great Salt Lake sediments and other shoreline substrates where it also fills depressions and can be mixed with biofilms. The mucus is a semistratified solution in which micrite precipitates in the bottom layer, epitaxial overgrowths on fibrous prisms occur in the intermediate layer and dissolution occurs at the tips of prismatic crystals in the upper acidic layer. Micrite can precipitate over fibrous palisades of crystals and form concentric layers. No calcification occurs in the upper layer of the mucus which is more acidic than the lower layer where the tips of the fibrous crystals showed dissolution features (Reitner and others, 1997). Dissolution features (figures 28 and 22) in some of our intraclast samples from mid-Stansbury Island appeared as discontinuities within the epitaxial prisms not at the tips. These sublinear discontinuities suggest laminations and possibly multiple growth events, but may represent a nonuniform surface for crystal growth, nonuniform crystal growth, or a zone of dissolution. The epitaxial overgrowths cements appear vaguely laminated, because of small scale dissolution within the crystals (figure 22). One could interpret this as a $CaCO_3$ recycling mechanism similar to that proposed by Reitner and others (1997) except our observations suggest that dissolution is occurring within the

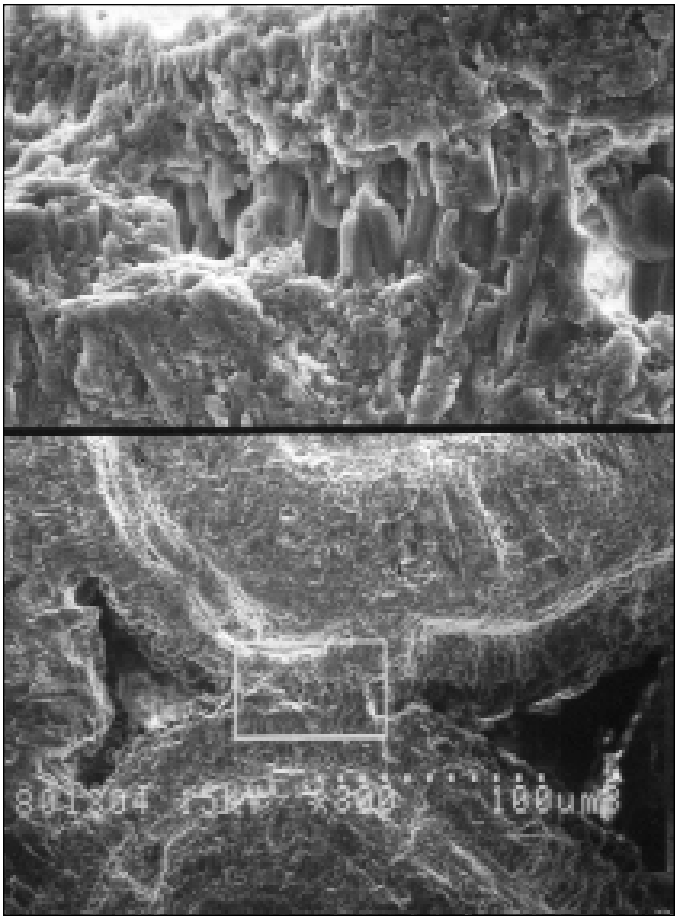

Figure 28. *SEM photomicrograph of cemented ooids in an intraclast from north point of Stansbury Island, showing rim cements of submicrocrystalline grains and prismatic aragonite. Note pitting and etching of some prismatic crystals suggesting dissolution in upper image. Lower magnification of the same rim cement that binds the ooids in bottom image (x300); box is detail in upper image (x1,500).*

crystal and reprecipitating at the top. The slight differences between interpretations result from slightly different observations of the location of dissolution and reprecipitation. Noting that mucus and biofilms can be mixed, the different observations probably can be explained by the variability in combinations of mucus and biofilms and the subtle differences in the process by which they produce different crystal morphologies. Reitner and others (1997) acknowledged an incomplete understanding of the process but provided good evidence that precipitation of the cement morphologies and fabrics in our micro-laminated crusts were mediated by organisms either directly in biofilms, or indirectly in mucus.

Our peloid cementstone crusts from the southern Stansbury Island location 5 are similar to the microbiolite crusts of Reitner and others (1997) from Antelope Island and share some similarities with the stromatolite samples of Pedone and Folks (1996) from southeastern Stansbury Island. The crust (peloid cementstone) at Stansbury Island's southern location is petrographically similar to Eardley's (1938) "clay-type" shingle from Rozel Point which he described as composed of numerous mineral grains cemented with $CaCO_3$ in which much clay was included. Eardley (1938) reported that granule sediment at Rozel Point formed when storm waves broke up the "clay-type" shingle or algal deposits with their associated cemented oolites. Our samples show clear forms of filamentous algae (figure 19) and are composed largely of subequant, anhedral aragonite of two different sizes. The dark outer margins are dominated by the less than 2 micron grains whereas the inner creamy white lamina consists mostly of the 10 to 20 micron anhedral crystals. The larger crystals appear to be similar to those described by Pedone and Folk (1996) in their stromatolites. The sequence of crystal forms they observed in laminae on egg cases is similar to that on peloids in our clasts. Few egg cases were observed in our clasts, but some of the peloids may have originally been egg cases. Brine shrimp feces, or pellets (figure 29), are common in the crusts and granules (figures 15 and 21). Many of the larger peloids (400 microns) in Salt Lake samples are actually pellets. Many of the peloids probably precipitated within the sediment as described by Macintyre (1985). The spherulitic form of the aragonite needle meshes (25 to 60 microns in diameter) probably are forming by direct precipitation similar to the peloids reported by Macintyre (1977, 1984) in submarine cements. The clotted textures reported by Reitner and others (1997) in their Antelope Island microbiolite crusts are probably peloids. They reported these crusts were of similar thickness (9 mm [0.35 inch]) to ours which averaged about 1 cm (0.4 inch). A biofilm on their crust was up to 600 microns thick and consisted primarily of two forms of cyanobacteria. The coccoid cyanobacteria were dominated by *Gloeocapsa* with lesser amounts of *Aphanothece*. *Aphanothece* is the prominent algae credited with building the Great Salt Lake stromatolitic bioherms (Eardley, 1966; Halley, 1976). The cement morphologies and crystal size described from bioherms (Halley, 1976) are similar to those described in granules by Eardley (1938) and herein. No biofilms were apparent in our samples but the dark layer with algal filaments and submicrocrystalline anhedral cements are probably the product of biofilms.

The granules (1 to 5 mm[0.04-0.2 inch]) at Stansbury Island are similar in appearance to the "grapestones" described from the Bahamas (Illing, 1954; others in Bathurst, 1976). Grapestones are grain aggregates formed by the cementing of one or more grains, the coalescing of chemical allochems as they crystallize out of a saturated solution adjacent to one another, or the reworking of previously cemented grains. Reworking of any of the cemented sediments by a variety of processes from wave energy to rupturing by confined gases could initiate the formation of these grains. The majority of our granules have cement fabrics similar to our peloid cementstone crusts although a few have micro-laminated crusts similar to those on the intraclasts. Our granule sands probably represent incipient cementation processes related to discontinuous, or disrupted biofilms, like those building the stromatolites.

Subequant, rounded, stubby-bladed isopachous cements were found in samples from two distinctly different settings: 1) from some of the intraclasts found submerged around the beachrock at Antelope Island (figure 4), and 2) from samples collected from the trench at Stansbury Island over 1 meter (3 feet) above current lake level. The uniform thickness of the fine blades and prisms around pores and grains indicate the cements formed in the phreatic zone which was saturated

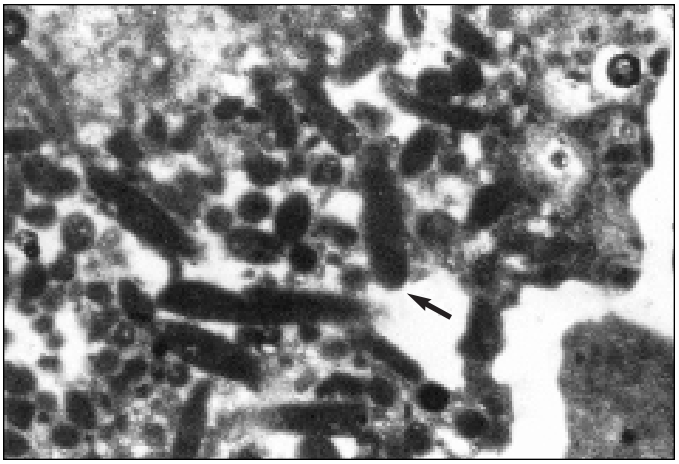

Figure 29. *Pellets (arrow) in granules are probably brine shrimp feces like those reported by Eardley (1938). Pellets are up to 400 microns in size. Thin section photomicrograph taken with plane transmitted light.*

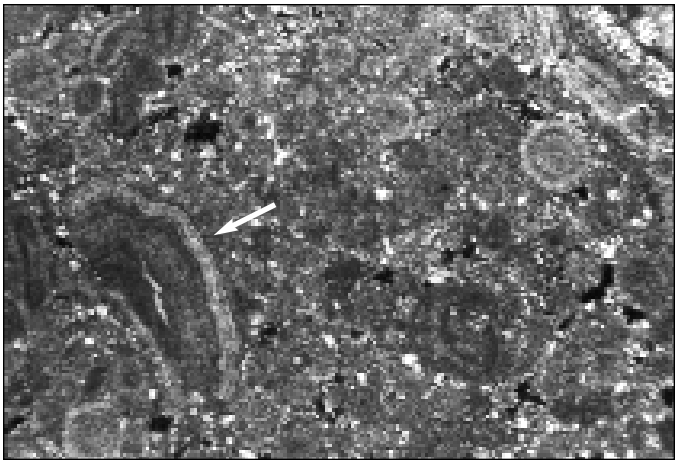

Figure 30. *Mississippian-age ooids and coated broken grains (arrow) from the subsurface of the Williston Basin, North Dakota. Halley (1977) demonstrated that hypersaline ooids characterized by radial fibrous fabrics are more susceptible to breakage than marine ooids with tangential fabrics, so coated, broken grains can indicate deposition in hypersaline conditions. Lack of cementation indicates subaqueous deposition distant from the strandline yet in a hypersaline setting. Compare these fabrics with those in ooids and micro-laminated crusts in figures 16 and 20, and with the coated broken grain in figure 14.*

with respect to aragonite. The subaerial samples are still aragonite but they have aberrant crystal forms. Subaqueous samples had some of the clear prism crystals, but they were rounded. Precipitation within the lake at an earlier, higher stand with lower salinities could explain the occurrence of these cements in both lake and supra-lake deposits. This interpretation is compatible with historical lake levels and water chemistries (Spencer and others, 1985). Aragonite is unstable at atmospheric conditions so one would expect that cements above present lake levels would alter to low-magnesium calcite or that the crystal habit would be modified within the meteoric phreatic zone (Longman, 1980). This may explain the more bladed appearance of the subaerial samples as compared to the somewhat fibrous bundle appearance of the subaqueous intraclast samples. The early stages of recrystallization could eliminate the fibrous fabric and yet maintain the bundles seen in SEM (figure 25), which in thin section would look like the rounded stubby blades in figure 24.

Gas Mediation of Cementation

Gas in the sediments is also contributing to the cementation process. Gas trapped by organic films in the water was observed forming a frothy foam in the center of a gas-eruption structure at Antelope island. Smaller sedimentary structures of cemented ooids collected in the same area have the form of domes and upturned, arcuate collars around 8 cm (3 inch) in diameter. Apical holes in some dome structures are interpreted to result from gas pressure increasing until the confining sediments rupture. Domes and collars rise about 2 cm (0.8 inch) above a flat-base flange of cemented sediment, suggesting that gas was below the cemented area and bulges formed in sediments that were weaker and/or more tensile. The collars are interpreted to form as a result of cementation of the sediments forming the walls of gas conduits or from the rupture of domed sediments before cementation was sufficient to preserve them as domes. Cementation had to be essentially contemporaneous with gas doming of the sediments or these structures would not have been preserved. Cementation in beachrock has been shown to occur within 12 hours by degassing of CO_2 from ground water (Hanor, 1978). Cloud (1960) briefly discussed the general role of gas in inducing cementation in sediments and more recently Reitner and others (1997) provided convincing evidence that ooid formation in Great Salt Lake is related to strong sulfate reduction in the sediments.

Oil seeps, black reducing sediments emitting a strong hydrogen sulfide smell, and frothy foams of bubbles all indicate the variety of sources and abundance of gases trapped in Great Salt Lake sediments. Although a deep, ancient source of mature hydrocarbons cannot be excluded as a source for gases in the sediments, organic material in Great Salt Lake is sufficiently abundant and the depositional conditions appropriate to produce biogenic gas during the Pleistocene. Organic deposits of animal, plant, and fecal material are of such great abundance that they form windrows of debris for miles along the beach where they decay and contribute a fetid odor (Eardley, 1938). Large amounts of organic matter are undoubtedly buried and incorporated into the sediment. This is indicated in numerous trenches dug into lake sediments that contained foul-smelling, sticky, impermeable clays (Seelos and others, 1975). Gas generation by decaying organisms produces various gases including some combination of carbon dioxide, methane, hydrogen, and hydrogen sulfide. The type of gas generated at shallow depths is primarily a function of the type of bacteria present, the type of organic material, and the occurrence of oxidizing or reducing conditions. Eardley (1938) concluded that the lake waters were a reducing environment and reported the emission of sulfurous fumes from the sediments. We believe gas generated in the sediments by the decaying process contributes to the cementation process and formation of eruption structures.

Gas-formed sedimentary structures similar in size and shape to the domes and collars have been reported in association with algal mats and were referred to as gas blisters

(Black, 1933; Clarke and Teichert, 1946;Ginsburg and others, 1954; Ginsburg, 1955; Kendall and Skipwith, 1968; and Davies, 1970). Algal gas blisters are generally preserved as small millimeter-scale fenestral pores and birdseye structures (Shinn and others, 1965) but cementation of gas structures the size of the domes reported here are rare. Laminated algal mats were not present at any of the locations we examined but they are not required for the formation of gas structures. Emery (1960) reported sand domes were formed in non-algal associated marine beach sediments in southern California. He postulated that the fine sediment was sufficient to trap the gas that lifted the sediment into domes.

A variety of components contribute to the trapping of gas beneath Great Salt Lake sediments, including algae, organic films, clays, and cements. The majority of our samples showed no evidence of algae in hand specimens, thin section or SEM images. Algal filaments are only seen in thin sections of the peloid cementstone crusts of central Stansbury (location 5) and are one of the major factors distinguishing them as a different crust type. A greenish cast on some of our grainstone samples was the only evidence for the presence of algae, biofilms or organic mucus. The heterotrophic cyanophytes described by Reitner and others (1997) probably contribute to the greenish cast we observed on these samples. Algae are abundant in the lake (Eardley, 1938), but most algae are seasonal and their standing crop was probably low during our March collection.

Clays are present as a very minor constituent in our grainstone samples (estimated to be less than a few percent) but are visually more abundant in the peloid cementstone crusts (figure 15 and 19). Eardley (1938) documented that clays are one of three major sediment types in the lake. In compiling a map of the distribution of the sediment types he noted clays are concentrated in the deeper portions of the basin and in embayments with restricted wave energy. Impermeable clays interbedded with potentially permeable brown sandy clays were reported in trenches dug at many locations around the lake (Seelos and others, 1975).

Carbonate cementation is widespread in Great Salt Lake sediments. Many processes are contributing to cementation in surface sediments, and in the vadose and shallow lacustrine phreatic environments. It is possible that some cementation is occurring at shallow depths within dysoxic sediment as Neuweiler (1997, p. 199) suggested for ooid formation. Beaches are dynamic and layers of sediment cemented near the surface could easily be buried. Trenches by others and our shallow probes have encountered buried cemented sediments. The imbricated nature of the plates forming eruption craters and the fact that there were more plates than could be reconstructed into a single layer suggest that more than one buried layer had been ruptured and the pieces had been forced up through the sediment. The angular edges of the fragments indicate brittle fracture from substantial force.

We believe that the gas is generated by the biodegradation of organic material; the gas is then trapped beneath impermeable layers of either cemented beds or clays. Gas moves up dip not only because of density differences, but also because rising lake levels increase the hydrostatic pressure on the sediments compressing the gas, thereby forcing the gas upwards along bedding planes. When the gas encounters a zone of weakness in poorly cemented sediment, or other types of seals, a bulge develops, or in some cases, the surficial layers burst, forming gas-eruption craters or the smaller circular upturned collars. A similar mechanism was proposed by Emery (1960) to explain gas domes in unconsolidated sediment. He postulated that the well-developed alternating laminae of coarse and fine sand allowed air to be driven by waves breaking on the beach to be forced along permeable layers until the air was so compressed that it could lift several centimeters of sand to form the domes. A compressive strength of 330 kg/m^2 (68 lbs/ft^2) was measured on aragonite-cemented sand layers of similar thickness in the Persian Gulf (Shinn, 1969). Gas pressures of the magnitude needed to break cemented sediment of this strength also could push fragments of cemented layers from shallow depths through unconsolidated sediment and produce gas-eruption structures in the form of upturned, imbricated plates of cemented sediment like those we observed.

Another mechanism for the formation of crater-like structures in Great Salt Lake was proposed by Eardley (1938) after observing “craterlets” formed along a bedrock sediment contact but he gave little information about their characteristics. No cemented sediments were described in association with his structures. The “craterlets” were postulated to have been created by the expulsion of cold concentrated brines from the dewatering of clays following compaction initiated by an earthquake. This mechanism does not explain our observations (e.g., bubbling froth and cemented gas domes) as well as does our proposal of gas expulsion.

Related Sedimentary Structures

Flat-pebble Conglomerates

Fragments of layers of cemented sediment were cemented together to form flat pebble conglomerates. Most flat-pebble conglomerates are fine-grained laminated muds and silts associated with peristrandline deposits (Shinn and others, 1965; Deffeyes and others, 1965). Because the available sediments are sand sized and cementation rates are so rapid, coarse-grain conglomerates are common. Other reports of coarse-grained flat-pebble conglomerate formation are few and associated with other hypersaline deposits in the Red Sea (Friedman and others, 1973) and the Persian Gulf (Taylor and Illing, 1969). If one encountered intraclasts in ancient conglomerates as large as those we report here, one would want to be cautious about assigning energy conditions to the formation of such a deposit.

Circular Structures

Circular structures similar to those we observed in large number on the west-cental side of Stansbury Island (figure 13) were first reported by Eardley in the 1950s (in Seelos and others, 1975, p. 91) but were not studied in detail until later (Stifel and Stokes, 1961; Stifel, 1964; and Seelos and others, 1975). The latter authors reported structures with shapes ranging from dumbbell to rounded with a size range from 0.3 to 9.3 meters (3 to 30 feet) in diameter. Stifel (1964) reported the average diameter to be 1.8 meters (6 feet). Extensive trenching by Seelos and others (1975) showed many of the structures were sediment-filled depressions whereas others

were diapir-like. The average depth of the disturbed beds shown in sketches of trenches through circular structures is 0.58 meters (1.9 feet) (Seelos and others, 1975). The structures are generally convex upward although near-vertical beds in two trenches appeared to be possible piercement structures and those examples had beds that extended to a depth greater than that of the trenches. It should be noted that at least three of the trenches showed "calcium-cemented" oolites that were "similar to shingles on the surface" (Seelos and others, 1975). The convex-upward internal structure of the ring structures may be due to collapse of the overlying beds after expulsion of gas. Earlier descriptions of trenching reported by Eardley (1966) revealed concave-upward structures. These latter structures and piercement structures are what one might predict for gas-escape structures. No conclusion about the origin of these structures was reached by previous authors although several theories were offered.

An alternative explanation may come from two types of sedimentary structures described from Death Valley (Hunt and others, 1966) that have similarities with the circular structures at Salt Lake. One type might be mistaken for the gas-eruption craters, and the other may have formed by processes similar to the large circular ring structures at Stansbury Island. The first is a circular collapse fracture system developed when salts are dissolved from below. The second occurs in areas of severe washing, where salts rise by capillary action to the surface, often forming circular spots. The spots consist of salt efflorescence and are from 30 to 60 cm (1 to 2 feet) in diameter surrounded by concentric belts of damp mud of similar diameter (Hunt and others, 1966). We also observed efflorescence in areas adjacent to Salt Lake circular structures (figure 8).

We suggest that there is more than one mechanism for forming the circular structures, but at least some of them may have formed by gas expulsion, as were the eruption craters in the cemented layers. Seelos and others (1975) described highly permeable sediments between impermeable clays or cemented oolite zones in the trenches they dug through circular structures at various locations around Salt Lake. The stratigraphy they described provides the criteria necessary for the formation of the eruption structures we observed; that is the permeable beds would serve as channels for gas movement and the impermeable clay and cemented layers would confine and trap the gas. When gas pressures become too high, gas structures can form in the confining beds. We know gas structures range from microscopic birdseye to meter-scale eruption craters. Cementation associated with gas seeping up along permeable beds might explain the crusts we collected on the perimeter of the circles we sampled and the concentric rings of pebbles Seelos and others (1975) reported in these structures at Dolphin Island.

Because cementation in Great Salt Lake appears to be associated with extremes in hypersalinity, one might expect concentrations of cemented sedimentary structures and constituents to be more common and widespread at low lake level stands during periods of highest salinity. Beachrock would be a valuable indicator of the shoreline at those times. Concentrations of the associations of cemented sedimentary structures and constituents described above can help in characterizing strata deposited during periods of hypersaline conditions. As ancient basins like Great Salt Lake filled and the period and frequency of extreme hypersaline conditions increased, cemented horizons in time and space could become more common and cementation more thorough and pervasive. Hydrocarbon reservoir rock, traps and seals could all form by different degrees of early cementation.

Throughout geologic history, there have been both large lakes and epicontinental seas that experienced periods of hypersalinity. The recognition of the types of cements and textural associations described above will aid in distinguishing between these different environments. Misidentifying lacustrine hypersaline ooids as open-marine ooids can significantly affect paleoenvironmental interpretations (compare figure 30 with 14; Gerhard and others, 1978).

CONCLUSIONS

Quaternary precipitation of aragonite cements in Great Salt Lake has not only produced great volumes of sediments, but also a wide array of cement morphologies, fabrics, and sedimentary structures by a range of processes. Calcium carbonate ions carried by rivers into the confined lake basin from surrounding Paleozoic carbonate terrain are concentrated by evaporation to precipitate great volumes of aragonite during low lake levels when the salinity is highest.

Five distinct crystal morphologies were recognized in samples collected along the shoreline: (1) subequant, anhedral submicrocrystalline grains and microcrystals; 2) bundles of subhedral prisms to blades; 3) subequant, rounded stubby-blades; 4) equant, euhedral microcrystalline prisms; and 5) needles. These crystal morphologies, alone or in combination, are present in many different fabrics including meniscus, pendant, rinds (partial and isopachous), peloidal (clotted), radial fibrous, epitaxial overgrowths, and laminated crusts.

Two forms of laminated crusts are present, micro-laminated with lamina on the scale of a few microns to a few tens of microns, and macro-laminated crusts with lamina on the scale of a few millimeters. Micro-laminated crusts are most common on intraclasts and beachrock along the shoreline, whereas the macro-laminated crusts occurred as fragments associated with large circular ring structures on sandy mud flats.

Several mechanisms are contributing to the precipitation of cements including aragonite-saturated hypersaline waters, direct organic mediation by cyanobacteria, indirect organic mediation by soluble organic matter, and interstitial gas. Unique gas-eruption structures result in part from this mechanism in the form of fossil bubbles (domes), upturned collars, and eruption craters. All of these structures are preserved in cemented ooid grainstones in a range of forms and ages. Recent structures were observed bubbling gas from the center of concentric circles of imbricated plates of ruptured cemented sediment, whereas relict structures were defined by circular depressions in ruptured layers of cemented sediment that were often filled with debris.

Other structures formed because of the different cementation processes include ooids, granules, intraclasts, flat-pebble conglomerates, intraformational breccia, and beachrock. Cement fabrics and crystal morphologies associated with Great Salt Lake beachrock have some similarities and differ-

ences with beachrock in both normal-marine and marginal-marine hypersaline settings. Close examination of cement morphologies should be helpful in discriminating between environments.

REFERENCES

Bathurst, R.G.C., 1976, Carbonate sediments and their diagenesis: New York, Elsevier, Developments in Sedimentology, no. 12, 658 p.

Binkley, K.L., Wilkinson, B.H., and Owen, R.M., 1980, Vadose beachrock cementation along a southeastern Michigan marl lake: Journal of Sedimentary Petrology, v. 50, no. 3, p. 953-962.

Black, M., 1933, The algal sediments of Andros Island, Bahamas: Royal Society of London, Philosophical Transactions, Series B, v. 222, p. 165-192.

Carozzi, A.V., 1962, Cerebroid oolites: Illinois State Academy of Science Transactions, v. 55, p. 239-249.

Clarke, E. de C., and Teichert, Curt, 1946, Algal structures in a western Australian salt lake: American Journal of Science, v. 244, p. 271-276.

Cloud, P.E., 1960, Gas as a sedimentary and diagenetic agent: American Journal of Science, Bradley Volume, v. 258-A, p. 35-45.

Davies, G.R., 1970, Algal laminated sediments, western Australia, *in* Logan, B.W., Davies, G.R., Read, J.F., and Cebulski, D.E., editors, Carbonate sediments and environments, Shark Bay, western Australia: American Association of Petroleum Geologists Memoir 13, p. 169-205.

Dean, W.E. and Fouch, T.D., 1983, Lacustrine environment *in* Scholle, P.A., Bebout, D.G., and Moore, C.H., editors, Carbonate depositional environments: American Association of Petroleum Geologists Memoir 33, p. 98-130.

Deffeyes, K.S., Lucia, F.J., and Weyl, P.K., 1965, Dolomitization of Recent and Plio-Pleistocene sediments by marine evaporite waters on Bonaire, Netherland Antilles, *in* Pray, L.C. and Murray, R.C., editors, Dolomitization and limestone diagenesis: Society of Economic Paleontologists and Mineralogists Special Publication 13, p. 71-88.

Eardley, A.J., 1938, Sediments of Great Salt Lake, Utah: American Association of Petroleum Geologists Bulletin, v. 22, no. 1, p. 1305-1411.

Eardley, A.J., 1966, Sediments of Great Salt Lake, *in* Stokes, W.L., editor, Guidebook to the Geology of Utah, no. 20: Utah Geological Society, p. 105-120.

Emery, K.O., 1960, The sea off southern California - A modern habitat of petroleum: New York, John Wiley & Sons, Inc., 366 p.

Eugester, H.P. and Hardie, L.A., 1978, Saline lakes, *in* Lerman, Abraham, editor, Lakes – chemistry, geology, and physics: New York, Springer-Verlag, p. 273-293.

Freeman, Tom, 1962, Quiet water oolites from Laguna Madre, Texas: Journal of Sedimentary Petrology, v. 32, p. 475-483.

Friedman, G.M., Amiel, A.J., Braun, M., and Miller, D.S., 1973, Generation of carbonate particles and laminates in algal mates – examples from sea marginal hypersaline pool, Gulf of Aqaba, Red Sea: American Association of Petroleum Geologists Bulletin, v. 57, p. 541-557.

Frishman, S.A. and Behrens, E.W., 1969, Geochemistry of oolites, Baffin Bay, Texas (abstract): Geological Society of America, Abstracts with Programs, v. 1, part 7, p. 71.

Gerhard, L.C., Anderson, S.B., and Berg, J., 1978, Mission Canyon porosity development, Glenburn field, North Dakota, Williston Basin, *in* 1978 Williston Basin Symposium: Montana Geological Society, p. 177-188.

Ginsburg, R.N., 1953, Beachrock in south Florida: Journal of Sedimentary Petrology, v. 36, no. 1, p. 85-92.

Ginsburg, R.N., 1955, Recent stromatolitic sediments from south Florida: Journal of Paleontology, v. 29, no. 4, p. 723-724.

Ginsburg, R.N., Isham, L.B., Bein, S.J., and Kuberg, J., 1954, Laminated algal sediments of south Florida and their recognition in the fossil record: Miami University Institute of Marine Science, Marine Laboratories, unpublished report no. 54-21, 33p.

Halley, R.B., 1976, Textural variations within Great Salt Lake algal mounds, *in* Walter, M.R., editor, Stromatolites: New York, Elsevier, Developments in Sedimentology, [no.] 20, p. 435-445.

Halley, R.B., 1977, Ooid fabric and fracture in the Great Salt Lake and the geologic records: Journal of Sedimentary Petrology, v. 47, no. 3, p. 1099-1120.

Hanor, J.S., 1978, Precipitation of beachrock cements - mixing of marine and meteoric water versus CO_2 degassing: Journal of Sedimentary Petrology, v. 48, p. 489-502.

Hunt, C.B., Robinson, T.W., Bowles, W.A., and Washburn, A.L., 1966, Hydrologic basin, Death Valley, California: U.S. Geological Survey Professional Paper 494-B, p. 138.

Illing, L.V., 1954, Bahamian calcareous sands: American Association of Petroleum Geologists Bulletin, v. 38, p. 1-95.

Kahle, C.F., 1974, Ooids from Great Salt Lake, Utah, as an analogue for the genesis and diagenesis of ooids in marine limestones: Journal of Sedimentary Petrology, v. 44, p. 30-39.

Kelts, K., and Hsu, K.J., 1978, Freshwater carbonate sedimentation, *in* Lerman, Abraham, editor, Lakes – chemistry, geology, physics: New York, Springer Verlag, p. 295-323.

Kendall, C.G., St. C., and Skipwirth, Sir P.A. d' E., 1968, Recent algal mats of a Persian Gulf lagoon: Journal of Sedimentary Petrology, v. 38, p. 1040-1058.

Lomando, A.J., Schreiber, B.C., and Harris, P.M., editors, 1994, Lacustrine reservoirs and depositional systems: Society of Economic Paleontologist and Mineralogists Core Workshop no. 19, 381 p.

Longman, M.W., 1980, Carbonate diagenetic textures from near-surface diagenetic environments: American Association of Petroleum Geologists Bulletin, v. 64, p. 461-487.

Loreau, Jr., and Purser, B.H., 1973, Distribution and ultra-

structure of Holocene ooids in the Persian Gulf, *in* Purser, B.H., editor, The Persian Gulf: New York, Springer Verlag, p. 279-328.

Macintyre, I.G., 1977, Distribution of submarine cements in a modern Caribbean fringing reef, Galeta Point, Panama: Journal of Sedimentary Petrology, v. 47, p. 503-516.

Macintyre, I.G., 1984, Extensive submarine lithification in a cave in the Belize Barrier reef platform: Journal of Sedimentary Petrology, v. 54, no. 1, p. 221-235.

Macintyre, I.G., 1985, Submarine cements – The peloidal question, *in* Schneidermann, Nahum, and Harris, P.M., editors, Carbonate cements: Society of Economic Paleontologists and Mineralogists Special Publication no. 36, p. 109-116.

Moore, C.H., 1973, Intertidal carbonate cementation, Grand Canyon, West Indies: Journal of Sedimentary Petrology, v. 43, p. 591-602.

Muller, G., Irion, G., and Forstner, U., 1972, Formation and diagenesis of inorganic Ca-Mg carbonates in the lacustrine environment: Naturwissenschaften, v. 59, p. 158-164.

Multer, H.G. and Hoffmeister, J.E., 1971, Holocene cementation on skeletal grains into beachrock, Dry Tortugas, Florida, *in* Bricker, O.P., editor, Carbonate cements: Johns Hopkins University Studies in Geology, no. 19, p. 25-26.

Neuweiler, F., 1997, Introduction - Part II - International Geologic Conference Proceedings No. 380, *in* Neuweiler, F., Reitner, J., and Monty, C., editors, Biosedimentology of Microbial Buildups, International Geologic Conference Proceedings Project No. 380, Proceedings of 2nd Meeting, 1996: Facies, v. 36, p. 195.

Pedone, V.A., and Folk, R. L., 1996, Formation of aragonite cement by nannobacteria in the Great Salt Lake, Utah: Geology, v. 24, no. 8, p. 763-765.

Picard, M.D. and High, L.R., 1972, Criteria for recognizing lacustrine rock, *in* Rigby, J.K. and Hamblin, W.K., editors, Recognition of ancient sedimentary environments: Society of Economic Paleontologists and Mineralogists Special Publication 16, p. 108-145.

Reitner, J., Arp, G., Thiel, V., Gautret, P., Galling, U., and Michaelis, W., 1997, Organic matter in Great Salt Lake ooids (Utah, USA) - First approach to a formation via organic matrices, *in*, Neuweiler, F., Reitner, J., and Monty,C., editors, Biosedimentology of Microbial Buildups - International Geologic Conference Proceedings Project No.380 - Proceedings of 2nd Meeting, 1996: Facies, v. 36, p. 210-219.

Sandberg, P.A., 1975, New interpretations of Great Salt Lake ooids and of ancient non-skeletal carbonate mineralogy: Sedimentology, v. 22, p. 497-537.

Seelos, A.G., Oldroyd, J.D., and Alton, D.R., 1975, Depression structures in unconsolidated sediments of Great Salt Lake, Utah: Utah Geological amd Mineralogical Survey, Utah Geology, v. 2, no. 2, p. 91-102.

Shinn, E.A., 1969, Submarine lithification of Holocene carbonate sediments in the Persian Gulf: Sedimentology, v. 12, p. 109-114.

Shinn, E.A., Ginsburg, R.N., and Lloyd, R.M., 1965, Recent supratidal dolomite from Andros Island, Bahamas, *in* Pray, L.C. and Murray, R.C., editors, Dolomitization and limestone diagenesis: Society of Economic Paleontologists and Mineralogists Special Publication no. 13, p. 112-123.

Spencer, R. J., Eugster, H. P., and Jones, B. F., 1985, Geochemistry of Great Salt Lake, Utah II - Pleistocene-Holocene evolution: Geochimica et Cosmochimica Acta, v. 49, p. 739-747.

Stifel, P.B., 1964, Geology of the Terrace and Hogup Mountains, Box Elder County, Utah: Salt Lake City, University of Utah Ph.D. dissertation, 174 p.

Stifel, P.B., and Stokes, W.L., 1961, Some unusual sedimentary structures along the shores of Great Salt Lake (abstract): Proceedings, Utah Academy of Sciences, Arts, and Letters, v. 38, p. 131.

Taft, W.H., 1968, Yellow Bank, Bahamas: A study of modern marine carbonate lithification (abstract): American Association of Petroleum Geologists Bulletin, v. 52, p. 551.

Taylor, J.C.M. and Illing, L.V., 1969, Holocene intertidal calcium carbonate cementation, Qatar, Persian Gulf: Sedimentology, v. 12, p. 69-107.

THE WATERS SURROUNDING ANTELOPE ISLAND GREAT SALT LAKE, UTAH

by
J. Wallace Gwynn
Utah Geological Survey

ABSTRACT

Antelope Island and its northern and southern causeways to the mainland separate two distinctive and dynamic bodies of water, both part of the Great Salt Lake system. The south causeway from the island to the mainland was constructed in about 1952. The Davis County causeway was constructed in 1969 and rebuilt in 1992 after the 1980s flooding.

The salinity of the south arm fluctuates inversely with lake elevation. At lake elevations below the top elevations of the two causeways, Farmington Bay is isolated and its salinity is less than half that of the south arm. At lake elevations above the tops of the two causeways, Farmington Bay becomes one with the south arm and their salinity is about equal. Density stratification was observed in the south arm in 1966 and existed there until mid-1991 when it disappeared due to diminished heavy, deep return flow brine from the north arm through the Southern Pacific Railroad causeway. The ion ratios of the major ions and cations (sodium, potassium, magnesium, calcium, chloride and sulfate) are about the same in both bodies of water. Farmington Bay acts as a biological treatment lagoon for the plant nutrients nitrogen and phosphorus in the Jordan River. The biota in the two bodies of water are significantly different because of their different salinities. Raw sewage was emptied into Farmington Bay from Salt Lake City for many years prior to the construction of treatment plants during the 1950s to 1960s.

Six mineral-extraction industries presently operate on Great Salt Lake, three each on the south and north arms. Products generated include sodium chloride, magnesium chloride, potassium sulfate, magnesium metal, chlorine gas, and dietary supplements.

From the 1930s to the present, there have been numerous proposals to convert Farmington Bay or the entire east embayment into freshwater bodies through diking between the islands and the mainland. During the 1980s flooding period, diking proposals were aimed at protecting individual entities, such as sewage-treatment plants, or large areas of shoreline from flooding. To date, none of the major proposals has come to fruition, due mainly to high project costs, and environmental and health-issue concerns.

INTRODUCTION

Antelope Island is the largest of the four major islands in the south arm of Great Salt Lake, covering about 23,850 acres (figure 1). It is 15.5 miles in length, trending in a north-south direction, with a maximum width of 4.5 miles. The island's highest peak reaches an elevation of 6,596 feet above mean sea level, or about 2,396 feet above a 4,200-foot nominal lake level (USGS, 1974). To the east of Antelope Island lies Farmington Bay, a shallow body of water having a maximum depth of seven to eight feet at a lake elevation of 4,200 feet. Earth-fill causeways extend from the north and south ends of the island to the mainland; these causeways isolate Farmington Bay from the south arm of Great Salt Lake (GSL). The surface area enclosed by these two dikes, the eastern shore of Antelope Island, and the mainland covers about 76,700 acres. The northern and western shores of Antelope Island border the main south-body arm of GSL, which covers about 550,505 acres, and has a maximum depth of about 32 feet at the 4,200-foot lake elevation (Waddell and Fields, 1977). Numerous Davis County communities lie along the narrow, densely populated strip of land between the east shore of Farmington Bay and the Wasatch Range to the east.

The main body of the south arm, including Farmington and Bear River Bays, receives nearly all of the freshwater inflow to the lake (figure 1). The Bear and Weber Rivers contribute about 79 percent of the total inflow (Arnow and Stephens, 1990) and enter the Ogden Bay portion of the lake, located to the northeast of Antelope Island, and north of Farmington Bay. The Jordan River contributes about 13 percent of the total inflow and empties into the southern end of Farmington Bay. Numerous streams from the Wasatch Range enter the bay along its eastern shore (figure 1) and contribute an additional five percent of the freshwater inflow. Montgomery (1984) summarizes the average annual surface inflows to the lake from 1931 to 1976 and for the wet year of 1983.

The purposes of this paper are to: (1) present the basic chemistry and yearly changes in salinity of the main body of the south arm of the lake, (2) provide a brief history of the two causeways that isolate Farmington Bay and their influence on the enclosed water, (3) recount the history of Farmington Bay as a receptacle for both untreated and treated sewage, (4) summarize the basic chemistry and changes in salinity of Farmington Bay, (5) discuss the south-arm extractive mineral industries, and (6) review the proposals to convert Farmington Bay into a body of freshwater. Discussion of the north arm of Great Salt Lake is minimal.

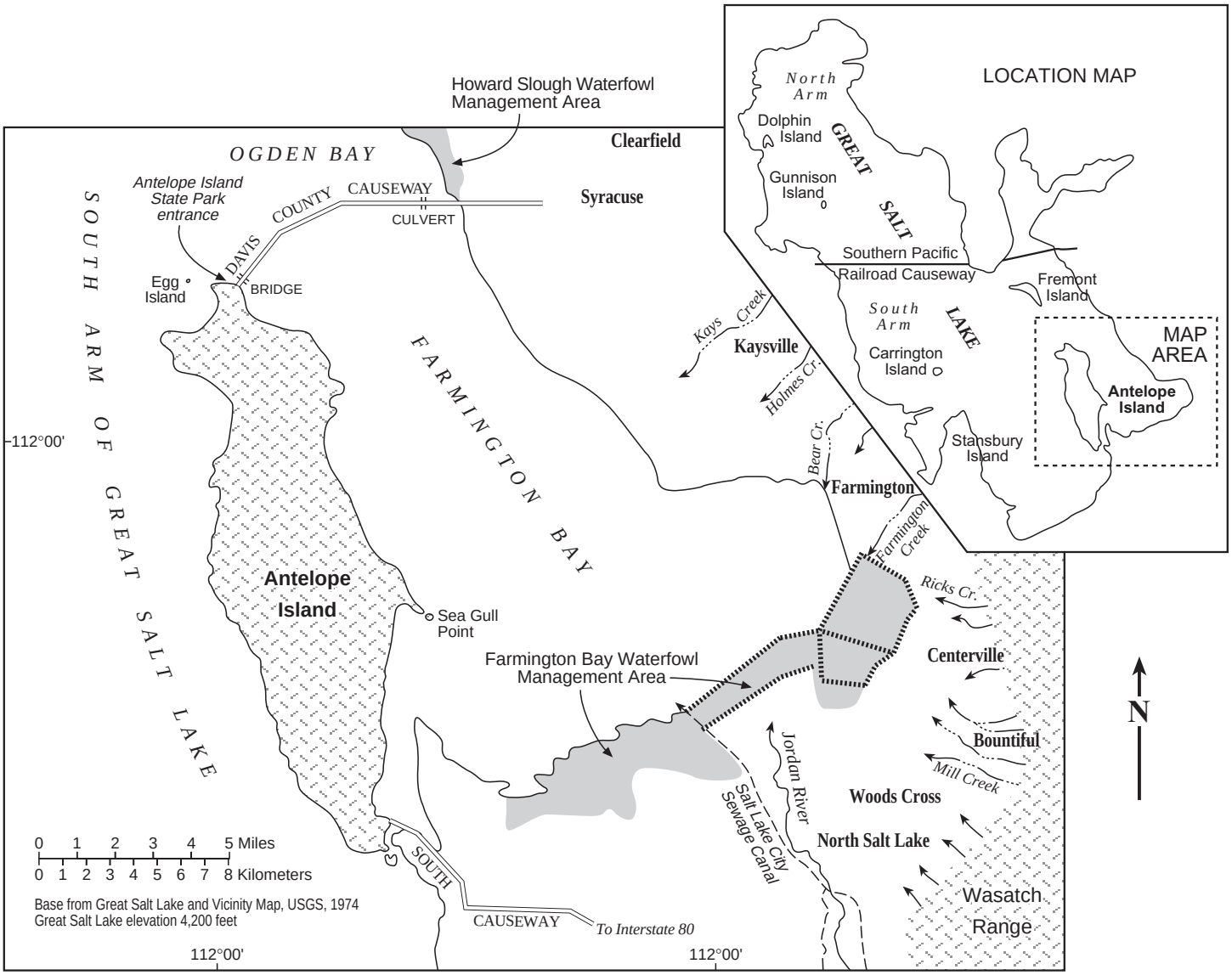

Figure 1. *General location map of Antelope Island, Farmington Bay, the south arm of Great Salt Lake, South and Davis County causeways, and waterfowl management areas.*

SALINITY, STRATIFICATION, AND CHEMISTRY OF THE SOUTH ARM

South-Arm Salinity

Lake Elevation Versus Salinity

Variation of the salinity of the south arm has an inverse relationship with the fluctuation of lake-surface elevation; salinity is lower when the lake elevation is higher. Figure 2 shows how both lake elevation and total dissolve solids (expressed in grams-per-liter g/L) vary annually between 1966 and 1997. During the early 1960s, when the lake was at its historic low (4,191.35 ft), the south-arm waters were nearly eight times saltier than typical ocean waters. During 1987, when the lake was at its historic high (4,211.85 ft), the south-arm waters were only 1.4 times saltier than ocean waters. At a nominal south-arm elevation of 4,200 feet, south-arm waters contain about 130 grams-per-liter (11 to 12 percent salt) and are about 3.3 times as salty as the ocean.

Stratified Brines

In 1966, Utah Geological Survey (UGS) personnel observed, through vertical-density profiling of the water column, the existence of a stratified brine condition in the south arm. A dense, dirty, fetid brine was observed at the bottom of the lake, initially below an elevation of about 4,175 feet, but below an elevation of about 4,180 feet after about 1972. Above this dense brine lay a clean, lighter brine. Figure 3 shows the area underlain by the dense brine at the 4,180-foot top elevation. This deep, dense brine originated from the return flow of heavy north-arm brine that migrated from north to south through the lower portion of the Southern Pacific Railroad (SPRR) causeway which separates the south and north arms of the lake. South-arm stratification continued through the 1980s flooding period until mid-1991 when it disappeared. The disappearance was caused in large measure by the greatly reduced volume of heavy north-arm brine migrating through the SPRR causeway into the depths of the south arm. This was due to a reduction in the causeway's hydraulic conductivity, caused by the addition and compaction of fill

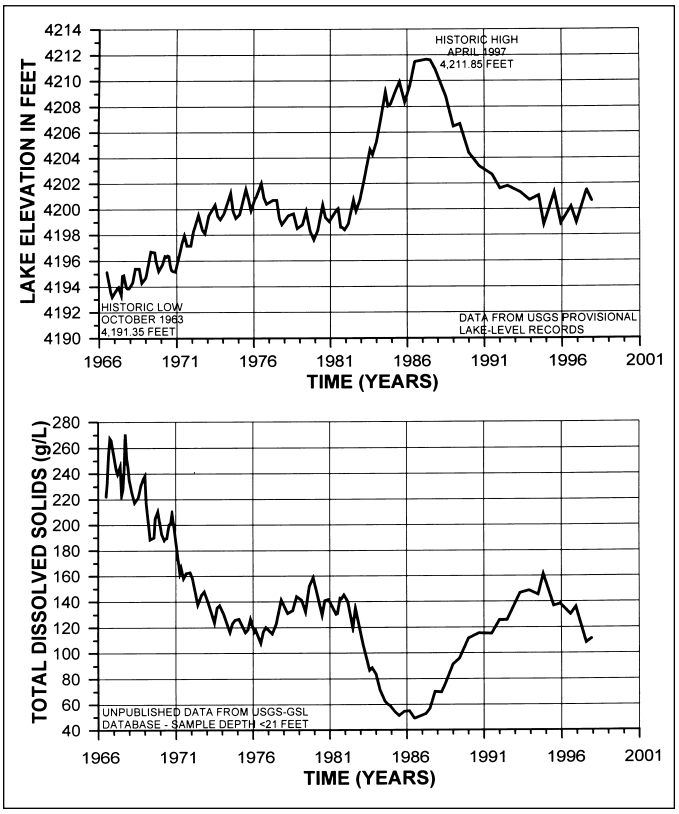

Figure 2. *(Top) Annual variation of the surface elevation of south arm of Great Salt Lake, Utah (1966-1997). (Bottom) Annual variation of the total-dissolved-solids of south arm of Great Salt Lake, Utah (1966-1997).*

material used to raise the tracks six to eight feet during the flooding period (1983 to 1987). Without a sufficient flow of north-arm brine southward, the volume of dense south-arm brine could not be maintained, and stratification disappeared through vertical mixing.

South-Arm Chemistry

While the salinity of the south arm changes with lake-surface elevation, its chemical composition (ion ratios) remains relatively constant. Table 1 shows the composition of the dissolved salts in Great Salt Lake. The composition of the dissolved salts in typical ocean water, and water from the Dead Sea are given for comparison.

Two earth-fill causeways provide access to Antelope Island but also isolate Farmington Bay from the main south arm of Great Salt Lake, especially when the lake's elevation is below the top (4,206 ft) elevations of the two dikes (figure 4). Because of this isolation, the bay's physical, chemical, and biological properties have become different from those of the south arm.

South Causeway

Between 1951 and 1952, the south causeway (figure 5) was built over an existing trail on the mud flats from the south end of Antelope Island eastward to the mainland (Harward, 1996). The work was done as a cooperative project between Davis County and the Island Improvement (Ranching) Company to prevent raw sewage, then being discharged into Farmington Bay, from polluting the southernmost beach-

Table 1. *Chemical composition of dissolved salts from Great Salt Lake, typical ocean, and Dead Sea waters on a dry-weight-percent basis (Gwynn, 1997).*

ION	GREAT SALT LAKE	TYPICAL OCEAN	DEAD SEA
Sodium	32.1	30.8	12.3
Potassium	2.3	1.1	2.3
Magnesium	3.7	3.7	12.8
Calcium	0.3	1.2	5.2
Chloride	54.0	55.5	67.1
Sulfate	7.6	7.7	0.1
Totals	100.0	100.0	99.8

es of the south arm (R. Harward, island resident, verbal communication, September 1997). The causeway also provided southern access to the island. Starting in 1978, a conveyor-belt route was constructed by the S.J. Groves Construction Company to move fill material from the island to the mainland for freeway construction. The conveyor belt was built atop the existing causeway southeastward from the island for a distance of about 3 miles. The present top elevation of the causeway is estimated to range from 4,205 (Clinton Baty, Great Salt Lake State Park harbor master, verbal communication, October 1997) to 4,206 feet (Tim Smith, Antelope Island State Park manager, verbal communication, August 1997). An elevation marker (USGS, 1972) on the causeway shows an elevation of 4,205 feet. Thus, when the lake-surface elevation is below about 4,205 to 4,206 feet, Farmington Bay is separated from the main body of the south arm at the southern end; when the lake elevation is above this elevation, there is some mixing of south arm and Farmington Bay waters.

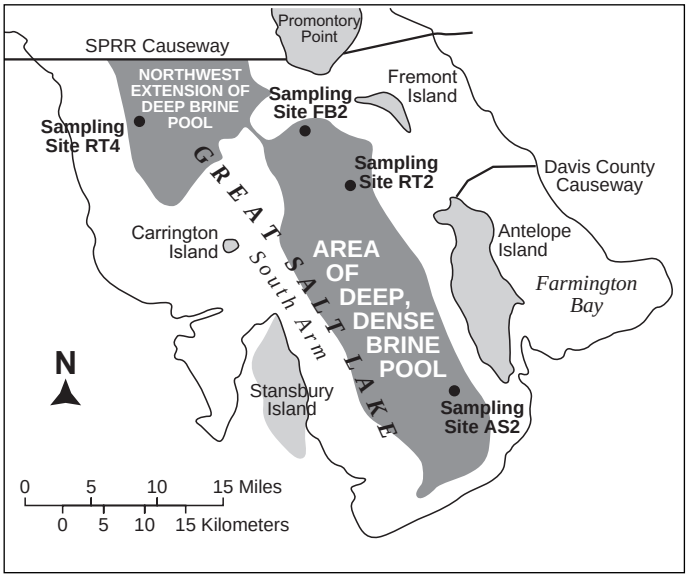

Figure 3. *South arm of Great Salt Lake showing the main and northwestern areas of the pre-1992 deep, dense brine pool.*

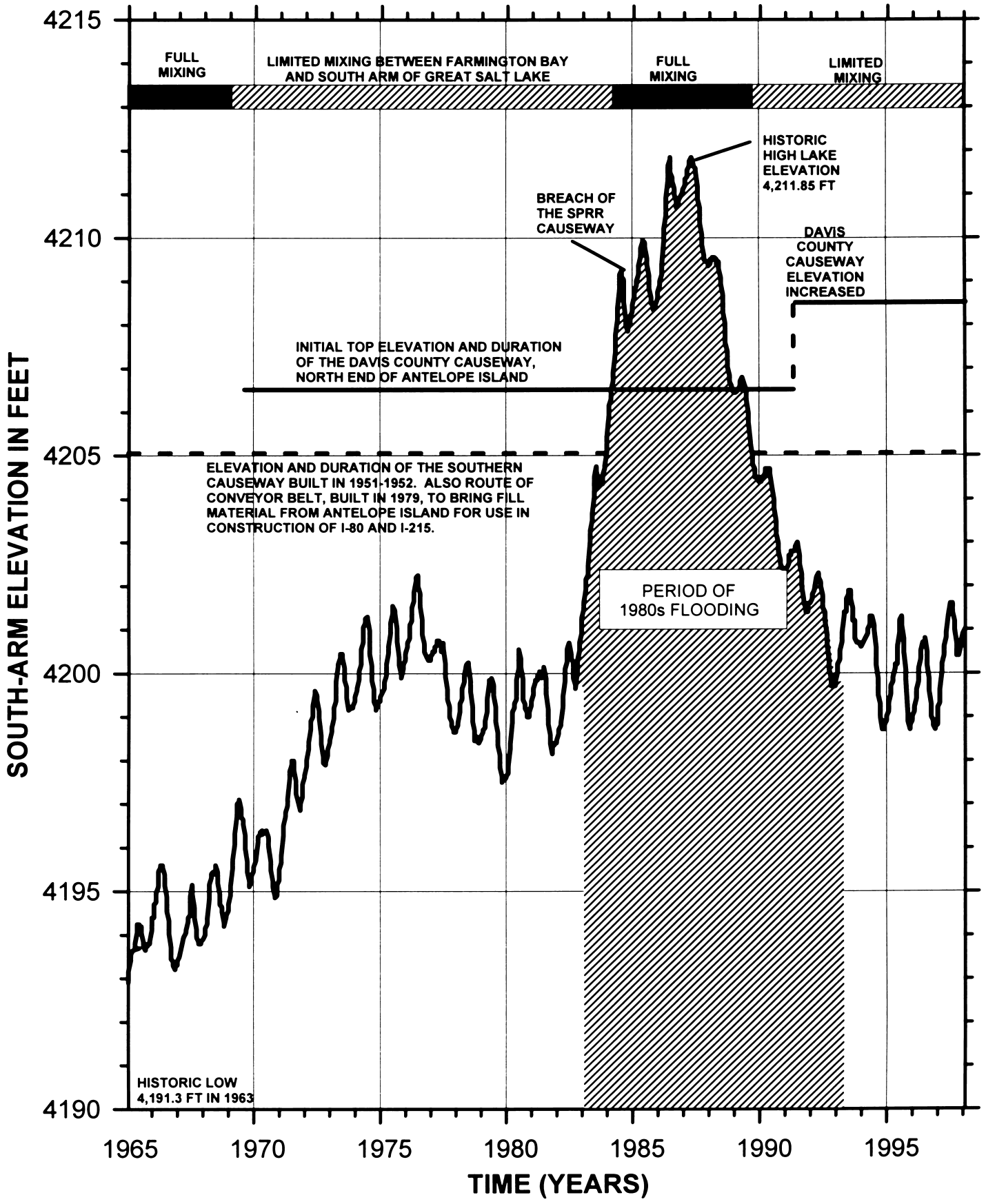

Figure 4. *Top elevations of the Davis County and south causeways, and the periods of full and limited mixing between Farmington Bay and south arm waters of Great Salt Lake, Utah.*

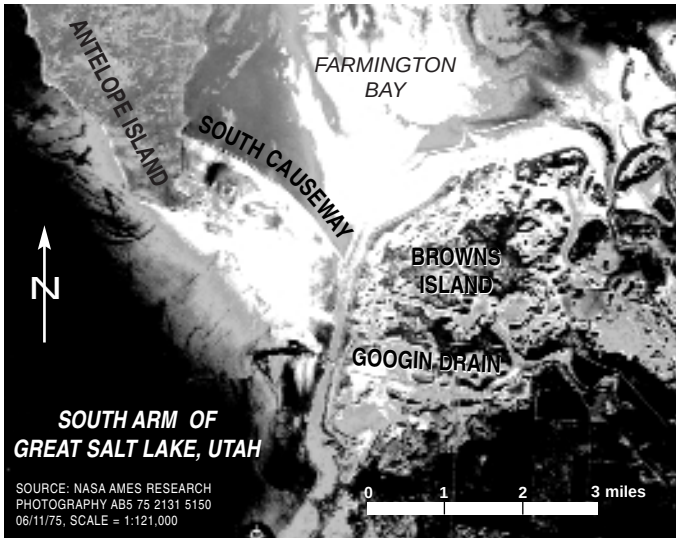

Figure 5. *Aerial photograph of Davis County causeway between the north end of Antelope Island eastward to the mainland.*

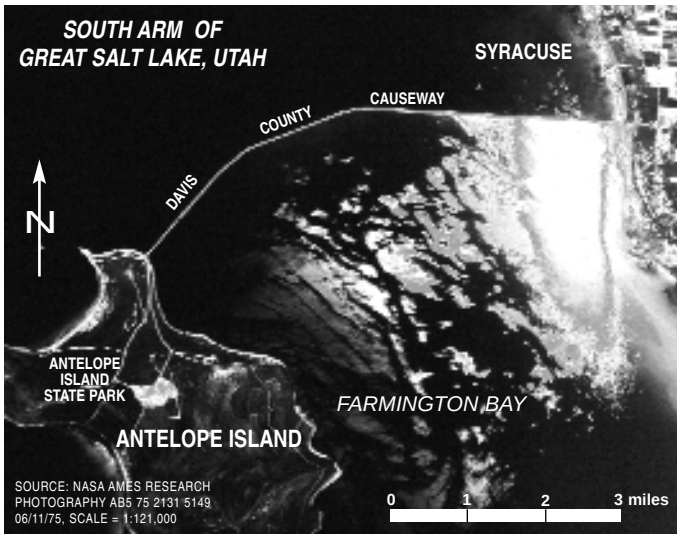

Figure 6. *Aerial photograph showing the Davis County causeway that extends between the north end of Antelope Island and the mainland.*

Davis County Causeway

Prior to 1969, there was no northern causeway separating Farmington Bay and the main body of the south arm, thus allowing the free movement and mixing of water between the two areas. During 1969, an earth-fill causeway was constructed by Davis County and the Utah Department of Transportation from the east shore of the lake, near Syracuse, westward to the northern end of Antelope Island (figure 6). The causeway separated Farmington Bay from the south arm proper and restricted mixing between the two areas except for flow through one narrow bridged opening, consisting of 10 precast box-culvert-type sections bolted together. The original top elevation of the northern causeway was about 4,206.5 feet (Smith, 1997).

In early 1984, the Davis County causeway was flooded when the lake surface rose from about 4,200 feet in elevation (1983) to its historic high of 4,211.85 feet (1986-1987); it remained submerged until mid-1989 when the lake receded below 4,206.5 feet. During that time, it is assumed that the waters of the south arm and Farmington Bay were free to mix; and that mixing was probably the greatest when the lake level was at its higher elevations. After 1989, when the lake level had receded, mixing again became restricted. In 1992, the causeway was rebuilt, through the combined efforts of the Utah Department of Transportation and Davis County, to an elevation of 4,208.5 feet along the eastern portion of the causeway (Saunders, 1994, and Saunders and Smith, 1994). During the same year, a new bridge was built near Antelope Island at the west end of the causeway. The bridge has a concrete deck supported by five 100-foot-long steel girders with a deck elevation of 4,213.5 feet. The road from the bridge west to the island has a top elevation of about 4209.85 feet. For additional control of the waters between Farmington Bay and the main body of the south arm, a box culvert was constructed about one mile from the east end of the causeway. This structure consists of two 10- by 15-foot box culvert sections laid side by side.

FLOW OF RAW AND TREATED SEWAGE INTO FARMINGTON BAY

From the time that the first sewers were installed in Salt Lake City (time uncertain) until the construction of sewage treatment plants in the 1950s and 1960s (figure 7), Farmington Bay was the recipient of Salt Lake City's raw sewage. Today, with rare exception, only treated effluent from sewage treatment plants servicing Salt Lake County and Davis County currently enters the bay. Under emergency conditions, individual sewage treatment plants are authorized by the Utah Division of Water Quality (UDWQ) to temporarily discharge raw sewage to the Jordan River or into Farmington Bay (Arne Hultquist, UDWQ, verbal communication, 1997).

Numerous investigators have studied the water quality and pollution of Farmington Bay caused by the introduction of both untreated and treated sewage. These include studies by: the Utah Department of Health and Davis County Health Department (1965), Bott and Shipman (1971), Carter and Hoagland (1971), Colburn and Eckhoff (1972), Searle (1976), Ford Chemical Laboratory (1977), Maxell and Thatcher (1980), Sturm (1983), Israelsen and others (1985), Chadwick and others (1986), and Sorensen and Riley (1988). Studies by these investigators include: types and distribution of pollutants in both water and sediments; types, distribution and survival of bacteria; water chemistry and water quality including the presence and distribution of heavy metals, nutrients and organics; odor-causing mechanisms; health and safety issues; and pollution-control measures.

SALINITY, STRATIFICATION, AND WATER CHEMISTRY OF FARMINGTON BAY

Farmington Bay Salinity

Salinity Changes Related to Lake Elevation

The overall salinity of Farmington Bay is affected by lake level, much like the south arm of the lake; as the lake

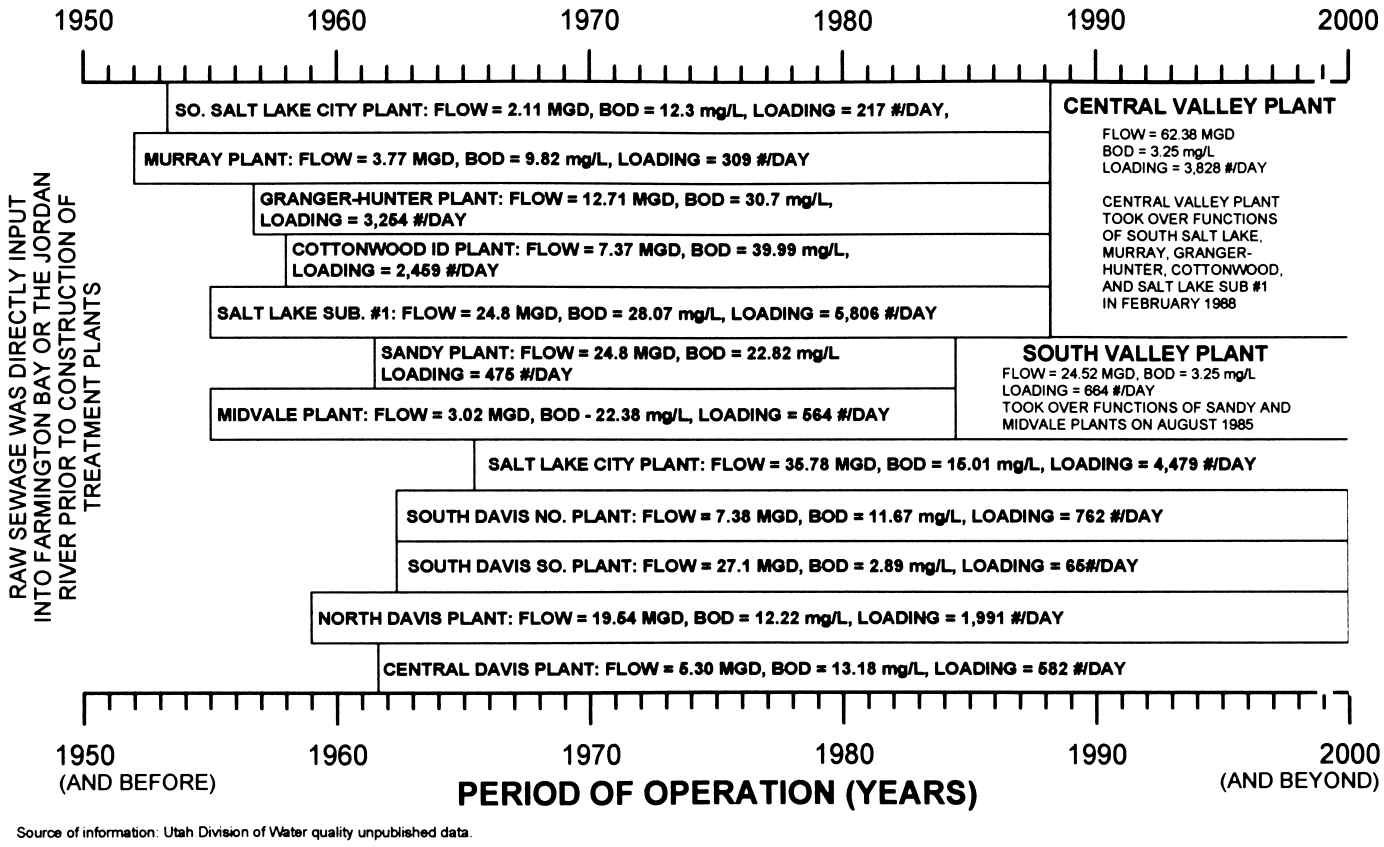

Figure 7. *Periods of operation, flow, BOD and loading, for individual sewage treatment plants in Salt Lake and Davis Counties which empty treated-sewage effluent into the Jordan River or directly into Farmington Bay.*

rises, salinity drops. Salinity is also influenced by the lake's elevation relative to the 4,205- to 4,206-foot top-elevation range of the south and Davis County causeways. Below this elevation range, Farmington Bay is isolated from the main south arm of the lake by the two causeways, with the exception of low-volume, bi-directional flow through the opening(s) in the Davis County causeway. Bi-directional flow is the phenomena of two brines of differing densities flowing in opposite directions through the same opening. Averaged water-quality data from Bott and Shipman (1971), Maxell and Thatcher (1980), Hansen (1981), and the Utah Division of Water Quality (1994-1996) suggest that, at lake elevations below 4,205 feet, the salinity of Farmington Bay is about half that of the south arm. Above the 4,205 to 4,206-foot elevation range, there is direct communication between Farmington Bay and the south arm which allows increased mixing as the lake rises. Under these sustained conditions, data from Sorensen and Riley (1988) suggest that the salinities of the south arm and Farmington Bay become the same.

South-to-North Salinity Gradient

When the water of Farmington Bay is isolated from the south arm, a salinity gradient exists which increases from south to north within the bay (Utah Department of Health and Davis County Health Department, 1965; Bott and Shipman, 1971; Maxell and Thatcher, 1980). This gradient is thought to be attributable to two factors: (1) fresh water enters the bay at the south end, mixing with the resident salty water. As the mixed water moves towards the openings in the Davis County causeway, water is removed at the surface by evaporation causing it to be come saltier; and (2) the upper portion of Farmington Bay water probably increases in salinity as it mixes with the underlying tongue of higher-density brine (discussed below) that extends into the bay from the bridged opening in the Davis County causeway.

Farmington Bay Stratification and Bi-Directional Flow

Stratification

Bott and Shipman (1971), and Sturm (1983) documented the existence of brine stratification in Farmington Bay, consisting of a layer of dense brine at the lake's bottom overlain by a layer of less-dense brine. The source of the dense brine was the north-to-south underflow of heavier south-arm water through the bridged opening in the Davis County causeway. Bott and Shipman's (1971) data suggest that the interface between the two layers of brine within Farmington Bay was about 5 feet deep during June 1971; Sturm's (1983) data suggest the interface depth was between 5 and 6 feet deep during July 1981.

Bi-Directional Flow

Bi-directional flow exists at the Davis County causeway, and is discussed by Carter and Hoagland (1971), Colburn and Eckhoff (1972), Hansen (1981), and Sturm (1983). The north-to-south flow of denser south-arm brine through the Davis County causeway bridge is driven by hydrostatic pressure, while the south-to-north flows of overlying lighter water through this opening are driven by the existing hydrostatic head. Sturm (1983) shows that the depth to the bi-directional-flow interface within the bridged opening, during 1982 measurements, fluctuated between 4.75 feet and 6.25 feet under calm conditions. Under south-wind conditions, the depth to the interface became much deeper (8 to 10 feet), and the upper, south-to-north flows greatly increased. Under north-wind conditions, the depth to the interface diminished, sometimes to nothing, and the deep, north-to-south flows increased.

Farmington Bay Chemistry and Nutrients

(Nutrient section contributed by Doyle Stephens, USGS, 1997)

A comparison of a limited number of chemical analyses from Farmington Bay, mainly from the north end near the Davis County bridge, to analyses from the main south arm of the lake (figure 8), shows that there is no significant difference between the major-ion ratios within the two bodies of water. This is because the main source of salt for Farmington Bay comes from the south arm as return flow through the bridged opening.

Farmington Bay acts as a biological treatment lagoon for the plant nutrients nitrogen and phosphorus in the Jordan River. Typically, the Jordan River caries 3-4 mg/L of dissolved nitrogen (as nitrate and ammonium) and 1-2 mg/L of dissolved phosphorus into Farmington Bay. Most of these dissolved nutrients are removed from the water by algae, aquatic macrophytes, and bacteria within Farmington Bay. Between January and August 1997, sampling in Farmington Bay by the USGS at a site 5 miles south of the Davis County causeway found dissolved nitrate nitrogen always less than the reporting level (detection limit) of 0.05 mg/L, dissolved ammonia less than 0.02 mg/L, and total dissolved phosphorus less than 0.3 mg/L. Throughout the summer of 1997, there were massive blooms of green algae and cyanobacteria (blue-green “algae”). Salinity, at 1-meter depth, ranged from 3.8 percent in January to 6 percent in August.

South Arm and Farmington Bay Biota

(Section contributed by Don Paul,
Utah Division of Wildlife Resources, 1997)

Great Salt Lake (GSL) biology varies between locations that have different salinities. Antelope Island and its causeways divide two locations of differing salinities, namely, Farmington Bay and the south arm of the lake (figure 1). The balance between inflow to, and evaporation from, the lake coupled with the terminal (no outlet) nature of the GSL cause frequent shifts in lake elevation and salinity and, consequently, the biology of various isolated lake locations.

Living organisms have difficulty coping with the osmotic stress of high concentrations of salt ions; only a few are successful. However, even with high salt concentrations, different ecological systems can exist side by side where these salinities are locally variable. An excellent example of such local variation is the south arm of GSL and Farmington Bay which are separated by the Davis County causeway, as described in the following examples. During May 1996, GSL elevation was 4,200.7 feet and the salinity of the south arm was 12.2 percent, whereas the salinity of Farmington Bay was 5.6 percent (Doyle Stephens, USGS, personal communication, November, 1997).

The south arm fosters a relatively simple system of some 20 species of algae and 10 species of protozoa when the salinities are at 115 g/L (Rushforth and Felix, 1982). Four macro invertebrates coexist with these microscopic species. These macro invertebrates include two species of brine flies which typically inhabit the area along the shoreline, small numbers of a corixid, and a species of brine shrimp that occupies the entire reach of the south arm. The constant shifting of the GSL elevation and shoreline fosters macro invertebrates that are reproductively flexible and seasonally abundant, that is, brine flies and brine shrimp. At salinities above 115 g/L the south arm ecosystem is relatively predator free and the brine shrimp and fly populations go unchecked, increasing within the limits of the algae production, which seems to be nitrogen limited. The brine shrimp species in GSL, *Artemia fransiscana*, is an effective filter-feeder capable of reducing the algae in the south arm water column by mid-summer to an extent that the shrimp become food-stressed.

In contrast to 1997 salinity conditions, the high-lake-level conditions during the 1980s significantly reduced the salinity to 50 g/L in the south arm. At that time, the south-arm biology was similar to that of the current (1997) Farmington Bay condition. These diluted conditions effectively reduced brine shrimp production and densities enough that both the avian species and the brine shrimp harvest industry, reliant on the *Artemia* resource, were nonplused in their activities in the south arm. Insect predation (corixids), on what few brine shrimp were produced, was significant in nearshore areas, especially around underwater structures. The ecology became more complex with dilution, shifting away from a brine shrimp- and brine fly-dominated system to a more competitive ecosystem in the south arm. North of the Southern Pacific Railroad causeway, conditions improved for some brine shrimp production as salinities fell below 20% and consequently there was a limited brine shrimp harvest and some Eared Grebe and Wilson’s phalarope use of the macro invertebrates in that region of the lake during high lake years. Bird-use estimates were considerably lower during these years for species keying on summer and fall populations of brine shrimp and flies at Great Salt Lake.

Farmington Bay, with its lower salinities, supports a larger number of species and a more complex interaction between trophic (nutrient) levels with many more checks and balances. The predacious corixid *Trichocoixa verticalis* is a flighted insect that is known to prey on brine shrimp, especially the smaller *nauplii* and sub-adults. This predator flourishes in lower salinities of 50 g/L. At these salinities, *T. verticalis* mean densities were 52 individuals/m^3 (Wurtsbaugh, 1992). In Farmington Bay during April 1997, *T. verticalis* individuals numbered 100/m^3 (Doyle Stephens, USGS, verbal l communication, 1997). Subsequently, the population of *Artemia*

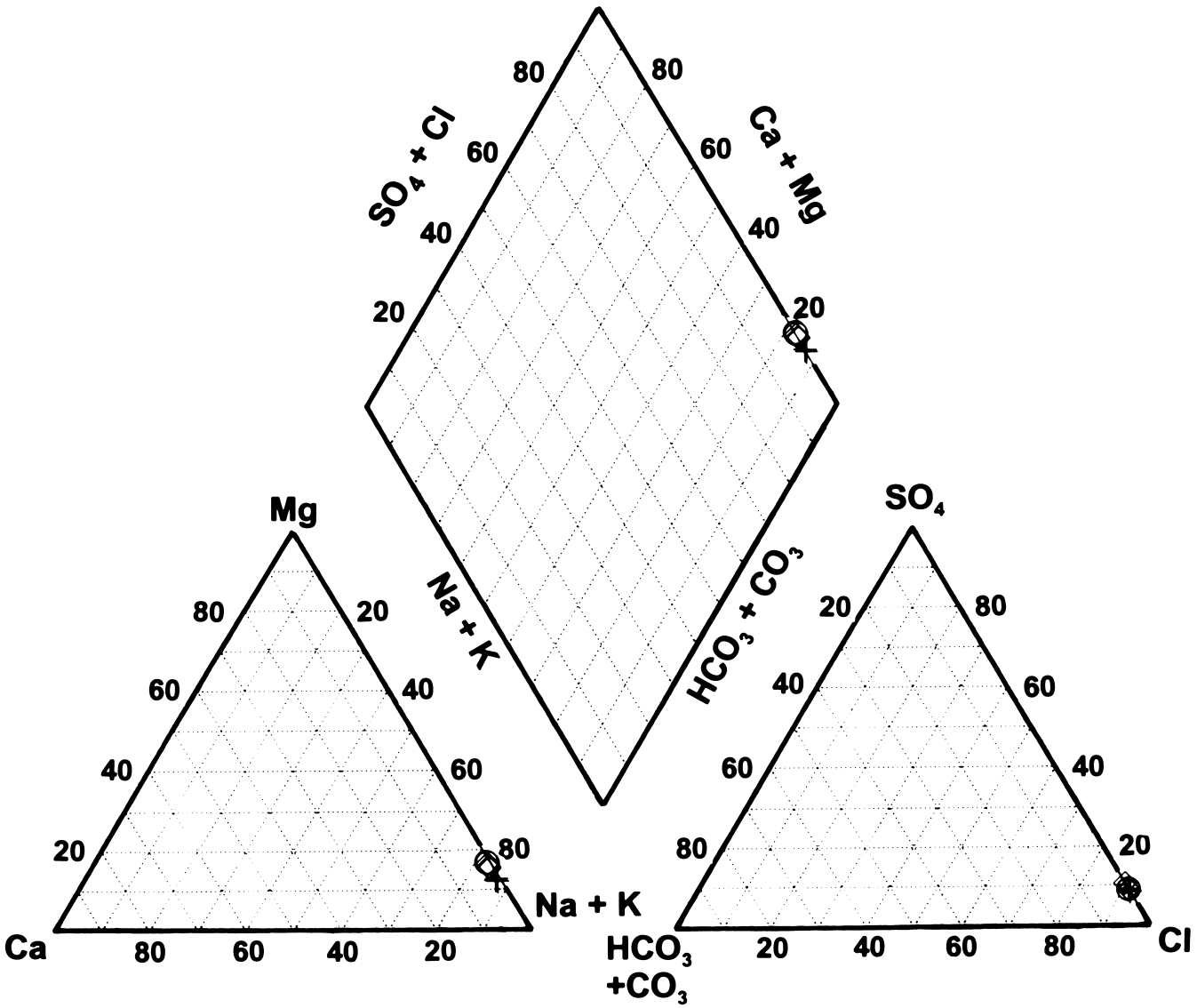

EXPLANATION

DIAMONDS (Sample analyses from Utah Department of Health, unpublished

Average of 8 samples from Farmington Bay, 100 feet south of the Antelope-Syracuse causeway, 1977-1978.

Average of 59 samples from Farmington Bay, at the Antelope-Syracuse causeway bridge (south side), 1980-1982.

Average of 6 samples from Farmington Bay, in the main deep channel, 1977-1978.

Average of 8 samples from Farmington Bay, NE of Seagull Point, 1977-1978

CROSSES (Samples analyses from UGS-GSL database, unpublished)

Average of 2 samples from Farmington Bay, south of Antelope-Syracuse bridge, 0.5 foot depth, 1976-1977.

Average of 2 samples from Farmington Bay, south of Antelope-Syracuse bridge, 15 foot depth, 1976-1977.

Average of 2 samples from Farmington Bay, south of Antelope-Syracuse bridge, 25 foot depth, 1976-1977.

CIRCLES (Sample analyses from UGS-GSL database, unpublished)

Average of 48 samples from South Arm, sites AS2/FB2, 0.5 foot depth, 1977-1983.

Average of 48 samples from South Arm, sites AS2/FB2, 15 foot depth, 1977-1983.

Average of 48 samples from South Arm, sites AS2/FB2, 25 foot depth, 1977-1983.

Figure 8. *Trilinear plot showing chemical compositions of waters from Farmington Bay and the south arm of Great Salt Lake.*

in Farmington Bay was suppressed by predation. In addition, predation by other macro invertebrates and zooplankton in the Farmington Bay complex ties up much of the available invertebrate food resources in the water column.

When the south arm is at 115 g/L salinity and the system is brine-fly and brine-shrimp dominated, these invertebrates are released to the next trophic level and predatory opportunists, the birds. Significant numbers of some species and suites of species of birds depend upon these macro-halofiles (invertebrates). The Great Salt Lake was designated a Hemispheric Shorebird Reserve by the Western Hemispheric Shorebird Reserve Network in 1990 because it supports millions of shorebirds. These shorebird numbers are supported by significant wetland resources located on the east side of the lake, including Farmington Bay Wildlife Management area (figure 1), and by the copious halophiles of the Great Salt Lake. Besides the recognition for shorebird populations, the Great Salt Lake ecosystem supports notably high numbers of other species as compared to continental, hemispheric, and world populations. The waters surrounding Antelope Island are often the producers of the food that fuels these birds.

MINERAL EXTRACTION INDUSTRIES

Common salt was extracted from Great Salt Lake by trappers and explorers as early as 1825, and became the principal source of salt for the early Mormon settlers beginning in 1847. Since that time, there have been numerous salt industries on the lake (Clark and Helgren, 1980), mainly along the lake's southern shore. Small operations were also located in Spring Bay on the extreme north end of the lake, at Promontory Point, and on the mud flats west of Syracuse (within the present bounds of Farmington Bay). Today, six active mineral-extraction industries operate on the lake which contribute significantly to the local economies. These companies, the source of their brine (arm of the lake), and the products they produce, are shown in table 2.

Table 2. *Active mineral-extraction industries on Great Salt Lake, Utah (after Gwynn, 1997).*

COMPANY NAME	ARM OF LAKE	PRODUCTS
Magnesium Corporation of America	South	Primary magnesium metal, alloys, and chlorine gas
(MAGCORP) Cargill Salt Company	South	Sodium chloride products
Morton Salt Company	South	Sodium chloride products
IMC Kalium Ogden Corporation	North	Potassium sulfate (fertilizer), magnesium chloride products
IMC Salt	North	Sodium chloride products
North Shore Ltd. Partnership - Mineral Resources International	North	Concentrated brines that are processed into dietary supplements

CHRONOLOGY OF DIKING STUDIES AND PROPOSALS RELATED TO THE SOUTH ARM OF GREAT SALT LAKE

Studies, and Early Proposals for Freshwater Embayments (1930-1965)

Numerous proposals have been put forth over the years to create freshwater bodies out of the entire east embayment (the general area east and north of Antelope and Fremont Islands), or out of Farmington Bay, through the construction of dikes between the islands and the mainland. Richards (1965, 1972) reviews the past studies of the east embayment as a freshwater reservoir, none of which have been implemented. The chronology and a short description of these studies up to 1972 are summarized in appendix A and illustrated in figure 9.

Flooding Years (1983-1987)

Lake-Level Control Alternatives

In water year 1983, Great Salt Lake began its historic rise from a low elevation of about 4,200 feet to its historic high of 4,211.85 feet in 1986-1987. As the lake rose, extensive flooding occurred around the lake, causing many millions of dollars in damage, mainly around the south arm. During this time, several lake-level control measures were investigated, including upstream development, breaching the SPRR causeway, West Desert pumping, and diking (Allen and others, 1983; and Utah Division of Water Resources, 1984). Of these alternatives, the SPRR causeway breach was constructed in 1984, and West Desert pumping was implemented in 1987.

Diking Alternatives

Diking alternatives were proposed during the flooding years (1983-1987) mainly to protect large areas around the perimeter of the lake or to protect individual entities such as sewage-treatment plants. A number of these proposals included the construction of dikes between Antelope Island and the mainland, or between Antelope and Fremont Islands and the mainland. The major diking alternative proposals presented during the flooding years include: Creamer and others (1985), Holland and Spiers (1985), Chadwick and others (1986), Rollins and others (1987), and Sorensen and Riley (1988). The lake began to drop after 1987, and none of the above-listed diking schemes was implemented.

Some dikes were constructed within or in proximity to Farmington Bay (Anderson, 1985). For example, a dike around the South Davis North Wastewater Treatment Plant was built during 1985 and 1986. Two sections of dike were constructed through the eastern part of Farmington Bay west of Farmington and Centerville by Utah Power and Light Company during late 1984 and early 1985. These dikes were constructed to protect power-transmission towers from ice loading. Phillips Petroleum also raised the dikes around its wastewater holding ponds west of Bountiful.

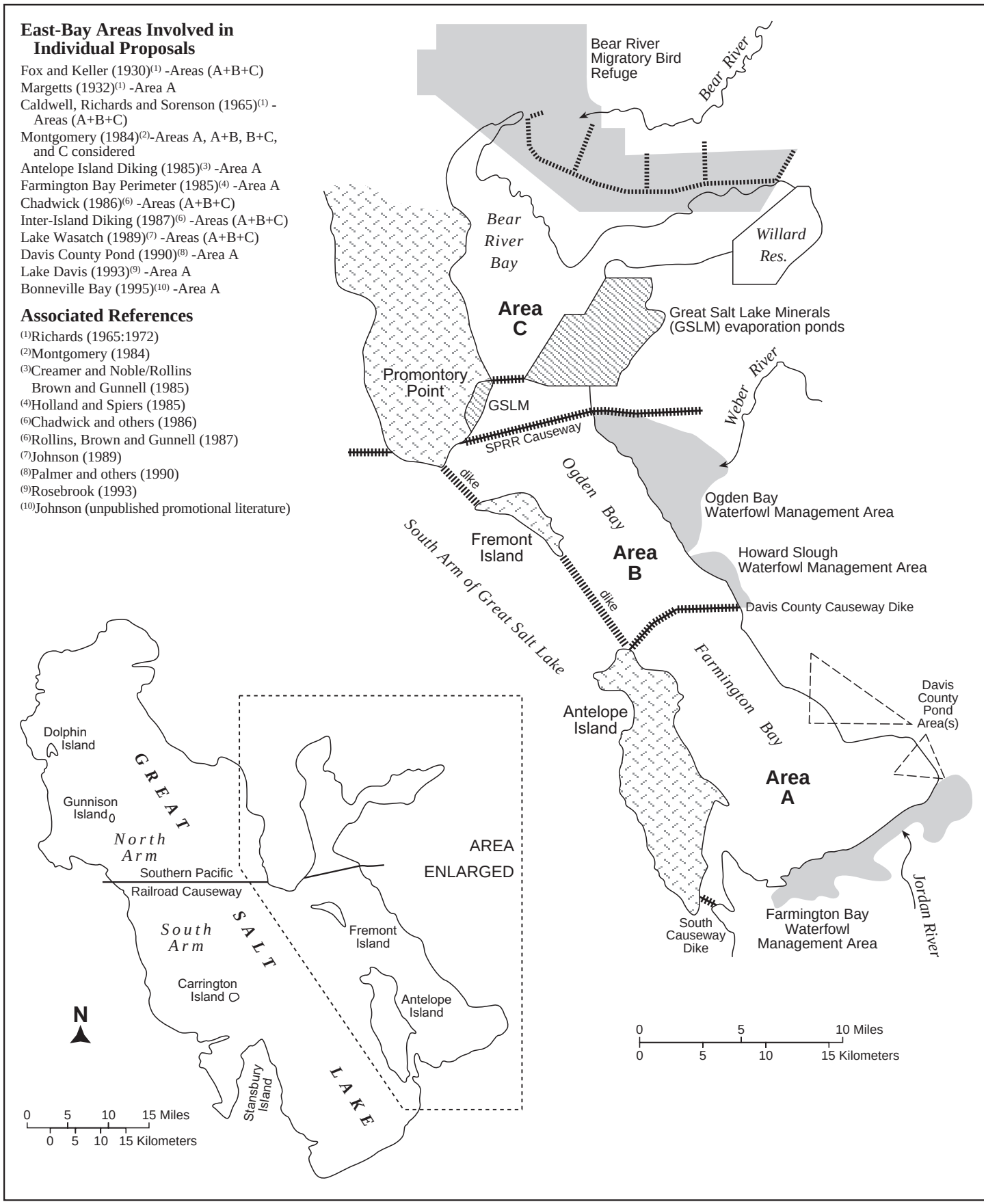

Figure 9. *Areas of east embayment involved in the various proposed diking schemes to create freshwater bodies, and the location of proposed dikes, solar-evaporation-pond areas, and waterfowl-management areas.*

Post-Flooding Years (1987-present)

After the flooding years, attention was again returned to the creation of freshwater impoundments, within Farmington Bay or the entire east bay, through various diking schemes. The first of these was proposed in 1989 by the Lake Wasatch Coalition (Johnson, 1989). The proposed freshwater Lake Wasatch would have been formed through diking from the south shore of the lake to the south tip of Antelope Island, from the north end of Antelope Island to the south tip of Fremont Island, and from the north end of Fremont Island to Promontory Point (figure 9). This proposal failed because of the high construction costs and concern about disrupting the GSL ecosystem (Woolf, 1993).

Also in 1989, The Utah Legislature, through the "Great Salt Lake Development Authority Act" (Smedley and others, 1989), formed the Great Salt Lake Development Authority (GSLDA) to investigate the technical, economic, and environmental feasibility of an inter-island diking project that would create the freshwater Lake Wasatch in the eastern half of Great Salt Lake. The recommendations of the GSLDA (Great Salt Lake Development, 1990) were as follows:

(1) Development of "Lake Wasatch" through a Great Salt Lake inter-island diking project, as defined in Utah Code Ann. §17A-2-1603 (9), does not appear to be economically or environmentally feasible.

(2) Proposals to create small freshwater lake or water storage reservoir in Farmington Bay deserve further study.

(3) Public access to Antelope Island should be restored as quickly as possible.

In mid-1990, a preliminary design report was issued by the Utah Division of Water Resources (Palmer and others, 1990) for a diked water impoundment, called the Davis County Pond, as part of the Bear River Development Project. The purpose of the work was to study, test, and recommend an area or areas for final pond design. Two recommended areas were: (1) the eastern end of Farmington Bay from the Farmington Bay Waterfowl Management area on the south to Shepards Lane on the north, and (2) a triangular area along the northeastern shore of Farmington Bay, bounded on the south by a western extension of Shepards Lane and on the west by a southerly extension of 1,000 West street in Syracuse (figure 9).

In January 1993, Davis Lake (figure 9) was proposed by the Davis County Commission (Rosebrook, 1993). This proposed project, a scaled-down version of Lake Wasatch, would have converted Farmington Bay into a freshwater body by using the existing dikes at both the north and south ends of Antelope Island.

In early 1995 (pre-February), the Bonneville Bay proposal emerged, which called for the creation of a freshwater reservoir similar to Davis Lake (figure 9). The unique feature put forth in this proposal was the use of new technology, the "Wasatch Wall Pile Dike System," developed by Don D. Johnson in 1985, (promotional literature) in the construction of both the north and south dikes.

To date, none of the proposals to change either Farmington Bay or the entire east embayment into freshwater reservoirs has come to fruition. In spite of the many advantages cited by the proponents of these projects, questions related to sediment pollution, health hazards, eutrophication potential, wastewater-treatment plant costs, water salinity, mosquito production potential, and flooding issues (Chadwick and others, 1986; Sorensen and Riley, 1988; Stauffer and Austin, 1995) remain understudied and unanswered.

REFERENCES

Allen, M.E., Christensen, R.K., and Riley, J.P., 1983, Some lake level control alternatives for the Great Salt Lake: Utah Water Research Laboratory, Utah State University, Water Resources Planning Series UWRL/P-83/01, 101 p.

Anderson, D.L., 1985, Executive summaries - Great Salt Lake studies: Utah Department of Natural Resources, Division of Water Resources, 47 p.

Arnow, Ted, and Stephens, Doyle, 1990, Hydrologic characteristics of the Great Salt Lake, Utah- 1847-1986: U.S. Geological Survey Water-Supply Paper 2332, 32 p.

Bott, Cordell, and Shipman, S.T., 1971, Water chemistry and water quality of Farmington Bay, *in* Carter, C.K., project director, Some ecological considerations of Farmington Bay and adjacent Great Salt Lake State Park: University of Utah, p. B1-B27.

Carter, James, and Hoagland, Timothy, 1971, Geological and hydrological characteristics of Farmington Bay, *in* Carter, C.K., project director, Some ecological considerations of Farmington Bay and adjacent Great Salt Lake State Park: Salt Lake City, University of Utah, p. A1-A-27.

Chadwick, D.G., Jr., Riley, J.P., Seierstad, A.J., Sorensen, D.L., and Stauffer, N.E., Jr., 1986, Expected effects of in-lake dikes on water levels and quality in the Farmington Bay and the east shore areas of the Great Salt Lake, Utah: Utah Water Research Laboratory, Utah State University, 91 p.

Clark, J.L., and Helgren, Norman, 1980, History and technology of salt production from Great Salt Lake, *in* Gwynn, J.W., editor, Great Salt Lake - a scientific, historical and economic overview: Utah Geological and Mineral Survey Bulletin 116, p. 203-217.

Colburn, A.A., and Eckhoff, D.W., 1972, Pollution input from the lower Jordan Basin to Antelope Island Estuary, *in* Falkenborg, Donna, editor, The Great Salt Lake and Utah's water resources: Proceedings of the first annual conference of the Utah Section of the American Water Resources Association, Salt Lake City, Utah, November 30, 1972, p. 104-120.

Creamer & Noble Engineers, and Rollins, Brown & Gunnel, Inc., 1985, Final design report for Great Salt Lake-Antelope Island diking, executive summary: Unpublished consultants report, prepared for the Utah Department of Transportation, pp. I1-I24.

Ford Chemical Laboratory, 1977, An investigation of bacteria concentrations in specific areas of the Great Salt Lake: Ford Chemical Laboratory, Unpublished report prepared for Utah State Division of Health, Department of Social Services, 30 p.

Great Salt Lake Development Authority, 1990, Report of the

Great Salt Lake Development Authority to Governor Norman Mangerter, Senator Arnold Christensen, and Representative Craig Moody: Great Salt Lake Development Authority Board of Directors (December 10), 5 p.

Gwynn, J.W., 1997, Brine properties, mineral extraction industries, and salt load of Great Salt Lake, Utah: Utah Geological Survey Public Information Series 51, 2 p.

Hansen, D.E., 1981, A hydrologic model to determine water quality management of the Farmington Bay and Farmington Bay bird refuge: Logan, Utah State University, M.S. thesis, 67 p.

Harward, M.R., 1996, Where the buffalo roam - life on Antelope Island: M.R. Harward, 382 W. 3300 S., Bountiful, Utah 84010, 87 p.

Holland, F.L., and Spiers, K.L.,1985, Farmington Bay area perimeter diking alternative - final design report, executive summary: James M. Montgomery Consulting Engineers, Inc. published report prepared for the Utah Division of Water Resources, Utah Department of Natural Resources, 15 p.

Israelsen, C.E., Sorensen, D.L., Seierstad, A.J., and Brennard, Charlotte, 1985, Preliminary identification, analysis, and classification of odor-causing mechanisms influence by decreasing salinity of the Great Salt Lake: Utah Water Research Laboratory, Utah State University, prepared for the Utah Department of Natural Resources, Utah Division of Water Resources, 63 p.

Johnson, D.D., 1989, Lake Wasatch - the great freshwater lake: 1071 E. 250 N., Bountiful, Utah , 97 p. (unpublished collection of promotional information packets on Lake Wasatch).

Maxell, M.H., and Thatcher, L.M., 1980, Coliform bacteria concentrations in Great Salt Lake waters, *in* Gwynn, J.W., editor, Great Salt Lake - a scientific, historical and economic overview: Utah Geological and Mineral Survey Bulletin 116, p. 323-335.

Montgomery, J.M., 1984, Great Salt Lake diking feasibility study - volume I: James M. Montgomery, Consulting Engineers, Inc. unpublished report prepared for Utah Department of Natural Resources, Project No. 1609.003, Utah Division of Water Resources, 293 p.

Palmer, Jim, Leeflang, Bill, Everitt, Ben, and Aubrey, Dan, 1990, Preliminary design report for proposed reservoir in Farmington Bay of the Great Salt Lake: Utah Department of Natural Resources, Utah Division of Water Resources, 125 p.

Richards, A.Z., Jr., 1965, A preliminary master plan for the development of the Great Salt Lake--over a period of the next 75 years: Caldwell, Richards & Sorensen, Inc., unpublished report prepared for the Great Salt Lake Authority, 32 p.

-----1972, Review of past studies of the east embayment as a freshwater reservoir, *in* Falkenborg, Donna, editor, The Great Salt Lake and Utah's water sources: Proceedings of the first annual conference of the Utah Section of the American Water Resources Association, Salt Lake City, Utah, November 30, 1972, p. 180-189.

Rollins, Brown and Gunnell, Inc., and Creamer & Noble Engineers, 1987, Great Salt Lake inter-island diking project: unpublished consultants report, v. 1, section 1, 9 p.

Rosebrook, Don, 1993, Davis has fresh plans for Antelope Island: Deseret News, January 6-7 1993 edition, p (?).

Rushforth, S.R. and Felix, E.A., 1982, Biotic adjustments to changing salinities in the Great Salt Lake, Utah: Microbial Ecology (US), v. 8, p. 157-161.

Saunders, G.E., 1994, Massive spread footing key to causeway reconstruction: Roads & Bridges, August edition, p. 26-27.

Saunders, G.E,. and Smith, S.W., 1994, Causeway reopening benefits people and wildlife: Public Works, February edition, p. 34-36.

Searle, R.T., 1976, The Great Salt Lake: Office of Legislative Research, State of Utah, Research Report No. 7, 274 p.

Smedley, S.M., and Bain, Walt, Burningham, K.R., Woddoups, M.G., and 24 other legislators, 1989, Great Salt Lake Development Authority: 1989 General Session [of the Utah Legislature], H.B. No. 208, 57 p.

Smith, S.W., 1997, Memo from S.W. Smith, Director of Davis County Public Works, to D.R. McConkie, Davis County Commissioner, 1 p.

Sorensen, D.L. and Riley, J.P., 1988, Great Salt Lake inter island diking-water quality considerations, final report: Utah Water Research Laboratory, Utah State University, prepared for Utah Department of Natural Resources, Division of Water Resources, 261 p.

Stauffer, Norm and Austin, Lloyd, 1995, Proposal to convert Farmington Bay into a freshwater bay: Memorandum to D. Larry Anderson, Director of Utah Division of Water Resources, dated July 17, 1995, 4 p.

Sturm, P.A., 1983, Farmington Bay project report: Utah Geological and Mineral Survey Open-File Report 86, 56 p.

U.S. Geological Survey, 1972, Antelope Island South Quadrangle, Utah: U.S. Geological Survey, 7.5 minute series orthophotomap (topographic), scale 1:24,000.

U.S. Geological Survey, 1974, Great Salt Lake and vicinity, Utah: U.S. Geological Survey topographic map, scale 1:125,000.

Utah Division of Water Quality, 1994-1996, unpublished laboratory-analysis reports: Utah Division of Water Quality, Utah Department of Environmental Quality (20 analyses).

Utah State Department of Health and Davis County Health Department, 1965, Preliminary investigation of pollution of Great Salt Lake east of Antelope Island: Utah State Department of Health and Davis County Health Department, unpublished report 13 p.

Waddell, K.M., and Fields, F.K., 1977, Model for evaluating the effects of dikes on the water and salt balance of Great Salt Lake, Utah: Utah Geological and Mineral Survey Water-Resources Bulletin 21, 54 p.

Woolf, Jim, 1993, Davis wants to convert bay into freshwater reservoir: Salt Lake Tribune, January 7, 1993.

Wurtsbaugh, W.A., 1992, Food-web modifications by an

invertebrate predator in the Great Salt Lake (USA): Oecologia., v. 89, p. 168-175.

APPENDIX A

Chronology and description of past studies of the east embayment as a freshwater reservoir (modified from Richards 1965, 1972)

May, 1930: L.E. Fox and T.L. Keller, in a work titled "Putting Great Salt Lake to work," propose a three-part dike extending westerly from the mainland to the south end of Antelope Island, and northerly from the north end of Antelope Island to the south end of Fremont Island, and from the north end of Fremont Island to the Promontory Point (figure 9).

March, 1932: S.G. Margetts, in a work titled "Report on proposed freshwater lake," recommended a smaller freshwater lake be developed in Farmington Bay by damming the 146 square-mile area between the mainland and the south end of Antelope Island and between the north end of Antelope Island and the mainland at Syracuse (figure 9).

June, 1933: R.A. Hart and N.E. McLaughlan, published a work titled "Abstract of report on laboratory tests of feasibility of freshening the proposed diked-off portion of Great Salt Lake."

July, 1933: D.A. Lyon, published a work titled "Report of sub-committee appointed to investigate technical problems that present themselves in connection with the proposed diking of Great Salt Lake for the purpose of creating a body of fresh water."

December, 1933: J.L. Crane, provided a summary report on Great Salt Lake diking project, and concluded that the "smaller reservoir" known as the Farmington Bay Project would be feasible from the standpoint of engineering construction. He recommended that the diking project be undertaken by the State of Utah.

July, 1935: T.C. Adams, reported to the Utah State Planning Board on additional engineering studies that he had been commissioned to make by said board to substantiate certain recommendations of the 1933 Crane report.

1955: The Utah Legislature asked the Utah State Road Commission to initiate a study of the advisability of constructing the inter-island dikes, and particularly to address the availability of water.

1956: Dames & Moore and Caldwell, Richards & Sorensen, Inc, provided a joint report to the Utah State Road Commission on the availability of water.

1957: Caldwell, Richards & Sorensen, Inc. prepared a report for an advisory committee to the State Road Commission titled "An engineering report and opinion on the quantity and quality of water which may become available for use by industry, agriculture and for improved recreation from the east embayment reservoir of Great Salt Lake if the inter-island dikes were to be built."

1963: The Utah State Legislature enacted the "Great Salt Lake Authority," with the responsibility to plan, formulate and execute a program for the development of the mainland, the islands, the minerals, and the water within Great Salt Lake meander line as established by the United States Surveyor General for industrial, recreational, agricultural, industrial, and chemical purposes.

January, 1963: D.R. Mabey published an article in the Utah Engineering and Science Magazine titled "Tailings--a new resource?" which addressed the possibility of using tailings from Kennecott Copper Corporation to construct the inter-island dikes.

January, 1965: Caldwell, Richards & Sorensen, under the direction of the Great Salt Lake Authority, published a report titled "Preliminary master plan for the development of Great Salt Lake over the next 75 years." This plan envisioned constructing a massive landfill in the southern half of Farmington Bay using Kennecott tailings, and through the construction of dikes, creating three freshwater bays: (1) a south bay east of Antelope Island, (2) a central bay east of Fremont Island, and (3) a northern bay within the present Bear River Bay (figure 9).

The waters surrounding Antelope Island, Great Salt Lake, Utah - Gwynn

CONSTRUCTION MATERIALS, ANTELOPE ISLAND

by
Fitzhugh D. Davis
Utah Geological Survey (retired)

ABSTRACT

Sand and gravel, flagstone (slate), quartzite, and other metamorphic rocks found on Antelope Island are actual and potential sources of construction materials. Sand and gravel have been used for road construction, slate has been prospected for use as roofing material, and quartzite has been used as riprap for highway embankment protection. Several rock units in the Farmington Canyon Complex would make durable, strong, and attractive ornamental and building stone.

CONSTRUCTION MATERIALS

Several varieties of construction materials have been identified on Antelope Island. These include sand and gravel, flag and roofing stone (slate), quartzite for rip-rap and crushed stone, and metamorphic rocks for decorative or facing stone. The location of described deposits are indicated on the index map (figure 1).

Sand and Gravel

History

Sand and gravel resources on Antelope Island have been exploited to build roads, highways and causeways. A few case histories are presented to illustrate past usage and to describe the nature of the deposits.

Syracuse-Antelope Island causeway: In 1967, the Utah Department of Transportation (UDOT) investigated two potential sources of sand and gravel on the northern part of the island for use in construction of a causeway from Syracuse to Antelope Island. The first area was in the N½, NW ¼, section 32, T. 4 N., R. 3 W., (UDOT material site number 06069). Thirteen holes, ranging in depth from 2 to 27 feet (0.6 to 8.2 m), were augured in this lake terrace deposit. Granular material was present to at least a depth of 27 feet (8.2 m).

Seven samples of material from different holes and depths were obtained for testing. One sample was taken just for absorption and wear tests. For the other samples the gravel content averaged 31 percent, the sand content averaged 56 percent, and the silt and clay portion averaged 13 percent. However, two samples were obtained from thin gravel lenses that greatly biased the gravel percentage; the actual sand content of the deposit was larger. Liquid limits ranged from non-plastic to 26, plasticity indexes ranged from non-plastic to 7, and the gravel had a wear of 19.1 percent. Material from this deposit, at least until 1969, was used as fill on the causeway.

The second area in the northern part of the island was in the NW ¼, SE ¼, section 4, T. 3 N., R. 3 W., (UDOT material site number 06070). Five holes were augered that ranged from 9 to 20 feet (2.7 to 6.1 m) in depth. Four samples were taken from different depths in two holes for testing. The gravel content of the samples averaged 38 percent, the sand content averaged 57 percent, and the silt and clay portion averaged 5 percent. Apparently, material from this site was never used.

In 1969, the UDOT opened a pit in the NE ¼, SW ¼, section 31, T. 4 N., R. 3 W., (figure 2, UDOT material site number 06068). It revealed 30 feet (9.1 m) of sand, and thick, lenticular gravel beds in a shoreline deposit. Three cut-bank samples were obtained from different levels for testing. The average gravel component was 60 percent, the

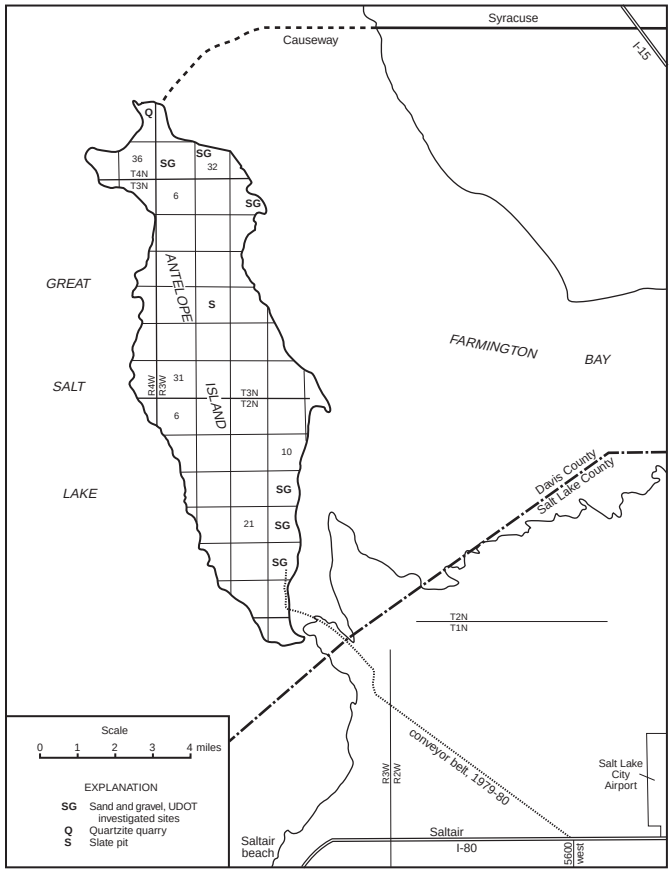

Figure 1. *Index map showing locations of described deposits.*

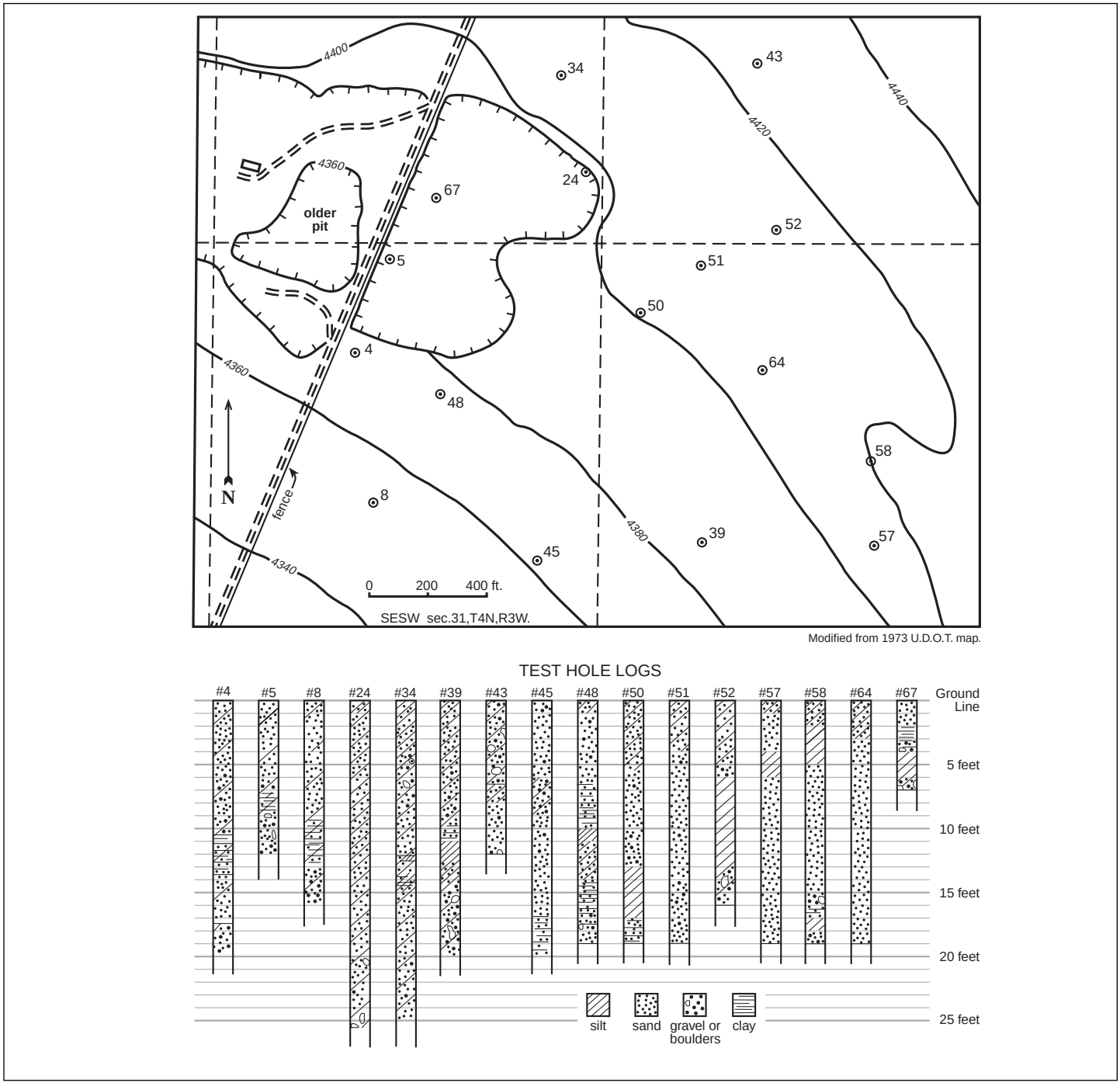

Figure 2. *Map of Utah Department of Transportation material site 06068 on the north part of Antelope Island. Representative test holes and corresponding logs are shown.*

average sand content was 31 percent, and the average silt and clay portion was 9 percent. Liquid limits ranged from 18 to 29, plasticity indexes ranged from non-plastic to 6, the swell was zero on all samples, and the gravel wear averaged 38 percent.

During 1969 and again in early 1973, a total of 67 test holes were augured in this large deposit. The holes ranged from 3 to 30 feet (0.9 to 9.1 m) in depth and averaged about 18 feet (5.5 m). Figure 2 shows a representative number of the test holes plus the corresponding logs. Also, the 1987 pit outline is portrayed as well as the initial pit. From 1969 to the spring of 1984, a large amount of material from this pit was used as embankment on the causeway. However, by the end of 1973, all the gravel lenses had been excavated and all that remained was sand and silt (Allen K. Hunsaker, UDOT, personal communication, December, 1987). Therefore, from 1974 to 1984 a large quantity of sand and silt was used for maintenance of the causeway. During these years the pit, 35 to 40 feet (10.7 to 12.2 m) deep, was extended to the east and southeast. Test logs 5, 24, and 67 had correctly depicted the types of material in the deposit.

Interstate Highway 80: During 1975 and 1978 the UDOT investigated the alluvial fans and beach-sand deposits on the southeastern side of the island. A huge supply of embank-

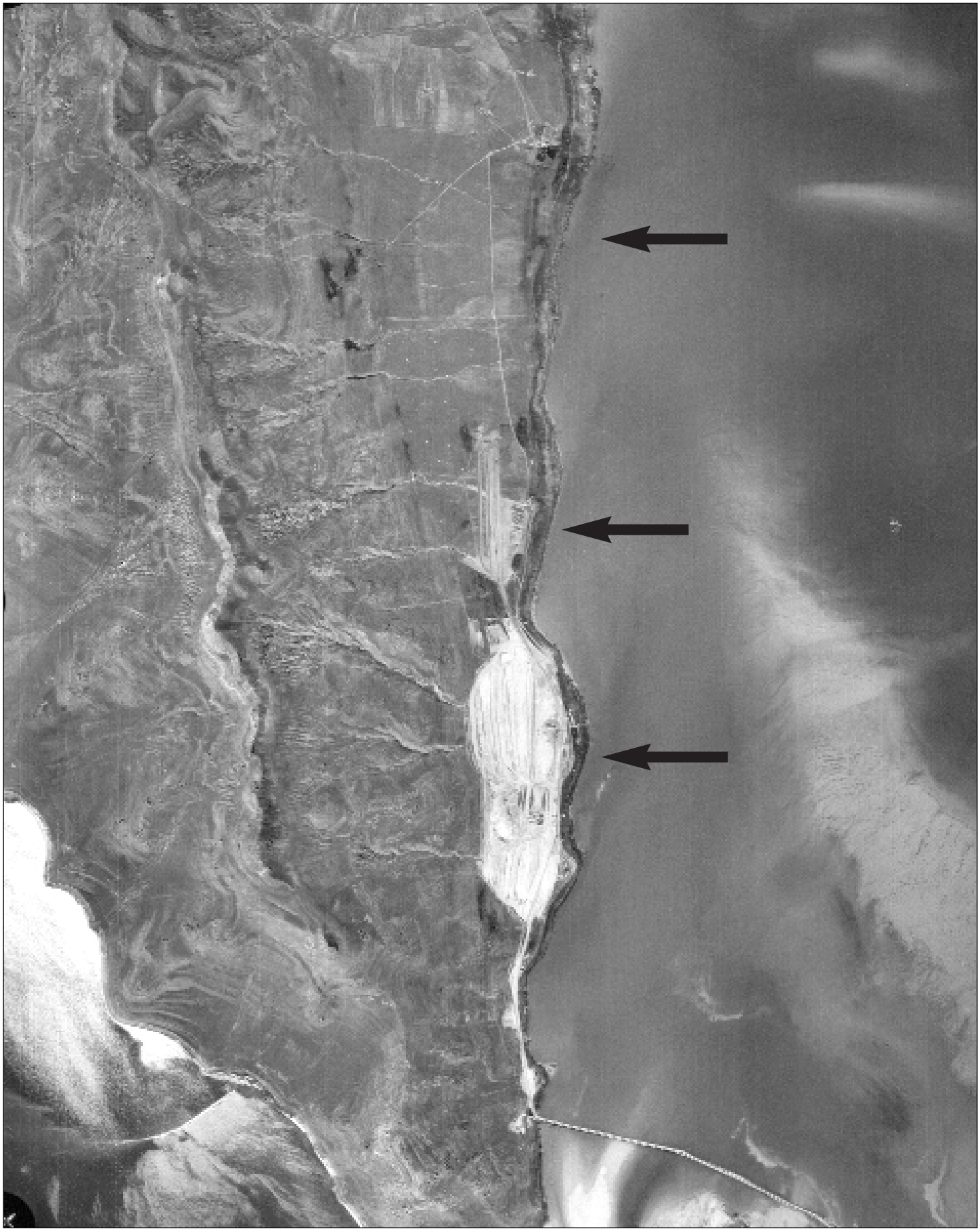

Figure 3. *Air photo of southern Antelope Island (taken June 20, 1980 by U.S. Department of Agriculture) shows the extent of the excavation for interstate highway construction material (bottom 2 arrows). Excavation eventually progressed northward (uppermost arrow).*

ment material was needed for interstate highway construction between Redwood Road (just east of the Salt Lake City airport) in Salt Lake City and Saltair Beach. The areas examined were in sections 15, 22, and 27, T. 2 N., R. 3 W. (figure 3).

During the two years 89 holes were augured and 20 holes were rotary drilled in these sections. The holes ranged in depth from 2 to 105 feet (0.6 to 32 m) and enough granular material was found to satisfy construction requirements. Sixty-one samples were obtained from different holes and depths for testing. Thirty-one samples were A-1-b material (American Association of State Highway Officials classification), 16 samples were A-2-4 material, and the remaining samples ranged from A-4(0) to A-7-5(12) material. In general, the gravel content of the samples was between 10 and 20 percent. The silt and clay percentages of the samples ranged from 7.3 to 95.9 percent, but sand was, by far, the largest volume of material.

In 1979 and 1980 about 16 million cubic yards (12.2 million cubic meters) of material were excavated from this part of the island for interstate highway construction (John T. McCleary, UDOT, personal communication, July, 1987). The excavation essentially removed the upper 10 to 15 feet (3 to 4.5 m) of the surficial deposits. The material was loaded onto a 13-mile-long (21 km) conveyor belt and carried southeasterly to a stockpile and loading facility near 5600 West and the I-80 route west of Salt Lake City. At the time, this conveyor belt system was the longest ever built in the world. The excavated areas were graded, contoured, and revegetated.

Antelope Island sand and gravel deposits

While mapping the geology of the island, Doelling and others (1990) examined many exposures, mostly in gullies, in the alluvial fans (Doelling and others, 1990 map unit Qaf) and the lacustrine sand and gravel deposits (map unit Qlg) around the perimeter of the island. In general, the gravel component ranges from 10 to 20 percent in nearly all the map units Qaf and Qlg deposits on the island. This contrasts with most commercial gravel deposits that have a 45 to 60 percent gravel content. The following comments pertain to the larger areas of Qaf and Qlg on the west side of the island:

Qaf in the W ½, section 20, T. 2 N., R. 3 W.: Eight feet (2.4 m) of alluvium is exposed in a gully. The gravel is 40 percent gneiss, 30 percent quartzite, 5 percent amphibolite, and 25 percent other metamorphic rocks. This is a large resource area, but sand comprises about 75 percent of the deposit.

Qaf in NE ¼, section 18, T. 2 N., R. 3 W.: Five feet (1.5 m) of alluvium is exposed in a gully. The gravel is 90 percent gneiss, 5 percent quartzite, and 5 percent other metamorphics. The deposit, however, is mostly sand with very little silt and clay.

Qaf in SW ¼, section 6 and N ½, section 7, T. 2 N., R. 3 W.: Ten feet (3 m) of sand and gravel are exposed in several places. The clasts are 94 percent gneiss, 3 percent amphibolite, 2 percent red granitic gneiss, and 1 percent quartzite. Gravel is more abundant (25 to 30 percent) in this deposit than in any other on the west side of the island. This is a large resource area and an average thickness of 20 feet (3 m) of sand and gravel seems reasonable.

Qlg and Qaf in NE ¼, section 24, T. 3 N., R. 4 W. and NW ¼, section 19, T. 3 N., R. 3 W.: Twelve to 15 feet (3.7 to 4.6 m) of alluvial and lacustrine deposits are exposed. The gravel is 85 percent gneiss, 10 percent amphibolite, and 5 percent schist and quartzite. However, sand comprises 60 to 70 percent of the material; silt and clay about 6 to 8 percent.

Qlg and Qaf in N ½, section 18, T. 3 N., R 3 W.: Fifteen feet (4.6 m) of Qlg are exposed in a gully. The deposit is about 80 percent beach sands. The clasts are 70 percent gneiss, 20 percent quartzite, 10 percent amphibolite, and comprise 10 to 12 percent of the deposit.

Quartzite

Crushed quartzite makes an excellent aggregate for concrete and bituminous mixtures. If a source is ever needed on the island, the Tintic Quartzite is abundant and a quarry could be easily located.

The Tintic Quartzite has been quarried for riprap in the NW ¼, NE ¼, section 25, T. 4 N., R. 4 W. Large, durable blocks and slabs of the quartzite were used to protect the causeway embankments.

Flagstone (slate)

In the west half of section 20 and the southeastern part of section 19, T. 3 N., R. 3 W., there are at least four slate prospects and one fair-sized slate pit in the upper part of the Kelley Canyon Formation. The slate pit in the NE ¼, NW ¼, section 20, T. 3 N., R. 3 W., is about 40 feet wide and 90 feet long. About 25 feet of thin-bedded, platy and laminated slate and hard shale are exposed. The rocks break into plates ¼ to 3 inches (0.6 to 7.6 cm) thick and the prospectors probably were looking for flagstone and possibly roofing material. The rock colors change vertically each 1/8 to 4 inches (0.3 to 10 cm) and they range through shades of brownish gray, grayish purple, light orange, light greenish gray, and medium brown. From the dump size adjacent to the pit, it appears that not too much slate was removed from the site. Much flagstone remains at the site.

Ornamental and Building Stone

Strong, hard, durable, and attractive rocks are available on the island for use as ornamental and building stone. Facing on building exteriors, sills, trim, facings, and steps can be fashioned in stone. Stone is used for interiors in flooring, wainscoting, steps, fireplaces, and baseboards. Three units in the Farmington Canyon Complex have ornamental and building stone potential: (1) quartz plagioclase gneiss (map unit XWfq), (2) red granitic gneiss (map unit XWfr), and (3) coarse-grained granite (map unit XWfc) (Doelling and others, 1990). All three have pleasing colors and fabrics. Units (1) and (2) have an attractive gneissic texture.

REFERENCE

Doelling, H.H., Willis, G.C., Jensen, M.E., Hecker, Suzanne, Case, W.F., and Hand, J.S., 1990, Geologic map of Antelope Island, Davis County, Utah: Utah Geological and Mineral Survey Map 127, 27 p., scale 1:24,000.

HYDROGEOLOGY OF ANTELOPE ISLAND, GREAT SALT LAKE, UTAH

by
Alan L. Mayo and Robert H. Klauk[1]
Department of Geology
Brigham Young University, Provo, Utah

[1] now at Warzyn Engineering, Inc., Milwaukee, Wisconsin

Reprinted from *Contributions to the solute and isotopic groundwater chemistry, Antelope Island, Great Salt Lake, Utah:* Journal of Hydrology, v. 127, p. 307-335, published in 1991 with kind permission from Elsevier Science - NL, Sara Burgerhartstraat 25, 1055 KV Amsterdam, the Netherlands.

ABSTRACT

The 43 square-mile (110 km^2) Antelope Island is predominantly composed of Precambrian gneiss similar to rocks in the Wasatch Range 20 miles (32 km^2) to the east. Three general types of ground-water systems have been identified on the basis of aquifer composition and dissolved solute content. The systems include ground waters which discharge from either crystalline or sedimentary rocks. Sedimentary ground-water systems contain ground water which is either Na-Cl rich or poor. All island ground water has anomalously high Na^+, Cl^-, or SO_4^{2-} concentrations when compared to ground waters that issue from similar bedrock in nearby areas. Crystalline ground-water systems discharge up to 1,400 feet (732 m) above lake level, and their combined dry-season discharge is estimated at 100 gallons/minute (400 l/min). Island ground-water systems may be statistically distinguished from each other and from other ground water in the region.

The solute chemistry of island ground water cannot be accounted for by the simple dissolution of aquifer minerals, and the water does not plot along fault-controlled thermal-water-precipitation or parent-aquifer-precipitation Cl^-/SO_4^{2-} mixing lines. Discharge elevations and Cl^-/SO_4^{2-} data also rule out mixing with residual salts from Pleistocene Lake Bonneville or brines of the Great Salt Lake for most island ground water.

Tritium data (>40 tritium units) suggest island ground-water systems are primarily recharged from modern meteoric water. Stable isotope deuterium and oxygen-18 data plot along an evaporation line which indicates that recharge water contains a component of evaporated Great Salt Lake water. Temporal variations in spring discharges, tritium concentrations, and discharge temperatures of less than 68°F (20°C) indicate short flow paths and shallow circulation. Excess Cl^- and SO_4^{2-} concentrations are attributed to the deposition of aerosols of windblown dust from nearby evaporate deposits and sea spray. Sulfur-34 isotope data suggest contributions to crystalline systems of reduced sulfur from nearby smelter plumes or other industrial smoke stacks. Excess Na^+ concentrations may be attributed to Great Salt Lake Desert aerosols from dust storms and precipitation events, to air-borne storm aerosols from lake sea spray, and to precipitation of saline lake water.

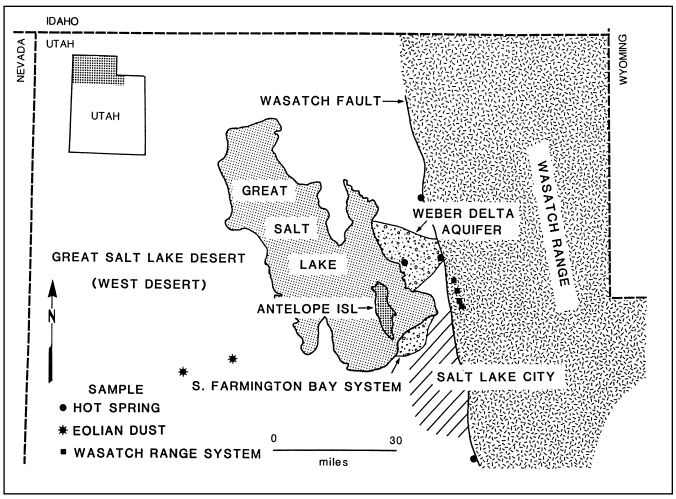

Figure 1. *Map showing the location of Antelope Island and Weber delta aquifer and southern Farmington Bay ground-water system. Sampling locations of hot springs, eolian dust and Wasatch Range ground water are also shown.*

INTRODUCTION

Antelope Island, the largest island in Utah's Great Salt Lake, is located about 20 miles (32 km) northwest of Salt Lake City (figure 1). The island covers approximately 43 square miles (110 km^2), and has a length of 15 miles (24 km) and a maximum width of 5 miles (8 km). The highest peak reaches an altitude of 6,597 feet (2,010 m) and the maximum relief above lake level is almost 2,400 feet (732 m).

As demonstrated by statistics, the chemical characters of various island ground waters are compositionally different from each other and from ground water in similar rock types in adjacent areas. Discharges from the crystalline bedrock sources have solute concentrations 3.7 times greater than solute concentrations in similar bedrock sources in the Wasatch Range located 20 miles (32 km) to the east. Discharges from the island's sedimentary aquifers systems, predominantly composed of Lake Bonneville sediments, also have anomalous concentrations of SO_4^{2-}, Na^+, and Cl^- compared to similar non-island ground-water systems. The purpose of this investigation is to determine the origin of the high solute concentrations in the island's ground water.

Methods of Study

Water-quality data from island ground water were collected and correlated with published water-quality data from similar rock sources in nearby terrains and from the Great Salt Lake. Anomalies were identified and potential sources of island ground water solutes and isotopes were identified.

The field investigation included locating springs, measuring discharges, evaluating structural and stratigraphic relationships, and collecting water samples. Geologic information was obtained from published sources. Temperature, pH, and HCO_3^- concentrations were determined in the field. Ions were analyzed by atomic absorption (AA), inductively coupled plasma (ICP), and specific ion methods. Water samples were collected and analyzed following U.S. Environmental Protection Agency (1981) procedures. Solute data were plotted on a trilinear (Piper, 1944) diagram for visual inspection. Saturation indices were calculated with the computer program WATEQF (Plummer and others, 1976).

Ground-Water Systems Defined

The solute and isotopic compositions of ground and lake waters from various sources located in the vicinity of southeastern Great Salt Lake, Utah, will be discussed (figure 1). Only the Weber Delta aquifer has been formally defined as an aquifer (Feth and others, 1966). The less formal designation of "ground-water system" will be used for other ground-water sources. The sources and their designations are:

1. Wasatch Range systems: ground water supported by Archean-age crystalline rocks located along the western edge of the Wasatch Range.
2. Weber Delta aquifer: ground water from the Weber Delta aquifer.
3. Thermal ground water: ground water from hot springs and wells located near the Wasatch fault and in the Weber Delta aquifer.
4. Southern Farmington Bay systems: ground water supported by off-shore Lake Bonneville deposits, located south of and adjacent to Farmington Bay, Great Salt Lake.
5. Island crystalline systems: ground water supported by Archean-age igneous and younger metamorphic rocks on Antelope Island.
6. Island sedimentary systems: ground water supported by Tertiary-age tuffs and by unconsolidated clays, sand, and gravels deposited on the flanks of Antelope Island from Lake Bonneville.
7. Water in the Great Salt Lake.

Both island sedimentary and southern Farmington Bay systems may be divided into two types on the basis of Na^+ and Cl^- concentrations. Although all ground waters in these systems have elevated Na^+ and Cl^- concentrations compared to other systems in the region, ground waters from these systems will be referred to as either Na-Cl poor or Na-Cl rich (based on local comparisons). Most ground-water discharges in each system are Na-Cl poor.

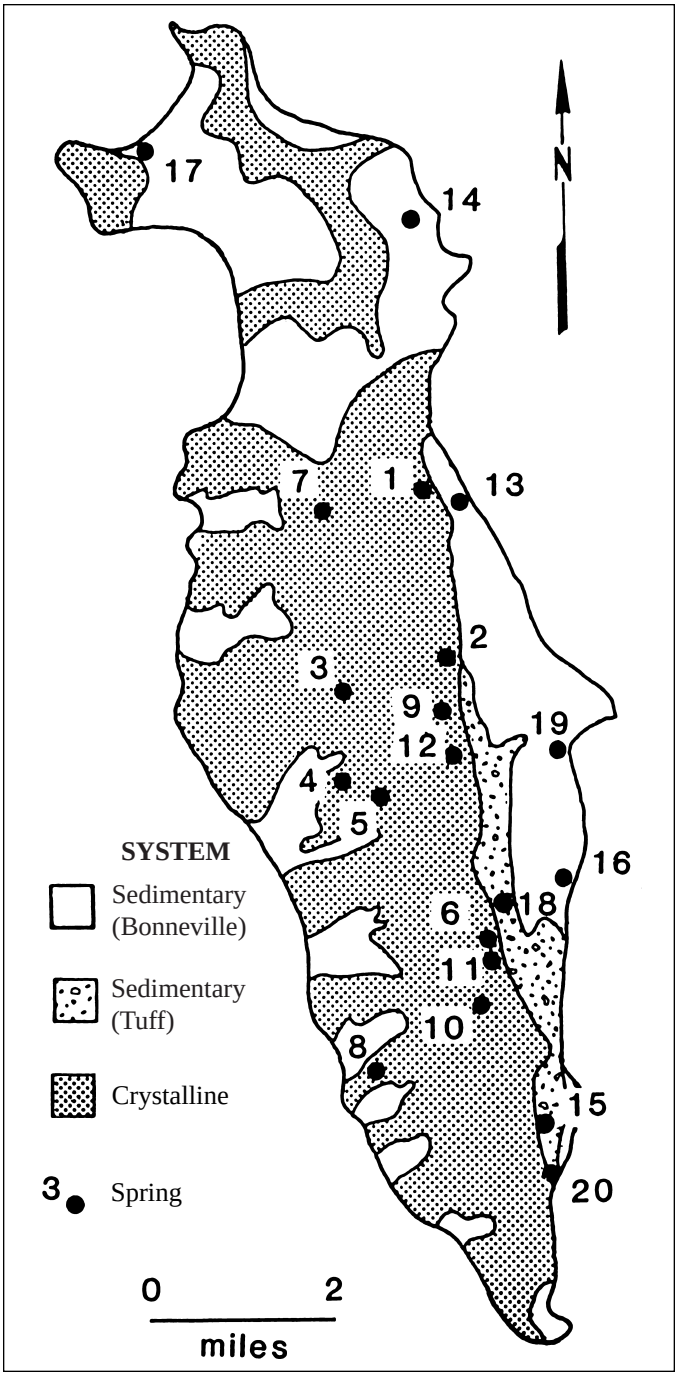

Figure 2. *Generalized geologic map of Antelope Island showing ground-water systems and sampling locations.*

Geologic and Hydrogeologic Setting

The oblong island (figure 2) has a bedrock core of Archean-age gneiss with lesser amounts of fractured Proterozoic slate and dolomite and Cambrian quartzite (Doelling and others, 1990; Goode, 1978). Bedrock types found on the island also crop out in the Wasatch Range. Antelope Island and other islands in the lake, such as Stansbury Island located to the west, are Basin-and-Range-style horst blocks separated from each other and from the Wasatch Range to the east by a graben containing as much as 13,000 feet (4,000 m) of detritus (Goode, 1978). A cover of Tertiary-age clastic sediments and Pleistocene-age Lake Bonneville unconsolidated clay, sand, and gravel deposits flank the bedrock core. Lake Bon-

Table 1. *Physical and chemical characteristics of Antelope Island ground water, Great Salt Lake, Utah*

Sample[1]	Location[2]	Aquifer[3]	Discharge[4] (gpm)	Elevation (ft)	Temp (°C)	pH	meq l^{-1} Ca^{2+}	Mg^{2+}	Na^{+}	K^{+}	HCO_3^{-}	SO_4^{2-}	Cl^{-}	mg l^{-1} SiO_2	$\delta^{18}O$ (‰) (SMOW)	$\delta^{2}H$ (‰) (SMOW)	$\delta^{13}C$ (‰) (PDB)	$\delta^{34}S$ (‰) (CD)	^{3}H (TU)
Island Crystalline Systems																			
1	T3N R3W 21bba	Gneiss	3	4400	15	7.7	1.65	0.97	2.52	0.03	2.79	0.92	1.35	10	-	-	-	-	-
2	T3N R3W 33abb	Gneiss	4	4620	10	8.3	1.80	0.99	2.52	0.03	2.95	0.83	1.21	12	-	-	-	-	-
3	T3N R3W 32bcd	Gneiss	3	5360	14	7.7	1.80	0.90	2.57	0.03	2.39	0.98	1.72	7	-	-	-	-	-
4	T2N R3W 5bcd	Gneiss	3	4800	13	9.0	1.30	0.74	3.39	0.05	2.57	1.19	1.51	9	-14.7	-115.3	-	-	-
5	T2N R3W 5dcb	Gneiss	<0.1	4900	20	9.2	2.20	1.23	5.22	0.05	3.31	2.06	3.17	-	-	-	-	-	-
6	T2N R3W 16aab	Gneiss	4	4550	13	7.8	3.89	1.97	4.79	0.13	4.00	1.92	4.80	25	-	-	-	-	-
7	T3N R3W 19add	Metamorphic	3	5000	10	8.4	2.79	1.89	3.57	0.05	3.38	1.23	3.67	7	-15.1	-115.5	-12.9	+2.0	-
8	T2N R3W 20cad	Gneiss	0.3	4369	16	7.9	3.79	2.39	8.70	0.23	4.54	3.12	6.70	7	-13.7	-109.8	-11.7	+0.6	42.3
9	T3N R3W 33cab	Granite	2.5	4800	13	8.1	2.10	1.48	2.78	0.03	3.25	1.17	1.83	8	-14.9	-113.6	-	-	46.1
10	T2N R3W 16dcd	Gneiss	20	4900	14	7.7	3.99	1.65	5.22	0.03	3.18	1.83	5.64	64	-	-	-	-	-
11	T2N R3W 16adb	Gneiss	2.5	4600	13	8.8	3.39	1.73	4.79	0.10	3.70	1.77	4.65	16	-	-	-	-	-
12	T2N R3W 4bad	Granite	1	4800	16	8.1	1.70	1.07	2.61	0.05	2.26	1.25	1.97	8	-	-	-	-	-
mean				4758	14	8.2	2.53	1.42	4.06	0.07	3.19	1.52	3.19	14.4	-14.6	-113.5	-12.3	+1.3	44.2
Island Sedimentary Systems																			
13	T3N R3W 21aca	Bonneville	<1	4240	13	8.1	3.54	1.56	5.22	0.05	3.02	0.75	6.35	-	-	-	-	-	-
14	T3N R3W 4bbc	Bonneville	1	4280	15	8.2	2.05	0.91	2.52	0.08	2.03	1.66	2.17	6	-14.3	-112.5	-14.6	+4.2	-
15	T2N R3W 27bca	Tuff	4	4380	14	7.3	8.98	1.41	23.93	0.33	8.79	3.54	25.03	9	-	-	-	-	-
16	T2N R3W 10aac	Bonneville	2	4220	14	8.0	3.64	2.22	7.83	0.36	4.26	1.50	9.87	41	-14.5	-114.7	-12.9	+8.1	-
17	T4N R4W 35adb	Bonneville[5]	-	4230	9	9.9	4.99	3.04	10.44	0.33	7.08	2.08	9.17	15	-	-	-	-	-
18	T2N R3W 9dda	Tuff	13	4460	15	7.9	3.14	1.73	4.09	1.73	3.08	1.54	4.02	18	-14.8	-119.8	-12.0	+7.8	
19	T2N R3W 3abc	Bonneville[5]	>10	4240	15	8.6	1.95	1.40	5.66	0.23	4.47	0.73	3.81	9	-	-	-		
20	T2N R3W 34bab	Bonneville[6]	5	4230	14	7.9	8.48	5.43	23.49	0.26	4.06	3.12	27.50	14	-	-	-	-	-
mean (all sites)				4285	13.6	8.2	4.60	2.21	10.40	0.42	4.60	1.87	10.99	16	-14.5	-115.7	-13.2	+6.7	-
mean (Na-Cl poor; w/o 15 and 20)				4278	13.5	8.4	3.22	1.81	5.96	0.46	3.99	1.38	5.90	17.8					
mean (Na-Cl rich; with 15 and 20)				4305	14	7.6	8.73	3.42	23.71	0.30	6.43	3.33	26.27	11.5	-	-	-	-	-

[1] See Figure 2 for map locations.

[2] Reference Salt Lake Base Line and Meridian. Location is: T-Township, R-Range, section number, quarter section, quarter-quarter section, quarter-quarter-quarter section (a=northeast, b=northwest, c=southwest, d=southeast).

[3] Bonneville: sand and gravel deposits from Lake Bonneville; Tuff: tuffaceous sandstone and conglomerate (Tertiary); Metamorphic: diamicite, dolomite and slate (Late Proterozoic); Granite: granite gneiss (Early Proterozoic); Gneiss: gneiss, amphibolite, and schist (Archean). After Doelling and others, 1990.

[4] Does not include base flow discharge from all island springs.

[5] Thin Bonneville over Cambrian Tintic Quartzite.

[6] Thin Bonneville over gneiss.

Table 2. *Physical and chemical characteristics of ground-water discharge from areas in the vicinity of Antelope Island.*

Sample[1]	Location[2]	Temp (°C)	pH	meq l^{-1}							mg l^{-1}	$\delta^{18}O$	$\delta^{2}H$	$\delta^{13}C$	$\delta^{34}S$
				Ca^{2+}	Mg^{2+}	Na^{+}	K^{+}	HCO_3^{-}	SO_4^{2-}	Cl^{-}	SiO_2	(‰)	(‰)	(‰)	(‰)
						Southern Farmington Bay Ground-Water Systems[3] (all sites are wells)									
21	T1N R1E 19baa	19	8.0	1.25	1.32	10.44	0.05	5.23	0.07	8.46	22	-	-	-	-
22	T1N R2E 24dac	27	8.2	0.65	0.32	6.96	0.10	4.14	0.05	4.23	32	-	-	-	-
23	T1N R2E 8abd	19.5	8.1	1.25	1.48	12.18	0.06	3.30	0.10	12.41	22	-	-	-	-
24	T1N R2E 15bcd	20	8.2	0.55	0.56	6.96	0.05	3.30	0.05	3.95	24	-	-	-	-
25	T1N R2E 21acd	21.5	8.0	0.80	0.49	9.14	0.16	4.48	0.04	6.21	53	-	-	-	-
26	T1N R2E 21cab	18	8.3	0.33	0.39	13.05	0.06	6.79	0.09	7.05	22	-	-	-	-
27	T1N R2E 22daa	15.5	8.0	1.00	1.32	12.62	0.07	5.80	0.07	10.16	22	-	-	-	-
28	T1N R2E 23bbd	16.5	8.2	0.65	0.90	14.79	0.06	6.25	0.10	9.87	22	-	-	-	-
29[4]	T1N R2E 26cda	18	7.7	1.80	0.90	7.83	0.05	3.04	0.54	7.05	13	-	-	-	-
30[4]	T3N R1W 25dab	16	7.4	2.99	1.23	7.83	0.06	3.80	0.07	8.75	25	-	-	-	-
31	T1N R2E 16caa	22.5	7.8	3.49	1.73	20.45	0.31	3.12	0.17	23.70	48	-	-	-	-
32	T1N R2E 7caa	17.5	7.8	4.59	7.49	41.76	0.09	4.88	0.46	50.78	22	-	-	-	-
33	T1N R2E 7ccc	13.5	8.0	3.64	6.83	73.95	0.11	3.54	7.08	73.35	21	-	-	-	-
34[4]	T1N R1W 10aac	16	7.3	2.40	1.32	23.06	0.72	7.43	0.15	21.16	53	-	-	-	-
mean (all sites)		18.6	7.9	1.81	1.88	18.64	0.14	4.65	0.65	17.65	28.6	-	-	-	-
mean (Na-Cl poor)		19.3	7.9	1.43	1.00	12.11	0.15	4.72	0.12	10.25	29.8	-	-	-	-
mean (Na-Cl rich 32 & 33)		15.5	7.9	4.12	7.16	57.95	0.10	4.21	3.77	62.07	21.5				
						Weber Delta Aquifer[4] (all sites are wells)									
35	T3N R1W 4bca	16.5	7.7	1.75	0.67	1.22	0.06	3.24	0.02	0.42	21	-	-	-	-
36	T3N R1W 5dda	18	7.7	1.40	0.45	1.31	0.07	2.78	0.05	0.39	32	-	-	-	-
37	T3N R1W 5ddb	17	7.3	2.00	1.15	2.00	0.16	5.28	0.08	0.48	29	-	-	-	-
38	T3N R1W 5ddb	18.5	7.9	1.40	0.62	1.48	0.06	2.78	0.01	0.48	22	-	-	-	-
39	T4N R1W 3ccd	12.5	7.4	3.09	1.23	0.70	0.04	3.92	0.50	0.56	16	-	-	-	-
40	T4N R1W 8dcd	14	7.7	2.45	0.90	0.65	0.03	3.16	0.33	0.37	17	-	-	-	-
41	T4N R1W 16bdd	15.5	7.8	1.50	0.54	0.52	0.02	2.08	0.10	0.28	17	-	-	-	-
42	T4N R2W 7bac	15.5	7.9	2.50	0.99	1.17	0.06	4.02	0.05	0.51	20	-	-	-	-
43	T4N R2W 20ada	16.5	8.0	2.10	0.90	0.83	0.08	3.34	0.02	0.34	21	-	-	-	-
44	T5N R1W 26bbc	16	7.6	2.64	1.07	1.17	0.04	3.92	0.29	0.85	19	-	-	-	-
45	T5N R1W 27dcc	12.5	7.5	3.49	1.32	0.70	0.04	4.30	0.50	0.68	12	-	-	-	-
46	T5N R1W 29bdb	11	7.4	3.49	1.48	0.74	0.05	4.62	0.58	0.56	12	-	-	-	-
47	T5N R1W 29bdc	11	7.3	3.54	1.56	0.91	0.06	5.04	0.54	0.56	12	-	-	-	-
48	T5N R1W 30ada	11.5	7.4	3.49	1.48	0.83	0.05	4.68	0.56	0.51	12	-	-	-	-
49	T5N R1W 35aaa	12.5	7.4	3.04	1.15	0.74	0.03	3.66	0.50	0.68	13	-	-	-	-
50	T5N R2W 22dcd	16.5	7.6	2.99	1.23	0.65	0.05	3.66	0.52	0.37	14	-	-	-	-
51	T5N R3W 25cdc	16	7.8	1.80	0.90	1.26	0.04	3.60	0.02	0.39	20	-	-	-	-
mean		14.8	7.6	2.51	1.04	0.99	0.06	3.77	0.27	0.50	18.2	-	-	-	-
						Wasatch Range Ground-Water Systems[5] (all sites are springs)									
52	Little spg	12.5	7.5	0.95	0.66	0.74	0.05	1.61	0.46	0.25	-	-	-	-	-
53	Baer spg	13	7.3	0.60	0.49	0.57	0.03	1.11	0.33	0.22	-	-	-	-	-
54	Crooked spg	14.5	8.1	1.00	0.33	0.39	0.03	1.38	0.29	0.17	-	-	-	-	-
55	Military spg	13	7.6	1.00	0.33	0.39	0.03	1.21	0.25	0.14	-	-	-	-	-
mean		13.3	7.7	0.97	0.45	0.52	0.03	1.42	0.35	0.20	-	-	-	-	-

Thermal Ground Water[6,7] (all sites are springs)														
56 Wasatch spg	42	7.9	19.91	5.68	67.77	1.46	4.31	13.20	70.24	12	-16.0	-128	-6.7	+11.5
57 Beck spg	56	7.6	37.23	8.97	201.19	4.12	3.88	18.26	213.55	24	-16.8	-129	-4.4	-
58 Utah spg	58	6.4	48.60	1.89	286.59	20.99	3.65	3.77	362.50	28	-15.1	-136	-	-
59 Ogden spg	56	7.0	15.72	0.49	130.02	8.05	4.00	2.00	139.08	41	-16.0	-136	-	-
60 Hooper spg	57	6.8	10.18	5.92	107.14	5.22	3.85	0.62	130.99	24	-15.8	-140	-	-
mean	53.8	7.1	26.30	4.59	158.54	7.97	3.94	7.57	183.27	25.8	-15.9	-134	-5.6	+11.5
Causeway Well														
61[8] T4N R3E 19caa[3]	-	-	2.55	1.73	8.78	0.12	3.06	0.25	9.87					

[1] See table 1 and figure 1 for locations.
[2] Reference Salt Lake City Base Line and Meridian.
[3] Data from Seiler (1986).
[4] Data from Plantz and others (1986).
[5] Unpublished data, Utah Health Department (1988).
[6] Data from Cole (1983).
[7] $\delta^{13}C$ and $\delta^{34}S$ unpublished data by authors.
[8] Data from Bolke and Waddell (1972).

Table 3. *Mean solute chemistry of ground water in the vicinity of Antelope Island.*

Type[1]	Number of samples	°C	pH	meq l^{-1}								mg l^{-1}
				Ca^{2+}	Mg^{2+}	Na^{+}	K^{+}	HCO_3^{-}	SO_4^{2-}	Cl^{-}	total	SiO_2
Island crystalline systems	12	14.0	8.2	2.53	1.42	4.06	0.07	3.19	1.52	3.19	15.98	14.4
Island sedimentary systems	8	13.6	8.2	4.60	2.21	10.40	0.42	4.60	1.87	10.99	35.09	16.0
Na-Cl poor systems[2]	6	13.5	8.4	3.22	1.81	5.96	0.46	3.99	1.38	5.90	22.72	17.8
Na-Cl rich systems[3]	2	14.0	7.6	8.73	3.42	23.71	0.30	6.43	3.33	26.27	72.19	11.5
S. Farmington Bay systems	14	18.6	7.9	1.81	1.88	18.65	0.14	4.65	0.65	17.65	45.43	28.6
Na-Cl poor systems[4]	12	19.3	7.9	1.43	1.00	12.11	0.15	4.72	0.12	10.25	29.78	29.8
Na-Cl rich systems[5]	2	15.5	7.9	4.12	7.16	57.95	0.10	4.21	3.77	62.07	139.38	21.5
Weber Delta aquifer	17	14.8	7.6	2.51	1.04	0.99	0.06	3.77	0.27	0.50	9.14	18.2
Wasatch Range systems	4	13.3	7.7	0.97	0.45	0.52	0.03	1.42	0.35	0.20	3.94	-
Thermal ground water	5	53.8	7.1	26.30	4.59	158.54	7.97	3.94	7.57	183.27	392.18	25.8

Type	Number of samples	log PCO_2	log saturation index (SI)						
			calcite	dolomite	gypsum	halite	quartz	chalcedony	mirabilite
Island crystalline systems	12	-3.06	0.32	0.63	-1.99	-6.65	0.45	-0.28	-6.75
Island sedimentary systems	8	-2.99	0.75	1.23	-1.77	-5.89	0.54	0.10	-6.21
S. Farmington Bay systems	14	-2.63	0.16	0.31	-3.22	-5.11	0.75	0.24	-6.84
Na-Cl poor systems[4]	12	-2.63	0.13	0.21	-3.42	-5.26	0.76	0.25	-7.20
Weber Delta aquifer	17	-2.33	0.07	-0.30	-2.86	-7.98	-0.63	0.11	-8.91
Wasatch Range systems	4	-2.81	-0.83	-2.00	-2.84	-8.69	-	-	-8.97
Thermal ground water	5	-1.72	0.64	0.68	-1.21	-3.58	0.23	0.62	-5.55

[1] See figures 1 and 2 for aquifer locations.
[2] Excludes samples 15 and 20.
[3] Samples 15 and 20.
[4] Excludes samples 32 and 33.
[5] Samples 32 and 33.

neville never completely covered the island, and lake sediments, commonly shoreline sands and clays, do not crop out above approximately 5,300 feet (1,600 m).

In the southern Farmington Bay, near the present lake level on the east and south sides of the island, the Lake Bonneville shoreline deposits grade into offshore deposits of sand and clay (Hintze, 1988; Marine and Price, 1964). Farther to the east (East Shore), Lake Bonneville sediments of the Farmington Bay facies grade into Lake Bonneville shoreline deposits at the base of the Wasatch Range. Northeast of the island at the base of the Wasatch Range, the Farmington Bay facies grade into several hundred feet of Weber Delta clastic sediments (Feth and others, 1966). The Weber Delta was deposited on the edge of Lake Bonneville by the Weber and Ogden Rivers as they emerged from the Wasatch Range. Numerous shallow wells have been completed in the southern Farmington Bay ground-water system and the Weber Delta aquifer. The spatial relationship between the various ground-water systems is illustrated in figure 1.

More than 80 cool-temperature, ephemeral, and perennial springs have been located on the island (Vaughn Hansen and Associates, 1976, unpublished report) Most perennial springs are located on the east side of the island and discharge from fractures and joints along the bedrock backbone of the island at elevations up to 5,360 feet (1,635 m) or along bedding contacts in the Lake Bonneville sediments that flank the bedrock core. Many of the shallow wells (<300 feet [<100m]) developed in the southern Farmington Bay ground-water system are flowing artesian, whereas the Weber Delta aquifer is unconfined near the mountain front and confined elsewhere.

SOLUTE AND ISOTOPE GEOCHEMISTRY

Samples from 20 island springs were analyzed for major ions and stable isotopes (δ^2H, $\delta^{18}O$, $\delta^{13}C$, $\delta^{34}S$, and ^3H)(table 1 and figure 2). Listed in table 2 are solute analyses and limited stable isotopic data of shallow ground-water samples from the southern Farmington Bay (Marine and Price, 1964; Seiler, 1986; Smith, 1961; Waddell and others, 1987) and Wasatch Range systems (Utah Department of Health, 1988, unpublished data), from the Weber Delta aquifer (Cole, 1982; Smith, 1961; Smith and Gates, 1963), and from thermal ground water (Cole, 1981, 1983). Solute analyses are summarized in table 3.

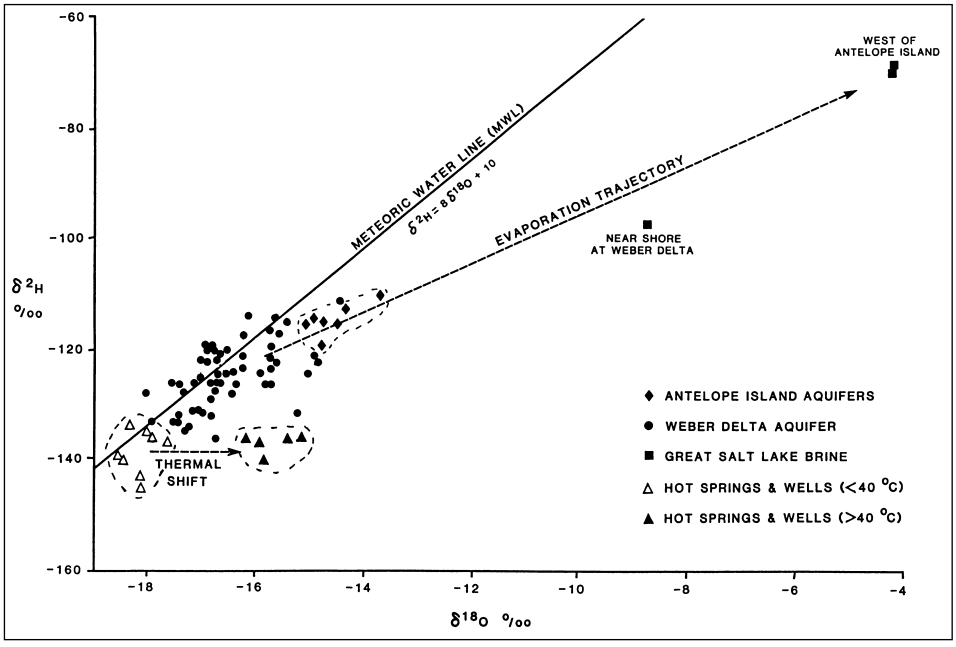

Figure 3. *Plot of δ^2H and $\delta^{18}O$ of various ground waters in vicinity of Antelope Island, Great Salt Lake, Utah. Salt Lake brine samples were collected west of the island and near shore at the Weber delta.*

Isotopes

The stable isotopic composition of environmental isotopes, such as hydrogen and oxygen of the water, carbon of bicarbonate, and sulfur, is expressed as the per mil ($^0/_{00}$) difference in the ratio of the heavy/light isotope in the sample relative to the ratio in the standard. For example, the stable isotopic composition of carbon is calculated as follows:

$$\delta^{13}C\ (^0/_{00}) = \frac{Rsample - Rstandard}{\bullet Rstandard} \times 1000$$

where $R = {}^{13}C/{}^{12}C$.

The stable environmental isotopes and reporting standards of interest to this investigation are listed below:

Isotope analysis	Ratio	Standard
δ^2H	$^2H/^1H$	SMOW (standard mean ocean seawater)
$\delta^{18}O$	$^{18}O/^{16}O$	SMOW (standard mean ocean seawater)
$\delta^{13}C$	$^{13}C/^{12}C$	PDB (Pee Dee Belmintella)
$\delta^{34}S$	$\delta^{34}S/\delta^{32}S$	CD (Canyon Diablo)

Hydrogen-2 and Oxygen-18 (δ^2H and $\delta^{18}O$)

δ^2H and $\delta^{18}O$ analyses for more than 50 Weber Delta aquifer and thermal ground waters (Cole, 1981, 1982, 1983) plot in figure 3 as three groups with respect to the continental Meteoric Water Line (MWL). Because Cole's Weber Delta aquifer numerical data were not published with location references, those data are not listed in table 2.

The MWL is defined as $\delta^2H = 8\delta^{18}O + 10\ ^0/_{00}$ (Craig 1961). Cole (1981) identified three groups of stable isotopic data with respect to the MWL:

1. Weber Delta ground-water data which plot near the MWL between δ^2H of -136 and -110 $^0/_{00}$. Cole (1981) suggested some Weber Delta data exhibit a possible evaporation trend.
2. Thermal ground-water data (68 to 104°F [20 to 40°C]) from sites

Table 4. *Isotopic analyses of Great Salt Lake brine.*

Sample[1]	Sampling Date	Depth (ft)	$\delta^{18}O$ (‰)	$\delta^{2}H$ (‰)	$\delta^{13}C$ (‰))	$\delta^{34}S$ (‰)
1	7/25/89	0.25	-4.2	-69	-1.4	+17.1
2	7/25/89	0.25	-4.1	-68	-1.4	+14.6
3[2]	-	-	-8.8	-98	-	-

[1] Sample 1 collected 3.5 miles west-southwest of Antelope Island; sample 2 collected 4 miles southwest of Antelope Island.
[2] Data from Cole (1983). Collected near shore at Weber Delta.

located near the Salt Lake Mining Company, which plot near the MWL at about $\delta^{2}H$ of -140 ‰.

3. Stable isotopic data for thermal ground water (>104°F [>40°C]) located along the Wasatch fault, which exhibit a positive $\delta^{18}O$ shift of 2.5 to 3.5 ‰. Cole (1981) attributed the $\delta^{18}O$ shifts to high-temperature oxygen exchange between rocks and water at depth.

Island stable isotopic data plot along the proposed evaporation trajectory of Cole (1981) and lie along the evaporation trajectory of Great Salt Lake brine (figure 3 and table 4). The plot of island ground-water isotopic data along the evaporation trajectory suggests that evaporated lake water, from the so called "lake effect," is a component of island precipitation. The slopes of the evaporation trajectories are variable (Fontes, 1990). The slope of the trajectory in figure 3 falls in the normal range of such trajectories. It is unlikely that the stable isotopic composition of island ground water can be attributed to soil zone evaporation, because steep island slopes preclude surface ponding of meteoric water prior to infiltration, and because standing bodies of surface water do not exist above spring-discharge elevations. As discussed in detail later, it is also unlikely that the location along the evaporation trajectory is the result of direct mixing of island ground water with Great Salt Lake brine because plausible mechanisms for mixing do not exist.

The "lake effect" is localized around the Great Salt Lake (Eubank and Brough, 1980), and it does not appear to influence the chemical or isotopic composition of high-elevation precipitation in the Wasatch Range. Stable isotopic compositions of high-elevation ground-water systems in the Wasatch Range plot near the MWL about a mean $\delta^{2}H$ of -132 ‰ . The high-elevation ground water is predominantly of the calcium carbonate type with low solute concentrations. Tritium (^{3}H) concentrations in high Wasatch Range ground water also indicate modern recharge water (Loucks and others, 1989).

Tritium (^{3}H)

Island stable isotopic data and tritium concentrations (>40 tritium units [TU]; table 1), suggest island ground waters are of a modern meteoric origin. Because of atmospheric ^{3}H contamination from post-1952 atmospheric testing of thermonuclear weapons, modern precipitation has ^{3}H concentrations >25 TU. Ground water recharged prior to 1952 has ^{3}H concentrations <4 TU. Modern recharge is consistent with an island water budget in which annual surface discharge is only 2.1 percent of annual precipitation. The budget is based on a mean annual precipitation of 16 inches (40.6 cm) and an island area of 43 square miles (110 km^{2}) and includes some spring discharge data not listed in table 1.

Carbon-13 and Sulfur-34 ($\delta^{13}C$ and $\delta^{34}S$)

Stable carbon isotopic compositions of water samples (table 1) from island crystalline (mean $\delta^{13}C$ = 12.3 ‰) and sedimentary systems (mean $\delta^{13}C$ = -13.2 ‰) suggest island ground waters acquire carbon from the congruent dissolution of soil zone carbonate minerals in the presence of soil zone CO_2 (gas). The $\delta^{13}C$ of all island ground water is consistent with typical soil zone $\delta^{13}C$ evolution where carbonate soil zone minerals (mean $\delta^{13}C$ = 0 ‰; Craig, 1963; Truesdell and Hulston, 1980; Muller and Mayo, 1986) are stoichiometrically dissolved by soil-zone carbonic acid (mean $\delta^{13}C$ = -26 to -20 ‰; Rightmire and Hanshaw, 1973; Fritz and others, 1978).

When sulfate concentrations are very low, the sulfate may be entirely of natural atmospheric sources. Sulfur concentration levels in island ground water (table 3) suggest additional bedrock or soil-zone sources or atmospheric contamination from sources such as smelter plumes and blowing gypsum dust. Sulfate belongs to two groups: 1) ^{34}S-enriched sulfate from the dissolution of evaporite minerals, and 2) ^{34}S-depleted sulfate from reduced sulfur sources such as sulfite minerals, pyrite, soil organic material, and anthropogenic sources. Sulfur fractionation tends to enrich the oxidized sulfate species in ^{34}S (i.e., $\delta^{34}S$ becomes more positive) and tends to enrich the reduced species in ^{34}S (i.e., $\delta^{34}S$ becomes more negative).

The isotopic composition of sulfate in ground water reflects the isotopic composition of the sulfur source. Oxidation of sulfide minerals, the dissolution of gypsum and anhydrite, smelter plumes, and sea spray are the potential sources

Table 5. *Bulk x-ray diffraction and bulk isotopic analyses of eolian deposits collected from the West Desert, Utah.*

Mineralogy (%)	Sample Site	
	Aragonite[1]	Knolls[2]
Amphibole	tr	-
Amorphous	7	1
Aragonite	13	14
Calcite	17	11
Chlorite	1	-
Cristobalite	4	-
Dolomite	5	5
Gypsum	tr	25
Illite/Smectite	5	2
K-Feldspar	4	10
Plagioclase	7	4
Pyrite	1	1
Quartz	34	27
Smectite	2	tr
$\delta^{13}C$ (‰)	+1.5	+1.0
$\delta^{34}S$ (‰)	+9.8	+16.4

[1]Collected from north side of Aragonite I-80 exit at north end of Cedar Mountains (54 miles (86 km) east of Utah-Nevada state line).
[2]Collected at Knolls I-80 exit from great salt flats (38 miles (61 km) east of Utah-Nevada state line). tr = trace

of sulfur in island ground waters. The typical $\delta^{34}S$ of magmatic pyrite is about 0 ‰ (Faure, 1986), a mean value -2.2 ‰ has been reported for Park City District pyrite in the nearby Wasatch Range (Thode and others, 1961), and acid mine drainage in the Wasatch Range has a mean value of -1.1 ‰ (Nielsen and Mayo, 1989). The $\delta^{34}S$ of evaporite rocks varies greatly and generally corresponds to the geologic age of deposition. The $\delta^{34}S$ of near-surface Great Salt Lake brine (mean $\delta^{34}S = {}^{+}15.9$ ‰, table 4) is consistent with the anticipated $\delta^{34}S$ range ($^{+}10$ to $^{+}20$ ‰) of Paleozoic gypsum and anhydrite sources in the central Wasatch Range (Holser and Kaplan, 1966). Gypsum in wind-blown deposits in the Great Salt Lake Desert (locally known as the West Desert) has $\delta^{34}S$ values of $^{+}9.8$ to $^{+}16.4$ ‰ (table 5). The deposits contain up to 25 percent gypsum as identified by x-ray diffraction (XRD) analyses.

Although the mean SO_4^{2-} concentrations in island sedimentary system ground waters are similar to the mean concentration in island crystalline system ground waters (table 3), the $\delta^{34}S$ data suggest different sulfur sources for crystalline and sedimentary systems. The mean $\delta^{34}S$ of two crystalline system ground-water samples is $^{+}1.3$ ‰, whereas the mean $\delta^{34}S$ of three sedimentary system ground-water samples is $^{+}6.7$ ‰ (table 1). The $\delta^{34}S$ composition of the sedimentary system ground water is similar to the mean $\delta^{34}S = {}^{+}7.1$ ‰ of carbonate aquifer ground waters in the Wasatch Range (Mayo and Loucks, 1992) and to the $\delta^{34}S$ values in precipitation near alpine lakes in the Rocky Mountains (Turk, 1990) and is consistent with isotopic fractionation accompanying the dissolution of evaporate minerals. The $\delta^{34}S$ of island crystalline system ground water (mean = $^{+}1.3$ ‰) is closer to the $\delta^{34}S$ (mean = -1.1 ‰) of mine drainage waters in the Wasatch Range (Nielsen and Mayo, 1989) and appears to have a major contribution from a reduced sulfur source.

Solute Geochemistry

Ground waters from island crystalline and sedimentary systems are distinguishable from each other and from non-island ground waters on the basis of the concentrations of one or more of the following: Na^+, Cl^-, SO_4^{2-}, and total solutes. Statistical differences in concentrations were determined with t-tests at a 95 percent confidence interval. Island crystalline system ground waters have mean Na^+, Cl^-, and total solute concentrations of 4.1, 3.2, and 16.0 milliequivalents/liter (meq l^{-1}), respectively, whereas Na-Cl poor island sedimentary system ground waters have mean Na^+, Cl^-, and total solute concentrations of 6.0, 5.9, and 22.7 meq l^{-1}, respectively (table 3). Na-Cl rich island sedimentary system ground waters have mean Na^+, Cl^-, and total solute concentrations of 23.7, 26.3, and 72.2 meq 1^{-1}, respectively.

The chemical composition of island ground waters cannot be solely attributed to the dissolution of aquifer minerals. If lithology were the principal factor controlling solute composition, island crystalline system ground water should be chemically similar to ground water in Wasatch Range systems and island sedimentary system ground water should be chemically similar to Weber Delta aquifer or southern Farmington Bay system ground water (table 3).

Island crystalline and Na-Cl poor sedimentary systems ground waters have mean solute concentrations about 4 and 2.5 times as great as those of ground waters in the Wasatch Range system and Weber Delta aquifer, respectively. Southern Farmington Bay system ground water is more saline than Na-Cl poor island sedimentary system ground water. Mean Na^+, Cl^-, and SO_4^{2-} concentrations of island crystalline ground water are about 8, 16, and 4 times as great, respectively, as those of ground water in the Wasatch Range crystalline system. Mean Na^+, Cl^-, and SO_4^{2-} concentrations in Na-Cl poor island sedimentary system ground waters are about 6, 12, and 4 times as great, respectively, as those of ground waters from the Weber Delta aquifer. The Na-Cl poor island sedimentary system ground water has a mean SO_4^{2-} content 11.5 times as great as that of Na-Cl poor southern Farmington Bay system ground water.

DISCUSSION

Factors which could contribute to the high Na^+, Cl^-, and SO_4^{2-} concentrations in island ground waters include:

1. Mixing with lake brines and/or the dissolution of residual salts precipitated from Lake Bonneville or the Great Salt Lake.
2. Contributions from deeply circulating thermal ground water associated with the Wasatch fault zone or other deep-seated normal faults.
3. Contributions to island sedimentary systems from shallowly circulating non-thermal ground water moving westward beneath the Great Salt Lake from the Wasatch Range.
4. Evaporated soil water from recent precipitation.
5. Aerosol contribution of salts from meteoric recharge water and from dry-fall aerosols.

Mixing with Lake Brine and/or Dissolution of Residual Lake Salts

An estimated 4.4×10^{10} tons (4.5×10^{13} kg) of solutes were removed from ancestral Lake Bonneville and the Great Salt Lake by diffusion into lake bed sediments and by precipitation of Na^+, Cl^-, and SO_4^{2-} bearing minerals (Spencer and others, 1985). However, it is unlikely that the dissolution of residual salts substantially affects the Na^+ and Cl^- content of most island crystalline system ground waters. One island crystalline system spring discharges above the highest Lake Bonneville stage (Bonneville shoreline, 5,250 feet [1,600 m]) and most island crystalline system springs discharge above 4,430 feet (1,350 m) (table 1). At lake levels between the Bonneville and Stansbury shorelines, 5,250 to 4,430 feet (1,600-1,350 m) (Doelling and others, 1990), Na^+ and Cl^- were conserved in Lake Bonneville waters (Spencer and others, 1985); thus Na^+ and Cl^- concentrations in island crystalline system ground waters cannot be directly attributed to lake sources.

At all lake levels, calcite precipitated and minor amounts of SO_4^{2-} precipitated or diffused into lake sediments (Spencer and others, 1985). Supersaturation of most island ground water with respect to calcite (tables 3 and 6) suggests that

Table 6. *Calculated log PCO_2 and saturation indices[1] (SI) of water samples collected on Antelope Island and adjacent areas.*

Sample	log PCO_2	log saturation index (SI) calcite	dolomite	gypsum	halite	quartz	chalcedony	mirabilite
		Antelope Island Crystalline Ground-Water Systems						
1	-2.54	-0.15	-0.53	-2.23	-7.18	0.38	-0.14	-7.21
2	-3.15	0.42	0.56	-2.17	-7.19	0.42	-0.13	-7.11
3	-2.52	-1.11	-0.54	-2.11	-6.99	0.25	-0.28	-7.12
4	-3.93	0.89	1.51	-2.18	-6.92	0.34	-1.88	-7.72
5	-4.07	1.39	2.63	-1.85	-6.45	0.19	-0.48	-6.53
6	-2.55	0.33	0.33	-1.62	-6.30	0.82	0.28	-6.34
7	-3.21	0.72	1.18	-1.90	-6.52	0.31	-0.24	-6.60
8	-2.72	0.35	0.52	-1.48	-5.91	0.23	-0.31	-5.80
9	-2.90	0.36	0.53	-2.00	-6.93	0.32	-0.21	-6.95
10	-2.51	0.20	-0.01	-1.63	-6.19	1.21	0.20	-6.34
11	-3.57	0.25	1.19	-2.65	-6.30	0.61	0.07	-6.29
12	-3.03	0.17	0.15	-2.05	-6.93	0.27	-0.25	-7.10
mean	-3.06	0.32	0.63	-1.99	-6.65	0.45	-0.28	-6.75
		Antelope Island Sedimentary Ground-Water Systems						
13	-2.97	0.49	0.58	-2.04	-6.13	0.32	0.49	-7.74
14	-3.05	0.41	0.47	-1.99	-6.90	0.16	-0.36	-7.10
15	-1.70	0.44	0.56	-1.27	-4.94	0.81	0.29	-4.94
16	-2.69	0.55	0.87	-1.80	-5.78	1.01	0.49	-6.10
17	-4.80	2.16	4.06	-1.69	-5.69	0.50	-0.05	-5.47
18	-2.71	0.31	0.36	-1.78	-6.44	0.64	0.12	-6.64
19	-3.27	0.94	1.74	-2.29	-6.32	0.33	-0.20	-6.66
20	-2.64	0.68	1.16	-1.33	-4.91	0.55	0.02	-5.01
mean	-2.99	0.75	1.23	-1.77	-5.89	0.54	0.10	-6.21
		Southern Farmington Bay Ground-Water Systems						
21	-2.56	0.29	0.65	-3.50	-5.73	0.66	0.29	-7.35
22	-2.81	0.26	0.37	-3.84	-6.20	0.69	0.22	-8.14
23	-2.87	0.18	0.50	-3.42	-5.50	0.65	0.15	-7.15
24	-2.95	0.00	0.08	-3.97	-6.21	0.68	0.18	-7.88
25	-2.61	0.09	0.06	-3.92	-5.92	1.00	0.51	-7.82
26	-2.56	0.10	0.32	-4.00	-5.71	0.67	0.16	-7.02
27	-2.54	0.17	0.47	-3.64	-0.56	0.72	0.17	-7.05
28	-2.71	0.22	0.60	-3.66	-5.51	0.70	0.18	-6.79
29	-3.19	-0.08	-0.41	-2.45	-5.92	0.45	-0.06	-6.67
30	-2.13	-0.10	-0.58	-3.14	-5.83	0.77	0.25	-7.49
31	-2.59	0.28	0.36	-2.47	-5.03	0.95	0.28	-6.70
32	-2.46	0.41	1.07	-2.50	-4.42	0.69	0.18	-5.58
33	-2.84	0.22	0.70	-1.52	-4.03	0.74	0.21	-3.76
34	-2.04	0.20	0.15	-3.05	-5.01	1.10	0.58	-6.32
mean	-2.63	0.16	0.31	-3.22	-5.11	0.75	0.24	-6.84
meanw/o 32 and 33	-2.63	0.13	0.21	-3.42	-5.26	0.76	0.25	-7.20
		Weber Delta Aquifer						
35	-2.46	0.00	-0.40	-3.79	-7.92	0.68	0.17	-9.58
36	-2.52	-0.13	-0.71	-3.42	-7.91	0.84	0.33	-9.13
37	-1.85	-0.16	-0.53	-3.16	07.66	0.82	0.30	-8.57
38	-2.72	0.07	-0.17	-4.23	-7.78	0.67	0.16	-9.84
39	-2.11	-0.07	-0.59	-2.19	-8.04	0.63	0.10	-8.49
40	-2.49	0.08	-0.30	-2.43	-8.25	0.63	0.10	-8.77
41	-2.76	-0.15	-0.75	-3.07	-8.46	0.61	0.08	-9.49
42	-2.58	0.40	0.41	-3.28	-7.86	0.68	0.16	-9.19
43	-2.75	0.38	0.41	-3.79	-8.18	0.68	0.38	-9.98
44	-2.29	0.12	-0.14	-2.48	-7.64	0.65	0.13	-8.44
45	-2.17	0.11	-0.24	-2.15	-7.96	0.51	-0.03	-8.51
46	-2.05	0.02	-0.41	-2.09	-8.01	0.53	-0.01	-8.31
47	-1.91	-0.04	-0.52	-2.12	-7.92	0.52	-0.01	-8.17
48	-2.04	0.31	-0.38	-2.11	-8.01	0.52	-0.02	-8.26
49	-2.14	-0.10	-0.68	-2.19	-7.93	0.54	-0.10	-8.44
50	-2.32	0.15	-0.07	-2.19	-8.26	0.51	-0.01	-8.73
51	-2.52	0.14	-0.01	-3.85	-7.93	0.67	0.14	-9.58
mean	-2.33	0.07	-0.30	-2.86	-7.98	0.63	0.11	-8.91
		Wasatch Range Ground-Water Systems						
52	-2.58	-0.81	-1.82	-2.61	-8.33	-	-	-8.37
53	-2.53	-1.33	-2.79	-2.91	-8.49	-	-	-8.74
54	-3.33	-0.38	-1.29	-3.02	-9.06	-	-	-9.59
55	-2.80	-0.78	-2.08	-2.82	-8.86	-	-	-9.19
mean	-2.81	-0.83	-2.00	-2.84	-8.69	-	-	-8.97
		Thermal Ground Water						
56	-2.51	1.18	2.16	-0.72	-4.17	0.06	1.18	-4.99
57	-2.23	1.16	2.03	-0.54	-3.32	0.21	1.16	-4.79
58	-1.01	0.11	-0.85	-1.20	-2.96	0.28	-0.09	-5.35
59	-1.52	0.39	-0.39	-1.63	-3.66	0.43	0.06	-5.93
60	-1.34	0.38	0.47	-1.97	-3.77	0.19	0.81	-6.68
mean	-1.72	0.64	0.68	-1.21	-3.58	0.23	0.62	-5.55

[1] Saturation: log SI = 0.00 ± 0.1

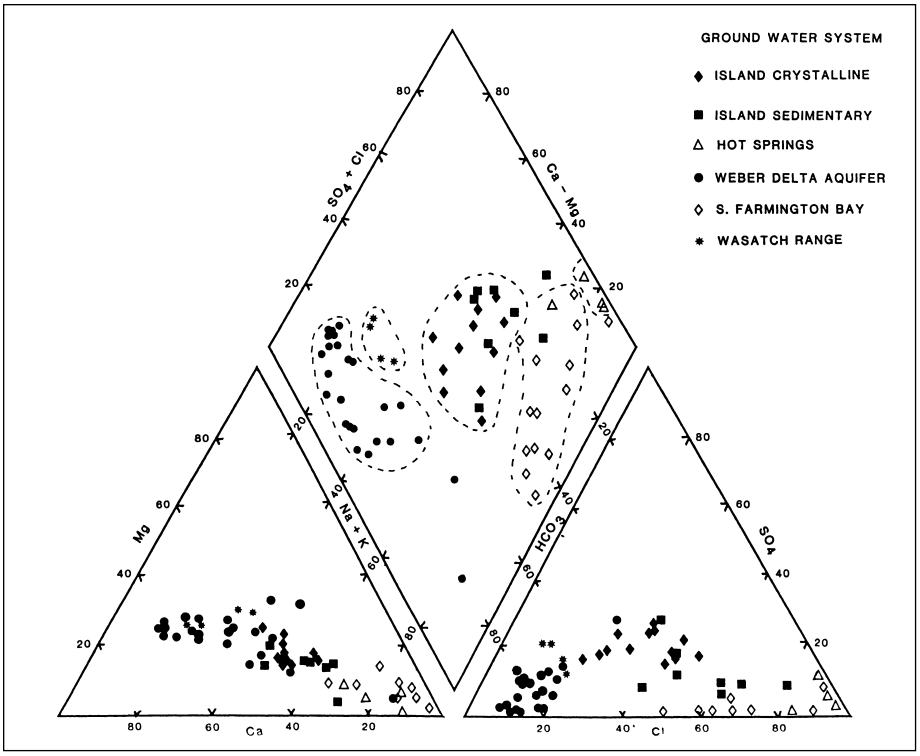

Figure 4. *Trilinear diagram of ground-water analyses of water samples collected in the vicinity of Antelope Island.*

factors other than calcite dissolution control the Ca^{2+} concentrations. Possible controls are discussed later. Because the lake level has been below most island crystalline system spring discharge elevations for the past 15,000 years (Spencer and others, 1984), ample time has passed for the more active bedrock ground-water flow systems to leach minor amounts of highly soluble residual material from fractures in the crystalline rocks. Additionally, the mean $\delta^{34}S$ of island crystalline system ground waters suggests a reduced sulfur source rather than the dissolution of an oxidized sulfur source such as gypsum.

Discharge elevations preclude modern brine from mixing with island sedimentary system ground waters which discharge as springs. However, late Pleistocene and historic fluctuations of lake levels (Currey and others, 1984; Spencer and others, 1985; Doelling and others, 1990) could have influenced the Na^+, Cl^-, and SO_4^{2-} content of ground water in island sedimentary and southern Farmington Bay systems by brine diffusion, infiltration, or mineral precipitation. Both halite and mirabilite have precipitated from lake brine since 1930 (Eardley, 1966; Whelan, 1973; Butts, 1980), and since 1955, halite precipitation has controlled the lake's Cl^- content (Spencer and others, 1985).

Solute data of water from both the Wasatch Range system and the Weber Delta aquifer tend to plot near the Ca-Mg-HCO_3 domain in the trilinear diagram (figure 4). Southern Farmington Bay system ground water is of the Na^+ - Cl^- type and island sedimentary system ground water has an affinity for the Na^+ - Cl^- type (figure 4). The Na^+ and Cl^- concentrations and stable sulfur isotopic data suggest interaction between southern Farmington Bay system ground water and diagenetic mineral precipitates and/or lake brine and interactions between island sedimentary system ground water and diagenetic mineral precipitates.

It is reasonable to assume that Cl^- and SO_4^{2-} are conservative ions in study area ground waters because all ground waters are undersaturated with respect to all minerals containing these species (table 3). Other species, particularly cations, cannot be considered conservative because of possible ion exchange reactions or precipitation due to mineral supersaturation. Thus, the relationships between SO_4^{2-} vs. Cl^- concentrations in figure 5 may be used to evaluate both Cl^- and SO_4^{2-} sources. In the figure, island sedimentary and southern Farmington Bay system ground waters plot away from the precipitation-brine mixing line, suggesting that mixing with brine is minimal at most locations.

The relationship between island and southern Farmington Bay system ground-water SO_4^{2-} concentrations (figure 5) is also worthy of note. The mean SO_4^{2-} concentration of Na-Cl poor southern Farmington Bay system ground water is only marginally greater than the mean in Salt Lake City precipitation (Christensen and others, 1984) and is an order of magnitude less than the mean SO_4^{2-} concentration of island ground waters (tables 3 and 7).

The low SO_4^{2-} content of most southern Farmington Bay system ground waters is an enigma because the ground water flows through offshore Lake Bonneville sediments. Observed concentrations suggest either a paucity of sulfate-bearing minerals in the ground-water system or sulfate reduction.

Table 7. *Summary of solute concentrations in northern Sierra Nevada and Salt Lake City, Utah precipitation.*

	meq l^{-1}						
Location	Ca^{2+}	Mg^{2+}	Na^+	K^+	HCO_3^-	SO_4^{2-}	Cl^-
Northern Sierra Nevada[1]	0.019	0.007	0.019	0.008	0.048	0.019	0.014
Salt Lake City[2]	0.118	0.031	0.057	0.007	0.084	0.112	0.049

[1] After Feth and others (1964).
[2] After Christensen and others (1984).

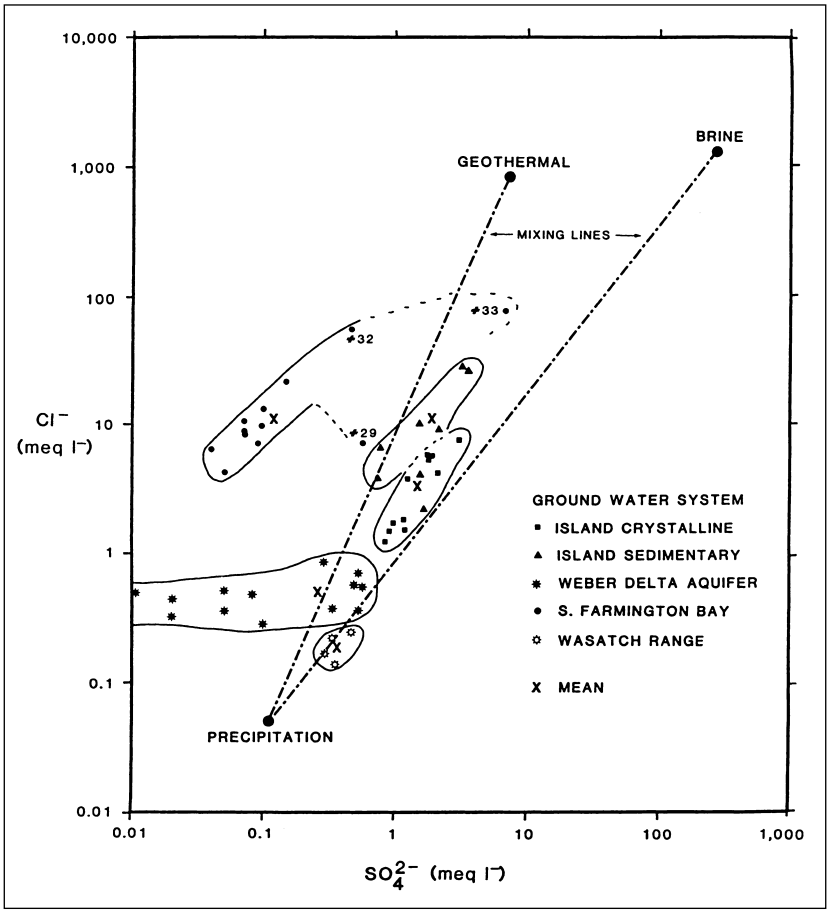

Figure 5. *Plot of Cl^- vs. SO_4^{2-} concentrations in water samples collected in the vicinity of Antelope Island. Dashed lines represent linear mixing of precipitation with geothermal and lake-brine sources.*

The ground-water system should contain sulfate-bearing minerals but, to date, no field or laboratory data indicate sulfate reduction or another process in the ground-water system which would reduce the sulfur content.

Contribution from Circulating Thermal Water

Thermal ground waters discharge 20 miles (32 km) east of Antelope Island along normal faults at the base of the Wasatch Range (Goode, 1978; Cole 1981, 1983). The thermal systems are believed to be recharged high in the Wasatch Range and, based on geochemical thermometers, to attain water temperatures as great as 248°F (120°C) and to circulate to depths as great as 2 miles (3 km) (Cole, 1981, 1983). Thermal discharges are of the Na^+ - Cl^- type (figure 4) and have mean Na^+, Cl^-, SO_4^{2-} concentrations of about 158.5, 183.2, and 7.6 meq l^{-1}, respectively (table 3). Mixing of thermal ground waters with ground water from the overlying, shallow, cool-temperature Weber Delta aquifer has been noted near the base of the Wasatch Range (Cole, 1981).

Mixing of thermal fluids with island ground water is a possible source of the high Na^+, Cl^-, and SO_4^{2-} concentrations observed in island ground waters. Thermal ground water could migrate along sedimentary aquifers beneath the Great Salt Lake or upward along normal faults cutting the island. A mean elevation difference >2,000 feet (>600 m) between the crest of the Wasatch Range and the crest of the island could provide an adequate hydraulic gradient.

The δ^2H, $\delta^{18}O$, and $\delta^{34}S$ compositions of island ground water do not preclude nor suggest mixing with thermal ground water, because only small amounts of thermal water are needed to mix with precipitation to obtain the stable isotopic and total solute concentrations observed in island ground waters. However, the following analysis suggests thermal contributions are unlikely.

Neither island crystalline or sedimentary system ground waters plot along the thermal-precipitation water mixing line in figure 5. PHREEQE (Parkhurst and others, 1980) calculations demonstrate that thermal ground waters will remain undersaturated with respect to Cl^- and SO_4^{2-} bearing minerals when cooled to island ground-water discharge temperatures or when mixed with precipitation. Therefore, mineral precipitation cannot occur and the mixed water must receive similar contributions of Cl^- concentrations in island crystalline, Na-Cl poor sedimentary and Na-Cl rich sedimentary system waters require thermal ground-water contributions of 1.6 and 3.0 and 14.1 percent, respectively, whereas observed mean SO_4^{2-} concentrations require thermal ground-water contributions of 15.5, 14.7, and 40.4 percent, respectively. These percentages are based on the assumption that unmixed island crystalline and sedimentary system ground waters are similar to their ground-water counterparts in Wasatch Range systems and the Weber Delta aquifer. If the southern Farmington Bay system is the appropriate counterpart for the island sedimentary system, mixing would require the unlikely proposition that thermal ground-water SO_4^{2-} mixes and thermal ground-water Cl^- does not.

Contribution From Non-thermal Ground Water Beneath the Great Salt Lake

Ground-water systems in the East Shore area extend beneath the Great Salt Lake and ground-water movement is generally eastward toward Antelope Island (Bolke and Waddell, 1972). The East Shore area is located between the Weber Delta and Salt Lake City. Bolke and Waddell (1972) identified a Na^+ - Cl^- type water from the 423 to 475 foot (129-145 m) depth interval in a flowing artesian well which tapped the ground-water system beneath the lake. The well was located 0.5 miles (0.8 km) northeast of Antelope Island and was constructed on the causeway connecting Antelope Island with the east shore mainland.

Based on a cursory examination of the water quality from the well and from springs located at the north end of the island, Bolke and Waddell (1972) suggested that some Antelope Island ground water may contribute to ground-water systems beneath the Great Salt Lake. Because the hydraulic head of the aquifer beneath the lake is above lake level, it is possible that ground-water systems beneath the lake may contribute to island ground-water systems. In 1969 when the water quality sample was collected, the well free flowed 280

gallons/minute (gpm) ($17.71s^{-1}$) and the static head rose to an elevation of about 4,250 feet (1,295 m), which is above the discharge elevation of several island sedimentary system springs (table 1).

Although the Na^+ and Cl- contents of the two groundwater systems are similar, SO_4^{2-} data suggest that groundwater systems beneath the Great Salt Lake do not contribute significant quantities of water to island sedimentary groundwater systems. The SO_4^{2-} content of the well water is only 0.25 meq l^{-1}, whereas the mean SO_4^{2-} island sedimentary system which discharges below 4,250 feet (1,295 m) is 1.64 meq 1^{-1}.

Evaporated Soil Water from Recent Precipitation

Mean Na^+, Cl^-, and SO_4^{2-} concentrations in Salt Lake City precipitation (table 7) are 0.057, 0.049, and 0.112 meq l^{-1}, respectively (Christensen and others, 1984). Chemical composition of precipitation data are not available for Antelope Island. Mean Na^+, Cl^-, and SO_4^{2-} loads of Antelope Island ground waters are considerably greater than those of Salt Lake City precipitation. It is not unreasonable to expect the solute content of recharge water to be enriched with respect to precipitation due to the concentrating effect of evapotranspiration (E-T). When the anticipated effect of aquifer mineral dissolution is accounted for, the ratios of conservative ions should be similar in precipitation and recharge water. The Wasatch Range system and Weber Delta aquifer are the assumed counterparts for the island crystalline and sedimentary aquifers, respectively. The southern Farmington Bay system is not appropriate because of its low SO_4^{2-} content. Island bedrock, Na-Cl poor sedimentary, and Na-Cl rich sedimentary system ground waters have Na^+ plus Cl^- concentrations about 62, 98, and 458 times greater, respectively, than Salt Lake City precipitation, whereas SO_4^{2-} concentrations in respective island ground waters are only about 10, 10, and 27 times as great. Differences in mean Cl^-/SO_4^{2-} ratios further suggest that the E-T concentration of recharge precipitation alone cannot account for the high Na^+, Cl^-, and SO_4^{2-} concentrations observed in island ground waters. The ratios are 0.44 in Salt Lake City precipitation, 2.1 in island bedrock systems, 4.3 in Na-Cl poor island sedimentary systems, and 22.9 in Na-CI rich island sedimentary systems. Mean Na^+/SO_4^{2-} ratios are similar to mean Cl^-/SO_4^{2-} ratios.

Meteoric and Aerosol Contributions

Snow in the northern Sierra Nevada Range has mean Na^+, Cl^-, and SO_4^{2-} concentrations of 0.019, 0.014, and 0.019 meq 1^{-1}, respectively (Feth and others, 1964). Precipitation data from 6 stations located at elevations below the Bonneville shoreline near Salt Lake City show mean solute concentrations up to 6 times of those in precipitation in the Sierra Nevada Range (table 7). Storm tracks affecting the Great Salt Lake area are predominantly from the Pacific Ocean located 600 miles to the west (Richardson, 1974). The Cl^-/Na^+ ratio in sea water is about 1.8. The Cl^-/Na^+ ratio in Pacific storm precipitation decreases from about 1.4 along the California coast to about 0.5 along the eastern edge of the Sierra Nevada Range. In the immediate area of the Great Salt Lake, an increase in the ratio to about 1.0 is attributed by Junge and Werby (1958) to the effects of wind-blown dust and lake brines. Island crystalline systems, Na-Cl poor island sedimentary systems, and Na-Cl rich island sedimentary systems have Cl^-/Na^+ ratios of about 0.8, 1, and 1.1, respectively.

High Na^+, Cl^-, and SO_4^{2-} concentrations in ground waters have been attributed to cyclic salting (i.e., salt input to ground water from precipitation containing ocean, saline lake and playa-derived aerosols, sea spray, etc.) and dust-derived aerosols associated with dry fall and precipitation. Precipitation from sea salt sources, such as the ocean or the Great Salt Lake, tend to be enriched in Na^+ and Cl^- ions with respect to rain from atmospheric moisture which is derived from fresh water sources. However, SO_4^{2-} in precipitation tends to have a terrestrial rather than saline water origin (Berner and Berner, 1987; Munger, 1982). In Australia, Evans (1982), Hingston and Gailitis (1976), and Van Dijk (1969) demonstrated significant contributions to the Na^+ and Cl^- content of ground waters from cyclic salt in precipitation in low volume recharge regimes and from sea spray in the form of dry fall. In the Edwards Aquifer, Texas, Rightmire and others (1974) attributed a mean ground-water SO_4^{2-} concentration of 0.4 meq 1^{-1} and concentrations as great as 1.7 meq 1^{-1} to dust aerosols.

Sources of cyclic salt and dust borne aerosols in island recharge water include dust blown off large salt flats and soils developed on Lake Bonneville evaporite-rich sediments in the desert west of the Great Salt Lake, airborne salts released as white cap spray accompanying wind storms on the lake, and cyclic salt in precipitation originating as evaporated lake water.

GEOCHEMICAL EVOLUTION

A geochemical evolution model of island ground water must account for the observed solute and isotopic differences between the island ground-water system types as well as differences between island ground water and their ground-water system counterparts located elsewhere. The δ^2H, $\delta^{18}O$, and ^3H data indicate that island ground waters are recharged from modern meteoric water containing a component of evaporated Great Salt Lake water. The $\delta^{13}C$ data suggest island ground waters acquire carbon from the congruent, stoichiometric dissolution of soil zone carbonate minerals in the presence of soil zone CO_2 (gas).

Solute and isotopic data suggest that the chemical evolution of island ground water is dependent upon more than one of the following mechanisms:

1. Dissolution of aquifer minerals.
2. Mixing with Great Salt Lake brine, geothermal water or shallow artesian aquifer ground water beneath the Great Salt Lake.
3. The distribution of solutes in precipitation and wind-blown aerosols.

However, mixing lines (figure 5) suggest that it is unlikely that modern lake brines or geothermal fluids contribute significantly to the solute content of island ground water. The

Table 8. *Potential contribution of dissolved Cl^- and SO_4^{2-} in Antelope Island ground waters from the dissolution of aquifer minerals, precipitation, and wind-borne aerosols.*

Chloride Sources

Island Ground Water System	Mean Conc. (meq l^{-1})	Aquifer Contribution Source[1]	meq l^{-1}	%	Meteoric and Aerosol Contributions: Alternative A[2] Precipitation meq l^{-1}	%	Alternative A[2] Blown Aerosol meq l^{-1}	%	Alternative B[3] (X5) Precipitation meq l^{-1}	%	Alternative B[3] (X5) Blown Aerosol meq l^{-1}	%	Alternative C[4] (X10) Precipitation meq l^{-1}	%	Alternative C[4] (X10) Blown Aerosol meq l^{-1}	%
Crystalline	3.19	WR	0.20	6.3	0.05	1.6	2.94	92.1	0.25	7.8	2.74	85.9	0.49	15.4	2.50	78.3
Na-Cl Poor Sed.	5.90	WA	0.50	8.5	0.05	0.09	5.35	90.6	0.25	4.3	5.15	87.2	0.49	8.3	4.91	83.2
Na-Cl Poor Sed.	5.90	SFB	10.25	170.7[5]	0	0	0	0	0	0	0	0	0	0	0	0

Sulfate Sources

Island Ground Water System	Mean Conc. (meq l^{-1})	Aquifer Contribution Source[1]	meq l^{-1}	%	Meteoric and Aerosol Contributions: Alternative A[2] Precipitation meq l^{-1}	%	Alternative A[2] Blown Aerosol meq l^{-1}	%	Alternative B[3] (X5) Precipitation meq l^{-1}	%	Alternative B[3] (X5) Blown Aerosol meq l^{-1}	%	Alternative C[4] (X10) Precipitation meq l^{-1}	%	Alternative C[4] (X10) Blown Aerosol meq l^{-1}	%
Crystalline	1.52	WR	0.35	23.0	0.11	7.2	1.06	59.8	0.56	36.9	0.61	40.1	1.12	73.7	0.05	3.3
Na-Cl Poor Sed.	1.58	WA	0.27	19.6	0.11	8.0	1.00	72.4	0.56	40.6	0.55	39.9	1.12	81.2	0	0
Na-Cl Poor Sed.	1.58	SFB	10.12	8.7	0.11	8.0	1.15	83.3	0.56	40.6	0.70	50.7	1.12	81.2	0.14	10.1

[1] Mean concentration in Wasatch Range systems (WR), Weber Delta aquifer (WDA), and southern Farmington Bay systems (SFB).
[2] Contribution from precipitation as measured near Salt Lake City and wind-blown aerosols, when precipitation is not concentrated by E-T.
[3] Contribution from precipitation as measured near Salt Lake City and wind-blown aerosols, when precipitation is concentrated by an E-T factor of 5.
[4] Contribution from precipitation as measured near Salt Lake City and wind-blown aerosols, when precipitation is concentrated by an E-T factor of 10.
[5] Potential contribution from aquifer source exceeds ground-water content, so alternatives not possible.

chemical evolution of island ground water must, therefore, involve the accumulation of ions from the dissolution of aquifer minerals, solutes in precipitation, and wind-blown dust. It is not our intent to present a quantitatively unique mechanism; rather, it is to demonstrate a plausible mix of solute sources consistent with observations.

The excess Cl^- and SO_4^{2-} content of island crystalline and Na-Cl poor sedimentary system ground waters, with respect to their mainland and southern Farmington Bay system counterparts, can be accounted for by varying mixes of precipitation and aerosol sources (table 8). Contributions of Cl^- and SO_4^{2-} from the dissolution of aquifer minerals are assumed to equal the mean concentrations of their aquifer counterparts. The southern Farmington Bay system is a less likely mineralogical counterpart than is the Weber Delta aquifer, because the southern Farmington Bay system contains appreciable quantities of lake-bottom sediments and the ground water in the southern Farmington Bay system has a very low mean SO_4^{2-} content and a mean Cl^- content approximately two to three times as great as the mean content of island ground water.

Solutes in Salt Lake City precipitation, concentrated by an island E-T factor of 10, can account for most excess SO_4^{2-} and minor amounts of Cl^- observed in island ground waters. Reducing the E-T concentration factor to 5 requires a substantial percentage increase in windblown SO_4^{2-} but a much smaller percentage increase in windblown Cl^-. If solutes are not concentrated by island E-T, approximately 90 percent of the excess Cl^- and 60 to 70 percent of the excess SO_4^{2-} must be accounted for by wind-blown dust and white cap spray, dry fall deposition, or precipitation of brine.

The lack of precipitation and dry-fall depositional data from the island makes it difficult to quantify the depositional load that these sources contribute to island ground water. Wind storms often blow up clouds of salt dust from the West Desert prior to precipitation events (Eubank and Brough, 1980). When combined with light rain, the salt crystals form a precipitation brine responsible for dozens of power line fires each year in the West Desert. Because the island is located closer to particulate and aerosol sources (i.e., the salt flats of the West Desert, the sea spray of Great Salt Lake, and industrial smelter plumes) than are the precipitation/dry fall monitoring stations near Salt Lake City, it is reasonable to expect the depositional load on the island to be somewhat greater than that observed in Salt Lake City.

Regardless of the E-T concentration factor, the calculated contribution attributed to windblown Cl^- in the island sedimentary systems is about two times as great as that of island crystalline systems, whereas the windblown SO_4^{2-} contribution remains about equal in both ground-water systems. The idea of greater windblown Cl^- contributions to lower elevation systems (i.e., the island sedimentary system) is consistent with the anticipated stratification of sea spray and saltdust during wind storms. The greatest concentration of large salt particles and chloride-rich sea spray should be near lake level. However, stratification of windblown Cl^- may not totally explain the elevated Cl^- content of island sedimentary system ground water. Most island sedimentary systems are located on the prevailing lee side (east side) of the island where the effects of windblown Cl- stratification should be reduced. Some of the apparent excess Cl^- may be the result of brine diffusion, infiltration, or mineral precipitation when lake levels were previously higher. The local occurrence of Na-Cl rich island sedimentary ground-water systems, at the southeast edge of the island, suggests such sources.

Although a mix of precipitation, dry fall, and West Desert wind storm dust contributions can account for most excess Cl^- and SO_4^{2-} concentrations in island ground water and the $\delta^{34}S$ (table 1) of island sedimentary systems (mean $\delta^{34}S = +6.7\ ^0/_{00}$), these sources cannot account for the $\delta^{34}S$ of island crystalline system ground water (mean $\delta^{34}S = +1.3\ ^0/_{00}$). Because the SO_4^{2-} content of island crystalline system ground water is considerably greater than the non-island ground-water systems, the $\delta^{34}S$ of island crystalline system ground water requires more in situ sulfur dissolution than anticipated or an external source of reduced sulfur in addition to the isotopically heavy sulfur contributed from sea spray and West Desert dust. Nearby smelter and other industrial plumes are a potential source of reduced sulfur. Greater contributions of isotopically light sulfur to the island crystalline systems, which are located at the higher elevations, may result from the stratified deposition of sea spray, sea fog, and dust storm deposited Cl^- and SO_4^{2-} and smelter plume sulfur. The island's higher elevations are more likely to intercept smelter plume gases than are the lower elevations.

Nonconservative cations, such as Na^+, Ca^{2+}, and Mg^{2+}, are also found in greater concentrations in island ground waters than in their aquifer counterparts located to the east. PHREEQE (Parkhurst and others, 1980) calculations at ground-water discharge temperatures indicate that calcite and dolomite supersaturation of island ground waters cannot be attributed to the common ion and ionic strength effects associated with the introduction of windblown calcite, dolomite, gypsum, and halite. Observed supersaturation may be attributed to wet and dry fall of more soluble saline lake mineral species such as epsomite ($MgSO_4 \cdot 7H_2O$), glauberite ($Na_2Ca(SO_4)_2$), magnesite ($MgCO_3$), mirabilite ($Na_2SO_4 \cdot 10H_2O$), thenardite (Na_2SO_4), and tychite ($Na_6Mg_2(SO_4)(CO_3)_4$), and to aerosol contamination from industrial stacks in the West Desert.

With existing data, it is not possible to assign percentage contributions to natural and air pollution sources of the observed differences in island crystalline and sedimentary system ground-water $\delta^{34}S$ contents and to the apparent excess of nonconservative cations. The island's crystalline bedrock itself is not highly mineralized; however, the island is a linear fault block which is parallel to and tectonically related to the highly mineralized fault blocks to the south. The island is also located in the pathway of smelter and other industrial plumes originating in Magna and the West Desert which carry sulfur and other elements.

Quantification of the contribution to island ground-water chemistry from natural and air pollution sources of aerosols, dust, and sea spray, requires additional study. Such a study would entail soil sampling and synoptic snow, wet-fall and dry-fall monitoring on the island.

REFERENCES CITED

Berner, E.K., and Berner, R.A., 1987, The global water cycle: Prentice Hall, Englewood Cliffs, New Jersey, 397 p.

Bolke, E.L., and Waddell, K.M., 1972, Ground-water conditions in the East Shore area, Box Elder, Davis and Weber Counties, Utah 1960-1969: Utah Department of Natural Resources Technical Publication 35, 59 p.

Butts, D.S., 1980, Factors affecting the concentration of Great Salt Lake brines, *in* Gwynn, J.W., editor, Great Salt Lake - A scientific, historical and economic overview: Utah Geological and Mineralogical Survey Bulletin 116, p. 116-168.

Christensen, RC., Stephens, D.W., Pyper, G.E., McCormack, H.F., and Weigel, J.F., 1984, Quality and quantity of runoff and atmospheric deposition in urban areas of Salt Lake County, Utah: U.S. Geological Survey Water-Resources Investigation Report 84-4011, 223 p.

Cole, D.R., 1981, Isotopic and ion chemistry of waters in the East Shore area, northern Utah: Geothermal Research Council, Transactions, v. 5, p. 63-66.

Cole, D.R., 1982, Tracing fluid sources in the East Shore area, Utah: Groundwater, v. 20, no. 5, p. 586-593.

Cole, D.R., 1983, Chemical and isotopic investigations of warm springs associated with normal faults in Utah: Journal of Volcanology and Geothermal Research, v. 16, p. 65-98.

Craig, H., 1961, Isotopic variations in meteoric waters: Science, v. 133, p. 1702-1703.

---1963, The isotopic geochemistry of water and carbon in geothermal areas, *in* Nuclear geology on geothermal areas; Spoleto, Italy, September 9-13, 1963: Cons. Naz. Ric. (Nuclear Geology Laboratory), Pisa, 53 p.

Currey, D.R., Atwood, Genevieve, and Mabey, D.R., 1984, Major levels of Great Salt Lake and Lake Bonneville: Utah Geological and Mineralogical Survey Map 73, scale 1:750,000.

Doelling, H.H., Willis, G.C., Jensen, M.E., Hecker, Suzanne, Case, W.F., and Hand, J.S., 1990, Geologic map of Antelope Island, Davis County Utah: Utah Geological and Mineral Survey, Map 127, 27 p., scale 1:24,000.

Eardley, A.J., 1966, Sediments of Great Salt Lake, *in* Stokes, W.L., editor, Great Salt Lake: Utah Geological Society, Guidebook to Geology of Utah, number 20, p. 105-120.

Eubank, M.E., and Brough, R.C., 1980, The Great Salt Lake and its influence on the weather, *in* Gwynn, J.W., editor, Great Salt Lake - A scientific, historical and economic overview: Utah Geological and Mineralogical Survey Bulletin 116, p. 279-283.

Evans, W.R., 1982, Factors affecting water quality in a regional fractured rock aquifer: Australian Water Research Council, Conference on Groundwater in Fractured Rock, Conference Series 5, p. 57-69.

Faure, Gunter, 1986, Isotope Geology, 2nd edition: New York, Wiley and Sons, 589 p.

Feth, J.H., Rogers, S.M., and Roberson, C.E., 1964, Chemical composition of snow in the northern Sierra Nevada and other areas: U.S. Geological Survey Water-Supply Paper 1535-J, 39 p.

Feth, J.H., Barker, D.A., Moore, L.G., Brown, R.J., and Veirs, C.E., 1966, Lake Bonneville; geology and hydrology of the Weber Delta District, including Ogden, Utah: U.S. Geological Survey Professional Papers 518, 74 p.

Fontes, J.C., 1980, Environmental isotopes in groundwater hydrology, *in* Fritz, P. and Fontes, J.C., editors, Handbook on environmental isotope geochemistry, volume 1, The terrestrial environment: Elsevier, Amsterdam, p. 75-140.

Fritz, Peter, Reardon, E.J., Barker, J., Brown, R.M., Cherry, J.A., Killey, R.W.D., and McNaughton, D., 1978, The carbon isotope geochemistry of a small ground-water system in northeastern Ontario: Water Resources Research, v. 14, no. 6, p. 1059-1067.

Goode, H.D., 1978, Thermal waters of Utah: Utah Geological and Mineral Survey Report of Investigations 129, 183 p.

Hingston, F.J., and Gailitis, V., 1976, The geographic variation of salt precipitated over Western Australia: Australian Journal of Soil Research, v. 14, p. 319-335.

Hintze, L.F., 1988, Geologic History of Utah: Brigham Young University Geology Studies, v. 20, part 3, 181 p.

Holser, W.T., and Kaplan, I.R., 1966, Isotope geochemistry of sedimentary sulfur: Chemical Geology, v. 1, p. 93-135.

Junge, C.E., and Werby, R.T., 1958, The concentration of chloride, sodium, potassium, calcium and sulfate in rainwater over the United States: Journal of Meteorology, v. 15, p. 417-425.

Loucks, M.D., Mayo, A.L., and Brimhall, W.H., 1989, Fault control of groundwater flow in the central Wasatch Range, Utah, evaluated by geochemical means: Geological Society of America Abstract with Programs, v. 21, no. 5., p. 108.

Marine, I.W., and Price, D., 1964, Geology and ground-water resources of the Jordan Valley, Utah: Utah Geological and Mineralogical Survey, Water Resource Bulletin 7, 68 p.

Mayo, A.L., and Loucks, M.D., 1992, Ground-water flow systems in the central Wasatch Range, Utah: Utah Geological Survey, Contract Report 92-6, 116 p.

Muller, A.B., and Mayo, A.L., 1986, ^{13}C variation in limestone on an aquifer-wide scale and its effects on groundwater ^{14}C dating models: Radiocarbon, v. 28, no. 3, p. 1041-1054.

Munger, J.W., 1982, Chemistry of atmospheric precipitation in the north central United States - Influence of sulfate, nitrate, ammonia and calcareous soil particulates: Atmospheric Environment, v. 16, no. 7, p. 1633-1645.

Nielsen, P.J., and Mayo, A.L., 1989, Chemical and isotopic investigation of the cause of acid and neutral mine discharges in the central Wasatch Range, Utah, *in* Cordy, G.E., editor, Geology and hydrology of hazardous-waste mining-waste, and repository sites in Utah: Utah Geo-

logical Association Publication 17, p. 121-134.

Parkhurst, D.L., Thorstenson, D.C., and Plummer, L.N., 1980, PHREEQE - A computer program for geochemical calculations: U.S. Geological Survey Water-Resources Investigation Report 80-96, 193 p.

Piper, A.M., 1944, A graphic procedure in the geochemical interpretation of water analysis: Transactions, American Geophysical Union, v. 25, p. 914-928.

Plantz, G.G., Appel, C.L., Clark, D.W., Lambert, P.M., and Puryear, R.L., 1986, Selected hydrologic data from well in the East Shore area of the Great Salt Lake, Utah, 1985: Utah Department of Natural Resources, Basic-Data Report 45 [also as U.S. Geological Survey Open-File Report 86-139], 75 p.

Plummer, L.N., Jones, B.F., and Truesdell, A.H., 1976, WATEQF - A FORTRAN IV version of WATEQF, a computer program for calculating chemical equilibrium of natural waters: U.S. Geological Survey Water-Resources Investigation Report 76-13, 61 p.

Richardson, A.E., 1974, Climate, *in* Austin, L.H., editor, Great Salt Lake - Climate and hydrogeologic systems: Utah Department of Natural Resources, Division of Water Resources, p. 11-17.

Rightmire, C.T., and Hanshaw, B.B., 1973, Relationship between the carbon isotope composition of soil CO_2 and dissolved carbonate species in ground water: Water Resources Research, v. 9, no. 4, p. 958-967.

Rightmire, C.T., Pearson, F.J., Back, W., Rye, R.O., and Hanshaw, B.B., 1974, Distribution of sulfur isotopes of sulfates in ground waters from the principal artesian aquifer of Florida and Edwards aquifer of Texas, United States of America, *in* Isotope techniques in ground-water hydrology, 2: International Atomic Energy Agency, Vienna, Austria, v. II, p. 191-207.

Seiler, R.L., 1986, Selected hydrologic data for Salt Lake Valley, Utah, October 1968 to October 1985: Utah Department of Natural Resources, Basic-Data Report 44 [also as U.S. Geological Survey Open-File Report 86-249], 57 p.

Smith, R.E., 1961, Records and water-level measurements of selected wells and chemical analyses of ground water East Shore area, Davis, Weber, and Box Elder Counties, Utah: Utah State Engineer [Department of Natural Resources], Basic-Data Report 1, 35 p.

Smith, R.E., and Gates, J.S., 1963, Ground-water conditions in the southern and central parts of the East Shore area, Utah, 1953-1961: Utah Geological and Mineralogical Survey, Water Resource Bulletin 2, 41 p.

Spencer, R.J., Baedecker, M.J., Eugster, H.P., Forester, R.M., Goldhaber, M.B., Jones, F.B., Keltz, K., McKenzie, J., Madsen, D.B., Rettig, S.L., Rubin, M., and Bowser, C.J., 1984, Great Salt Lake, and precursors, Utah - The last 30,000 years: Contributions to Mineralogy and Petrology, v. 86, p. 321-334.

Spencer, R.J., Eugster, H.P., and Jones, B.F., 1985, Geochemistry of Great Salt Lake, Utah II - Pleistocene-Holocene evolution: Geochemica et Cosmochemica Acta, v. 49, p. 739-747.

Thode, H.G., Monster, J., and Dunford, H.B., 1961, Sulphur isotope geochemistry: Geochemica et Cosmochemica Acta, v. 25, p. 150-174.

Truesdell, A.H., and Hulston, J.R., 1980, Isotopic evidence on environments of geothermal systems, *in* Fritz, Peter, and Fontes, J.C., editors, Handbook on environmental isotope geochemistry, volume 1, The terrestrial environment: Elsevier, Amsterdam, p. 179-226.

Turk, J.T., 1990, Use of stable-sulfur isotopes to identify sources of sulfate in alpine lakes in the Rocky Mountains: Geological Society of America Abstracts with Programs, v. 22, no. 6, p. 48.

U.S. Environmental Protection Agency, 1981, Methods for chemical analysis of water samples: U.S. Environment Protection Agency, EPA 6000-4-81-020, unpaginated.

Van Dijk, D.C., 1969, Relic salt, a major cause of recent land damage in Yass Valley, Southern Tablelands, N.S.W.: Australian Geography v. 11, p. 1-12.

Waddell, K.M., Seiler, R.L., and Solomon, D.K., 1987, Chemical quality of ground water in Salt Lake Valley, Utah, 1969-1985: Utah Department of Natural Resources, Division of Water Rights, Technical Publication 89, 56 p.

Whelan, J.A., 1973, Great Salt Lake, Utah - Chemical and physical variation of the brine, 1966-1972: Utah Geological and Mineralogical Survey, Water Resource Bulletin 20, 29 p.

ENGINEERING GEOLOGY CONSIDERATIONS FOR PARK PLANNING, ANTELOPE ISLAND STATE PARK, DAVIS COUNTY, UTAH

by
Suzanne Hecker[1] and William F. Case
Utah Geological Survey

[1] now at U.S. Geological Survey, 345 Middlefield Rd., Menlo Park, CA 94025

ABSTRACT

In the mid-1980s, historically high levels of Great Salt Lake caused damage to park facilities on Antelope Island and destroyed the causeway linking the park to the mainland. Information on the engineering geology of Antelope Island can be used to improve park facilities and reduce the risk from geologic hazards and poor construction conditions.

Certain characteristics of the geologic environment need to be considered in park planning. During wet cycles, Great Salt Lake may reach static levels of 4,217 feet (1,285.3 m), and wave- and wind-elevated levels locally may reach 6.5 feet (2 m) higher. A probabilistic assessment of the earthquake ground-shaking hazard along the Wasatch Front indicates that peak ground accelerations of approximately 0.20 to 0.30 g have a one-in-ten chance of being exceeded in 50 years on the island. A slope-failure hazard exists locally in colluvial and Lake Bonneville deposits, along the modern shore, and beneath cliffs. Flash-flood and debris-flow hazards exist on alluvial fans. Areas in the southern two-thirds of the island may have a relatively high potential for radon emission. Particular soil types on the island may be expansive, compressible, erodible, impermeable, or susceptible to liquefaction or hydrocompaction.

The distribution of most geologic hazards can be defined, and many locations on the island have conditions suitable for construction. Lacustrine sand and gravel deposits are widespread and have engineering characteristics that are generally favorable for foundations. However, facilities and roads built close to the modern shoreline may be susceptible to lake flooding and erosion, slope failures, shallow ground water, and burial by active sand dunes. Well-graded (poorly sorted) alluvial-fan deposits are generally most suitable for wastewater disposal, although they may be subject to flooding or be underlain by low-permeability, fine-grained lacustrine deposits.

INTRODUCTION

The purpose of this study is to provide an overview of the geologic and hydrologic characteristics relevant to development of park facilities on Antelope Island. The information is meant to be used as a guide for general planning. Adequate site characterization for facilities would require more detailed engineering geology studies. The scope of work for this study consisted of a literature review, examination of aerial photographs and topographic maps, field checking, and limited soil sampling and testing. Much of the basic geologic information presented in this paper is based on mapping at 1:24,000-scale by Doelling and others (1990).

Pre-existing shoreline park facilities at the north end of Antelope Island were largely destroyed by rising levels of Great Salt Lake during the mid-1980s. Between 1982 and 1986, the lake rose approximately 12 feet (3.7 m), to 4,212 feet (1,283.8 m)(Arnow and Stephens, 1990), flooding picnic areas and destroying the causeway connecting the island with the mainland. Following recession of the lake to below 4,205 feet, the park was given $750,000 to restore damaged facilities on the island, and Davis County spent $3.8 million to rebuild the causeway (Tim Smith, manager, Antelope Island State Park, verbal communication, 1997). The information presented in this paper is intended for use in reducing the likelihood that future lake-level rises and other potential hazards, as well as unfavorable construction conditions, will adversely impact future development of the park. Most of this report was written in 1990, prior to redevelopment of park facilities on Antelope Island.

GEOLOGY

Doelling and others (1990) divided the geologic units on Antelope Island into seven groups: 1) high-grade metamorphic rocks of the Archean(?) and Lower Proterozoic Farmington Canyon Complex; 2) diamictite of the Upper Proterozoic Mineral Fork Formation; 3) metasedimentary rocks of the Upper Proterozoic Kelly Canyon Formation; 4) the Cambrian Tintic Quartzite; 5) sedimentary rocks of an Eocene or younger conglomeratic unit; 6) mostly tuffaceous rocks of the Miocene-Pliocene Salt Lake Formation; and 7) unconsolidated to partly consolidated Quaternary deposits. As will be discussed in subsequent sections, the various unit lithologies differ in their significance for evaluating engineering geology on the island.

Rock Units

The Farmington Canyon Complex, which has been divided into eleven map units on Antelope Island (Doelling and others, 1990), comprises the core of the island (figure 1). It

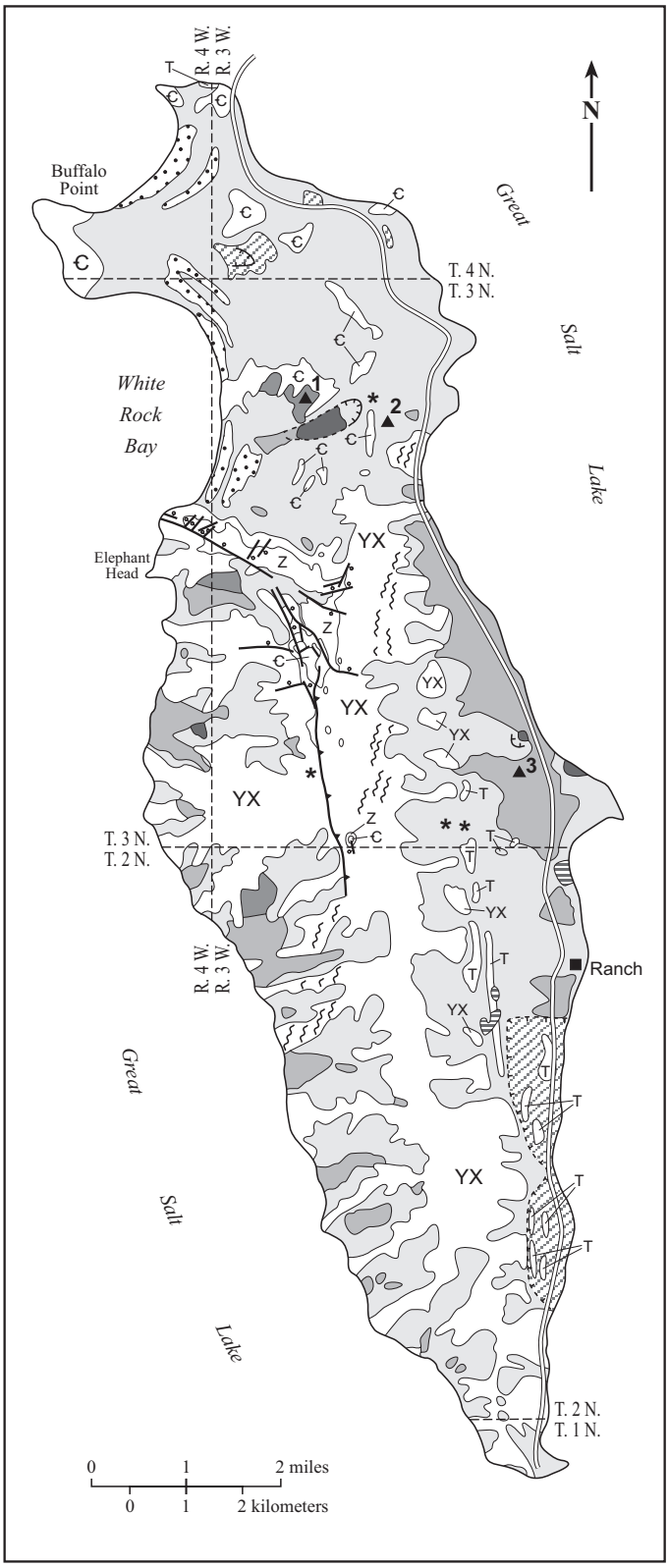

EXPLANATION

- Lacustrine sand and gravel
- Alluvial-fan deposiots
- Wind-blown sand
- Fine-grained lacustrine deposits
- Marsh and lagoonal deposits
- Landslide deposits; *too small to map
- Disturbed ground
- T — Tertiary conglomeratic unit and Salt Lake Formation
- C — Tintic Quartzite
- Z — Mineral Fork and Kelley Canyon Formation
- YX — Farmington Canyon Complex
- Normal fault
- Thrust fault
- Shear zone
- Landslide main scarp
- ▲1 Soil sample location

Figure 1. *General geology of Antelope Island, emphasizing distribution of unconsolidated deposits with significance for engineering geology. Simplified from Doelling and others (1990).*

consists dominantly of layered gneiss, migmatitic gneiss, granite, schist, and amphibolite, with steeply southeast-dipping foliation. These rocks show extensive ductile deformation and have been locally intruded and silicified. In many areas of the island, chloritization attributed to retrograde metamorphism and intense shearing has affected rocks of the Farmington Canyon Complex and younger Proterozoic and Cambrian metasedimentary rocks. The shear zones range from a few feet (1 m) to nearly a mile (1.6 km) in width and generally trend northeast. Joint sets are well developed in many of the Farmington Canyon Complex rocks.

Upper Proterozoic and Cambrian rocks, found on the northern half of Antelope Island (figure 1), are only slightly metamorphosed and have retained original sedimentary characteristics. The Mineral Fork Formation consists of diamictite and the Kelley Canyon Formation consists of a lower dolomite member and an upper slate member. The Tintic Quartzite consists of dense quartzite and lesser amounts of metaconglomerate. A number of faults have been mapped that displace rocks of the Mineral Fork and Kelley Canyon Formations, and it is likely that similar faults cut the Farmington Canyon Complex and the Tintic Quartzite. Most faults on the island are small-displacement, high-angle normal faults. Cretaceous(?) quartz veins, generally less than 10 feet (3 m) thick, are common in all of the Precambrian and Cambrian rocks on Antelope Island (Doelling and others, 1990).

East-dipping Tertiary rocks are exposed along the southeast side (where surficial deposits have been excavated) and at the north tip of the island (figure 1). The conglomeratic

unit is comprised of coarse conglomerate locally interbedded with mudstone, claystone, and limestone. The mudstone and claystone beds are bentonitic. Rocks identified as the Salt Lake Formation consist of tuffaceous sandstone, volcanic ash, tuff, conglomerate, and poorly consolidated sandstone (Doelling and others, 1990).

Unconsolidated Deposits

Unconsolidated Quaternary deposits mantle much of Antelope Island. Lacustrine processes associated with late Pleistocene Lake Bonneville and the much smaller Holocene Great Salt Lake deposited sediment and sculpted prominent shorelines up to an elevation of 5,250 ft (1,600 m), across roughly 90 percent of the island (Doelling and others, 1990). Four major shorelines (from highest to lowest: Bonneville, Provo, Stansbury, and Gilbert shorelines), which represent stillstands of the fluctuating lake between about 27,000 and 11,000 years ago, are generally well developed but locally discontinuous on the island.

Lacustrine sand and gravel deposits are widespread (figure 1) and vary in grain size, sorting (grading), and cementation. Sand is the most abundant grain-size fraction of most deposits. Concentrations of boulders characterize some shoreline deposits; locally well-developed tufa and calcium-carbonate-cemented sands and gravels (beachrock) discontinuously cap some wave-cut platforms and beach deposits, mainly on and between the Stansbury and Provo shorelines (see Doelling and others, 1990 for shorelines).

Ooids (accretionary sand grains of calcium carbonate) are present in varying amounts in beach deposits of Holocene age, but are especially abundant along the west side of the island. In the Unified Soil Classification System (USCS)(table 1), these oolitic deposits are clean, poorly graded (well sorted) sands (SP).

Fine-grained offshore sediments (mixtures of sand, silt, and clay) underlie various thicknesses of regressive beach deposits and Holocene alluvial fans. These lacustrine fines, although locally exposed in various settings, typically lie at or near the surface in wave-sheltered areas southeast of bedrock headlands on the west side of the island (figure 1). The results of laboratory analyses of plastic and liquid limits for several samples of the finer of two facies of lacustrine fines indicate that the sediments are silt and clay (ML and CL; figure 2).

Holocene lagoons and marshy areas surrounding springs, located mostly near the modern shore on the east side of the island (figure 1), are sites where organic-rich sand, silt, and clay have accumulated. Typical lagoon and marsh deposits are probably OL soil (table 1), although laboratory data are not available for these deposits.

Post-Bonneville surficial processes have redeposited lacustrine sediments (as well as sediments derived directly from weathered bedrock) in alluvial fans, eolian dunes, landslides, and colluvium. Poorly sorted (well graded), dominantly coarse-grained alluvium is found in channels of ephemeral streams and in alluvial fans on broad, gently to moderately sloping piedmont surfaces (figure 1). This alluvium has been deposited in successive flash-flood and debris-flow events during Holocene time.

Table 1: *Generalized Unified Soil Classification System.*

Major divisions			Group symbols	Typical names
Coarse-grained soils (More than half of material is larger than No. 200 sieve size)	Gravels (More than half of coarse fraction is larger than No. 4 sieve size)	Clean gravels (Little or no fines)	GW	Well-graded gravels, gravel-sand mixtures, little or no fines
			GP	Poorly graded gravels, gravel-sand mixtures, little or no fines
		Gravel with fines (Appreciable amounts of fines)	GM	Silty gravels, gravel-sand-silt mixture
			GC	Clayey gravels, gravel-sand-silt mixture
	Sands (More than half of coarse fraction is smaller than No. 4 sieve size)	Clean sands (Little or no fines)	SW	Well-graded sands, gravelly sands, little or no fines
			SP	Poorly graded sands, gravelly sands, little or no fines
		Sands with fines (Appreciable amounts of fines)	SM	Silty sands, sand-silt mixtures
			SC	Clayey sands, sand-clay mixtures
Fine-grained soils (More than half of material is larger than No. 200 sieve size)	Silts and clays (Liquid limit less than 50)		ML	Inorganic silts and very fine sands, rock flour, silty or clayey fine sands, or clayey silts with slight plasticity
			CL	Inorganic clays of low to medium plasticity, gravelly clays, sandy clays, silty clays, lean clays
			OL	Organic silts and organic silty clays of low plasticity
	Silts and clays (Liquid limit greater than 50)		MH	Inorganic silts, micaceous or diatomaceous fine sandy or silty soils, elastic silts
			CH	Inorganic clays of high plasticity, fat clays
			OH	Organic clays of medium to high plasticity, organic silts
	Highly organic soils		Pt	Peat and other highly organic soils

Wind-blown sand is a component of Gilbert-age (about 10,000 to 11,000 yr B.P.) and younger shore-zone deposits in bays along the northwestern side of the island (figure 1). The sand (SP; table 1) is primarily derived from the Tintic Quartzite; younger deposits along the present shoreline are rich in ooids. Holocene coastal dunes adjacent to the modern shoreline are sparsely vegetated and active.

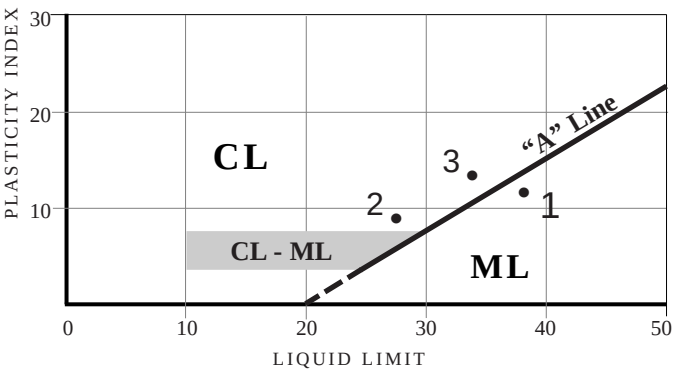

Figure 2. *Plasticity Chart, Unified Soil Classification System, showing laboratory test results for three samples of fine-grained lacustrine deposits (soil samples 1, 2, and 3; see figure 1 for collection sites). See table 1 for soil-symbol (ML and CL) descriptions.*

Landslides have formed in lacustrine sediments and in colluvium (figure 1), mostly above the Bonneville shoreline. Several landslides are located on the flanks of wave-built terraces and other lacustrine ridge forms. Recent slumps, some probably associated with the wet period of the early 1980s, are found in steep colluvial slopes and along the modern wave-cut shore.

Colluvium and talus deposits (including rock-fall debris; generally GM or GC; table 1) have developed typically near the base of moderate-to-steep slopes. Some of the thickest accumulations are above the Bonneville shoreline within the upper portions of drainage basins and are comprised of weathered rock fragments and soil derived from the Farmington Canyon Complex.

Extensive gravel mining along the southeast margin of the island has left a thin, recontoured veneer of sand and gravel deposits, underlain by Tertiary rocks (disturbed ground; figure 1). Surface disturbances associated with gravel mining at the island's north end and artificial fill containing spoil from gravel mining and drilling operations cover smaller, scattered areas.

Ground Water

Unlike other islands in Great Salt Lake, Antelope Island has numerous springs, which issue from both rock and unconsolidated deposits. Springs above an elevation of 4,400 feet (1,341 m) on the east side of the island generally have the best chemical quality (Doelling and others, 1990). Most of the ground-water discharge points are located along the margins of the island and are submerged during high levels of the lake. Low-gradient areas adjacent to springs and the lake shore are probably underlain by ground water at shallow depths. Shallow perched water may exist locally above low-permeability fine-grained deposits.

A study of the geochemistry of Antelope Island ground water found that island aquifers are primarily recharged from modern meteoric water, which has short flow paths and shallow circulation (Mayo and Klauk, 1991, this volume). High concentrations of Cl^- and $SO_4^=$ in the ground water are attributed to aerosols from atmospheric dust and lake spray, and precipitation of evaporated saline lake water (Mayo and Klauk, 1991, this volume).

GEOLOGIC HAZARDS

An extensive coastline, proximity to active faults, and steep, rocky slopes combine to produce a variety of geologic hazards on Antelope Island. The hazards with the most significance for park planning are earthquake ground shaking, lake flooding, erosion, slope failure, alluvial-fan (flash) flooding, problem soil, shallow ground water, and radon.

Earthquakes

Antelope Island lies within the Intermountain seismic belt, a zone of diffuse seismicity that trends north-south through the center of Utah (Smith and Sbar, 1974). The island is part of a mountain-range block on the eastern margin of the Basin and Range Province. The East Great Salt Lake fault (EGSLF) bounds the west side of the range block; its trace is concealed beneath the lake and is less than a mile (<1.6 km) west of Antelope Island. The west-dipping Wasatch fault zone (WFZ), which marks the province boundary, is about 10 miles (16 km) east of the island (figure 3). The WFZ is the most active known fault zone in the region. The central segments of the fault zone have repeatedly experienced large surface-faulting earthquakes (magnitude > 7) during the Holocene, with recurrence intervals for individual segments of about 1,200 to 2,600 years (McCalpin and Nishenko, 1996). The rate of slip on the EGSLF during the late Quaternary may be half the Holocene rate for segments of the WFZ, but the EGSLF may be similarly capable of generating large earthquakes (Pechmann and others, 1987).

The only surface-faulting earthquake in the Great Salt Lake region in historical time was the 1934 magnitude 6.6 earthquake in Hansel Valley, about 50 miles (80 km) northwest of Antelope Island (figure 3). The largest earthquakes since 1850 in the vicinity of the island were two events in 1910 and 1914 that had estimated magnitudes of 5.5 and occurred near Salt Lake City and Ogden, respectively (figure 3; Arabasz and others, 1980).

The greatest earthquake hazard on Antelope Island is ground shaking resulting from either a moderate-size earthquake, which could occur anywhere in the area, or from a large earthquake on a known fault in the region, particularly the WFZ or EGSLF. On Antelope Island, strong ground shaking could initiate landslides and rock falls, generate large waves (seiches) in Great Salt Lake, and cause liquefaction of susceptible saturated soil.

Strong ground shaking alone can damage buildings not designed or constructed to withstand the high lateral forces of earthquakes. Youngs and others (1987) used probabilities of earthquake occurrence from a variety of sources in northern Utah, including the WFZ and the EGSLF, to obtain a probabilistic assessment of the ground-shaking hazard for the Wasatch Front region. Their analyses indicate that for soil sites on Antelope Island, peak horizontal ground accelerations with a 10 percent probability of being exceeded in 50 years vary from about 0.20 g to 0.25 g (g is the acceleration of gravity). For areas underlain by rock, the corresponding peak accelerations range from about 0.25 g to 0.30 g.

Antelope Island lies within the region designated by the 1997 Uniform Building Code (UBC) as seismic zone 3 (Inter-

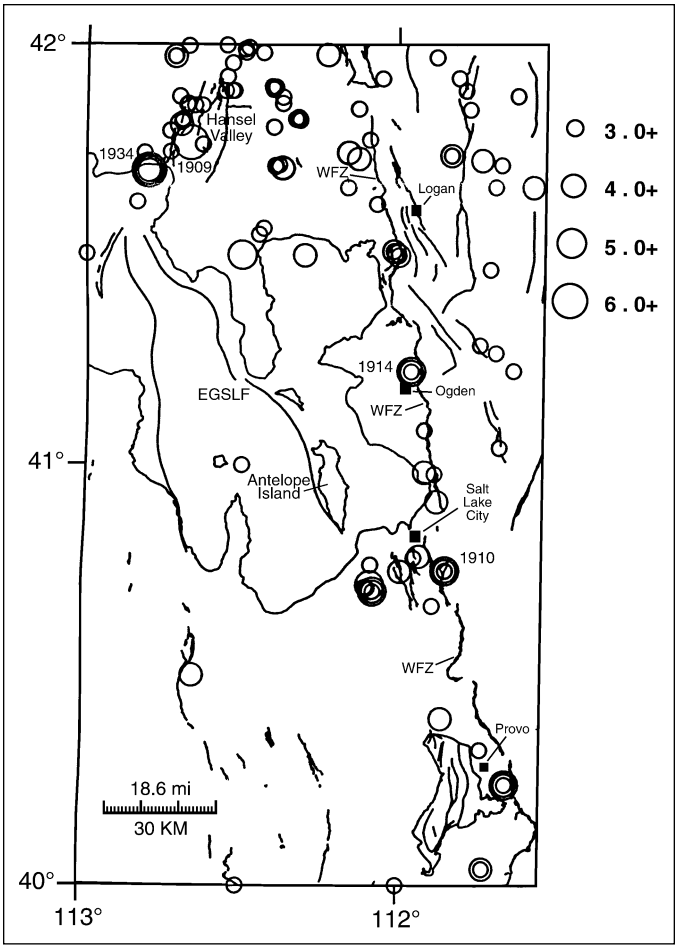

Figure 3. *Regional map of Quaternary faults and earthquake epicenters for all independent main shocks of about magnitude 3.0 or greater, 1850-1990. Earthquakes of estimated magnitude 5.5 or greater are labeled with year of occurrence. Faults discussed in text are also labeled (EGSLF = East Great Salt Lake fault; WFZ = Wasatch fault zone). Epicenter data from University of Utah Seismograph stations; fault data from compilation by Utah Geological Survey.*

national Conference of Building Officials, 1997). Seismic provisions of the UBC specify minimum earthquake-resistant design and construction standards to be followed for the seismic zone. In general, the boundary between zones 3 and 4 is intended to correspond to an effective peak acceleration of 0.3 g. The basis for the probabilistic ground-shaking evaluation of Youngs and others (1987) is similar to the basis for the UBC requirements, and the resulting ground-shaking values presented above are within the range specified for seismic zone 3.

Lake Flooding and Shore Erosion

Fluctuations in the level of Great Salt Lake have caused flooding and erosion in coastal areas. Above-average precipitation in the early 1980s caused a dramatic rise in the level of the lake, which destroyed causeway access to the island and inundated public beaches (figure 4). The lake reached a peak elevation of approximately 4,212 feet (1,283.8 m) in 1986 and again in 1987. This historic highstand level, which is 20 feet (6 m) higher than the 1963 historic lowstand and 10 feet (3 m) higher than the average lake level (Currey and others, 1984; Arnow and Stephens, 1990; Atwood and Mabey, this volume), has been equaled only once in historical times, in the 1870s, and equaled or exceeded at least three other times during the past 700 years (McKenzie and Eberli, 1985; Murchison, 1989; Atwood, 1994; Atwood and Mabey, this volume). The highest level reached by Great Salt Lake in post-glacial times is 4,220 to 4,221 feet (1,286.5 m), less than 10 feet (3 m) higher than the recent historic high (Currey and others, 1988; Murchison, 1989; Atwood, 1994; Atwood and Mabey, this volume). Murchison (1989) constrained the age of this highstand to between 3,440 and 1,400 yr B.P.

Based on a study of abandoned Great Salt Lake shorelines on Antelope Island, combined with previous study results (McKenzie and Eberli, 1985; Karl and Young, 1986; Murchison, 1989), Atwood (1994) and Atwood and Mabey (this volume) speculated on the nature of future lake-level cycles. They estimated that a rise of Great Salt Lake comparable to or greater than the historic highstand of 4,212 feet (1,283.8 m) occurs with an average frequency of about once every hundred years and should be considered within the range of normal fluctuations. The lake level attained during a particular wet cycle depends on the beginning level of the lake, as well as the duration and intensity of the cycle. A highstand altitude of 4,215 feet (1,284.7 m), where the lake expands into the Great Salt Lake Desert, may have an average recurrence interval of a few hundred years. Higher lake levels, up to 4,217 feet (1,285.3 m), occur at some greater, unknown interval. Atwood (1994) and Atwood and Mabey (this volume) proposed that development plans for areas near Great Salt Lake should account for static lake levels that may reach 4,215 feet (1,284.7 m), but will probably not exceed 4,217 feet (1,285.3 m).

The upper altitude of flooding and wave-erosion hazards on the island lies above the maximum static level of the lake and varies spatially with lake-bed and beach geometry and exposure to storm waves and seiches. The elevation of the 1986-87 shorelines surveyed at nineteen locations on Antelope Island vary from 0.6 to 6.3 feet (0.2 to 1.9 m) above the static lake level of 4,212 feet (1,283.8 m) and are highest on the southwest side of the island (Atwood, 1994; Atwood and Mabey, this volume). Changes in water level induced by sustained winds or earthquakes can cause seiches in Great Salt Lake, with an oscillation period (determined by lake configu-

Figure 4. *Debris from picnic facilities at north end of Antelope Island destroyed during mid-1980s rise of Great Salt Lake.*

ration) of about 6 hours and a lake-level rise of perhaps two feet or more (Lin and Wang, 1978; see Atwood, 1994 and Atwood and Mabey, this volume, for discussion). Seiches observed during the 1909 magnitude 6 earthquake in Hansel Valley may have raised the water surface 12 feet (3.7 m) at the Lucin cutoff railroad trestle north of Antelope Island (Lowe, 1990).

The West Desert pumping project, begun after the dramatic rise of Great Salt Lake in 1986-87, was designed to increase total lake evaporation by transferring water into an evaporation pond west of the Newfoundland Mountains. Pumping, as well as consumptive water use, may help reduce the severity of future lake-level maxima, but will not prevent future high lake cycles or eliminate the threat of future flooding (Harty and Christenson, 1988; Atwood, 1994; Atwood and Mabey, this volume).

Slope Failures and Alluvial-Fan Deposition

A slope failure hazard exists on Antelope Island in areas of wave erosion along the modern shore, on and beneath abandoned wave-built lake terraces, and on steep colluvial slopes above the Bonneville shoreline. The character and probable cause of landsliding differs in different areas of the island, although all mapped landslides (figure 1) appear to have originated in slopes greater than about 20 percent.

The largest slope failure on the island is a prehistoric earth flow on the northwest side above White Rock Bay (figure 1). Sand and gravel in the slide moved as far as one-half mile or more (>0.8 km) across gentle to moderate (8 to 17 percent) slopes. Overlapping lobes of material, low mounds, and levees along the margins suggest a failure mode that probably involved relatively fast-moving, water-saturated material.

Fine-grained lacustrine deposits that are exposed in stream cuts just north of the earth flow are inferred to also underlie the slopes that failed. Layers of fine-grained deposits create a zone of low permeability that during times of prolonged or rapid infiltration may become saturated and/or allow development of a perched water table in overlying deposits. These types of saturated conditions, perhaps in conjunction with earthquake ground shaking, may have contributed to initiation of the earth flow. The lacustrine fine-grained unit, as observed in exposures near the earth flow, is comprised of a clean fine-sand facies overlying a more silt- and clay-rich (and less permeable) facies (figure 5). Assuming the necessary moisture conditions, it is possible that strong ground shaking during an earthquake caused the sandy deposits to liquify, resulting in the earth flow.

The earth-flow deposit has well-defined hummocky morphology uncut by shorelines, and thus is less than 13,000 years old, the approximate time when Lake Bonneville dropped below an elevation of 4,400 feet (1,341.1 m) during its recession from the Provo shoreline (Currey and Oviatt, 1985). The landslide is probably more than a few hundred years old, based on the vegetation cover and the accumulation of ponded, fine-grained sediments at the head of the deposit.

The earth flow incorporated coarse-grained material from the outer edge of a Provo shoreline terrace. Along the margin of the terrace adjacent to the landslide main scarp, there are

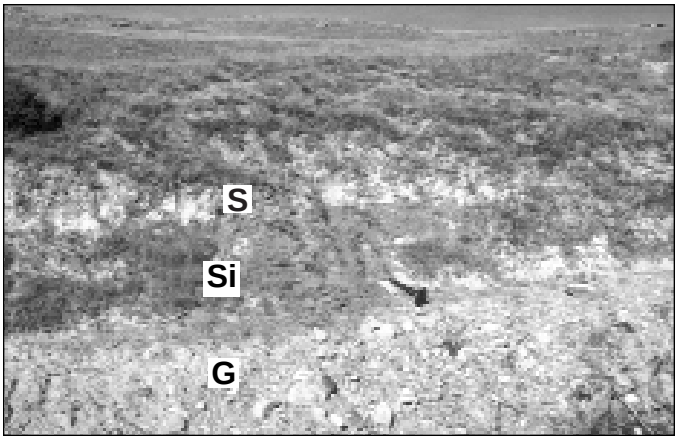

Figure 5. *Exposure of fine-grained offshore deposits (sandy facies, S; silty facies, Si) and transgressive shore-zone gravels (G) of Lake Bonneville. Collection site for soil sample 1 on figures 1 and 2.*

Figure 6. *Aerial view of a rotational landslide in lacustrine sands and gravels (north of soil sample location 3, figure 1).*

arcuate lineaments and scarps with small offsets that appear to be the result of ground cracking and incipient landsliding. These features, which may have formed under the same conditions as the earth flow, indicate that the slope may be unstable.

Several smaller landslides, mostly slumps, have occurred elsewhere on the island in Lake Bonneville and younger sand and gravel deposits (figures 1 and 6). One slump is located close to the earth flow, having formed in the same lake terrace deposit. Wave erosion and ground-water sapping along the modern shore have created other unstable slopes, leading to recent slumping.

Above the Bonneville shoreline, extensive weathering and erosion of gneiss, schist, and metasedimentary rock has produced locally thick mantles of colluvium on steep slopes. Weathering is especially pronounced in rocks that have been mechanically and geochemically weakened by faulting, shearing, and chloritization. The largest landslide mapped above the Bonneville shoreline formed in colluvium at the north end of a major thrust fault near the crest of the island (the Daddy Stump Ridge fault of Doelling and others, 1990). Approximately one-third of the ~600-foot-long (180 m) landslide complex has recently reactivated as a shallow slide with several feet of down-slope movement (figure 7). This reactivated slide is one of many small, fresh-looking slope failures and tensional fractures in steep colluvial slopes on the island.

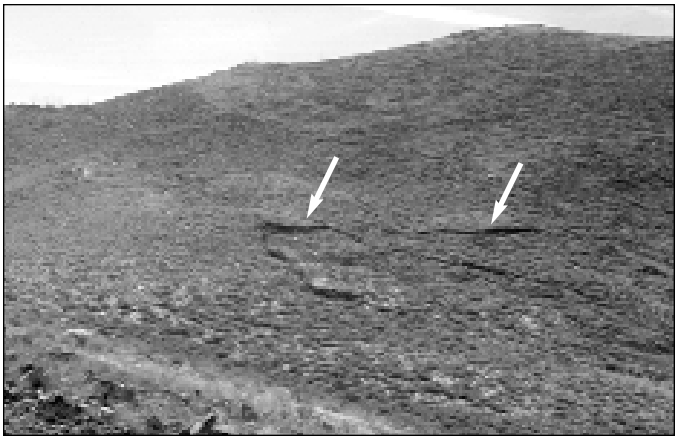

Figure 7. *Recent slope failure in older landslide and colluvial deposits below crestline of the island (at north end of thrust fault, figure 1). View to the south. Arrows point to fresh main-scarp fractures (about 1989).*

These features are similar to the partially detached landslide masses that formed during the wet years of the early 1980s in Farmington Canyon Complex colluvium in the Wasatch Range (Wieczorek and others, 1983), and may have a potential for further movement and perhaps mobilization as debris flows and debris floods.

Numerous debris-flow and flood events during post-Bonneville time have built extensive alluvial fans on both sides of the island (figure 1). Debris-slide scars and fresh, unvegetated alluvial-fan deposits (figure 8), as well as active, unincised fan surfaces, provide evidence that debris-flow and flood processes are ongoing. Areas of coalescing fans on the east side of the island contrast with areas of "disturbed ground" (figure 1) at the southeast end, where extensive gravel mining has removed most of the unconsolidated deposits. Despite the removal of geologic information in these mined areas, debris-flow and flood hazards can be assumed to be present because the topographic setting is similar to areas of fan deposition farther north and locally small debris flows have flowed into the disturbed area.

A study of alluvial-fan deposits in Davis County found that sedimentation and flooding events on fans are characterized by phases, corresponding to differences in sediment-to-water ratios and resulting flow processes (Keaton and Mathewson, 1987). Plastic debris flows and viscous transitional flows, with relatively high sediment concentrations, present a hazard due to impact and burial and occur in proximal (apex) and medial areas of fans. Hyperconcentrated sediment flows and normal streamflows carry less sediment and are more common, but less damaging. They present a hazard of flood inundation and occur mainly on distal fan surfaces and in stream channels (Keaton and others, 1988). While debris flows and transitional flows are relatively rare, flooding and sedimentation from hyperconcentrated and normal streamflows are likely during any normal snow-melt or cloudburst-storm event.

Accumulations of rock-fall debris are associated with some of the higher elevation beach deposits containing large boulders, and with bedrock promontories on the island's west side. A rock-fall hazard generally exists at the base of steep slopes beneath perched lacustrine boulders and outcrops of sheared and fractured bedrock.

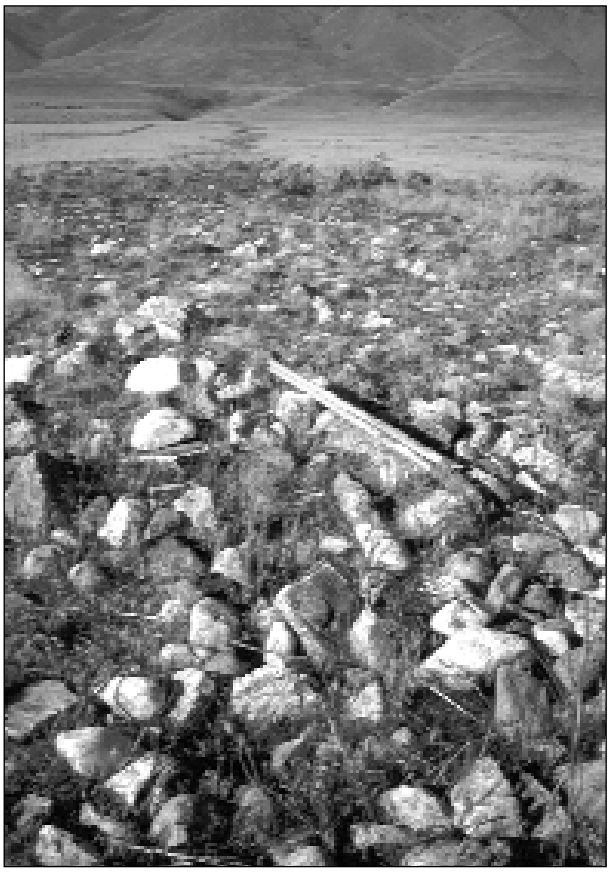

Figure 8. *Recent alluvial-fan deposit on the east side of Antelope Island.*

Problem Soil and Shallow Ground Water

Several types of soil conditions on Antelope Island may pose hazards to park development. Fine-grained lacustrine deposits at variable depths beneath surficial sand and gravel may create unstable ground conditions and present potential engineering problems. Other deposits that may pose challenges for engineering are compressible organic soils in shore and spring areas, possible hydrocompactible soil on alluvial fans, and local expansive soil on fans, colluvial slopes, and certain weathered bedrock.

Atterberg limits were determined for three samples of lacustrine fines from the north end and east side of the island (figure 1; samples 2 and 3 were collected from fine-grained deposits exposed in drainage cuts). The test results (plasticity indices of 12.0, 8.0, and 13.0; corresponding to liquid limits of 38.0, 27.6, and 33.3, for samples 1, 2, and 3, respectively) show the soils to be silt (ML; sample 1) and lean clay (CL; samples 2 and 3). However, the data for all three samples plot close together near the "A" line separating clay-like and silt-like materials on the plasticity chart (figure 2), which indicates that fine-grained lacustrine soil from different areas on the island may have similar engineering properties. The test results indicate a low shrink-swell potential, but rather poor soil drainage. Fine-grained organic soil on the island has not been laboratory tested, but is likely to be classified OL (table 1), having moderate-to-high compressibility, some

shrink-swell potential, and poor drainage.

Soil on alluvial fans and on colluvial slopes probably has a range of engineering properties, corresponding to variations in local composition. Soil derived from Precambrian metamorphic rocks may have low to moderate shrink-swell potential, whereas soil derived from the Tintic Quartzite probably has low to very low shrink-swell potential. Soil derived from tuffaceous rocks of the Salt Lake Formation and the bentonitic claystone and mudstone beds identified in the Tertiary conglomeratic unit has the potential to be expansive. Certain types of alluvial-fan deposits may be susceptible to hydrocompaction, particularly dry, low-density, debris-flow deposits near fan apices.

Other problem soil conditions on Antelope Island include sand-dune activity and soil erosion. Blowing sand from sparsely vegetated dunes on the north end of the island (figure 1) may be deposited on roads and may bury or be eroded from beneath structures (figure 9). Erosion is a hazard on steep slopes underlain by surficial deposits, particularly when surfaces and vegetation are disturbed, sediments are compacted, and runoff is channelized. This is evidenced by deep gullies that have developed along old off-road vehicle trails (figure 10).

Shallow ground water, especially in combination with problem soil types, presents several problems for development. Water less than 10 feet (3 m) deep can cause unstable slopes, unstable building foundations, and flooding of subsurface facilities. Also, ground water less than about 30 feet (9 m) deep in areas with susceptible soil creates a potential for liquefaction. In general, shallow ground water can be expected in low-gradient areas near Great Salt Lake and in the vicinity of springs. Shallow ground water may also develop locally and intermittently above the low-permeability lacustrine fines. This may be a particular problem if water is introduced by park development.

Radon

Radon, a common radioactive gas of geologic origin, is hazardous only when it becomes concentrated in buildings or natural enclosures; outdoor radon concentrations never reach hazardous levels (see Sprinkel and Solomon, 1990; Black, 1993 for discussion of radon hazards in Utah). A statewide assessment of relative radon-hazard potential (at 1:1,000,000-scale) identified the north end of Antelope Island (area underlain mainly by Cambrian Tintic Quartzite) as having moderate indoor radon-hazard potential and the rest of the island (underlain mainly by the Farmington Canyon Complex) as having high radon-hazard potential (Black, 1993). The assessment is based on a consideration of three geologic factors that influence radon-hazard potential: uranium concentration in source materials, soil permeability, and depth of ground water. Low soil permeability and shallow ground water block the flow of soil gas and thereby reduce the radon-hazard potential. Higher radon-gas hazards are based on the general association of mapped rock types with concentrations of uranium-bearing minerals (Sprinkel, 1987). The Precambrian Farmington Canyon Complex and Tertiary units such as the Salt Lake Formation are known to contain uranium-bearing strata (Sprinkel, 1987).

Figure 9. *Wind-blown sand covering road in area of beach facilities at north end of Antelope Island.*

Figure 10. *Gullies and debris fans formed in lacustrine sands and gravels along old off-road vehicle trails on northeast side of island.*

A preliminary ground radiometric survey of equivalent uranium concentration on Antelope Island (Utah Geological Survey, unpublished data) indicated that areas on the west side of the island underlain by granitic gneiss of the Farmington Canyon Complex have relatively high radon potential. Some areas of prominent shearing in the Farmington Canyon Complex appear to have similar potential. In other areas of the Farmington Canyon Complex, particularly along the high central portion of the island, the survey values seem anomalously low. However, this result is consistent with the relatively low readings obtained in a survey of indoor radon concentrations in areas underlain by soil derived from the Farmington Canyon Complex along the Wasatch Range front in Weber and Davis Counties (Sprinkel and Solomon, 1990). From the ground survey, the north end of the island, which is comprised of Tintic Quartzite (figure 1), appears to have a relatively low potential for radon. Locally along the east side of the island, relatively high radiometric concentrations correlate with the Salt Lake Formation.

In a study of radon-hazard potential along the Wasatch Front near Sandy and Provo, Solomon and others (1994) found that Quaternary deposits with the highest potential for an indoor-radon hazard are well-drained upper Pleistocene lacustrine sediments related to the transgressive phase of Lake Bonneville, as well as younger alluvial and colluvial deposits overlying these transgressive sediments. Sediments below the Provo (regressive) level were found to be less well

drained and to have lower hazard potential.

FACILITY SITING CONSIDERATIONS

Factors important in siting facilities include the bearing capacity (shear strength and compressive strength) of earth materials and ease of excavation, as well as problem-soil, slope-stability, and other hazards previously discussed. Included below are summaries of these siting conditions as they relate to buildings, roads, trails, shoreline facilities, and waste-disposal facilities. These assessments of siting conditions are based on generalized characteristics of rock and unconsolidated deposits; local conditions may vary.

Foundation Conditions

Rock Units

The following characteristics of rock units are deduced from brief excursions and generalized physical properties of specific rock types; no tests were run on Antelope Island rock units.

Ledge-forming and slope-forming rock units present different foundation conditions on Antelope Island. Ledge-forming rock units are strongly indurated, resist weathering, generally occur on steep slopes, and have high compressive and shear strengths, except where they are fractured. Slope-forming rock units are weakly indurated, easily weathered, erode to gentle slopes, and have a wide range of compressive and shear strength values.

Excavation of ledge-forming rock units requires ripping and blasting, subject to the extent and spacing of fractures. Slopes in hard rock are typically steep, except on the north end of the island where the Tintic Quartzite is exposed near ground level. Ground water is usually deep, except near springs along the base of the mountains, because of high fracture permeability. The ledge-forming rock units include: some Farmington Canyon Complex gneisses and granites; the dolomite member of the Kelley Canyon Formation; the Tintic Quartzite; and tuffaceous sandstone, tuff, and conglomerate of the Salt Lake Formation.

The ease of excavation of slope-forming rock units depends on the degree of weathering of the rock, extent of fracturing, and rock strength. Slope-forming rock units may require ripping and blasting below the weathered, surficial layer. Slope-forming rock units include the following: schistose layers in gneiss, chloritized and hematitized gneiss, and amphibolite of the Farmington Canyon Complex; slate member of the Kelley Canyon Formation; Mineral Fork Formation diamictite; and fine-grained strata of the Salt Lake Formation.

Unconsolidated Deposits

Unconsolidated deposits include all Quaternary geologic units. Some deposits are semi-consolidated where they are cemented by calcium carbonate (forming beachrock and tufa). Soil types on the island, classified using the Unified Soil Classification System, include well-graded sand and gravel (GW), poorly-graded sand (SP), silt (ML), and lean clay (CL).

Sand and gravel beach deposits, which consist predominantly of granular materials, generally have low compressibility. Shear strengths are generally high. These deposits are relatively easy to excavate, except where they contain especially large grain sizes. Excavation in tufa and beachrock may also be difficult. Beach deposits are generally stable in slopes below the angle of repose, but are subject to raveling in steeper slopes, and may be unstable at lesser slopes when wet.

Wind-blown sand deposits and some beach deposits are composed of clean, poorly-graded sand (SP). Compactibility of beach and dune sand is low; compressive strength is generally high; and excavation is relatively easy. Sands are porous and permeable and, except near a source of water, are dry. Shrink-swell potential and susceptibility to frost heave are low.

Alluvial-fan deposits and colluvium are well graded, containing gravel to clay-sized particles. Compressive and shear strengths are variable, depending on the amount of gravel and fines in the deposit. Holocene alluvial-fan deposits may be subject to collapse by hydrocompaction; a laboratory consolidation test is necessary to determine the collapse potential of a particular soil. Alluvial-fan and colluvial materials are relatively easy to excavate, except where boulders are common. Shrink-swell potential and susceptibility to frost heave are variable, depending on the rock source and clay content of the deposit. Ground water may be locally shallow in alluvial-fan deposits.

Lagoon and marsh environments contain low-strength, compressible organic silts and clays (OL) subject to subsidence from oxidation and decomposition, providing generally poor foundation conditions. Shallow ground water in these environments can cause foundation-stability difficulties.

Deep-water, fine-grained Lake Bonneville sediments (ML and CL) may underlie many surficial deposits around the island. Excavations in areas of unconsolidated deposits may encounter the unit at depths ranging from near surface to perhaps more than 45 feet (14 m), the maximum known depth of sand and gravel deposits measured in gully exposures (Fitzhugh D. Davis, Utah Geological Survey, verbal communication, 1990). The deposit may be moderately difficult to excavate because of the relatively high dry strength of clays. Atterberg limits determined for three samples (figure 2) indicate a low shrink/swell potential and poor soil drainage. The deposits are likely to impede ground-water infiltration, creating local perched water tables. Slopes underlain by this unit may be unstable, particularly when wet, as evidenced by the large earth flow on the north end of the island (see section on slope failure and alluvial-fan flooding).

Roads and Trails

The location of roads, and hiking and biking trails on the island should be carefully planned, particularly on slopes underlain by unconsolidated materials that are easily compacted and eroded. Existing roads and off-road vehicle trails have caused severe erosion problems on the island. On steep slopes underlain by granular lake deposits, roads and trails are deeply rutted (figure 10). Surface runoff concentrates and increases erosion in the tire-compacted surfaces. The problem has been worsened by vehicles that avoid the ruts and thereby expand the damaged area. Roads and trails must be designed and drainage must be controlled to mitigate exces-

sive slope erosion.

Other problems to be considered in siting roads and trails include slope failures, wave erosion, and sand-dune migration. Roads should be placed above and away from shoreline areas susceptible to erosion and slope failures caused by lake-level fluctuations, storm waves, and seiches (see Geologic Hazards section). During the mid-1980s lake-level rise, waves eroded portions of the causeway. Wave erosion continues to threaten some areas along the east-side road. Sand dunes have migrated onto roads at the north end of the island (figure 9).

Shoreline Facilities

Park facilities built along the shoreline may be susceptible to the following hazards: 1) wave erosion; 2) slope failure due to wave erosion and ground-water sapping; 3) sand-dune migration; 4) lake-level fluctuations; and 5) foundation settlement due to compression of saturated organic soil (see Geologic Hazards section). Any in-lake structures such as piers, jetties, or groins will also be subject to lake-level fluctuations and perhaps worse foundation problems. In addition, these structures may impede the longshore drift of sediment, affecting deposition patterns and the stability of down-current beaches.

Wastewater Disposal

The suitability of an area for wastewater disposal in a soil absorption field is dependent on the soil permeability and clay content, slope, flood hazard, depth to ground water, and depth to rock. Soil must have permeability that is high enough to allow wastewater to move through it, but not so high as to allow wastewater to discharge to the surface or mix with ground water before being renovated. Percolation rates must be between 1 and 60 minutes/inch (0.39 and 23.6 minutes/cm) and slopes must be less than 25 percent to meet state health department requirements. The soil-absorption field should not be susceptible to flooding, erosion, or ponding of surface water. Drain lines are required to be at least 3 feet (0.9 m) above bedrock or impervious strata, at least 1 foot (0.3 m) below ground surface, covered by at least 1 foot (0.3 m) of filter material, and at least 2 feet (0.6 m) above the anticipated highest level of ground water. This ground-water level shall be at least 4 feet (1.2 m) below finished grade (Utah Department of Environmental Quality, 1996a). The best soil type is silty/clayey sand (SM/SC) with less than 25 to 30 percent clay.

On Antelope Island, well-graded alluvial-fan deposits are probably the most suitable material for soil-absorption fields. However, active portions of alluvial fans are susceptible to debris flows and floods, and may be underlain by shallow water tables. Permeability may be low enough, and filtering and cation-exchange capacity of soils may be sufficient for renovation of wastewater in these deposits. These factors may not be adequate in many other surficial deposits, such as dune and beach deposits. Fine-grained lacustrine deposits, if present at shallow depths below a soil-absorption field, may produce a perched water table and flood the system. Wastewater may also move downslope through the subsurface along the top of the fine-grained unit and come to the surface or flow into Great Salt Lake prior to being renovated.

Wastewater disposal in sewage lagoons is possible on Antelope Island, although careful consideration must be given to hazards and the potential for lake contamination. Most of the larger areas of gentle slopes required for lagoons are near the lake and are presumably underlain by less-permeable, fine-grained lacustrine deposits that may direct seepage from a lagoon into the lake. Liners would be required and, although some material of sufficiently low permeability for a clay liner may be found on the island, most material would likely need to be imported. Most of the suitable areas for sewage lagoons are on the north and east sides of the island.

Landfills

Landfills are permanent solid-refuse holding sites and should be sited to minimize transfer of materials from the landfill into the environment. Solomon and Klauk (1989) listed the following considerations for landfill siting: (1) the site should have workable geologic materials that can be economically excavated; (2) the host materials should be relatively impervious if the pit is unlined; (3) the geologic material used for the cover should also be relatively impervious, as well as compactable; (4) there should be no geologic hazards, such as flooding, erosion, or slope failure, that will expose waste to the environment; (5) the slope of the ground surface should be sufficiently gentle for ease of working the landfill and maintaining slope stability, yet steep enough to prevent water from ponding on the landfill; (6) ground-water quality should be continuously monitored, from the time of construction and continuing after the landfill has been abandoned; and (7) the bottom of the landfill should be at least 5 feet (1.5 m) above the seasonally high ground-water level. According to the Utah Department of Environmental Quality (1996b), a landfill site should not be located within 1,000 feet (305 m) of a national, state, or county park.

In general, the coarse-grained lake, eolian, and alluvial-fan deposits that dominate the surficial deposits of the island are poorly suited as host or cover material for a landfill. A liner would be required and fine-grained material would need to be blended with the sand and gravel to provide suitable cover. Some finer grained alluvial-fan and lake deposits may be locally suitable for cover but, as with sewage lagoons, liner material would likely need to be imported. Areas of fine-grained lake deposits and weathered soft rock, such as that found in gravel excavations on the southeast side of the island, may be suitable host material. However, expansive clays found in the weathered rock may not be suitable for cover, both because such clay is not workable when wet and because it cracks excessively when dry. In all cases, geologic hazards such as flooding and slope failure need to be identified during siting studies, but in most cases hazards can be avoided or mitigated.

CONCLUSIONS

Geologic information is important to successful development and management of park resources on Antelope Island. Geologic hazards and difficult site conditions must either be avoided or accommodated in design and construction of facilities. Local variations in slope, materials, and processes can

influence suitability of sites for buildings, roads, or waste disposal.

Strong earthquake ground shaking may effect the entire island and initiate landslides, rock falls, and liquefaction in susceptible material. Antelope Island is within seismic zone 3 of the Unified Building Code, and probabilistic analyses of ground shaking in the region indicate that peak ground accelerations of roughly 0.20 to 0.30 g (varying with location between rock and soil sites) have a 10 percent chance of being exceeded in 50 years on the island (Youngs and others, 1987).

The margins of the island adjacent to Great Salt Lake may be subject to flooding and erosion from earthquake- or wind-induced seiches of the lake, storm waves, or rising lake levels. For planning purposes, the lake may be expected to reach static levels as high as 4,215 to 4,217 feet (1,284.7 to 1,285.3 m), with wave-elevated levels up to 6.5 feet (2 m) higher, depending on site exposure and topography (Atwood, 1994; Atwood and Mabey, this volume).

Slope-failure hazards exist in several different settings on the island. Moderate to steep slopes in coarse-grained Lake Bonneville deposits, particularly deposits underlain by a layer of low-permeability lake fines, may be unstable under conditions of excessive moisture and/or strong ground shaking. Landslides may also occur in colluvial slopes above the Bonneville shoreline and in wave-eroded areas along the modern shoreline. A rock-fall hazard may be present in areas below cliffs of fractured rock and below steep bouldery slopes. Debris flows and flash floods are a hazard on alluvial fans, which have been built from successive flow and flood events during the past 10,000 years.

Shallow ground water and expansive, compressible, hydrocompactible, and erodible soils are found locally and present difficulties for development. Soils derived from tuffaceous and bentonitic rocks of the Salt Lake Formation and Tertiary conglomeratic unit, or from metamorphic rocks of the Farmington Canyon Complex may have significant shrink-swell potential. The fine-grained lacustrine sediments thought to be widespread at shallow depths on the island appear from laboratory testing to have low shrink-swell potential, but poor soil drainage. Shallow ground water, found either perched above these fines or in the vicinity of springs or Great Salt Lake, may create unstable foundation conditions and flood underground facilities. Compressible organic soil is commonly found in areas of shallow ground water and in marsh or lagoon environments. Holocene debris-flow deposits on alluvial fans may be susceptible to hydrocompaction. Some sediments, notably lacustrine sand and gravel deposits on steep slopes and wind-blown sand, are easily eroded when vegetation is removed or runoff is channelized.

Indoor radon-hazard potential is considered to be high within the southern two-thirds of the island (Black, 1993). This area is underlain by the Farmington Canyon Complex and the Salt Lake Formation, map units that are known to contain uraniferous strata (Sprinkel, 1987). In contrast, the north end of the island, where the Tintic Quartzite is exposed, appears to have moderate to low radon-hazard potential.

Few serious problems face construction of buildings, roads and trails, shoreline facilities, wastewater disposal systems, or landfills on Antelope Island. The ease of excavating rock for building foundations ranges from relatively easy for slope-forming rock units to relatively difficult for ledge-forming rock units. Unconsolidated deposits present few excavation difficulties, unless they are cemented by calcium carbonate or contain boulders. Compressive and shear strengths of rock units range from high for ledge-forming rock units to variable for soft-rock units. Physical properties of unconsolidated deposits are a function of grain size and type of deposit. The compressive and shear strengths of sand and gravel deposits are generally high, whereas well-graded alluvial-fan and colluvial deposits, which contain silt and clay, have variable compressive and shear strengths.

Traffic on roads and trails that cross slopes underlain by unconsolidated materials may produce ruts and increase erosion. Properly engineered roadbeds and drainage will be required to alleviate such erosion problems. Routes should consider slope stability in siting and design, and those close to shorelines should consider fluctuating lake levels, wave erosion, and active sand dunes, as should all shoreline facilities. The direction of longshore drift should be considered for in-lake facilities to avoid loss of sand at swimming beaches and filling of marina harbors. Structures near the shoreline may also encounter problems with shallow ground water and/or organic-rich soils.

Alluvial-fan deposits are probably the most suitable unconsolidated unit on the island for wastewater disposal in soil absorption systems. Clay content in the deposits may be sufficient to maintain the percolation rates necessary to renovate wastewater. However, some alluvial-fan locations are unacceptable because of surface- and ground-water flooding potential. Fine-grained lacustrine sediments or weathered soft-rock Tertiary units found on the southeast side of the island may be most suitable as host materials for a landfill, although it is likely that imported liner material would be required at any site. Some alluvial-fan sediments may be suitable as cover material for a landfill, but most other unconsolidated materials are less suitable. Landfills must be sited to avoid or designed to mitigate geologic hazards such as flooding, slope instability, and shallow ground water.

In planning park facilities, care should be taken to consider engineering geologic conditions. For all essential facilities or facilities for human occupancy, an engineering geologic report assessing geologic hazards and foundation conditions should be performed to recommend appropriate avoidance and mitigation strategies. For waste-disposal systems, studies are required to assess site conditions with regard to hazards, soil permeability, potential to contaminate ground or surface water (particularly the lake), and availability and suitability of local materials for liners and cover. Geologic hazards on the island are generally localized and for the most part can be mitigated. Sites well-suited for disposal of wastes, particularly landfills or sewage lagoons, are probably few and should be carefully chosen and designed.

REFERENCES

Arabasz, W.J., Smith, R.B., and Richins, W.D., 1980, Earthquake studies along the Wasatch front, Utah -- Network monitoring, seismicity, and seismic hazards: Bulletin of the Seismological Society of America, v. 70, p. 1479-1499.

Arnow, Ted, and Stephens, Doyle, 1990, Hydrologic characteristics of the Great Salt Lake, Utah--1847-1986: U.S. Geological Survey Water Supply Paper 2332, 32 p.

Atwood, Genevieve, 1994, Geomorphology applied to flooding problems of closed-basin lakes...specifically Great Salt Lake, *in* Geomorphology and Natural Hazards, 25th Binghamton Symposium in Geomorphology: Geomorphology, v. 10, p. 197-219.

Black, B.D., 1993, The radon-hazard-potential map of Utah: Utah Geological Survey Map 149, scale 1:1,000,000.

Currey, D.R., and Oviatt, C.G., 1985, Durations, average rates, and probable causes of Lake Bonneville expansions, stillstands, and contractions during the last deep-lake cycle, 32,000 to 10,000 years ago, *in* Kay, P.A., and Diaz, H.F., editors, Problems of and prospects for predicting Great Salt Lake levels: Salt Lake City, Center for Public Affairs and Administration, University of Utah, p. 9-24.

Currey, D.R., Atwood, Genevieve, and Mabey, D.R., 1984, Major levels of Great Salt Lake and Lake Bonneville: Utah Geological and Mineral Survey Map 73, scale 1:750,000.

Currey, D.R., Berry, M.S., Douglas, G.E., Merola, J.A., Murchison, S.B., Ridd, M.K., Atwood, Genevieve, Bills, B.G., and Lambrechts, J.R., 1988, The highest Holocene stage of Great Salt Lake, Utah: Geological Society of America Abstracts with Programs, v. 20, no. 6, p. 411.

Doelling, H.H., Willis, G.C., Jensen, M.E., Hecker, Suzanne, Case, W.F., and Hand, J.S., 1990, Geology map of Antelope Island, Davis County, Utah: Utah Geological Survey Map 127, 27 p., scale 1:24,000.

Harty, K.M., and Christenson, G.E., 1988, Flood hazard from lakes and failure of dams in Utah: Utah Geological and Mineral Survey Map 111, 8 p., scale 1:750,000.

International Conference of Building Officials, 1997, Uniform Building Code: Whittier, California, International Conference of Building Officials, variously paginated.

Karl, T.R., and Young, P.J., 1986, Recent heavy precipitation in the vicinity of Great Salt Lake; just how unusual?: Journal of Climate and Applied Meteorology, v. 25, p. 353-363.

Keaton, J.R., and Mathewson, C.C., 1987, Proposed ideal alluvial fan stratigraphy for risk assessment: Geological Society of America Abstracts with Programs, v. 19, no. 7, p. 723.

Keaton, J.R., Anderson, L.R., and Mathewson, C.C., 1988, Assessing debris flow hazards on alluvial fans in Davis County, Utah, *in* Fragaszy, R.J., editor, Proceedings of the 24th symposium on engineering geology and soils engineering, Coeur d'Alene, Idaho: Idaho Department of Transportation, Boise, Idaho, p. 89-108.

Lin, Aching, and Wang, Lo, 1978, Wind tides of the Great Salt Lake: Utah Geolgical and Mineralogical Survey, Utah Geology, v. 5, no. 1, p. 17-25.

Lowe, Mike, 1990, Earthquake-induced ground failure in sensitive clays, vibratory settlement, seiches, surface-drainage disruptions, and increased ground-water discharge, Davis County, Utah, *in* Gori, P.L., editor, Assessment of Regional Earthquake Hazards and Risk along the Wasatch Front, Utah, volume IV: U.S. Geological Survey Open-File Report 90-225, p. MM1-MM16.

Mayo, A.L., and Klauk, R.H., 1991, Contributions to the solute and isotopic groundwater geochemistry, Antelope Island, Great Salt Lake, Utah: Journal of Hydrology, v. 127, p. 307-335.

McCalpin, J.P., and Nishenko, S.P., 1996, Holocene paleoseismicity, temporal clustering, and probabilities of future large (M > 7) earthquakes on the Wasatch fault zone, Utah: Journal of Geophysical Research, v. 101, no. B3, p. 6233-6253.

McKenzie J.A., and Eberli G.P., 1985, Late Holocene lake-level fluctuations of the Great Salt Lake (Utah) as deduced from oxygen-isotope and carbonate contents of cored sediments, *in* Kay, P.A., and Diaz, H.F., editors, Problems of and Prospects for Predicting Great Salt Lake Levels: Salt Lake City, Center for Public Affairs and Administration, University of Utah, p. 25-39.

Murchison, S.B., 1989, Fluctuation history of Great Salt Lake, Utah, during the last 13,000 years: Salt Lake City, University of Utah, Ph.D. dissertation, 137 p.

Pechmann, J.C., Nash, W.P., Viveiros, J.J., and Smith, R.B., 1987, Slip rate and earthquake potential of the East Great Salt Lake fault, Utah [abstract]: EOS, Transactions of the American Geophysical Union, v. 68, no. 44, p. 1369.

Smith, R.B., and Sbar, M.L., 1974, Contemporary tectonics and seismicity of the western United States with emphasis on the Intermountain Seismic Belt: Geological Society of America Bulletin, v. 85, no. 8, p. 1205-1218.

Solomon, B. J., and Klauk, R. H., 1989, Regional assessment of geologic conditions for sanitary landfills in Sevier County, Utah: Utah Geological and Mineral Survey Special Study 71, 15 p.

Solomon, B.J., Black, B.D., Nielson, D.L., Finerfrock, D.L., Hultquist, J.D., and Linpei, Cui, 1994, Radon-hazard-potential areas in Sandy, Salt Lake County, and Provo, Utah County, Utah: Utah Geological Survey Special Study 85, 49 p.

Sprinkel, D.A., 1987 (revised 1988), The potential radon hazard map, Utah: Utah Geological and Mineral Survey Open-File Report 108, 4 p., scale 1:1,000,000.

Sprinkel, D.A., and Solomon, B.J., 1990, Radon hazards in Utah: Utah Geological and Mineral Survey Circular 81, 25 p.

Utah Department of Environmental Quality, 1996a, Individual Wastewater Disposal Systems, R317-501 through R317-513, Utah Administrative Code: Utah Department of

Environmental Quality, Division of Water Quality, 59 p.

Utah Department of Environmental Quality, 1996b, Proposed Administrative Rules, Solid Waste Permitting and Management Rules, R315-301 through R315-320: Department of Environmental Quality, Division of Solid and Hazardous Waste, 77 p.

Wieczorek, G.F., Ellen, Stephen, Lips, E.W., Cannon, S.H., and Short, D.N., 1983, Potential for debris flow and debris flood along the Wasatch Front between Salt Lake City and Willard, Utah, and measures for their mitigation: U.S. Geological Survey, Open-File Report 83-635, 45 p.

Youngs, R.R., Swan, F.H., Power, M.P., Schwartz, D.P., and Green, R.K., 1987, Analysis of earthquake ground shaking hazard along the Wasatch Front, Utah, *in* Gori, P.L., and Hays, W.W., editors, Assessment of Regional Earthquake Hazards and Risk along the Wasatch Front, Utah, volume II: U.S. Geological Survey Open-File Report 87-585, p. M1-M110.

THE GEOLOGY OF ANTELOPE ISLAND, Davis County, Utah

King and Willis

Miscellaneous Publication 00-1
Utah Geological Survey
a division of
Utah Department of Natural Resources

ISBN 1-55791-647-0